IMPACT OF *STAPHYLOCOCCUS AUREUS* BIOFILM CONDITIONED MEDIUM ON INFLAMMATION AND EPITHELIALIZATION IN HUMAN KERATINOCYTES

by

Patrick Robert Secor

A dissertation submitted in partial fulfillment
of the requirements for the degree

of

Doctor of Philosophy

in

Cell Biology and Neuroscience

MONTANA STATE UNIVERSITY
Bozeman, Montana

January 2011

©COPYRIGHT

by

Patrick Robert Secor

2011

All Rights Reserved

APPROVAL

of a dissertation submitted by

Patrick Robert Secor

This dissertation has been read by each member of the dissertation committee and has been found to be satisfactory regarding content, English usage, format, citation, bibliographic style, and consistency and is ready for submission to the Division of Graduate Education.

Dr. Thomas Hughes

Approved for the Department of Cell Biology and Neuroscience

Dr. Thomas Hughes

Approved for the Division of Graduate Education

Dr. Carl A. Fox

STATEMENT OF PERMISSION TO USE

In presenting this dissertation in partial fulfillment of the requirements for a doctoral degree at Montana State University, I agree that the Library shall make it available to borrowers under rules of the Library. I further agree that copying of this dissertation is allowable only for scholarly purposes, consistent with "fair use" as prescribed in the U.S. Copyright Law. Requests for extensive copying or reproduction of this dissertation should be referred to ProQuest Information and Learning, 300 North Zeeb Road, Ann Arbor, Michigan 48106, to whom I have granted "the exclusive right to reproduce and distribute my dissertation in and from microform along with the non-exclusive right to reproduce and distribute my abstract in any format in whole or in part."

Patrick Robert Secor

January 2011

TABLE OF CONTENTS

1. INTRODUCTION....1

Context....1
Objectives....2

2. BACKGROUND....4

Literature Reviewed....4
Biology and Immunology of Acute Wound Healing....4
Inhibition of Healing in Chronic Wounds....7
Bacterial Biofilm and *S. aureus* Infection of Chronic Wounds....10
Epidermal Keratinocytes and Their Functions in Immunity....12
Cytokine Biology....13
Signal Transduction in Activated Keratinocytes....16
Mitogen Activated Protein Kinase....17
Transcription Factors....20
Intracellular Calcium Release....22
Physiology of Wounded Human Skin....23

3. PHYLOGENETIC CHARACTERIZATION OF CHRONIC WOUND BIOFILM MICRO-COMMUNITIES....25

Introduction....25
Materials and Methods....26
DNA Extraction from Debridement Samples....26
PCR and DGGE....26
Cloning and Sequencing....27
Results....28
Estimation of Bacterial Diversity by DGGE and Sequencing of 16S rDNA....28
Characterization of Bacterial Populations in Diabetic Foot Ulcers, Venous Leg Ulcers, and Pressure Ulcers....32
Discussion....34

4. DEVELOPMENT OF A NOVEL *IN VITRO* BIOFILM DISEASE MODEL AND CHARACTERIZATION OF *S. AUREUS* BIOFILM CONDITIONED MEDIUM....38

Introduction....38

TABLE OF CONTENTS– CONTINUED

Materials and Methods....39
Cell Culture....39
S. aureus Biofilm Culture Conditions and Preparation of Biofilm Conditioned Medium....40
S. aureus Planktonic Culture Conditions and Preparation of Planktonic Conditioned Medium....40
Population Density Measurements of *S. aureus* Cultures....41
1D SDS-PAGE....42
Nuclear Magnetic Resonance (NMR) Metabolite Profiling....43
Organic Extraction of Conditioned Medium....43
High-Performance Liquid Chromatography Mass Spectrometry (HPLC/MS) Analysis 44
HPLC....44
ESI-MS....44
Q-TOF-MS....44
ICP-MS....45
Results....45
Characterization of *S. aureus* in the Biofilm Disease Model and *S. aureus* Biofilm Conditioned Medium....45
S. aureus Biofilm Produces Mixed Acid Fermentation Products....49
Hydrophobic Small Molecules Production in *S. aureus* Biofilm and Planktonic Cultures....57
Oxygen Tension in Planktonic *S. aureus* Cultures Impacts Production of Aureusimine AandB 61
Discussion....63

5. *S. AUREUS* BIOFILM CONDITIONED MEDIUM INDUCES A DISTINCT INFLAMMATORY RESPONSE AND INHIBITS PROCESSES ASSOCIATED WITH EPITHELIALIZATION IN HUMAN KERATINOCYTES....71

Introduction....71
Materials and Methods....71
Cell Culture....71
Bacterial Strains and Culture Conditions....72
Conditioned Medium Microarray....72
Co-Culture Microarray....73
RT-qPCR....75
Microscopy....75

TABLE OF CONTENTS– CONTINUED

Terminal Deoxynucleotidyl Transferase
dUTP Nick End Labeling (TUNEL) Assay....76
Measurement of Intracellular Calcium Levels....77
Cytokine Detection by Enzyme Linked Immunoassays (ELISA)....77
Detection of MAPK Phosphorylation Using Cell-Based ELISAs....78
Inhibition of MAPK....78
Results....79
Epithelialization....79
S. aureus Biofilms Induce
Changes in Keratinocyte Morphology....79
S. aureus Biofilms Induce Apoptosis in Human Keratinocytes....84
Increase of Intracellular Calcium
Levels in BCM Stimulated Keratinocytes....87
Inflammation....89
S. aureus Biofilm Upregulates Genes
Associated with Inflammation in Human Keratinocytes....89
S. aureus BCM and PCM Induce Differential Temporal
Cytokine and Chemokine Production in Human Keratinocytes....92
S. aureus BCM and PCM Differentially Modulate MAPK
Phosphorylation in Human Keratinocytes....96
XME Genes Upregulated in Human
Keratinocytes Exposed to Bacterial Secreted Products....100
Discussion....102
Inflammation....102
Transcriptional Analysis of Human
Keratinocytes Exposed to BCM....103
Cytokine Production in BCM Treated Keratinocytes....104
MAPK Signaling....105
Xenobiotic Metabolizing Enzymes are
Induced by BCM in Human Keratinocytes....107
Epithelialization....111
Morphologic Changes
and Apoptosis Induced by BCM....112
A Model of the Effects of Bacteria on Wound Healing....114

6. CONCLUSIONS AND SUMMARY OF RESULTS....117

APPENDICES....119

TABLE OF CONTENTS– CONTINUED

APPENDIX A: MS2 Data for Aureusimine A.....120
APPENDIX B: MS2 Data for Aureusimine B.....125
APPENDIX C: BCM/PCM Microarray Data.....130
APPENDIX D: Co-Culture Microarray Data 140
APPENDIX E: Fibroblast Morphology and Apoptosis.....154
APPENDIX F: The Small GTPase GEM and Cell Morphology.....156
Introduction.....157
Materials and Methods.....158
Microarray.....158
RT-qPCR 158
GEM Immunostaining.....158
Protein Kinase C Detection.....158
shRNA Interference.....158
Results and Discussion.....159
APPENDIX G: Peroxisome and Lysosome Depletion in Keratinocytes Treated with BCM 164
APPENDIX H: Unknown Cell Types Present in HFK Culture Resistant to Ill Effects of BCM.....166

REFERENCES CITED.....172

LIST OF TABLES

Table Page

1. Bacterial Genera Identified by Culture Data as Related to DGGE Banding Patterns of Chronic Wound Debridement Samples.....29

2. Bacteria Identified by Traditional Culturing Techniques From Debridement Samples from 37 Chronic Wounds.....30

3. BLAST Results from Sequenced 16S rDNA Sequences from 31 Debridement Samples.....31

4. Results from DGGE Band Excision and Sequencing.....33

5. Bacteria Cultured During Standard Care from the Three Wound Groups.....34

6. Aureusimine A and B Production in Different Bacterial Strains.....60

7. Pro-Inflammatory Genes Upregulated in BCM Treated HFKs.....90

8. Inflammatory Genes Significantly Regulated in HFKs in the *S. aureus* Biofilm Co-Culture Model After 24 hours of Co-culture.....91

9. Transcription Factors Induced in PCM and BCM Treated Keratinocytes after Four Hours.....92

10. DUSP Genes Activated in HFKs by BCM after Four Hours of Contact.....96

11. Genes with Xenobiotic Metabolic Activity are Upregulated in Keratinocytes Exposed to *S. aureus* Biofilm.....100

12. Genes Involved in the Aryl Hydrocarbon Receptor Pathway are Regulated by *S. aureus* Biofilm Secreted Factors in Human Keratinocytes.....100

13. Functional Enrichment Using the DAVID Functional Analysis Tool Revealed Several Genes Related to Oxidative Stress and DNA Damage in Response to BCM.....102

LIST OF FIGURES

Figure Page

1. The Three Main Phases of Wound Healing.....7

2. Generalized Scheme of MAPK Signaling.....18

3. Image of a Typical DGGE Gel Showing Results from 13 Chronic Wound Specimens.....29

4. DGGE Profiles for Diabetic Foot Ulcers, Venous Leg Ulcers, and Pressure Ulcers.....32

5. Image of the *in vitro* Biofilm Disease Model.....46

6. Population Density Curves for *S. aureus* Biofilm and Planktonic Cultures Over a Four Day Period.....47

7. 1D SDS-PAGE and Total Protein Concentrations in BCM, PCM, and EPI.....48

8. Extracellular DNA in BCM and PCM.....49

9. NMR Raw Spectrum BCM.....50

10. Hierarchical Clustering of Metabolite Concentrations in BCM, PCM, and EPI as Revealed by Nuclear Magnetic Resonance.....51

11. Hierarchical Clustering of Excreted Metabolites from Human Keratinocytes Exposed to BCM, PCM, or EPI.....53

12. Growth Curves for *S. aureus* Under Open, Aerobic, Sealed Aerobic, and Anoxic Conditions.....54

13. pH Values for BCM and PCM Produced Under Differing Oxygen Tensions.....55

14. Hierarchical Clustering of Metabolite Concentrations in Planktonic Cultures of *S. aureus* Under Differing Oxygen Tensions.....56

LIST OF FIGUES – CONTINUED

Figure Page

15. High Performance Liquid Chromatography
Mass Spectrometry Analysis of BCM, PCM, and EPI.....57

16. Chemical Structures of Aureusimine A and B.....58

17. Extracted Ion Chromatogram and UV absorbance for m/z 245 and m/z 229.....59

18. Production of Aureusimine A and B under
Various Oxygen Tensions in Planktonic *S. aureus* Cultures.....62

19. Production of Aureusimine A and B
Under Various Oxygen Tensions at Similar Phases of Planktonic Growth.....63

20. Time Lapse Microscopy of HFKs in Contact with BCM.....80

21. F-Actin and β-Tubulin Structures in
BCM and PCM Treated HaCaT Keratinocytes.....82

22. Prevention of BCM Induced Morphology by Taxol.....83

23. Nuclear Morphologies in
HFKs Treated with BCM or PCM.....84

24. Percentage of HFKs Staining Positive for TUNEL.....85

25. Cell Counts and Percentage of HaCaT
Keratinocytes Staining Positive for TUNEL.....86

26. Intracellular Calcium Levels in BCM and PCM Treated
HFKs Correlate with BCM Induced Morphology Changes.....87

27. Intracellular Calcium Levels in
BCM and PCM Treated HaCaT Keratinocytes.....88

28. Cytokine and Chemokine Production in Keratinocytes
after 24 Hours of Exposure to BCM or PCM.....93

LIST OF FIGUES – CONTINUED

Figure Page

29. Cytokine and Chemokine Production in Keratinocytes After 24 Hours of Exposure to BCM or PCM, Normalized to pg/100,000 Non-Apoptotic Cells.....95

30. Mitogen Activated Protein Kinase Phosphorylation in HaCaT Keratinocytes Exposed to PCM or BCM.....97

31. Mitogen Activated Protein Kinase Inhibition and Cytokine Production in HaCaT Keratinocytes.....98

32. Mitogen Activated Protein Kinase Inhibition and Impacts on HaCaT Morphology.....99

33. CYP1A1 and CYP1B1 Expression in HFKs Exposed to *S. aureus* Biofilm.....101

34. Illustration of the aryl hydrocarbon receptor (AhR) pathway.....109

35. Overview of the Potential Mechanisms of Pathogenesis Induced by Secreted Factors from either *S. aureus* Biofilm or Planktonic Cultures.....115

Appdx 1. Morphology of Primary Human Fibroblasts Exposed to BCM.....155

Appdx 2. Apoptosis Induced by BCM in Human Foreskin Fibroblasts.....155

Appdx 3. Genes Upregulated by BCM Relating to Cell Morphology.....159

Appdx 4. Expression of GEM Over 24 Hours of Exposure to BCM.....160

Appdx 5. GEM Immunostaining.....161

Appdx 6. Over Expression of GEM and Impacts on Cell Morphology.....161

Appdx 7. Protein Kinase C Staining of BCM treated HFKs.....162

Appdx 8. shRNA Knockdown of GEM and Cell Morphology.....163

Appdx 9. Peroxisome Depletion in BCM Treated HFKs.....165

LIST OF FIGUES – CONTINUED

Figure Page

Appdx 10. Lysosome Depletion in BCM Treated HFKs.....165

Appdx 11. Unknown Cell Type Resistant to BCM Induced Apoptosis.....167

Appdx 12. Unknown Cell Type Morphologies.....168

Appdx 13. Protein Kinase C Not Induced in Unknown Cell Types.....169

Appdx 14. Re-population of Culture Wells by
Unknown Cell Types after Exposure to BCM.....170

ABSTRACT

Chronic wounds are characterized by prolonged inflammation and failure to epithelialize and do not respond well to conventional treatment. Bacterial biofilms are a major impediment to wound healing. The effective treatment of chronic wounds requires a better understanding of the relationship between bacterial biofilms and human skin. Human keratinocytes are the most abundant cell type in the epidermis and play essential roles in the inflammatory and epithelialization phases of wound repair. The aim of this dissertation was to determine the effect of biofilm-conditioned medium (BCM) and planktonic-conditioned medium (PCM) on inflammatory and epithelialization processes in keratinocytes. The phylogeny of chronic wounds was characterized to select a model pathogen. *Staphylococcus aureus* was found to be prevalent in chronic wounds. A novel *in vitro* model was developed to facilitate host-pathogen investigations between *S. aureus* biofilms and human keratinocytes. *S. aureus* BCM contained fermentation products and metabolites that regulate virulence. After four hours of exposure to BCM, pro-inflammatory genes were upregulated in keratinocytes relative to PCM. ELISA analysis of cytokine production in BCM-treated keratinocytes confirmed that after four hours of exposure, cytokine levels were higher relative to PCM-treated keratinocytes. However after 24 hours of exposure, BCM stalled the production of cytokines, suppressed activation of the mitogen activated protein kinases JNK and p38, and induced the release of intracellular calcium in keratinocytes. Processes relating to epithelialization such as the disruption of cytoskeletal components and induction of apoptosis were induced by BCM in keratinocytes. BCM induced a distinct inflammatory response and inhibited processes related to epithelialization. Collectively, the results provide insight into the formation and persistence of chronic wounds. The use of biofilm-based models of disease such as the *in vitro* model described herein will aid in the development of new biofilm based treatment strategies, not only for chronic wound infections, but all biofilm-based disease.

CHAPTER 1

INTRODUCTION

Context

Bacterial biofilms are prevalent in nature and harbor unique properties relative to their planktonic counterparts. Biofilms are associated with increased resistance to antibiotics, radiation, osmotic shock, starvation, attack from other bacteria and fungi, and immune responses in infectious environments. Bacterial biofilms are increasingly accepted as a major barrier to healing in chronic wounds and several other diseases (i.e. pneumonia associated with cystic fibrosis and periodontal disease). Despite this, the bulk of the literature pertaining to *in vitro* models of bacterial infection focus primarily on the planktonic characteristics of bacteria. Models used to define the response of mammalian cell cultures to planktonic bacteria do not accurately reflect the nature of bacteria in a biofilm. Effective treatment of chronic wounds requires an understanding of the interactions between bacterial biofilms and host cells. The impacts of bacterial biofilms on the inflammatory and epithelialization phases of wound healing have not been well established in human skin. The impact of bacterial biofilms on wound healing processes in host cells could have implications for the pathogenesis of disease and the persistency of chronic infections.

Objectives

The overarching question addressed in this dissertation was as follows: Does biofilm-conditioned medium (BCM) impact wound-healing processes including inflammation and epithelialization in human skin?

The first objective was to select a model host and pathogen for use in an *in vitro* model of biofilm disease. Human keratinocytes were selected as a model host since they are involved in the inflammatory and epithelialization phases of wound-healing. Phylogenetic characterization of chronic wound micro-communities was used to identify bacterial species which were prevalent in chronic wounds. Both culture and molecular-based methodologies were employed in the investigation of microbial communities present in chronic wounds. The results revealed that *Staphylococcus aureus* was prevalent in these infections and was therefore selected as a model pathogen.

The second objective was to characterize *S. aureus* BCM. Conditioned medium from *S. aureus* biofilm and planktonic cultures was analyzed using metabolite profiling. *S. aureus* biofilms grown in ambient oxygen concentrations produced mixed-acid fermentation products indicating the presence of an anoxic niche within the biofilm. *S. aureus* biofilm also produced the virulence factors aureusimine A and B in greater quantities than planktonic cultures.

The final objective was to investigate the impact of *S. aureus* BCM on inflammation and epithelialization in human keratinocytes. *S. aureus* BCM induced sustained low-level inflammation, perhaps contributing to the persistent nature of biofilm-infected wounds. *S. aureus* BCM induced cytoskeletal rearrangements and

apoptosis in keratinocytes. The morphological changes in addition to the induction of apoptosis would likely inhibit wound epithelialization and lead to the advancement of the wound front. The *in vitro* biofilm model could be expanded to include different pathogens and mammalian cells to study other biofilm-based disease. Knowledge of biofilm pathogenesis could lead to new therapeutic and preventative strategies for biofilm-based diseases such as chronic wounds.

CHAPTER 2

BACKGROUND

Literature Reviewed

Biology and Immunology of Acute Wound Healing

An acute wound includes wounds such as burns, traumatic injuries, and surgically created wounds that heal in a timely fashion. The process of wound healing is an overlapping progression of events were certain factors are released in a predictable manner, triggering the three main phases of wound repair: inflammation, epithelialization (formation of neo-epidermis and granulation tissue), and tissue remodeling. For excellent reviews on wound healing, see [1, 2]. The three phases of wound healing are dynamic processes involving the secretion of soluble mediators by several cell types, degradation and formation of the extracellular matrix, and expansion of appropriate cell types, and loosely follows a temporal organization scheme.

When tissue is injured, blood vessels are disrupted leading to the extravasation of blood constituents. The resulting coagulation of blood constituents and the aggregation of platelets lead to the formation of a fibrin rich clot and swift initiation of the inflammatory phase of wound repair. Keratinocytes are important mediators of this initial inflammatory response since they are often the first cell type to experience injury and encounter microorganisms. The fibrin rich clot serves multiple purposes including: plugging severed blood vessels, filling any discontinuity in the wounded area, and providing a provisional matrix for cell migration [2]. Factors released by damaged tissue

and platelets in the clot recruit inflammatory leukocytes to the site of injury [3]. Infiltrating neutrophils and monocytes remove foreign particles and invading microorganisms from the damaged area and secrete important factors required for the progression of the wound repair process. If the wounded area is not substantially contaminated, the infiltrating neutrophil population becomes senescent after a few days and are destroyed by tissue macrophages [4]. If there are a substantial number of microorganisms present in the wound, a stronger inflammatory response is mounted resulting in the infiltration of many more neutrophils and other immune cells. If the body's immune system is overrun by an aggressive acute bacterial infection that reaches the circulatory system, septic shock and death are likely within hours. In a low bioburden wound, even after the resolution of invading neutrophils, monocytes continue to accumulate in the wounded tissue. Once in the affected area, infiltrating monocytes adhere to the extracellular matrix which induces them to differentiate into inflammatory or reparative macrophages [5]. Inflammatory and reparative macrophages function to debride damaged tissue, clear any remaining or newly contaminating pathogens, and digest apoptotic neutrophils [6]. The accumulation of macrophages in damaged tissue signals a transition from the inflammatory phase, (which lasts roughly 48 hours), to the tissue formation, or epithelialization, phase of wound repair.

The process of reestablishing a cutaneous cover begins within 2-10 days after injury, depending upon the severity of the wound. This stage of wound repair is characterized by the proliferation and migration of several cell types in the wounded area. The migration of keratinocytes into the wound bed is one of the first processes in this

stage. Migrating keratinocytes are basal in nature as they do not contain keratin or other matrix proteins. In contrast to basal keratinocytes, migrating keratinocytes express the integrins fibronectin and vitronectin, and collagen receptors which enable the migrating keratinocyte to crawl over the wound matrix and underlying dermis [1]. The formation of granulation tissue is a key process during this phase of wound healing. The formation of new vasculature in the wounded area through a process known as angiogenesis is essential in maintaining granulation tissue. Mature granulation tissue derives its name from the appearance of numerous newly formed capillaries in the new tissue. Fibroblasts contribute to the formation of granulation tissue when they are stimulated to proliferate and migrate into the wound and replace the fibrin rich clot with a collagen rich matrix [7]. Granulation tissue primarily consists of macrophages, fibroblasts, and connective tissue and provides new substrate for migrating keratinocytes [8]. Keratinocytes at the leading edge of migrating epithelium produce increased levels of various members of the matrix metalloproteinase (MMP) family which act to cleave the basal lamina, allowing keratinocytes to detach from the basal lamina and migrate [9]. After a monolayer of keratinocytes has been established over the wound surface, the formation of a new stratified epidermis is reestablished from the margins of the wound inward [10].

The third phase of wound repair, tissue remodeling, occurs in concert with tissue formation. The remodeling of the extracellular matrix, cell maturation, and apoptosis are involved in this phase of wound repair. Remodeling of the extracellular matrix and the maturation of newly formed epidermal tissue has been shown to occur at the same time granulation tissue is still invading the wound space in wounds larger than a small scratch

[11]. After the wounded area is covered with neoepidermis, fibroblasts differentiate into myofibroblasts and act to contract the wound [12]. Roughly 2-3 weeks after wounding, endothelial cells, fibroblasts, and macrophages remaining in the granulation tissue undergo apoptosis or exit the wound leaving predominantly acellular, collagen rich scar tissue. The collagen rich matrix undergoes remodeling over several months as type III collagen is replaced by type I collagen strengthening the scar tissue [13]. An overview of the major processes that occur and cell types involved in the three phases of wound healing is provided in Figure 1.

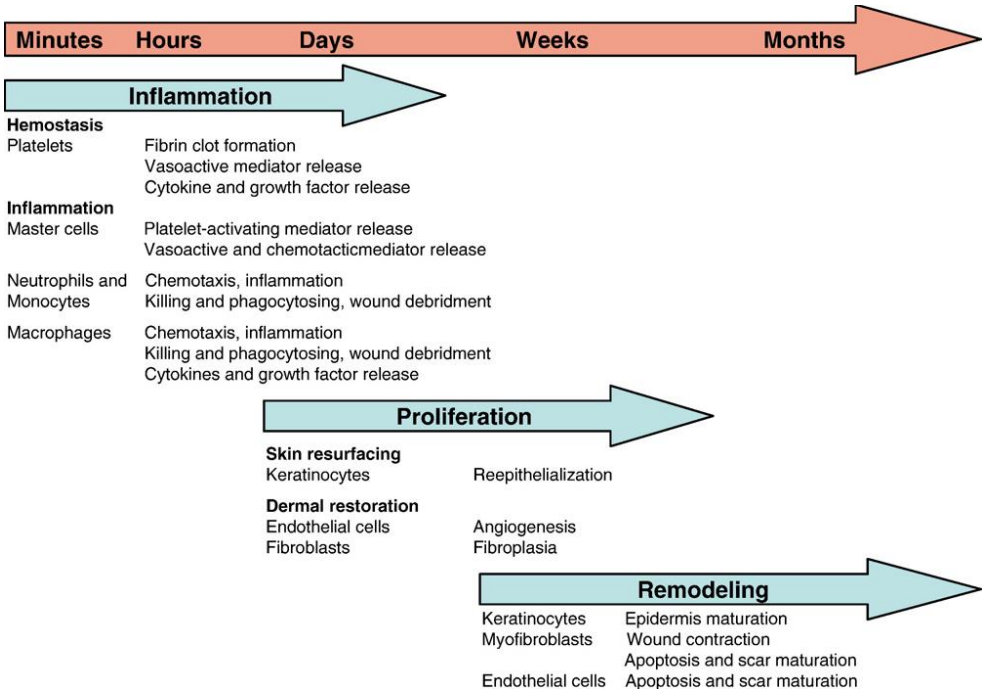

Figure 1. The overlapping progression of the three main phases of wound healing. Major events are shown along with the cell types mediating those events. Image adapted from Li, *et al* [14].

Inhibition of Healing in Chronic Wounds

There are three main types of chronic wounds: diabetic foot ulcers, venous leg ulcers, and pressure ulcers (DFUs, PFUs, and PUs). Underlying medical conditions (diabetes, pulmonary disease, etc.) and the location of the wound characterize which of

the three categories a non-healing wound falls into. Disruption of any of the phases involved in wound healing may lead to any of the three types of chronic wounds [14]. Bacterial contamination of damaged skin is unavoidable under normal circumstances. Microorganisms and foreign objects are destroyed in the inflammatory phase of acute wound healing and the progression of the healing process continues. However, wounds exposed to constant, abnormally high loads of bacteria, or people with compromised immune systems or underlying diseases that predispose them to bacterial infection or chronic inflammation, are susceptible to altered phases of wound healing. Acute wounds go through the three overlapping phases of healing in an orderly fashion while chronic wounds do not progress in an orderly process.

Some areas of chronic wounds are found in different phases of wound healing which leads to the loss of the necessary synchrony of events that lead to normal healing [15]. Chronic wounds have been described as being predominantly stuck in the inflammatory phase of wound healing. The production of several cytokines in chronically inflamed tissues recruit activated immune and inflammatory cells to the site of infection, were they amplify and perpetuate the inflammatory state. Conditions that lead to the failure of the wound healing process to exit the inflammatory phase include a layer of necrotic tissue encapsulating the wound, heavy bacterial burden, and/or high levels of foreign material that is resistant to phagocytosis or solublization during an acute inflammatory response [14].

If planktonic bacteria attach to an exposed surface like a traumatic wound and are not cleared immediately by the host immune system, they can form a microcolony which

then progresses to a biofilm. Early microcolonies evade opsonization as host antibodies do not recognize them [16]. Neutrophils and polymorphonuclear leukocytes nestle themselves into the biofilms extracellular matrix and become ineffective at killing bacteria in the biofilm [17-21].

Elevated neutrophil levels are observed in chronic wound infections leading to pathologic inflammation [22, 23]. Normal acute wound healing is characterized by a rapid influx of neutrophils followed by monocytes that mature into inflammatory macrophages, both components of the innate immune response. Resolution of inflammation can only occur if the neutrophils are eliminated from the affected area. Many inflammatory cytokines present in chronic wounds are capable of prolonging neutrophil survival by inhibiting spontaneous neutrophil apoptosis [24, 25].

High levels of proteolytic activity have been observed in chronic wound fluid. Inappropriate protease production (MMPs) may contribute to the inability of some chronic wounds to heal through the ill timed degradation of molecules in the extracellular matrix [26-28]. MMPs also regulate the release, activation, and silencing of growth factors, modify cell surface receptors, and regulate apoptosis and inflammation [29].

Chronic wounds contain keratinocytes with altered phenotypes [30]. Keratinocytes on the edge of chronic wounds do not migrate properly leading to the failure of the second phase of wound healing [31, 32]. The failure of keratinocytes to migrate properly at the wounds edge may lead to apoptosis in response to inappropriate matrix contact [33].

Bacterial Biofilm and Biofilm Infection of Chronic Wounds

The prolonged inflammation and failure of the epithelialization process in addition to a heavy microbial burden are common characteristics of chronic wounds. Microbial infection has been implicated in disrupting wound healing processes and microbes have been studied in the laboratory since they were described as the causative agents of infectious disease. Historically, bacteria grown suspended in liquid medium in the laboratory have been assumed to have similar properties to bacteria that cause infectious disease such as wound infections. Research over the past two decades has revealed that, in many environments, bacteria exist as a complex, multi-species surface associated community termed biofilm. Bacteria within these communities secrete an extracellular polymer matrix, form complex structures, and are phenotypically distinct from their planktonic counterparts [34, 35]. Bacteria within biofilm communities are orders of magnitude more resistant to antibiotics and biocides than planktonic bacteria [36]. Additionally, it has been documented that bacterial genes involved in biofilm formation are controlled by regulatory systems that also control the expression of virulence factors [37, 38].

It has been speculated for many years that bacteria colonizing chronic wounds exist as biofilm. The wound bed offers an ideal environment for bacteria to form a biofilm due to their susceptibility to contamination, the availability of nutrients, and an ideal surface for attachment. Chronic wound infections are persistent and are not cleared by the host's immune system and are resistance to traditional treatment strategies including systemic and topical antimicrobial agents [39]. Removal of the biofilm by

frequent debridement is one of the most clinically effective treatments to help heal chronic wounds [40]. James, *et al* recently showed that biofilms were prevalent in chronic wounds and rare in acute wounds, but the role biofilms play in preventing wound healing and mechanisms involved have yet to be determined [41].

Healthy human skin is colonized by large numbers of microorganisms classified as either the resident or transient microflora. The resident skin microflora includes coagulase-negative staphylococci (e.g., *Staphylococcus epidermidis, Staphylococcus hemolyticus, Staphylococcus hominis*) which are found in proportionally constant numbers in healthy human skin [42]. Organisms constituting the transient skin microflora temporarily colonize the surface of the skin due to contact with external sources and disrupt the homeostasis of the resident microflora. The prevalence of *S. aureus* skin colonization in the healthy human population is approximately 32% and is not considered a member of the resident skin microflora [43]. *S. aureus* infection of the skin initiates or induces persistence of many inflammatory skin disorders including atopic dermatitis and other chronic infections.

S. aureus is known to produce a wide range of virulence factors including hemotoxins, pore forming toxins, peptidoglycan (PG), lipoteichoic acid (LTA), and superantigens (e.g. toxic shock syndrome toxin-1, *Staphylococcal* enterotoxin). The impact of biofilm formation on virulence is controversial. Virulence factor gene expression in *S. aureus* cells within a biofilm have been shown to be downregulated when compared to planktonic *S. aureus* cultures [35]. Another study showed that biofilm formation had no effect on *S. aureus* virulence factor production [44], while several

studies highlight the necessity of regulatory elements associated with biofilm formation on the regulation of virulence [45, 46]. The role of biofilms in various infectious skin diseases is an area of active research leading to new insights in host/pathogen relationships.

Few studies have investigated the effects of bacterial biofilms on mammalian cells and those that have focus primarily on the well established biofilm infection associated with periodontal disease [47, 48]. Most studies investigating interactions between bacteria and cultured mammalian cells involve either direct contact with washed planktonic bacteria or the application of known or unknown soluble products from overnight cultures grown with constant agitation [49-55]. *S. aureus* was selected as a model organism for this research because it is an important human pathogen implicated in several infectious diseases including chronic skin infections [56-58].

Epidermal Keratinocytes and Their Functions in Immunity

Keratinocytes are by far the most abundant cell type in the epidermis. The view of the role keratinocytes play in cutaneous infection has changed drastically in the past two decades from a passive target of infection, to an active participant in the immune response to bacterial infection. A primary function of the epidermis is to act as a barrier to the environment and infectious organisms. The predominant mechanism in which keratinocytes function in innate immunity is through the recognition of conserved pathogen associated molecular patterns (PAMPs) which include bacterial cell wall components, bacterial DNA, flagella, PG, LTA, and other conserved prokaryotic structures [59]. PAMPs are recognized by cell surface receptors called toll like receptors

(TLRs) which are found on a variety of cell types including professional immune cells, endothelial cells, and cells of the epidermis. Human keratinocytes are constantly exposed to bacterial stimuli and express functional TLRs making them the first line of defense against pathogens in the skin [60]. In response to PAMPs, the keratinocyte is capable of producing immunomodulatory molecules including lipid-derived mediators of inflammation and protein cytokines [61]. Activation of TLR signaling by PAMPs ultimately results in the production of various cytokines which mediate various aspects of an inflammatory response (see cytokine biology section below) [59, 62].

Keratinocytes also express major histocompatibility complex (MHC) class II molecules in response to various pro-inflammatory and immune stimulation signals and thus play a role in adaptive immunity [63]. Activated keratinocytes expressing MHC II molecules produce increased amounts of cytokines in response to various *Staphylococci* superantigens [64]. Cytokine production by epidermal keratinocytes is initiated by various external signals which activate various intracellular pathways and is an important initial step in a normal immune response and in pathogenesis.

Cytokine Biology

Cytokines encompass a large and diverse family of small secreted proteins which mediate and regulate immunity and inflammation. Interleukins (IL) and chemokines are part of this family. Cytokines are capable of inducing their biological effects at very low concentrations (pg/ml to ng/ml) and act by binding specific cell surface receptors. Activation of cell surface receptors in turn activate second messengers which regulate

gene expression and cellular functions. Some cytokines act as primary cytokines, a cytokine that stimulates target cells to produce additional cytokines.

Tumor necrosis factor alpha (TNF-α) is a primary cytokine capable of inducing apoptosis in many cell types including keratinocytes [65], but this effect is often negated by the simultaneous induction of other pro-survival pathways activated in response to inflammation [66, 67]. TNF-α production by keratinocytes leads to the expression of adhesion molecules in endothelial cells and chemokine production in various epidermal and dermal cell types [68]. These changes lead to the attachment, diapedesis, and chemotaxis of immune cells into the affected area. The presence of additional inflammatory cells leads to the secretion of additional cytokines forming a positive feedback loop resulting in further TNF-α production and modulation of production of other cytokines [69].

Interleukin-1β (IL-1β) is a multifunctional primary cytokine that plays a role in both acute and chronic inflammation and is produced primarily by monocytes, macrophages, and polymorphonuclear phagocytes [70]. Other cell types known to produce IL-1β include fibroblasts, B cells, osteocytes, epithelial cells, and keratinocytes [71]. IL-1β affects nearly all cell types in the human body [72]. IL-1β is also known to affect the production of inflammatory molecules such as prostaglandins, leukotrienes, and cytokines and affects diverse innate immune processes [73]. IL-1β functions in a variety of activities such as immune cell recruitment, cell proliferation, tissue destruction, bone resorption, vascular smooth muscle cell contraction, blood pressure, and central nervous cell functions [74]. With such diverse roles, IL-1β has been described as a master or key

cytokine in many chronic diseases ranging from Alzheimer's disease [75], rheumatoid arthritis [76], periodontitis [77], and diabetes [78].

IL-6 was initially discovered through studies looking into mechanisms of B-cell terminal differentiation [79]. It was quickly realized that IL-6 possessed several additional biological activities beyond the activation of B-cells. IL-6 is capable of stimulating hepatocytes during inflammatory responses leading to systemic changes in acute phase serum protein compositions [80]. IL-6 is produced by T-cells, macrophages, fibroblasts, synovial cells, endothelial cells, glia cells, and keratinocytes in response to a variety of stimuli including cytokines such as TNF-α and IL-1β, and bacterial products [81]. IL-6 is overproduced in a variety of autoimmune and chronic inflammatory diseases such as rheumatoid arthritis, cardiac myxoma, psoriasis, and chronic inflammatory proliferative diseases [82].

CXC ligand-8 (CXCL-8, also known as IL-8) and other CXCL family members are potent chemo-attractants for neutrophils and are thus members of the chemokine family (CXC refers to the conserved cysteine “X” cysteine motif in this family were “X” represents any amino acid). Neutrophil infiltration is a hallmark of acute inflammation [83] while the inappropriate accumulation of neutrophils in inflamed tissue is a hallmark of chronic inflammation [22, 23]. CXCL family members preferentially bind the receptor CXCR2 (IL-8Rβ). Ligand binding and activation of CXCR2 in neutrophils has been shown to inhibit spontaneous neutrophil apoptosis leading to their accumulation in inflamed tissues [25]. Several cell types produce CXCL-8 including monocytes, T-cells, neutrophils, vascular endothelial cells, dermal fibroblasts, hepatocytes, human gastric

cancer cells, and keratinocytes [83]. During normal healing processes in healthy wounded tissue, CXCL-8 and other CXCL family members recruit neutrophils to a wounded area were angiogenesis is stimulated concomitantly with neutrophil recruitment resulting in the formation of granulation tissue [84].

Granulocyte/Macrophage-Colony Stimulating Factor (GM-CSF) is a major regulator of granulocyte and macrophage lineages at all levels of maturation. GM-CSF was first discovered in the lungs of mice treated with lipopolysacharide (LPS) highlighting a role for GM-CSF as a modulator of inflammatory responses to bacterial products [85]. GM-CSF can prime several cell types for increased cytokine production, particularly IL-1β and TNF-α [86]. GM-CSF activates and augments the functions of neutrophils, monocytes or macrophages, and dendritic cells leading to enhanced host defenses to a broad spectrum of pathogens [87]. GM-CSF has also been shown to play important roles in wound healing. Injection of GM-CSF into human skin induces regenerative differentiation of the epidermis and proliferation of keratinocytes [88]. Since GM-CSF is a keratinocyte mitogen and is produced by immune cells, fibroblasts, and keratinocytes themselves, GM-CSF has been recognized as an important autocrine and paracrine regulator of epidermal regeneration [89].

Signal Transduction in Activated Keratinocytes

Activated keratinocytes are keratinocytes that have been stimulated by bacteria and/or other environmental stresses present in wounded epithelium. Activated keratinocytes undergo a transformation from a cell destined for terminal differentiation to a migratory phenotype. This transformation requires the re-organization of the actin and

tubulin cytoskeleton to produce lamellipodia and filopodia. Activated keratinocytes also secrete inflammatory mediators such as cytokines initiating the inflammatory phase of wound repair while gearing up for the epithelialization phase.

Mitogen Activated Protein Kinases. Keratinocytes express functional TLRs which function in immunity by recognizing PAMPs. TLRs are prominent in the activation of mitogen activated protein kinase (MAPK) cascades [90]. MAPKs are a family of serine/threonine protein kinases found in all eukaryotic organisms which participate in signal transduction pathways with diverse physiological outcomes. All MAPKs include a central signaling theme which involves the activation of three tiers of core molecules: MAPK kinase kinases (MAPKKK), MAPK kinases (MAPKK), and MAPKs (Figure 2). MAPK cascades are activated by concurrent phosphorylation of tyrosine and threonine residues in the conserved activation loop of the kinase domain [91]. Deactivation of MAPK signaling is mediated primarily through dephosphorylation by dual specificity protein phosphatases (DUSPs) [92]. In mammals, MAPK cascades can be activated by a wide range of stimuli involving diverse receptor families. These receptor families include hormone and growth factor receptors acting through receptor tyrosine kinases (e.g. epidermal growth factor receptor), cytokine receptors acting through G protein-coupled seven-transmembrane receptors, and inflammatory cytokines of the TNF family [93].

MAPKs are intimately involved with fundamental biological processes such as embryonic development, innate and acquired immunity, cell differentiation, cell proliferation, and cell death [94]. MAPKs are major components of pathways regulating

the pathology of chronic inflammation [93] and mediate cellular responses essential to wound healing. MAPKs transduce signals relating to apoptosis [95-97], cytoskeletal rearrangements essential to the migration of keratinocytes [98, 99], keratinocyte differentiation [100], secretion of antimicrobial peptides [101], and responses to mechanical and osmotic stress [102, 103].

The stress-activated protein kinase/c-JUN NH_2-terminal kinase (JNK) and p38 MAPK are the major MAPK pathways activated by inflammatory cytokines and environmental stress [104]. The extracellular signal-regulated kinase 1 and 2 (ERK) MAPKs play roles in activities such as cell migration and mitosis and are also recruited in response to stress and inflammation [94].

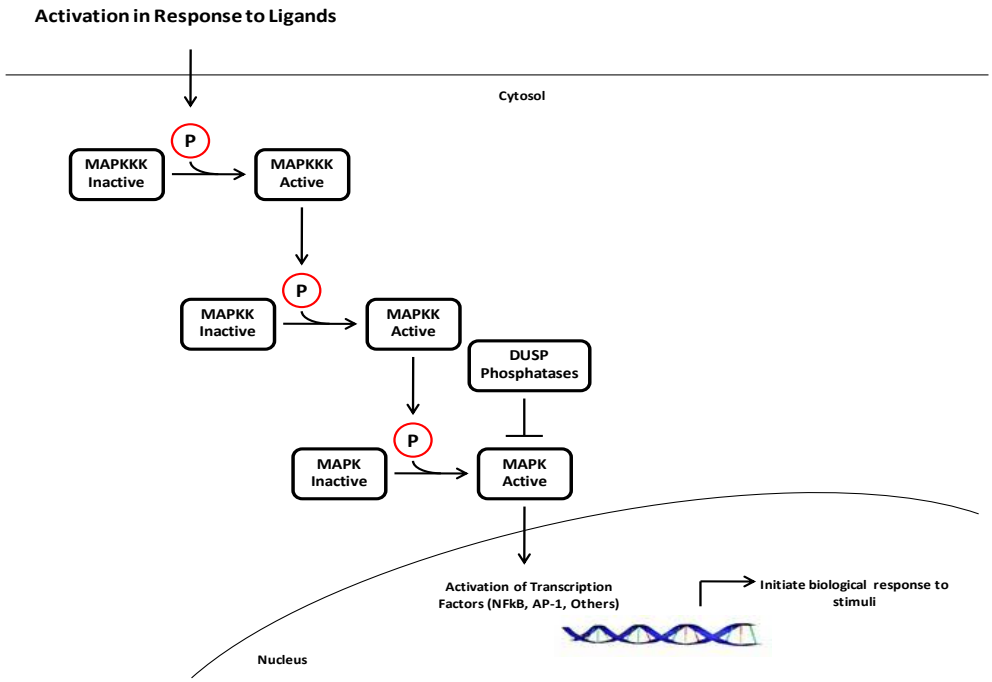

Figure 2. Generalized scheme of MAPK signaling. Diverse inputs such as cytokines, growth factors, and environmental stress lead to the activation of MAPK signaling. An extracellular stimulus leads to the phosphorylation of MAPKKKs which in turn phosphorylated MAPKKs, which activate MAPK proteins. Activated MAPKs regulate the activity of transcription factors resulting in a specific biological response to extracellular stimuli. Dual specificity protein phosphatases (DUSPs) de-activate MAPK signaling by dephosphorylating activated MAPKs. Activation of specific MAPKs (JNK, p38, and ERK) is described in the text.

JNK was first identified after exposing cells to stressful treatments such as exposure to ionization, osmotic shock, heat shock, mechanical shear, and protein synthesis inhibitors [105-107]. JNK has been shown to be activated by the inflammatory cytokines TNF-α and IL-1β which leads to the activation of the transcription factor c-JUN which activates genes associated with apoptosis, proliferation, and inflammation in response to cytokines, growth factors, chemical carcinogens, and bacterial infection (see transcription factor section below) [108, 109].

Evidence for a role of JNK in wound healing is conflicting with one study finding that JNK is not activated during wound healing in corneal epithelial cells [99] while other studies suggest that JNK is essential for normal wound healing to progress [110, 111]. These discrepancies are likely attributed to extracellular stimuli unique to different wound types, bacterial burden, and cell type.

The p38 MAPK is a 38-kDa polypeptide that is activated in response to stress such as endotoxin treatment and osmotic shock [112]. p38 is the target for two classes of anti-inflammatory drugs: pyridinyl-imidazole anti-inflammatory drugs and cytokine-suppressive anti-inflammatory drugs which block p38 dependent activation of AP-1 [113]. The p38 MAPK is activated by inflammatory cytokines and in most cases, the same stimuli that activates JNK also activates p38 [106]. A role in cell proliferation and migration in wound healing has been described for p38 in concert with ERK [99].

ERK1/2 are ~42 kDa MAPKs that are ubiquitously expressed in all tissues and are not considered to be stress related kinases like JNK and p38. ERK has been implicated in wound healing through the action of growth factors and acts to coordinate

the migration of groups of cells [114]. One study found that ERK was inactivated when migrating epithelial sheets meet at closing edges of wounds, but remained active at the open edges [98].

Collectively, JNK and p38 MAPK pathways are important mediators of cellular activities in response to stress, growth arrest, and apoptosis while the ERK cascade is a critical pathway for mitogenesis and differentiation [115-117]. However, ERK is also involved in pro-inflammatory responses [118]. The activation of NFkB and AP-1 is mediated by MAPK signaling and activation of these transcription factors by MAPK is known to lead to the production of TNF-α, IL-1β, IL-6, CXCL-8, CXCL-1, and GM-CSF [50, 119, 120].

Transcription Factors. Transcription factors are regulatory proteins that mediate changes in genes expression in response to extracellular stimuli. Activation of c-JUN by cell surface receptors linked to MAPK cascades is an example. c-JUN is a member of the activator protein-1 (AP-1) family of transcription factors which also includes Fos and activating transcription factor (ATF) family members. The AP-1 transcriptional complex consists of dimers of various combinations of Jun, Fos, and ATF proteins. AP-1 transcription factors are some of the most well studied transcription factors relating to wound healing activities in human keratinocytes [121]. AP-1 transcription factors regulate a variety of extracellular stimuli including apoptosis, proliferation, and inflammation in response to cytokines, growth factors, chemical carcinogens, and bacterial infection [108, 109]. AP-1 family members are regulated at the transcript level and act as early response genes which are rapidly transcribed in response to extracellular

stimuli [122]. Post-transcriptional modification through MAPK dependent phosphorylation of AP-1 transcription factors alters their DNA binding affinity leading to activation of target genes, namely cytokines and chemokines [123].

In addition to AP-1 activation, MAPKs activate the transcription factor Nuclear Factor-Kappa B (NFkB) [124-126]. NFkB regulates the expression of many genes involved in immune and inflammatory responses and often acts in synergy with AP-1 to mediate inflammatory responses [127, 128]. NFkB usually consists as a heterodimer consisting of the p65 (RelA) and p50 subunits [129]. In resting cells NFkB is sequestered in the cytosol by regulatory IkB proteins which prevent NFkB from entering the nucleus and activating target genes [130].

Stimulation of resting cells by cytokines, UV radiation, and bacterial products activates various kinase cascades which include MAPKs, resulting in the phosphorylation of IkB [131-133]. Phosphorylation of IkB causes a transformational change dissociating IkB from NFkB. Liberation of NFkB allows translocation to the nucleus were NFkB binds promoter regions of target genes. NFkB is also negatively by NFkBIA, a gene which encodes the protein IκBα. IκBα enters the nucleus and actively removes NFkB from DNA causing NFkB to be translocated back to the cytoplasm [134]. TNFAIP3 (A20). TNF-α induced protein (TNFAIP3 (A20)) is a transcription factor that also negatively regulates NFkB and protects cells from TNF-α induced apoptosis [135]. TNFAIP3 has been shown to regulate TLR2/4 mediated inflammation through inhibition of the NFκB pathway [136].

In wound healing, NFkB has been shown to be essential for the upregulation of MMPs and inflammatory cytokines required for normal wound healing [137, 138]. NFkB plays a protective role in cells stimulated by an inflammatory environment to produce pro-apoptotic signals by preventing apoptotic programs and stimulating pro-survival pathways [139].

Intracellular Calcium Release. The activation of keratinocytes is accompanied by an increase in intracellular calcium. Changes in cell morphology are initiated for keratinocyte migration which requires the release of internal calcium stores in addition to MAPK signaling cascades [140, 141]. The release of intracellular calcium is also required for cytoskeletal rearrangements that occur when activated keratinocytes return to their terminal differentiation program [142].

Inflammatory responses are also mediated by intracellular calcium. MAPK cascades and AP-1 activation are accompanied by an increase in intracellular calcium [121]. Activated keratinocytes expressing MHC II molecules signal through intracellular calcium dependent mechanisms often involving protein kinases A and C (PKA, PKC) [143, 144]. Release of intracellular calcium stores also occurs when keratinocytes are exposed to *S. aureus* superantigens [145]. Activation of these pathways can result in the production of cytokines and an inflammatory response through tyrosine kinase dependent mechanisms or induce cell death through PKC dependent mechanisms [146].

Physiology of Wounded Human Skin

One of the most influential factors relating to the physiology of both normal and infected skin is pH. The pH of the wound bed is both directly and indirectly associated with all aspects of healing, and inappropriate changes in pH inhibit the body's natural healing processes by interfering with every phase of wound healing. Human keratinocytes have been shown to produce high amounts of lactate both *in vivo* and *in vitro* contributing to the acidic nature of the skin [147]. This is thought to serve as a protective mechanism against invading pathogens. Chronic wounds have an alkaline pH ranging from pH 7.15-8.9, while normal healing wounds have a neutral pH witch acidifies to pH 5.5-6.0 as healing progresses [148]. Additionally, destructive bacterial proteases common in chronic wound infections have optimal catalytic activity in an alkaline environment [149].

Another important factor impacting the physiology of infected skin is the availability of oxygen. Oxygen concentration is an important parameter used to guide treatment of chronic wounds [150]. In wounds, oxygen levels affect the activity of antimicrobials, the oxidative killing of phagocytes, and the viability and population structure of microbes [151]. Chronic wounds are generally viewed as hypoxic and are routinely treated through intermittent hyperbaric oxygenation (HBO) of infected tissue which has proven successful in enhancing wound healing [152, 153]. HBO enhances wound healing by increasing the partial pressure of oxygen in the blood, attenuating keratinocyte apoptosis, and in many cases, reducing inflammation [154].

Bacterial biofilms contain both aerobic and anaerobic niches induced by differing oxygen and nutrient profiles. Anaerobic metabolism due to an anoxic niche in the core of bacterial biofilms has been described for many bacterial species, including *S. aureus* [155-157]. The oxidative state of biofilms has been shown to influence biofilm formation, biofilm persistence, and virulence factor production [158-160]. Wounds contain both anaerobic and facultative aerobic organisms, including *S. aureus* [41, 56]. Facultative anaerobes are capable of both aerobic and anaerobic respiration as well as fermentation.

Consumption of oxygen by host tissues and bacterial biofilms could quickly generate an anoxic environment in chronic wounds. An increase in fermentation products due to anaerobic metabolism in chronic wounds may contribute to the delayed healing and persistence of infection.

CHAPTER 3

PHYLOGENETIC CHARACTERIZATION OF CHRONIC WOUND BIOFILM MICRO-COMMUNITIES

Introduction

Culture based methodologies are routinely utilized by most clinical laboratories for the identification and quantification of microorganisms. Culture based identification of clinical samples biases results towards microorganisms that thrive under the synthetic conditions found in laboratory settings. This leads to the under-representation of important members of micro-communities. Using molecular techniques such as denaturing gradient gel electrophoresis (DGGE) and sequencing of 16S ribosomal genes, the composition of bacterial populations in the three major chronic wound types (DFUs, PFUs, PUs) were characterized. DGGE separates polymerase chain reaction (PCR) generated 16S ribosomal gene fragments (16S rDNA) based on sequence rather than molecular weight. Theoretically, each band present in a DGGE gel represents a single prokaryotic genus found within the wound micro-community. Bacterial community diversity (i.e. number of different genera) can be estimated from the number of bands present in each sample. To aid in the estimation of bacterial diversity in chronic wounds, culture data were collected from chronic wound debridement samples and compared to DGGE banding patterns for each wound analyzed. DNA extracted from pooled patient populations with the same type of chronic ulcer were also analyzed by DGGE, pyrosequencing of 16S rDNA, and full ribosomal shotgun sequencing of 16 S rDNA.

Sequencing of 16S rDNA revealed several bacterial populations prominent in chronic wound infections including: *Staphylococcus, Pseudomonas, Peptoniphilus, Enterobacter, Stenotrophomonas, Finegoldia,* and *Serratia* spp. Strict anaerobic organisms were also identified to varying degrees between the different wound types.

Materials and Methods

DNA Extraction from Debridement Samples

Chronic wound debridement specimens were homogenized and wound DNA was extracted using the Bio101 FastDNA® Spin for Soil Kit (MP BioMedicals, Solon, OH) and a Savant 101 bead beater (Fast Prep, Aurora, OH). Tissue samples with masses of 0.2-0.5 g were placed in the Lysing Matrix Tube as supplied in the kit (i.e., prefilled with beads), which was subsequently filled with sodium phosphate and extraction buffers. The tubes were processed in the bead beater for 45 seconds at a speed of 6.5. Extraction and cleaning of DNA was accomplished following kit protocols with no further changes. Extracted DNA from the specimens was immediately frozen at -70 °C and then placed in dry ice and transported to the Center for Biofilm Engineering.

PCR and DGGE

An assessment of bacterial diversity in chronic wound specimens was performed using the molecular techniques of PCR and DGGE. Primer reactions and DNA amplification were performed using a PTC-100 Programmable Thermal Controller (MJ Research, Waltham, MA) and universal Eubacterial primers, with a reverse primer containing a GC clamp. Specifically, the primers used were 518R (5'GTA TTA CCG

CGG CTG CTG G 3') and 357F (5' CGC CCG CCG CGC CCC GCG CCC GGC CCG CCGC CCC CGC CCC C CTA CGG GAG GCA GCA G 3') or 1070F (5'-ATG GCT GTC GTC AGC T-3') and 1392R (5'-CGC CCG CCG CGC CCC GCG CCC GGC CCG CCG CCC CCG CCC CAC GGG ACG GGC GGT GTG TAC-3') (Integrated DNA Technologies, Coralville, IA). Primer reactions and DNA amplification were performed using the following parameters: 94 °C for 2 minutes, 15 cycles of 94 °C for 45 seconds, 55 °C for 45 seconds, 72 °C for 45 seconds with a final extension step of 72 °C for 7 minutes. Verification of the presence of DNA was assessed in 1.5% agarose gels before analysis by DGGE. Positive controls for PCR were clinical isolates including *Pseudomonas aeruginosa*, *Staphylococcus epidermidis*, and *S. aureus*, and the negative control was sterile water. DGGE was performed on the 16S amplicons described above using the DCode™ DGGE system (Bio-rad). A 40%–70% denaturing gradient was optimal for separation of the approximately 450 bp 16S amplicons, where 7 M urea and 40% formamide is defined as 100%. Gels also contained an 8%–12% acrylamide gradient with a 12% native stacking gel. Different volumes of each sample were loaded for optimal visualization of bands with varying intensities. The gel was run at 60 V for 20 hours and was then stained with SYBR Gold® (Molecular Probes, Invitrogen, Carlsbad, CA) and visualized with a FluorChem™ 8800 fluorescence imager (Alpha Innotech Inc. San Leandro, CA).

Cloning and Sequencing

For bacterial identification, PCR products of approximately 200 bp and DNA from the excised DGGE bands were directly cloned using the TOPO TA Cloning Kit

(Invitrogen Inc., Carlsbad, CA), following the manufacturer's directions. For excised DGGE bands, the maximum amount of DNA (4 µl diffused DNA in TE buffer) was used in each of the cloning reactions following the manufacture's instructions. Plasmid preparation was performed using the Wizard Plus SV Miniprep DNA Purification System (Promega, Madison, WI), following the manufacturers' directions. The plasmid DNA was sequenced by Laragen Inc. Sequence data were analyzed using Basic Local Alignment Search Tool (BLAST) sequence searches (http://www.ncbi.nlm.nih.gov) to identify bacterial genera. Sequences for clones were analyzed in both the forward and reverse direction.

Results

Estimation of Bacterial Diversity by DGGE and Sequencing of 16S rDNA

To estimate the diversity of bacterial populations in chronic wounds, DNA from chronic wound specimens was analyzed by running PCR amplified 16S rDNA on DGGE gels. DGGE analysis of chronic wound debridement samples revealed that on average, DGGE banding patterns contained multiple bands with no two specimens sharing the exact same banding pattern (Figure 3). Information on wound types and culture data associated with Figure 3 are presented in Table 1. Several specimens cultured few or no organisms while analysis by DGGE revealed several bands indicating a more diverse population was present than indicated by culture data.

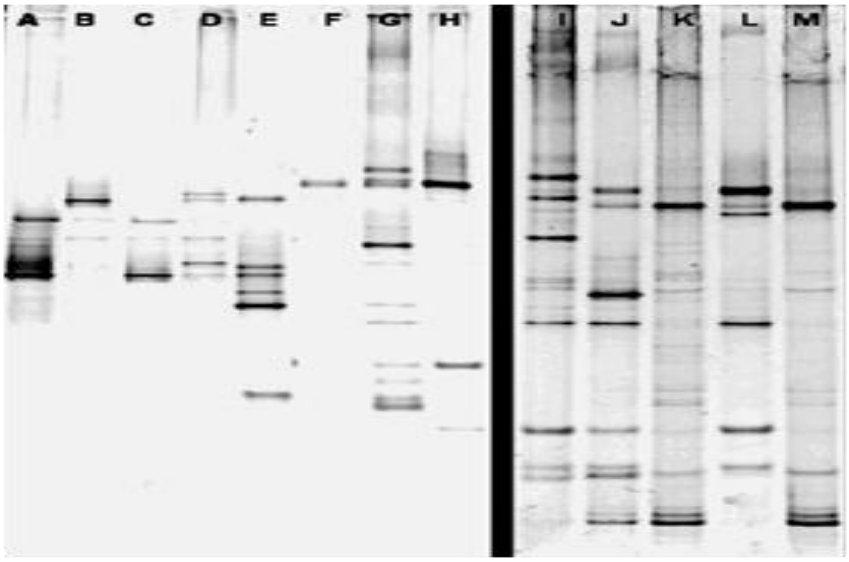

Figure 3. Image of a typical DGGE gel showing results from 13 chronic wound specimens. Most specimens revealed multiple bands and each specimen had a unique banding pattern. Letters correlate with culture data obtained at the clinic shown in table 1.

Table 1. Culture data associated with figure 3. Many wounds cultured few or no bacteria while analysis by DGGE revealed one or more bands indicating an underrepresentation of diversity by traditional culture techniques.

Gel Lane	**Number of distinct bands**	**Wound type**	**Genera/species cultured**
A	2	Non-healing surgical wound	*Enterobacter, Pseudomonas*
B	1	Venous leg ulcer	None
C	2	Calciphylaxis	*Pseudomonas, Staphylococcus*
D	5	Venous leg ulcer	*Escherichia coli, Staphylococcus aureus*
E	6	Diabetic foot ulcer	*Streptococcus* (Group B), *Citrobacter, Staphylococcus*
F	1	Venous leg ulcer	*Pseudomonas, Staphylococcus*
G	11	Chronic wound	*Enterococcus* (Group B), *Escherichia coli, Staphylococcus aureus*
H	3	Venous leg ulcer	*Pseudomonas*
I	8	Diabetic foot ulcer	*Enterococcus* (Group D)
J	9	Diabetic foot ulcer	*Citrobacter freundii, Staphylococcus aureus*
K	7	Decubitus ulcer	*Staphylococcus aureus*
L	6	Diabetic foot ulcer	*Staphylococcus*
M	5	Non-healing surgical wound	*Pseudomonas, Staphylococcus*

Bacterial genera in chronic wound micro-communities were identified by traditional culture techniques and 16S rDNA sequencing. Culture data were collected from 37 debridement samples and 16S rDNA analysis was performed on 31 debridement

samples for a total of 68 specimens. Culture data collected from debridement samples indicated the presence of polymicrobial communities consisting of several well known bacterial genera (Table 2). Identification of individual micro-community members was limited to the genus due to the short 16S PCR sequences required for DGGE. Sequencing of selected bands excised from various DGGE gels and construction of 16S clone libraries from various debridement samples revealed an extremely diverse bacterial community as compared to culture data (Table 3). Several genera of strict anaerobes were identified by 16S rDNA sequencing which were absent from culture data. These data underscore the utility of molecular methods to accurately identify bacteria present in chronic wounds.

Table 2. Bacteria genera identified by traditional culturing techniques from 37 chronic wound debridement samples. Data presented as a percentage of wounds positive for the genera indicated to the total number of wounds analyzed.

Genus	% Present in Chronic Wounds
Staphylococcus	65
Enterococcus	62
Pseudomonas	35
Proteus	24
Citrobacter	24
Enterobacter	24
Streptococcus	22
Escherichia	14
Morganella	8
Klebsiella	5
Acinetobacter	5
Serratia	3
Xanthomonas	3

Table 3. BLAST results from sequenced 16S rDNA sequences from 31 debridement samples revealed a diverse microbial population in chronic wound biofilms. *Pseudomonas* and *Staphylococcus* were the predominant genera identified.

Aerobic/ Facultative Anaerobic Bacteria*	Number of Patients in Which Organism Identified	% Present in Chronic Wounds
Achromobacter spp.	1	3
Acinetobacter spp.	5	16
Uncultured *beta Proteobacterium*	1	3
Burkholeria spp.	1	3
Citrobacter freundii	1	3
Corynebacterium spp.	1	3
Delftia acidovorans	1	3
Edwardsiella ictaluri	1	3
Enterobacter spp.	2	6
Enterococcus faecalis	2	6
Escherichia coli	1	3
Granulicatella adiacens	2	6
Haemophilus spp.	3	10
Klebsiella pneumoniae	1	3
Microbacterium paraoxydans	1	3
Morganella morganii	3	10
Pectobacterium carotovorum	2	6
Proteus mirabillis	2	6
Pseudomonas spp.	20	65
Uncultured *Pseudomoandales spp.*	1	3
Rhodococcus spp.	1	3
Serratia marcescens	1	3
Staphylococcus spp.**	10	32
Streptococcaceae bacterium	2	6
Streptococcus spp.	5	16
Anaerobic Bacteria		
Actinomyces odontolyticus	1	3
Anaerococcus vaginalis	1	3
Bacteroides fragilis	1	3
Bacteroidetes	1	3
Uncultured Clostridia bacterium	2	6
Dialister invisus	1	3
Finegoldia magna	1	3
Fusobacterium spp.	3	10
Peptococcus sp.	1	3
Peptoniphilus spp.	2	6
Prevotella oralis	1	3
Peptostreptococcus spp.	3	10
Porphyromonas somerae	3	10
Bacterium strain *Rauti*	1	3

*Species listed are the most probable species as identified by BLAST

**70% of *Staphylococcal* genera identified were probable *S. aureus* species

Characterization of Bacterial Populations in
Diabetic Foot Ulcers, Venous Leg Ulcers, and Pressure Ulcers

Wound micro-communities were analyzed in debridement samples from patients with one of the three main wound types: DFUs, VLUs, and PUs. Ten patients per wound type were analyzed by pooling extracted debridement DNA from each patient at equal concentrations prior to 16S PCR amplification and analysis.

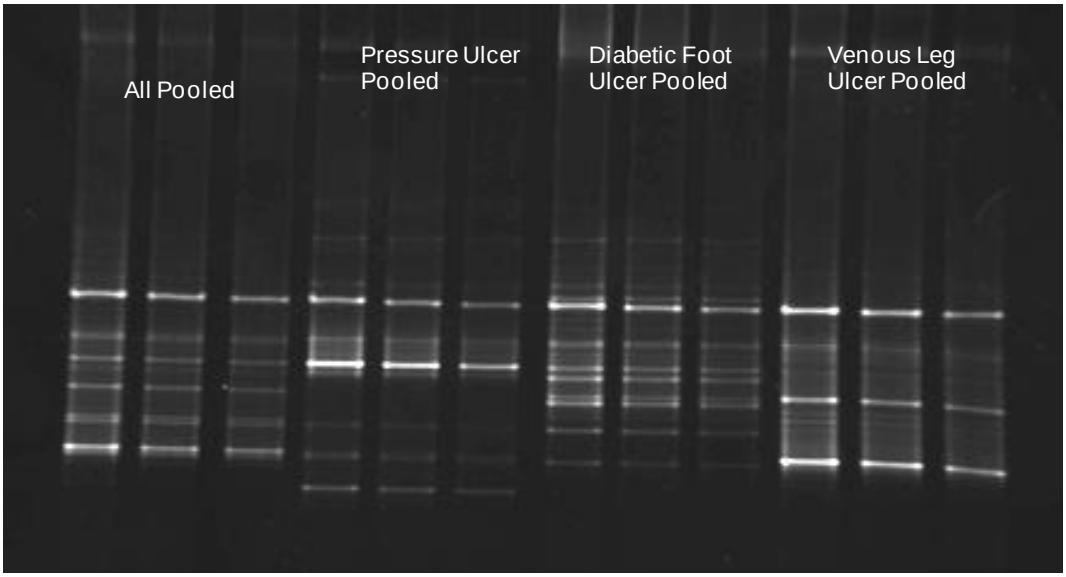

Figure 4. DGGE profiles for diabetic foot ulcers, venous leg ulcers, pressure ulcers, and all three wound types pooled. Notice the presence of both shared and unique bands. PCR products were diluted 1.5 fold 3 times to observe any faint bands or bands that may be present next to a larger band.

DGGE profiling of the pooled wound samples is shown in Figure 4. Some bands are shared between all wound types with varying intensities while many bands are unique to only one specific wound type. This indicates that while all wound debridement samples analyzed in this study shared certain bacterial populations, there were distinct differences in community composition between the three wound types. Various bands were excised, cloned, and sequenced. BLAST results from the sequenced DGGE bands are shown in Table 4. Bands shared by all wound types were often found to contain 16S

rDNA sequences from several different genera of bacteria between wound types. Therefore, bands shared by all wound types cannot be identified as a specific genus of bacteria.

Table 4. Results from DGGE band excision and sequencing. UWB refers to uncultured wound bacterium not found in the NCBI database.

Number of seqeunces	VLU Genus	Number of seqeunces	DFU Genus	Number of seqeunces	PU Genus
18	*Enterobacter* spp.	13	*Pseudomonas* spp.	34	*Serratia* spp.
17	*Pseudomonas* spp.	12	*Haemophilus* spp.	13	*Dialister* spp.
4	*Proteus* spp.	11	*Citrobacter* spp.	10	*Peptococcus* spp.
2	*Klebsiella* spp.	11	*Stenotrophomonas* spp.	3	*Pseudomonas* spp.
2	*Pectobacterium* spp.	10	*Morganella* spp.	2	*Citrobacter* spp.
2	*Erwinia* spp.	10	*Staphylococcus* spp.	2	*Morganella* spp.
1	*Serratia* spp.	5	*Acinetobacter* spp.	2	*Proteus* spp.
1	UWB	5	*Acinetobacter* spp.	1	*Haemophilus* spp.
1	*Haemophilus* spp.	4	*Morganella* spp.	1	*Klebsiella* spp.
		4	*Proteus* spp.	1	*Leminorella* spp.
		3	*Delftia* spp.	1	*Pectobacterium* spp.
		3	*Obesumbacterium* spp.	1	*Peptoniphilus* spp.
		2	*Dialister* spp.	1	*Prevotella* spp.
		2	*Mannheimia* spp.	1	UWB
		1	*Comamonas* spp.		
		1	*Grimontia* spp.		
		1	*Klebsiella* spp.		
		1	*Macrococcus* spp.		
		1	*Methylophaga* spp.		
		1	*Pantoea* spp.		
		1	*Pectobacterium* spp.		
		1	*Rahnella* spp.		
		1	*Serratia* spp.		
		1	*Streptococcus* spp.		
		1	UWB		

In addition to DGGE analysis of debridement samples, pooled DNA samples were analyzed by traditional culture methods, pyrosequencing and full ribosome shotgun sequencing in collaboration with Dowd et al [56]. Culture data were generated by analysis of the subject's medical record. Positive culture tests nearest to the date of sample collection for molecular analysis were recorded. All thirty subjects had culture

data in their medical records with the exception of one in the PU group. Many of the subjects were specifically cultured for both aerobic and anaerobic bacteria, but no obligate anaerobes were reported.

The results from these complimentary 16S rDNA methods compared to culture data revealed a much higher diversity in chronic wound bacterial populations. Collected evidence from DGGE, pyrosequencing, and full ribosomal shotgun sequencing indicated that chronic wounds are extremely complex polymicrobial communities.

Table 5. Bacteria cultured during standard of care from the three wound groups. The number of subjects within each wound type group with positive culture results for a bacterial genus is listed under the heading "subjects".

Subjects	VLU group	Subjects	DFU group	Subjects	PU group
4	*Enterococcus*	2	*Citrobacter*	4	*Staphylococcus*
3	*Staphylococcus*	2	*Enterococcus*	2	*Streptococcus*
2	*Enterobacter*	2	*Klebsiella*	2	*Enterococcus*
2	*Pseudomonas*	2	*Serratia*	1	*Escherichia*
1	*Klebsiella*	2	Staphylococcus	1	*Leclercia*
1	*Serratia*	2	*Streptococcus*	1	*Proteus*
1	*Citrobacter*	1	*Proteus*	1	*Pseudomonas*
1	*Acinetobacter*	1	*Pseudomonas*	1	*Acinetobacter*
		1	*Escherichia*	1	*Enterobacter*

Discussion

It has been known for some time that both acute and chronic wounds harbor multiple species of bacteria, including wounds without any signs of infection. This was evident in a review by Bowler et al where culture data from 62 published wound studies from the past four decades were examined [161]. *Staphylococcus aureus* was the most predominant isolate followed by coliforms, *Bacteroides* spp., *Peptostreptococcus*, *Pseudomonas aeruginosa*, *Enterococcus* spp., and *Streptococcus pyogenes*. Molecular techniques have been utilized in recent studies to characterize bacterial populations in

chronic wounds [56, 162, 163]. All such studies have found chronic wound micro-communities are more diverse than indicated by culture-based techniques. Overall, both culture and molecular based microbiological analyses have shown that wounds harbor diverse populations of bacteria. A single bacterial species responsible for chronic wound infections has not been identified and several species of bacteria have been cultured from both chronic and acute wounds. As chronic wounds do not seem to have a specific causative agent of disease, they violate Koch's postulates:

> 1. The microorganism must be found in abundance in all organisms suffering from the disease, but should not be found in healthy animals.
> 2. The microorganism must be isolated from a diseased organism and grown in pure culture.
> 3. The cultured microorganism should cause disease when introduced into a healthy organism.
> 4. The microorganism must be re-isolated from the inoculated, diseased experimental host and identified as being identical to the original specific causative agent.

However, a complex, polymicrobial causative agent for chronic diseases such as periodontal disease and chronic wounds is increasingly accepted.

DGGE banding patterns from chronic wound debridement samples revealed that, while some wounds shared certain bands, no two wounds shared identical banding patterns (Figure 3). This suggests that while some species of bacteria are common in many wounds, each wound micro-community is unique. DGGE banding profiles consistently produced several more bands than culture data indicated would be present (Figure 3, Table 1). These initial analyses indicated that culture data underrepresented the bacterial communities present in chronic wound infections.

To further address chronic wound bacterial community structure, 16S rDNA and culture data were compared from wound debridement samples (Tables 2 and 3). The diversity revealed by 16S rDNA analysis was far greater than indicated by traditional culture techniques. In addition to the greater number of bacterial genera identified, strict anaerobic genera were identified by 16S rDNA sequence analysis. No strict anaerobes were cultured from any wound analyzed, even though standard anaerobic culture techniques were applied.

The micro-communities from pooled DNA samples derived from ten patients per each of the three main wound types (DFUs, VLUs, and PUs) were analyzed by DGGE and 16S rDNA sequencing of excised bands. Each wound type produced a unique banding pattern which shared some bands (Figure 3). The finding that bands that denature at similar migration distances in the gel do not necessarily contain the same genera of bacteria indicated that DGGE analysis may under represent microbial diversity as well. This was considered a drawback to DGGE analysis. It was determined that DGGE is a tool best used for the qualitative analysis of bacterial diversity in complex communities rather than a quantitative method.

In collaboration with Dowd et al, sequence results from excised DGGE bands were compared to sequence results from complimentary 16S rDNA techniques [56]. The same DNA extracts from pooled patient populations with one of the three main wound types were analyzed by pyrosequencing and full ribosome shotgun sequencing. The complimentary comparison of the banding profiles and sequences produced by DGGE analysis, deep sequence coverage produced by pyrosequencing, and the species level

identification of bacterial community members by full ribosomal shotgun sequencing revealed that *Staphylococcus, Pseudomonas, Peptoniphilus, Enterobacter, Stenotrophomonas, Finegoldia,* and *Serratia* spp. are predominant populations of bacteria in chronic wound biofilms from the subjects analyzed in this study.

CHAPTER 4

DEVELOPMENT OF A NOVEL *IN VITRO* BIOFILM DISEASE MODEL AND CHARACTERIZATION OF *S. AUREUS* BIOFILM CONDITIONED MEDIUM

Introduction

An *in vitro* model to study the impact of bacterial biofilms on inflammatory and epithelialization processes in human epidermal cells was developed. *S. aureus* was chosen as a model pathogen since it was discovered in all of the three main wound types and is an important human pathogen associated with high rates of nosocomial infections. Keratinocytes form a physical barrier (the epidermis) to the outside environment, and are one of the first cell types to initiate inflammatory processes induced by invading microorganisms and environmental stresses associated with wounding. Additionally, the persistent nature of chronic wound infections is in part due to the failure of the epidermis to reestablish itself on the wound bed. Keratinocytes are thus involved in both the inflammatory and epithelialization phases of wound healing. Keratinocytes derived from human foreskin (HFKs) and the spontaneously immortalized keratinocyte cell line HaCaT (**H**uman **a**dult low **Ca**lcium **T**emperature) were selected as model epidermal cells. HaCaT keratinocytes are a widely used keratinocyte line which display similar responses to TLR ligands and migrate at similar rates as primary keratinocytes and are suitable for studies investigating innate immunity and cell migration [164, 165].

Research into the effects of disease causing bacteria has been overwhelmingly focused on the effects of planktonic bacterial cultures on different aspects of

pathogenesis. Several studies have been conducted that observed the effects of planktonic bacteria in exponential or stationary phase growth on various mammalian cell types [52, 53]. The formation of bacterial biofilms and their effects on pathogenic mechanisms is largely underrepresented in the literature. Bacterial biofilms occur frequently in nature and it can be argued that bacteria in a planktonic phenotype are the minority outside of the laboratory. Characterization of *S. aureus* biofilm and planktonic conditioned medium (BCM and PCM, respectively) was performed to evaluate fundamental differences between the planktonic and biofilm phases of growth. Analysis of *S. aureus* BCM could potentially elucidate mechanisms that impact wound healing processes in human keratinocytes. Our *in vitro* biofilm disease model is a more relevant way to study chronic wound infections than traditional planktonic based *in vitro* models.

Materials and Methods

Cell Culture

Human foreskin keratinocytes (HFKs) and the spontaneously immortalized human HaCaT keratinocyte cell line were used in these studies. Additionally, HaCaT keratinocytes undergo the same Biofilm Conditioned Medium induced morphology changes, induction of apoptosis, and increases in intracellular calcium as HFKs.

HFKs were cultured from newborn foreskin and passaged in serum free medium using methods previously described [166]. Cells were maintained in EpiLife® keratinocyte growth medium (Cascade Biologics, Portland, OR) supplemented with human keratinocyte growth supplement (HKGS; Cascade Biologics, Portland, OR).

Experiments were conducted with cell passages 4–10, using EpiLife® medium supplemented with HKGS (EPI). HaCaT keratinocytes were maintained and cultured under identical conditions. All cultures were kept in a humidified 5% CO_2 incubator at 37 °C.

S. aureus Biofilm Culture Conditions and
Preparation of Biofilm Conditioned Medium

Tissue culture inserts (35 mm diameter, 0.2 µm pore size, Nalge Nunc International, Rochester, NY) were placed into six well plates with 2.1 ml of EPI supplemented with human keratinocyte growth supplement in each well. An overnight culture of a clinical isolate of *S. aureus* (South West Regional Wound Care isolate #10943) was diluted in EPI to an optical density of 0.05 at 600 nm. Seven 10 µl drops of the diluted culture were placed on each insert and the biofilm was allowed to mature for three days at 37°C in a humidified 5% CO_2 atmosphere. Every 24 hours for four days thereafter, the growth medium was collected, pH adjusted to 7.2 (from pH 7.7), filter sterilized, pooled, and replaced with fresh EPI. The collected growth medium will be referred to as biofilm-conditioned medium (BCM). Alternatively, mature biofilms were transferred to 6-well plates with confluent keratinocytes and observed for various amounts of time. This will be referred to as the biofilm co-culture model.

S. aureus Planktonic Culture Conditions and
Preparation of Planktonic Conditioned Medium

To obtain a planktonic culture of *S. aureus* that most closely resembled the physiological conditions found in bacterial biofilms, mature three day old *S. aureus*

biofilms were re-suspended into 2.1 ml of EPI growth medium and grown at 37°C with constant agitation. Bacterial cells were centrifuged out of solution and the supernatant was collected, pH adjusted to 7.2 (from pH 6.9), and filter sterilized. This collected supernatant will be referred to as planktonic conditioned medium (PCM). The bacterial pellet was re-suspended in 2.1 ml fresh EPI growth medium and this process was repeated every 24 hours for four days and the supernatants pooled. Both *S. aureus* planktonic and biofilm cultures were maintained for four days and the conditioned medium pooled to help eliminate any day to day variations that might occur in overnight planktonic and biofilm cultures.

Planktonic cultures of *S. aureus* grown under varying oxygen tensions were grown in 30 ml EPI growth medium in glass tubes crimp sealed with a butyl rubber stopper maintained with constant agitation at 37°C. Cultures described as aerobic open were vented to ambient air with a needle and syringe filter. Cultures described as aerobic closed were inoculated with ambient air in the headspace and sealed. Cultures described as anoxic were purged with 0.2 µm filtered nitrogen for 30 minutes prior to inoculation. OD_{600} readings were obtained for all cultures at various times. Conditioned medium was harvested as described previously for PCM.

Population Density Measurements of *S. aureus* Cultures

Population densities were measured by reading the optical density of the culture at 600nm (OD_{600}). Planktonic measurements were taken after centrifuged planktonic bacterial pellets were re-suspended in fresh growth medium. An initial and final (day 0

and day 4) OD_{600} was measured for *S. aureus* biofilm by re-suspending the biofilm in the same volume of fresh EPI in which planktonic cells were re-suspended.

1D SDS-PAGE

Total protein from BCM, PCM, and EPI was quantified using a modified Lowry assay following the manufacturer's protocol (Thermo Scientific, Rockford, IL). Proteins from equal volumes (2 ml) of PCM, BCM, and EPI were precipitated by adding 50 µl 40% TCA and 150 µl acetone. Samples were vortexed and incubated at 4°C for 2 hours. Samples were then centrifuged at 10,000 RPM for 10 min at 4^{o}C. The supernatant was decanted and the protein pellet was washed in 500 µl acetone and centrifuged. This process was repeated and the protein pellet was allowed to air dry for 5 minutes at room temperature. Precipitated protein pellets were re-suspended in 50 µl sample buffer (3.8 ml dH_2O, 1.0 ml 0.5M Tris-HCL pH 6.8, 0.80 ml glycerol, 1.6 ml 10% SDS, 0.4 ml 2-β-mercaptoethanol, 0.4 ml 0.05% (W/V) bromophenol blue). Samples were incubated at 95^{0}C for 5 min. Samples were loaded onto 12% acrylamide gels (33.5 ml dH2O, 25 ml 1.5M Tris-HCL pH 8.8, 1.0 ml 10% SDS, 40 ml 30% acrylamide/bis, 500 µl 10% ammonium persulfate, 50 µl TEMED) with a 4% acrylamide stacking gel (3.05 ml dH2O, 1.25 ml .5M Tris-HCL pH 6.8, 50 µl 10% SDS, 0.65 ml 30% acrylamide/bis, 25 µl 10% ammonium persulfate, 5 µl TEMED). Gels were run in a Tris/Glycine running buffer at 60 mAmps until the dye front ran off of the gel. Gels were stained with Coomassie Blue (GE Healthcare Biosciences, Pittsburgh, PA).

Nuclear Magnetic Resonance (NMR) Metabolite Profiling

NMR metabolite profiling of bacterial conditioned medium was performed by the NMR Core facility at Montana State University. Samples of BCM, PCM, and EPI (400 ul) were diluted with 100 ul of concentrated NMR buffer and analyzed with NMR Samples were lyophilized and re-suspended in deuterated water and standard 1-D 600 MHz ^{1}H NMR spectra were acquired for all samples. NMR spectra were obtained on a Bruker 600 MHz magnet. Metabolites were quantified with Chenomx software. The Genesis software was used to generate a heat map of the metabolites and calculate ANOVA p-values.

Organic Extraction of Conditioned Medium

Conditioned medium was extracted into an equal volume of chloroform in glass test tubes and vortexed. The organic layer was removed to a fresh glass tube using glass Pasteur pipettes. The collected chloroform was then completely dried under a gentle stream of 0.2 µm filtered ambient air at room temperature and re-suspended into 100 µl chloroform. All samples destined to be analyzed and compared were prepared at the same time.

High-Performance Liquid
Chromatography Mass Spectrometry (HPLC/MS) Analysis

HPLC. Metabolites present in bacterial conditioned medium were routinely separated using an Agilent series 1100 high-performance liquid chromatograph equipped with an auto sampler, a fraction collector, a diode array detector, a temperature-controlled

column compartment, and a Hypersil BDS-C18 column (Agilent, 2.0x125 mm with 3 µm pore size). Solvents used were 0.1 % formic acid and 95% acetonitrile (0.1% formic acid) with a 5-95% gradient at a 0.4 ml/minute flow rate. Separation was performed at 25°C.

ESI-MS. Positive-mode electro spray ionization (ESI) mass spectra of bacterial conditioned medium were obtained using a series 6300 Agilent SL ion trap mass spectrometer. MS analysis was performed simultaneously with HPLC separation (HPLC/MS). For MS2 compound identification, fractions of each metabolite were collected at the time that their concentrations were the highest (between 8 and 9 minutes for aureusimine A and between 9.5 and 10.5 minutes for aureusimine B) and analyzed via direct infusion into the mass spectrometer. The MS parameters were as follows: nitrogen dry gas flow rate, 5 liters/ min; dry gas and vaporizer temperature, 350°C and 400°C, respectively; corona current, +4000 nA; and nebulizer pressure; 60 psi.

Q-TOF-MS. Samples were separated on a Agilent 1290 uHPLC with a Phenomenex Kinetex C-18 column (150 x 2.1 mm with 2.6 µm pore size). Solvents used were 0.1 % formic acid and 95% acetonitrile (0.1% formic acid) with a 5-95% gradient at a 0.4 ml/minute flow rate. Fractions containing m/z 229 and m/z 245 were collected based upon the time they eluted as determined by UV 322 nm detection. Collected fractions were directly injected into an Agilent 6520 quadrupole time-of-flight (Q-TOF) with a micro-syringe. MS2 was performed using collision energies ranging from 10-100V and acquired spectra were averaged.

ICP-MS. Filter sterilized (0.2 μm) samples were taken and preserved at 4 °C for analysis. Inductively coupled plasma mass spectrometry (ICP-MS) (Agilent 7500ce ORS, Foster City, CA, U.S.A.) with an Octopole Reaction System and a MicroMist glass concentric nebulizer was used to measure metal concentrations. The sample temperature was set at 2 °C and the radio frequency power was set to 1500 W. Argon was used as the carrier gas, at a flow rate of 0.64 L min^{-1}. The nebulizer pump was operated at 0.15 rotations per second (rps) and the sample pump was set to 0.1 rps. Measurements were compared with standards to calculate metal concentrations. Germanium and indium were used as internal standards to correct for drift over a series of runs.

Results

Characterization of *S. aureus* in the Biofilm Disease Model and *S. aureus* Biofilm Conditioned Medium

S. aureus biofilms grown on tissue culture inserts were used in either the co-culture model or for the production of BCM (Figure 5).

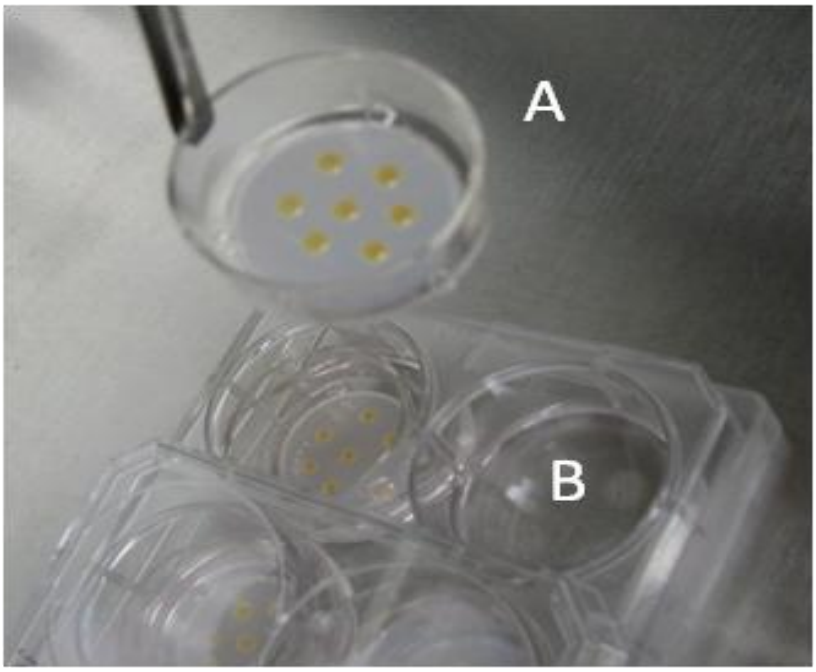

Figure 5. A. Three day old *S. aureus* biofilms grown on tissue culture inserts. B. EPI growth medium in contact with the biofilm (biofilm conditioned medium) was collected and replaced with fresh growth medium every 24 hours. Alternatively, mature biofilms (A) were placed in wells containing confluent keratinocytes (B) in the co-culture model.

Population density curves for both biofilm and planktonic cultures of *S. aureus* show that both cultures had comparable OD_{600} levels indicating similar growth rates and cell densities (Figure 6).

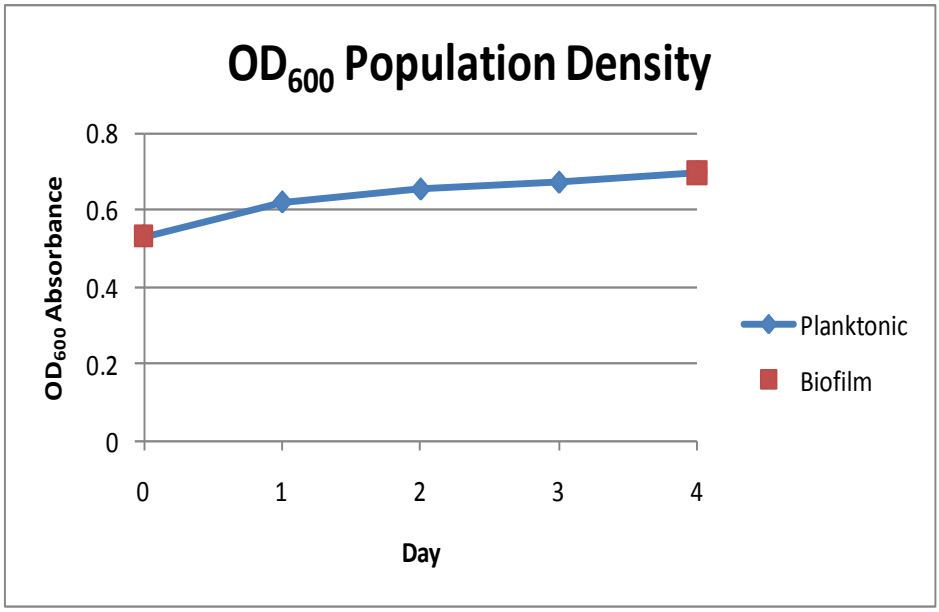

Figure 6. Population density curves for *S. aureus* biofilm and planktonic cultures over a four day period. Both cultures show stationary growth with comparable OD_{600} levels indicating that both culturing techniques produce similar culture densities. Data represents mean measurements from three individual cultures. Error bars on the order of 0.005 for all time points were too small to be charted.

The total protein concentration of PCM and BCM did not change drastically in any sample, but BCM was found to contain the highest amount of total protein (Figure 7). However, these data do not represent the total bacterial protein since the bacteria are consuming protein in the growth medium. Differences in bacterial proteins compositions were revealed by 1D SDS-PAGE (Figure 7). Several bands were found to be unique to each sample indicating differential protein production by *S. aureus* during planktonic and biofilm growth. Both planktonic and biofilm *S. aureus* consumed protein as indicated by the disappearance of large bands from the EPI control. Additionally, the BCM sample produced a smear in every gel run indicating the presence of bacterial proteases.

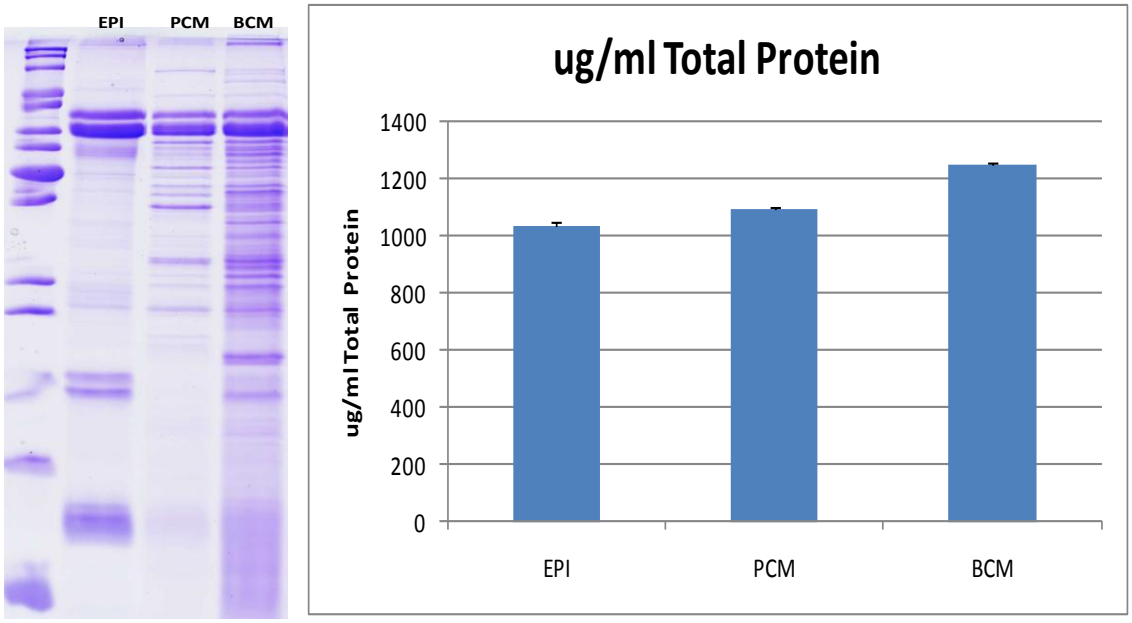

Figure 7. (Left) 1D SDS-PAGE of EPI, PCM, and BCM. Several unique bands are present in both the PCM and BCM samples. Smearing of the BCM sample was observed in all gels run indicating protease activity. (Right) Total protein in EPI, PCM, and BCM. BCM samples contained more total protein, but it is likely that the bacteria were consuming protein leaving the total bacterial protein concentration unknown.

Both BCM and PCM contained roughly equivalent amounts of extracellular DNA (Figure 8). A broader range of nucleic acid length was observed in DNA present in PCM (50-500 bp) while DNA present in BCM was between 50-100 bp in length. The tight range of extracellular DNA in BCM is likely a consequence of bacterial nuclease activity.

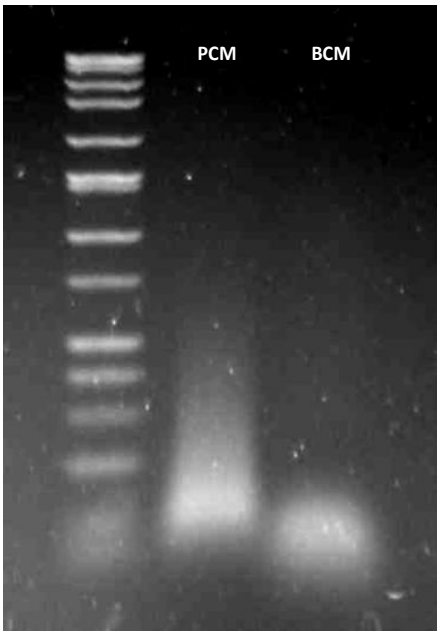

Figure 8. Precipitated DNA from 2 ml PCM or BCM. Both samples have roughly the same amount of DNA, but BCM ran without smearing. *S. aureus* biofilm are secreting DNA fragments between 50-100 bp while DNA present in planktonic cultures of *S. aureus* are between 50-500 bp. Ladder ranges from .05-10 kbp.

S. aureus Biofilm Produces Mixed Acid Fermentation Products

To investigate the complex metabolite compositions of planktonic and biofilm *S. aureus* secretions, NMR based metabolite profiling was applied to PCM, BCM, and EPI growth medium. With a lower limit of detection of 0.001 mM, 55 compounds were identified in *S. aureus* BCM, PCM, and EPI samples. It is important to note that this method of metabolite identification is limited to known standards in a library. As seen in Figure 9, several compounds are present which are not accounted for (orphan compounds). Compounds can be added to this library, but other methods are required for identification (i.e. HPLC/MS). A hierarchical clustering of known metabolite concentrations is shown in Figure 10.

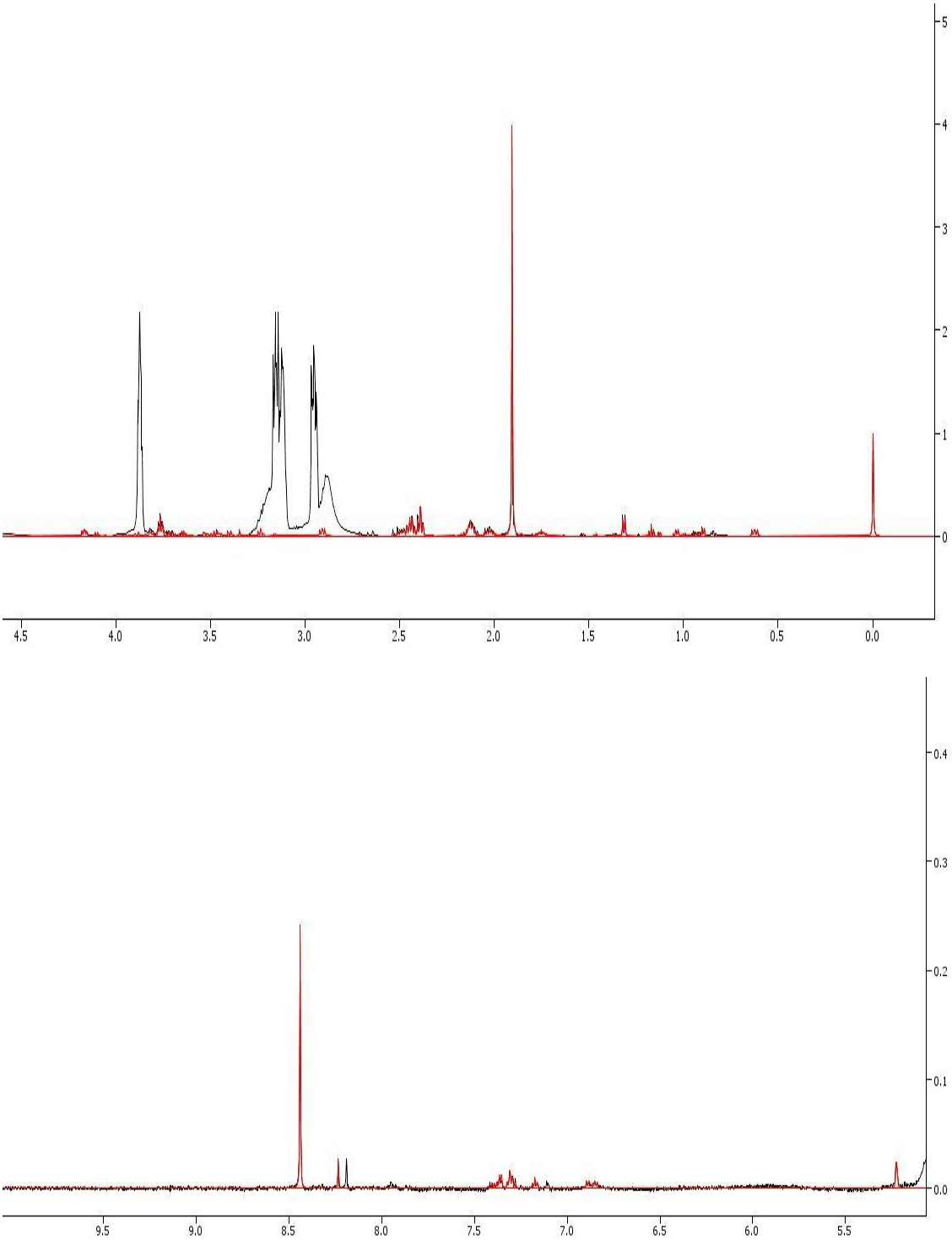

Figure 9. Raw spectrum produced by NMR analysis of BCM (note chemical shifts between 5-10 ppm are magnified, bottom). Compounds in the Chenomx library were identified (red) while several orphan compounds were observed (black). These orphan compounds are present in the sample, but compound identification is limited to known compounds in a library.

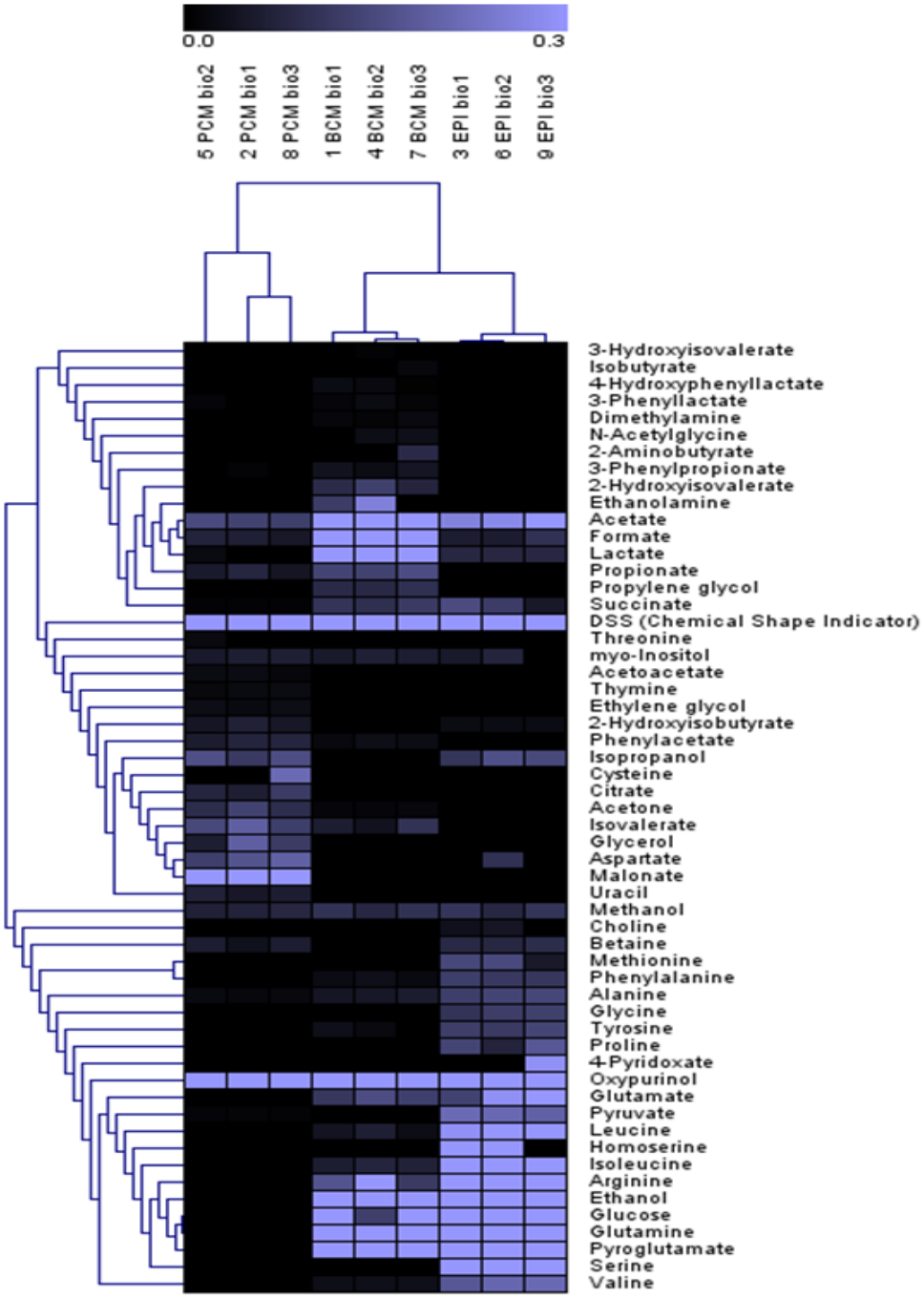

Figure 10. Hierarchical clustering (covariance distance) of metabolite concentrations in BCM, PCM, and EPI. Light colors indicate high metabolite concentrations, while black indicates metabolite concentrations below detection. Basic nutrients like glucose and amino acids were consumed more quickly in planktonic *S. aureus* cultures while *S. aureus* biofilm cultures were found to excrete the anaerobic fermentation products acetate, formate, lactate, and propionate. Results are consistent with the notion that bacterial biofilms harbor diverse metabolic niches including an overall more dormant metabolic state and anoxic areas deep within the biofilm. Triplicate biological replicates are indicated by 1, 2, and 3.

While both planktonic and biofilm cultures were found to consume glucose and amino acids, *S. aureus* planktonic cultures consumed more than *S. aureus* biofilm. *S. aureus* biofilm cultures selectively consumed amino acids over glucose and produced the fermentation products acetate, lactate, formate, and propionate. The lack of fermentation products in the planktonic culture supernatant indicates that glucose and other nutrients were consumed primarily through oxidative metabolic pathways.

Secreted metabolites from both planktonic and biofilm cultures of *S. aureus* were placed into contact with confluent HaCaT keratinocytes. The resulting metabolic profiles are shown in Figure 10. Relative to initial metabolite levels indicated by NMR analysis of PCM, BCM, and EPI, nutrients such as glucose and amino acids were only partially consumed by keratinocytes under all conditions. An increase in lactate, acetate, formate, and proprionate in all samples exposed to keratinocytes was observed indicating anaerobic glycolysis was occurring in HaCaT keratinocytes in our model. The absence of these fermentation products in the planktonic *S. aureus* culture followed by their appearance after incubation with the keratinocyte culture indicates they are produced by the keratinocytes. ICP-MS analysis of BCM, PCM, and EPI revealed that sodium, magnesium, potassium, and calcium levels were unchanged.

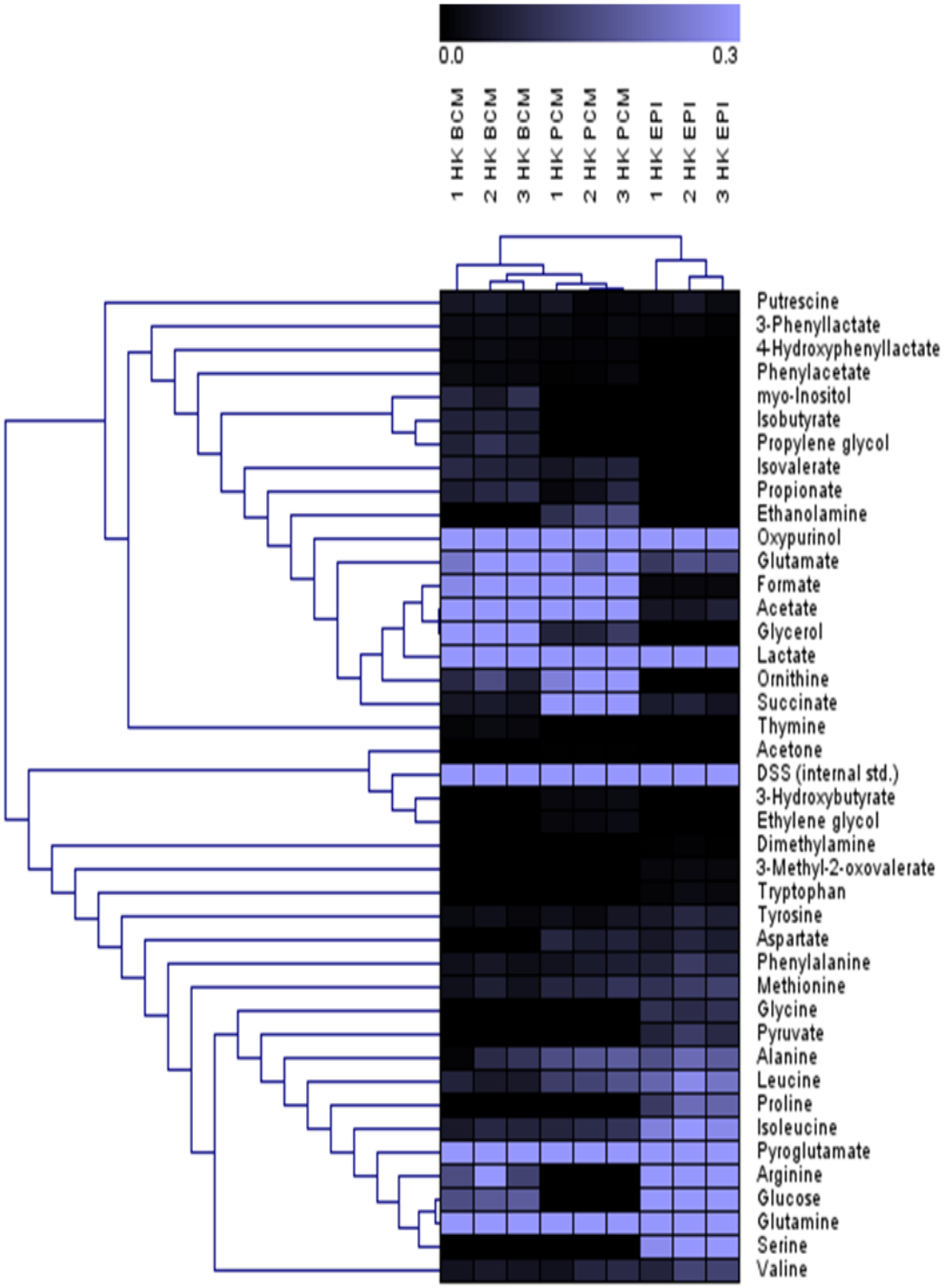

Figure 11. Hierarchical clustering (covariance distance) of excreted metabolites from human keratinocytes exposed to *S. aureus* metabolites in BCM, PCM, and EPI for four hours. Lactate production was observed in all conditions while the presence of other fermentation products such as acetate, formate, and propionate are present in samples exposed to bacterial products. Triplicate biological replicates are indicated by 1, 2, and 3.

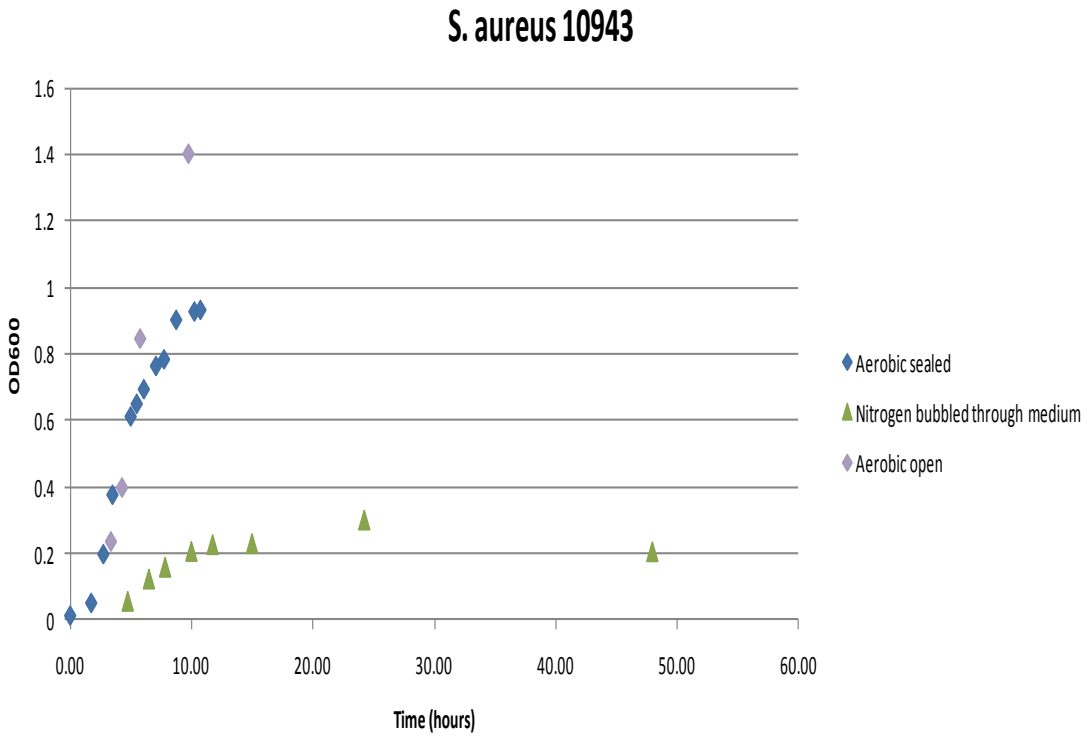

Figure 12. Growth curves for *S. aureus* under open, aerobic, sealed aerobic, and anoxic conditions. All cultures were grown planktonically with constant agitation at 37°C in EPI.

To further characterize secreted metabolite compositions from *S. aureus* biofilm, planktonic cultures grown under anoxic and aerobic environments were investigated. These conditions were selected to mimic the anoxic core and aerobic shell present in the biofilm. The expected growth patterns were observed with anoxic cultures growing slowly, open aerobic cultures growing very quickly, and sealed aerobic cultures growing modestly fast (Figure 11). It is important to note that the stationary phase open aerobic culture may have consumed all dissolved oxygen in the medium even though the headspace was exchanged to the atmosphere. In total, 33 metabolites were identified in planktonic *S. aureus* samples. Measured pH values revealed that all of the planktonic

cultures became more acidic over time while the biofilm was the only culture that actually increased its pH relative to the starting pH of EPI (Figure 12).

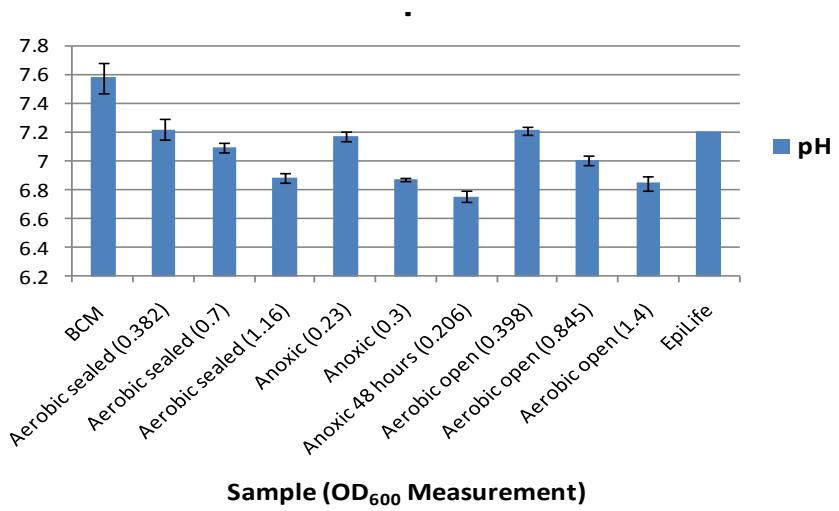

Figure 13. Planktonic cultures of *S. aureus* grown in EPI were harvested at various phases of growth and the pH was measured. EPI media had an initial pH of 7.2 and all planktonic cultures showed a decrease in pH over time regardless of the presence or absence of oxygen. BCM was the only sample were the pH increased above 7.2. Error bars represent standard deviation of the average of three experiments.

The hierarchical clustering of metabolites analyzed from *S. aureus* planktonic cultures cultivated under different oxygen tension is shown in Figure 13. Planktonic anoxic cultures of *S. aureus* contained higher concentrations of common fermentation products such as lactate and formate. The presence of these metabolites in planktonic anoxic *S. aureus* cultures in addition to the relatively low concentrations found in aerobic cultures confirms the presence of an anoxic niche in *S. aureus* biofilms. Metabolites such as glucose and other sugars were found to be consumed in anoxic cultures while they were not consumed in early exponential phase aerobic cultures or BCM. This indicates that while the metabolome of *S. aureus* biofilm is a mix between anoxic and aerobic

planktonic metabolomes, there are some unique metabolic activities that occur within the biofilm environment.

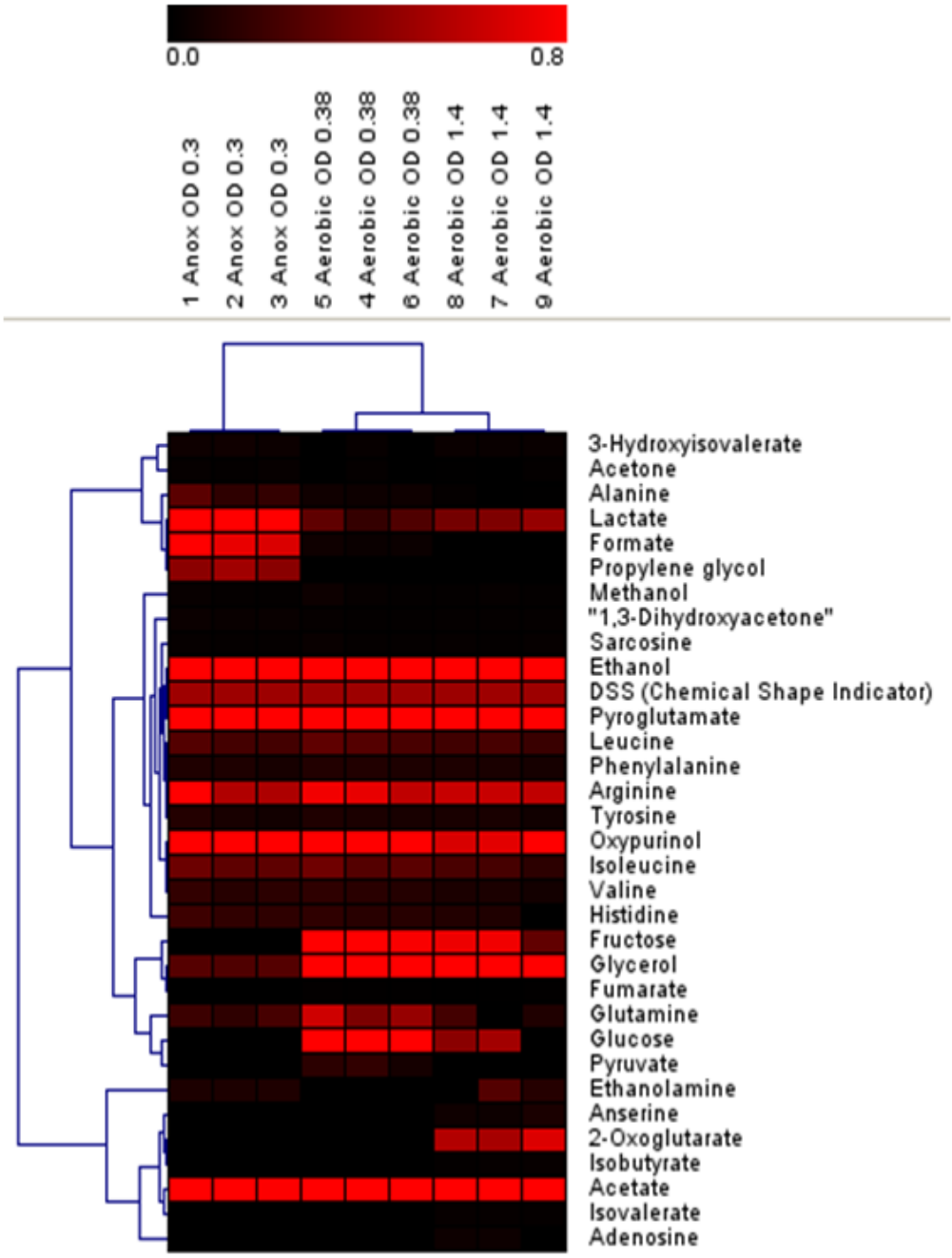

Figure 14. Hierarchical clustering (cosine correlation) of metabolite concentrations in anoxic, aerobic OD 0.38, and aerobic OD 1.4 planktonic *S. aureus* cultures. Bright red indicates high metabolite concentrations, while black indicates metabolite concentrations below detection. Fermentation products such as lactate and formate are present at high concentrations in anoxic cultures.

Hydrophobic Small Molecule Production in *S. aureus* Biofilm and Planktonic Cultures

Hydrophilic molecules are readily secreted from mammalian systems while hydrophobic molecules must be metabolized to a more water soluble form prior to elimination from the body. As a consequence, hydrophobic molecules are often much more toxic to mammalian cells than are hydrophilic molecules. To test the possibility that *S. aureus* biofilms were secreting small hydrophobic molecules that could diffuse freely into host cells, an organic extraction on BCM, PCM, and EPI medium was performed using chloroform. HPLC/MS analysis of chloroform extracts EPI, PCM, and BCM is shown in Figure 14.

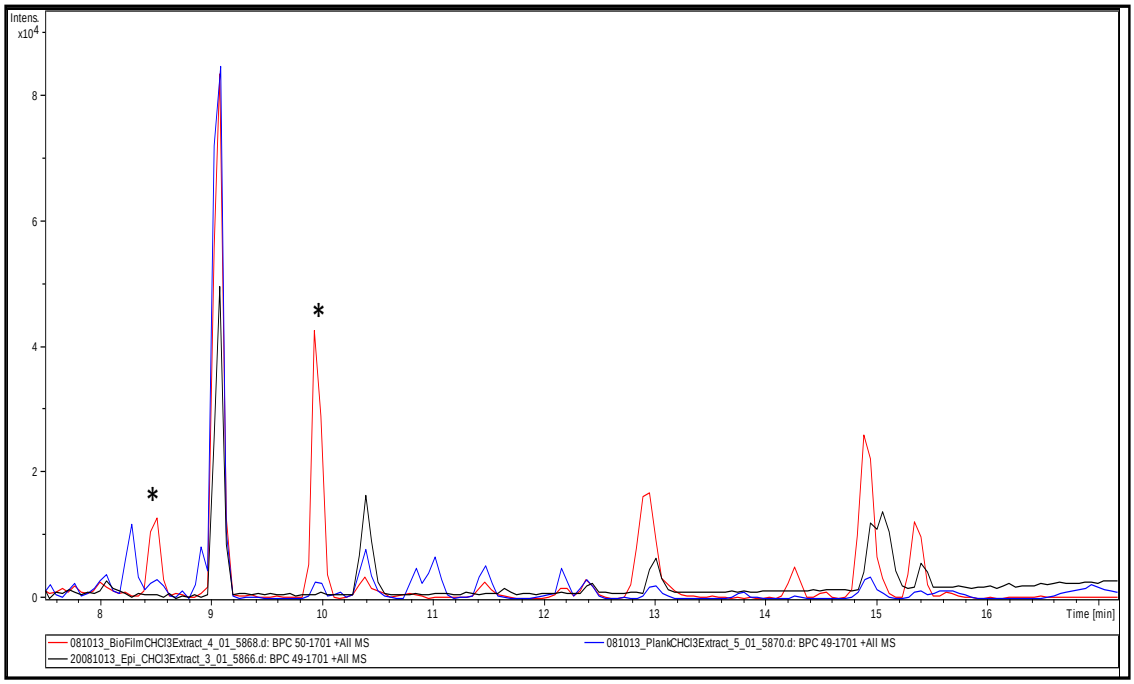

Figure 15. HPLC/MS base peak chromatogram displaying BCM (red), PCM (blue), and EPI medium (black). (*) represent peaks absent in EPI growth medium but present with high intensities in BCM samples relative to PCM samples (left * m/z=245.13, Right * m/z=229.13). Other peaks with high intensities in the BCM sample were found to be present in the growth medium and were not analyzed further.

Two peaks were present at high intensities in BCM relative to PCM which were absent in the growth medium. The ion with the highest intensity had an m/z ratio of 229.13 and the lower intensity ion had an m/z of 245.13. While this dissertation was being prepared, Wyatt et al published the structures of two non-ribosomal peptide secondary metabolites (aureusimine A and B) produced by *S. aureus* that regulated virulence [167]. Wyatt et al determined that these two compounds were synthesized by *S. aureus* through the combination of the amino acids valine and tyrosine (aureusimine A) and valine and phenylalanine (aureusimine B). The m/z of aureusimine A and B were reported by Wyatt et al as m/z 245.17 and m/z 229.13, respectively. The structures of the aureusimines are shown in Figure 15.

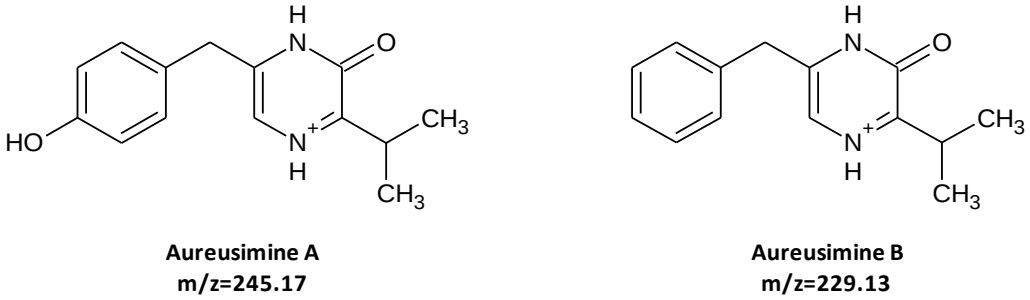

Aureusimine A
m/z=245.17

Aureusimine B
m/z=229.13

Figure 16. Structures the positive ions of *S. aureus* non-ribosomal peptide secondary metabolites published by Wyatt et al [167]. These compounds were shown to regulate virulence in *S. aureus* both *in vitro* and *in vivo*. These compounds were found to have the same molecular weight and UV absorbance spectra as the compounds identified in BCM.

Wyatt et al detected the aureusimines using Ultra Violet light (UV, 322 nm). They found that aureusimine A eluted first followed by aureusimine B. The ions described in this dissertation were also detected by 322 nm UV light which corresponded with extracted ion chromatograms (EICs) for m/z 245 and m/z 229 (Figure 17). Furthermore, based on the m/z of the eluting ions, the m/z which corresponded with aureusimine A

eluted first, followed by the ion correlating with aureusimine B. These data suggest that the ions described here are likely the same ions described by Wyatt et al.

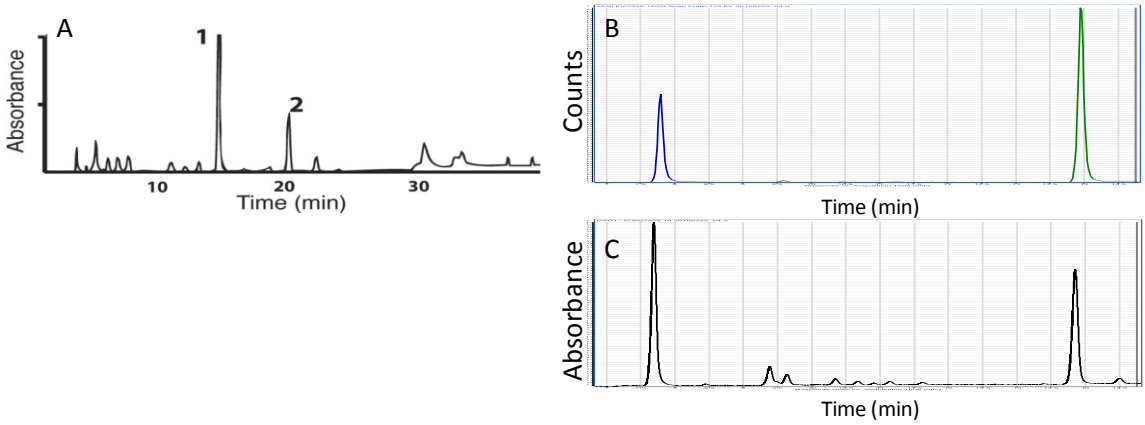

Figure 17. (A). Wyatt et al reported that aureusimine A (1) and B (2) absorbed UV radiation at 322 nm. EICs for m/z 245 and m/z 229 (B) correlated with UV absorbance at 322nm (C). The reproduction of UV absorbance at 322 nm indicates that m/z 229 and m/z 245 may be the aureusimines described by Wyatt et al.

In light of the publication of the structures of aureusimine A and B, MS2 experiments were carried out to identify the two ions present in high quantities in BCM relative to PCM. High resolution MS spectra obtained using a Q-TOF/MS provided high resolution masses for the two positive ions: m/z 245.1289 and m/z 229.1338. A high resolution chemical formula calculator was used to determine possible molecular formulas for the measured masses. The only possible chemical formulas for the two masses, within an acceptable error range of 1.5 ppm, were $C_{14}H_{17}N_2O_2$ and $C_{14}H_{16}N_2O$. These are the chemical formulas for the positive ions of aureusimine A and B, respectively. MS2 fragmentation of collected fractions of each ion directly injected into a Q-TOF/MS revealed that the expected fragmentation ions of aureusimine A and B were present (Appendices A and B, respectively). Both ions experienced similar losses of masses that corresponded to shared molecular features (i.e. loss of the isopropyl group)

while aureusimine A fragmentation patterns were consistent with the additional hydroxyl group in its tyrosine residue.

The production of aureusimine A and B in other strains of *S. aureus* and other Gram positive and Gram negative bacterial species were investigated using HPLC/MS and MS2 (Table 6). Interestingly, only Gram positive species were found to produce aureusimine A and B as none of the extracts from Gram negative bacteria contained either ion. The two MRSA strains were found to produce several times more aureusimine A and B than any other strain tested.

Table 6. Strains analyzed for aureusimine A and B. Relative production indicated by plus signs. Only Gram positive strains were found to produce the aureusimines. The MRSA strains tested produced the highest levels of the aureusimines.

Strain	Gram	Aureusimine A	Aureusimine B
S. aureus SWRWC 10943	+	++	++
S. aureus ALC 2035	+	++	+++
S. aureus SWRWC 113 (MRSA)	+	++++	+++++
S. aureus ATCC 33591 (MRSA)	+	++++	+++
S. aureus ATCC 29213	+	+	++
Coag (-) *Staph.* spp. SWRWC 129	+	+	+
Staphylococcus epidermidis (SWRWC clinical isolate)	+	+++	++
Enterococcus faecalis (SWRWC clinical isolate)	+	+	++
Pseudomonas aeruginosa SWRWC 215	-	-	-
Escherichia coli ATCC 8739	-	-	-

Oxygen Tension in Planktonic *S. aureus*
Cultures Impacts Production of Aureusimine A and B

The presence of mixed acid fermentation products in BCM and not in PCM indicated an anoxic niche was present in *S. aureus* biofilms. Since BCM contained relatively high levels of the aureusimines compared to PCM, it was hypothesized that the presence of an anoxic niche may contribute to the production of the small molecules observed in organic extracts of BCM. To test the production of the aureusimines in aerobic or anoxic environments, the same planktonic *S. aureus* cultures cultivated for metabolite analysis were analyzed for aureusimine A and B. Optical density readings were measured for all of the growth conditions (Figure 6) and the pH measured (Figure 12).

Culture supernatants were harvested based on OD_{600} readings (exponential or stationary growth phases) and extracted into chloroform for analysis of aureusimine production with HPLC/MS. Oxygen was found to influence the production of the aureusimines (Figures 18 and 19). All stationary phase cultures produced the aureusimines over time with the sealed aerobic culture producing the most. None of the aerobic cultures growing exponentially produced the ions while anoxic cultures were found to have the ions present during all phases of growth. Anoxic cultures produced the aureusimines at reduced levels compared to other cultures, but this is likely due to the low cell densities achieved during anoxic growth. The presence of aureusimine A and B was measured in freshly harvested BCM and in 8 week old BCM stored at -20°C. It was found that the aureusimines slowly decomposed over time.

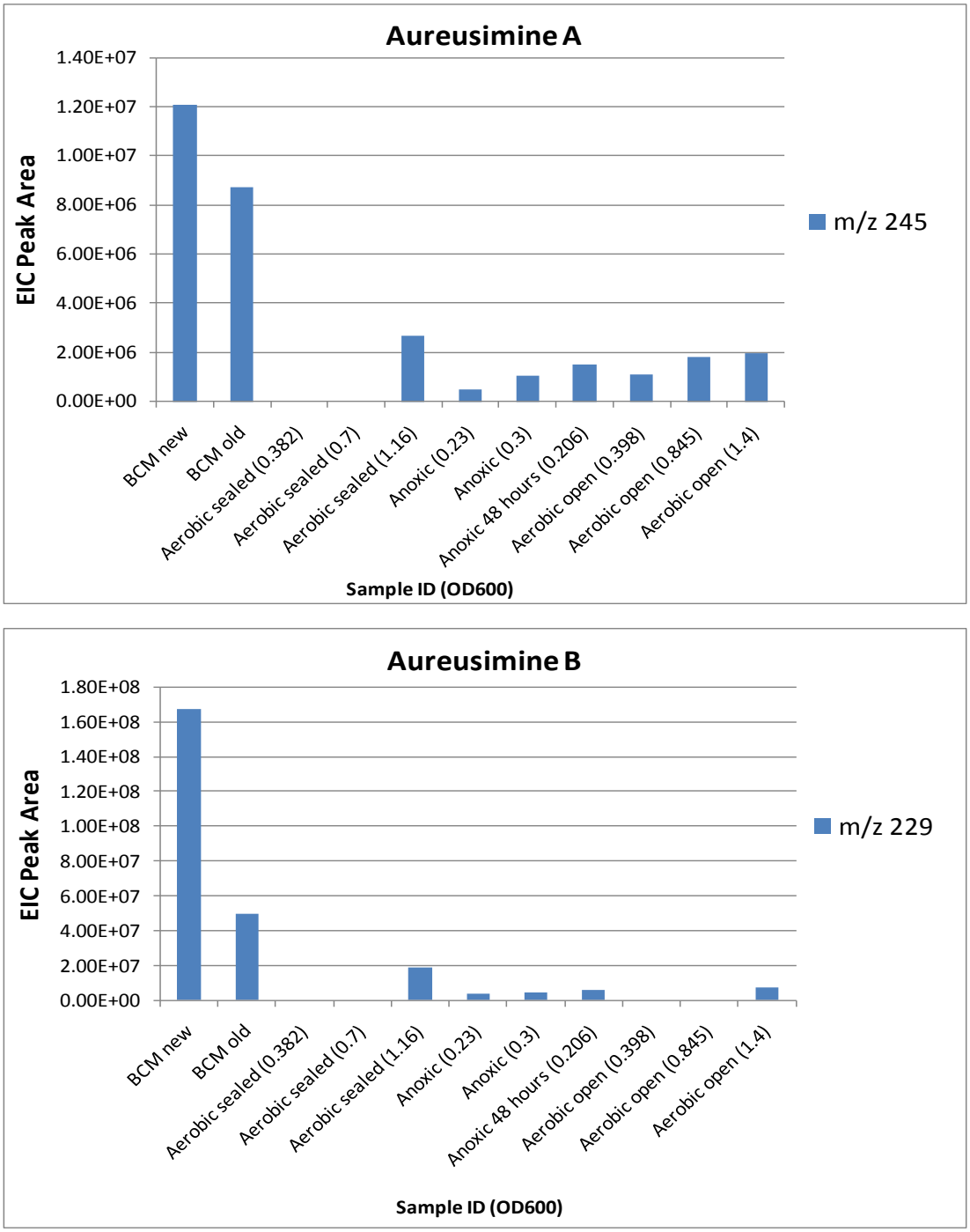

Figure 18. EIC peak areas indicate that as oxygen is consumed, the ions of interest are produced. Other than the BCM samples, the sealed aerobic sample collected during stationary growth contained the most aureusimines. No aureusimines were detectable in either aerobic culture until a stationary phase of growth was achieved. Anoxic cultures contained low levels of aureusimines at all time points indicating that although the anoxic cultures had low cell numbers, the low oxygen levels in those environments stimulated the synthesis of aureusimine A and B. Data representative of triplicate experiments.

Comparison of similar cell densities (OD_{600} 0.3-0.4) revealed that anoxic cultures did in fact produce more aureusimine A and B than similar cell densities of aerobic cultures (Figure 18). However, this could be attributed to a longer period of growth required to reach these population levels in anoxic cultures relative to aerobic cultures, resulting in the production of more of these molecules as a consequence of time rather than cell density.

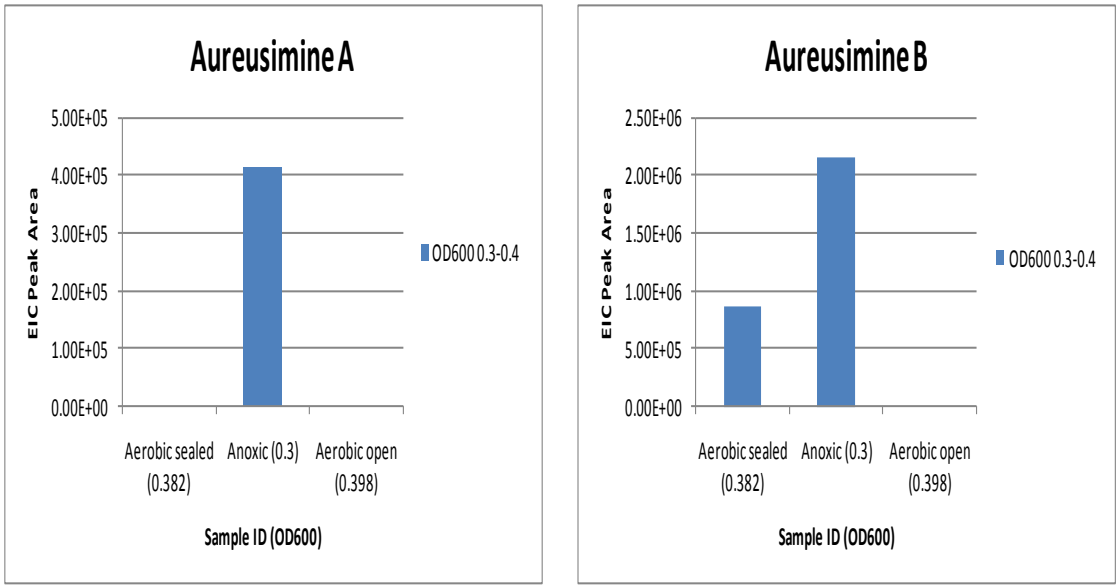

Figure 19. EIC peak areas of aerobic sealed, anoxic, and aerobic open cultures at similar OD600 readings between 0.3 and 0.4. At these similar cell densities, the anoxic cultures produced higher levels of the aureusimines. This further indicates that low oxygen tension is required for the production of these molecules. Data representative of triplicate experiments.

Discussion

S. aureus biofilm were grown on tissue culture insert membranes with a pore size smaller than the diameter of individual bacteria (0.2 µm pore size). No direct physical contact between the biofilm and keratinocytes was possible in this model without physically disrupting the biofilm by scraping it off of the membrane. Rather, interactions

between soluble products released from the biofilm and their effects on cultured keratinocytes were examined. Advantages of growing *S. aureus* biofilm on tissue culture inserts include: i) the biofilm and keratinocytes can be separated completely for study/maintenance with minimal disruption to either the host or pathogen, ii) the ability to separate the biofilm from the keratinocytes allows certain methods to be utilized for study without cross contamination (i.e. microarray analysis), iii) BCM can be produced in relatively large quantities and stored at -20 °C for future study.

Keratinocytes interacted with *S. aureus* biofilm in two ways: i) The biofilm co-culture model: Matured (three day old) *S. aureus* biofilms were placed in co-culture with confluent human keratinocytes or, ii) Bacterial conditioned medium model: *S. aureus* biofilms were matured for three days, placed in fresh growth medium, and after 24 hours, the biofilm conditioned medium was collected and given to confluent keratinocytes. A comparable co-culture model incorporating planktonic bacteria could not be readily devised. Planktonic cultures are maintained with constant agitation. This growth parameter for planktonic bacteria does not facilitate normal growth in mammalian cell cultures. Directly adding planktonic cells to keratinocytes would introduce effects caused by direct cell-cell contact between the host and pathogen, and the bacteria could be argued to form a biofilm over time. The fragile nature of the tissue culture insert membrane eliminated the possibility of agitating planktonic cultures inside of an insert with a magnetic stir bar or other mechanical mechanism. Because of these limitations, soluble excreted products from planktonic or biofilm *S. aureus* cultures grown in isolation and their effects on human keratinocytes were initially examined.

A planktonic culture similar in physiology, closely resembling the stationary growth of a biofilm, with similar cell densities was desired for comparison to the effects of *S. aureus* biofilm on human keratinocytes. To obtain such a culture, mature three day old biofilms were re-suspended into growth medium and grown at 37°C with constant agitation. This method effectively reverted *S. aureus* cells from a biofilm growth phase back to a planktonic growth phase.

Both the biofilm and planktonic cultures had comparable population densities and similar amounts of extracellular DNA and protein in the conditioned medium. 1D SDS-PAGE revealed that BCM and PCM consisted of different protein compositions rather than one simply having more or less of the same protein than the other. Smearing of the BCM samples indicated the presence of bacterial proteases. The presence of bacterial proteases in BCM may contribute to the pathogenesis of chronic wounds. Bacterial DNA has been shown to induce innate immune responses through recognition of conserved bacterial motifs [168]. Additionally, the presence of a narrow range of small fragments of extracellular DNA (~50-100 bp) in BCM may be indicative of nuclease activity in BCM. DNA processing by nucleases has been attributed to its pro-inflammatory nature in *S. aureus* [169].

Anoxic niches exist in bacterial biofilms, but the effect of oxygen deprivation caused by bacterial biofilms on the wound healing process has not been fully investigated. Increased oxygen levels in wounded tissue promotes the healing process by stimulating several activities including, degradation of necrotic wound tissue [170], collagen production [171, 172], neovascularization [173], phagocytosis [174], and

neutrophil-mediated oxidative microbial killing [175]. Presumably, oxygen levels in infected wounds would quickly be consumed by bacterial biofilms leading to the inhibition of the healing process. Oxygen levels in infected wounds are lower than oxygen levels in healthy skin [176]. Available oxygen in infected wounds has been shown to be primarily consumed by immune cells during the production of ROS to fight the invading microorganisms, leaving essentially no oxygen for the wound healing process [177].

S. aureus biofilms cultured in ambient air produced the mixed acid fermentation products propionate, formate, lactate, and acetate (Figure 9). These results indicated that *S. aureus* biofilms in our *in vitro* model harbor an anoxic niche. The presence of mixed acid fermentation products in BCM and not in PCM indicated that planktonic cultures of *S. aureus* were not growing in an anoxic environment. Planktonic anoxic cultures of *S. aureus* produced fermentation products found in BCM further supporting the presence of an anoxic core in the biofilm (Figure 11). Although several metabolites were shared between anoxic planktonic cultures and BCM, BCM is best described as a mix between the anoxic and aerobic metabolic profiles generated by NMR based metabolite profiling. However, the biofilm does contain unique metabolic profiles not found in the planktonic cultures, such as preferential amino acid metabolism over other available carbon sources such as glucose. Additionally, propionate, formate, lactate, and acetate production by bacterial biofilms in the oral cavity are known to be cytotoxic to human gingival keratinocytes, leading to damage of the gingival epithelium [178, 179]. The production

of fermentation products by *S. aureus* biofilm may contribute to the pathogenesis/ persistence of chronic wounds.

S. aureus biofilm caused an increase in pH in BCM (Figure 12). Additionally, *S. aureus* biofilms preferentially consume amino acids. Amino acid metabolism could lead to the liberation of the observed fermentation products, releasing ammonia through the deamination of amino acids, explaining the increase in pH in BCM. An increase in wound pH would inhibit the highly regulated progression of wound healing.

Bacterial conditioned medium and the EPI control in contact with keratinocytes for four hours produced mixed acid fermentation products (Figure 10). Fermentation products which were not present in PCM samples were present in PCM after contact with keratinocytes indicating that the keratinocytes were responsible for their production. The fermentation products produced by the keratinocytes are likely due to reduced levels of key nutrients such as glucose and amino acids originally present in the EPI culture medium. These depleted conditions may lead to the initiation of alternative metabolic pathways accounting for the production of the observed fermentation byproducts. The production of lactate by keratinocytes under all conditions including controls was observed. Lactate production by keratinocytes *in vivo* and *in vitro* helps to maintain the normally acidic nature of the skin, and the increased production of lactate in epidermal cultures in response to bacterial infection has been described [180].

NMR metabolite profiling provided a representation of hydrophilic compounds present in BCM. The presence of hydrophobic molecules was investigated using HPLC/MS. Hydrophobic molecules are, in general, more toxic to mammalian cells. This

is due to several factors including the accumulation of hydrophobic compounds in cell membranes and fatty tissues, the production of harmful ROS during their metabolism, and the transformed intermediates that are produced during their metabolism are often more harmful than the parent compound.

Two hydrophobic compounds were found to be produced in relatively high quantities by *S. aureus* biofilm relative to *S. aureus* planktonic cultures. While this dissertation was in preparation, Wyatt et al published the structures of two small non-ribosomal peptides produced by *S. aureus* which they named aureusimine A and aureusimine B [167]. Aureusimine A and B were found to regulate virulence genes in *S. aureus* and a mutant incapable of aureusimine production (Δ*ausA*) was not as virulent as the wild type. The small, hydrophobic molecules discovered in high quantities in BCM described in this dissertation were determined to be the aureusimines described by Wyatt et al.

The presence of aureusimine A and B in all Gram positive organisms tested suggests that this is a common metabolite produced during biofilm growth in many Gram positive species of bacteria (Table 6). Most importantly, aureusimine production was found to be several orders of magnitude higher in BCM relative to PCM. The higher levels of production of these molecules by *S. aureus* biofilm may induce the biofilm to become more virulent. This family of molecules could potentially be a therapeutic target for Gram positive species of bacteria in biofilm based diseases.

Wyatt et al isolated the aureusimines from planktonic cultures grown under fermentative conditions suggesting that a lack of oxygen may play a role in the

production of these molecules. The lower production of aureusimines in planktonic aerobic cultures of *S. aureus* relative to planktonic anoxic cultures suggests that aureusimine production is dependent upon an anoxic environment. The high production of aureusimine A and B in *S. aureus* BCM relative to PCM could be due to the anoxic niche present at the core of the biofilm. The relationship that these molecules share with oxygen availability and biofilm formation in *S. aureus* could possibly correlate with *S. aureus* virulence in general. Wounds infected with *S. aureus* biofilm could theoretically contain higher levels of aureusimine A and B due to the low oxygen tension induced by both the immune ROS burst, lack of functional vascularization, ischemia, and the anoxic nature of the biofilm.

Limitations of the *in vitro* model described in this dissertation are associated mainly with the biofilm and include the limited use of anaerobic bacteria, bacteria that swarm, and the absence of any physical contact between the biofilm and mammalian cells. Anaerobic bacteria cannot be incorporated into the co-culture version of this model as pure cultures due to the requirement of oxygen by the mammalian cell culture. This drawback may be overcome through the production of anaerobic bacteria conditioned medium in the absence of cultured cells. Alternatively, multispecies biofilms are capable of harboring anaerobic cultures due to pre-established anoxic niches deep within the biofilm. It was observed that bacteria that are capable of swarming (i.e., some isolates of *Pseudomonas aeruginosa*) quickly form a lawn of bacteria on the culture insert resulting in higher bacterial loads than intended. Non-motile species are ideal, but some strains capable of locomotion were found to form stable biofilms. Additionally, a lawn of

bacteria on the culture insert would likely deprive the cultured cells below the insert of oxygen.

A lack of physical contact between the biofilm and host cells absolutely influences any result observed utilizing this model. While this is very useful when techniques are employed that require the separation of the host and pathogen for analysis, effects induced by direct host/pathogen contact may be overlooked. These limitations are tolerable when taken in the light of the evidence presented in this dissertation. Experiments utilizing this *in vitro* model have provided clues about the potential effects of soluble products produced by bacterial biofilms in chronic wounds. Bacterial biofilms are widely accepted as the native phenotype in many natural settings including chronic wound infections. The underlying principal of this model could be applied to other infectious diseases by simply substituting bacterial species and cell cultures to suit various diseases. Studying the effects of bacterial biofilms rather than planktonic cultures using this *in vitro* model provides a more relevant way to study the biology of chronic wound biofilm infections.

CHAPTER 5

S. AUREUS BIOFILM CONDITIONED MEDIUM INDUCES A DISTINCT INFLAMMATORY RESPONSE AND INHIBITS PROCESSES ASSOCIATED WITH EPITHELIALIZATION IN HUMAN KERATINOCYTES

Introduction

Chronic wounds are unable to coordinate the phases of wound healing leading to an inflammatory environment in the wounded area that is unable to epithelialize. Keratinocytes are the main cell type in the epidermis and are essential in both the inflammatory and re-epithelialization phases of wound repair. The presence of bacterial biofilm in non-healing wounds is assumed by a growing number of physicians and clinicians to contribute significantly to the persistent nature of the wound. Often, patients with chronic wounds acquire pathogenic bacteria such as *S. aureus* through routine visits to hospitals and/or clinics. *S. aureus* is an important human pathogen that is associated with several skin diseases. The correlation of bacterial biofilms with chronic infections and not acute infections suggests that differential routes of pathogenesis in infected skin [41]. The effects of *S. aureus* planktonic and biofilm conditioned medium on wound healing processes in human keratinocytes were investigated using the *in vitro* biofilm disease model described in the previous chapter.

Materials and Methods

Cell Culture

As described in Chapter 4.

Bacterial Strains and Culture Conditions

As described in Chapter 4.

Conditioned Medium Microarray

Human foreskin keratinocytes (HFKs) were grown to 90% confluency in six well plates. Cells were then treated with 2 ml BCM, PCM, or fresh EPI for four hours. After treatment, the medium was removed and RNA was isolated using an RNeasy minikit (Qiagen, Valencia, CA) following the manufacturer's instructions for adherent cells. Extracted RNA was then ethanol precipitated and resuspended in water as previously described [181]. The following steps were performed at the Functional Genomics Core at Montana State University. RNA concentrations and purity were determined by measuring absorbencies at 260nm and 280nm on a GeneQuant spectrophotometer. RNA quality was evaluated using the RNA 6000 NanoChip assay on a 2100 Bioalyzer (Agilent Technologies, Palo Alto, CA). RNA integrity number results for all samples used exceeded 9.5 on a scale to 10.

Total RNA (500ng) was reverse transcribed, and amplified and biotin-labeled via in vitro transcription using the MessageAmp Premier kit (Ambion). The resulting cRNA was fragmented and hybridized to Affymetrix GeneChip Human Genome U133A 2.0 arrays (#900468, Affymetrix, Santa Clara, CA) at 45^{o}C for 16 hours with constant rotational mixing at 60 rpm. Washing and staining of the arrays was performed using the Affymetrix GeneChip Fluidics Station 450. Arrays were scanned using an Affymetrix GeneChip Scanner 7G and GCOS software version 1.4.

Microarray data were analyzed using FlexArray version 1.4. The Affymetrix CEL files were imported and normalized using GC-RMA. Genes were filtered for threshold signal intensities of at least 50 in one biological replicate. Analysis of Variance (ANOVA) was performed to identify statistically significant differences among the three conditions. 910 genes were identified (p-value < 0.01). The gene list was further trimmed to identify genes with fold-change differences of at least 1.5 in any comparison, resulting in 575 genes. The log2 values were imported into Genesis [182] for visualization and hierarchical clustering. Subsequent functional enrichment analysis was conducted using the database for annotation, **v**isualization and **i**ntegrated discovery (DAVID) software [183]. Data were submitted to Gene Expression Omnibus (NCBI) under accession GSE24118. A complete list of genes significantly regulated can be found in Appendix C.

Co-Culture Microarray

HFKs were grown to 90% confluency in six well plates. Mature *S. aureus* biofilms (three day old) grown on tissue culture inserts were placed in contact with the keratinocytes for 24 hours. After this time, RNA was extracted from the keratinocytes. RNA was sent to Research and Testing Laboratory (Lubbock, TX) and quantified using a spectrophotometry system (NanoDrop Technologies, Wilmington, DE). RNA quality was confirmed using a BioRad Experion system (BioRad, Hercules, CA). For each sample, 5 µg of RNA was converted to cDNA and labeled with either CyDye3-dCTP or CyDye5-dCTP (PerkinElmer , Waltham, MA) in a crossover dyeswap design using the LabelStar kit (Qiagen Inc.) and random nonomers (Integrated DNA Technologies,

Coralville, IA). Labeled cDNA was hybridized to the microarray using Agilent Hi-RPM hybridization solution in an Agilent Hybridization chamber (Agilent Technologies, Santa Clara, CA). A total of 8 arrays based upon the Agilent Human GE 4x44K v2 Microarray (4 biological replicates), were analyzed to obtain genes that were consistently and differentially regulated. Microarray images were captured using a Genepix 4000B (Molecular Devices Corporation, Union City, CA) laser scanner and images processed using GenePix 6.0 software (Molecular Devices Corporation). Microarray data analyses were performed using Acuity 4.0 software (Molecular Devices Corporation, Union City, CA). The signal intensity of each gene was globally normalized using LOWESS within the R statistics package. The normalized data was analyzed using commercial SAS 9.1.3 program (SAS Institute Inc. Cary, NC). An approximate F test on least-square means was used to estimate the significance of difference for each gene in each comparison. Data were analyzed based upon log ratio (635/532) values. Genes were included in the final dataset that exhibited at least 2.0-fold comparative regulation and p-values corrected for multiple comparisons based upon False Discovery Rate (FDR) < 1% (Benjamini-Hochberg $p < 0.01$). Annotations and functional enrichment analyses were derived using the DAVID website (david.abcc.ncifcrf.gov) to evaluate functional clustering and functional category enrichments with *Homo sapiens* as the background genome. Data were submitted to Gene Expression Omnibus (NCBI) under accession GSE24370. A complete list of genes significantly regulated can be found in Appendix D.

RT-qPCR

Keratinocytes were grown to 90% confluency in six well plates. Cells were then treated with BCM, PCM, or fresh EPI for various times. After treatment, the medium was removed and RNA was isolated using an RNeasy minikit (Qiagen, Valencia, CA) following the manufacturer's instructions for adherent cells. Extracted RNA was then ethanol precipitated as previously described [181]. RNA pellets were resuspended in 30 µl of water and quantified using the NanoDrop® ND-1000 UV-vis spectrophotometer (Thermo Fisher Scientific Inc. Wilmington, DE). Reverse transcription PCR (RT-PCR) was performed using the QuantiTech reverse transcription kit (Qiagen, Valencia, CA) following the manufacturer's instructions using 500 ng of template RNA. Quantitative PCR (qPCR) was carried out using the QuantiFast SYBR green PCR kit (Qiagen, Valencia, CA). All reactions contained 2 µl cDNA and 300 nM of each primer. Validated qPCR primer sets for CYP1A1 and CYP1B1 were purchased from SABiosciences, Frederick, MD.

Microscopy

Keratinocytes were grown to 80–90% confluence on 18 mm^2 cover slips placed in six-well plates. Afterwards, the keratinocytes were exposed to 2 ml of BCM or PCM. After various times of exposure, the keratinocytes were fixed in 4% paraformaldehyde in phosphate-buffered saline (PBS) for 15 minutes at 37 °C followed by three 5 minute washes in PBS. Cells were then permeablized with 0.2% Triton-X 100 for 5 minutes at room temperature, followed by three 5 minute washes in PBS. Keratinocytes were then stained for F-actin (BODIPY phalloidin, Invitrogen, Carlsbad, CA), β-tubulin (anti β-

tubulin monoclonal antibody conjugated to AlexaFluor 568, Cell signaling Technology, Danvers, MA) and DNA (TOPRO-3 Iodide, Invitrogen) following the manufacturer's instructions. The slides were then mounted using Vectashield® H-1000 (Vector Laboratories, Burlingame, CA) and imaged immediately. Laser scanning confocal microscopy (LSCM) was performed on a Leica TCS-SP2 AOBS confocal microscope with a 100x oil immersion objective unless otherwise noted. Control cultures were also stained and consisted of keratinocytes exposed to EPI.

Time lapse microscopy on keratinocytes exposed to BCM, PCM, or EPI was performed using light microscopy. Keratinocytes were grown to 80–90% confluence in 35 mm non-coated glass bottom Petri dishes (MatTek, Ashland, MA). Two hours before imaging, both the keratinocytes and the experimental solution were placed at room temperature to allow the temperature to equilibrate. Immediately before imaging, the cell culture medium was exchanged to the experimental solution and the cells were imaged using a 16x or 60x water immersion objective. Bright-field images were captured every 45 seconds for 4 hours with an 18-ms exposure rate.

Terminal Deoxynucleotidyl Transferase dUTP Nick End Labeling (TUNEL) Assay

TUNEL staining was used to investigate the induction of late stage apoptosis. Keratinocytes were grown to 80–90% confluence on 18 mm^2 cover slips placed in six-well plates. Afterwards, keratinocytes were exposed to 2 ml BCM, PCM, or EPI. At various time points, keratinocytes were fixed in 4% paraformaldehyde in PBS for 15 minutes at 37 °C followed by three 5-minute washes in PBS. The APO-BrdU TUNEL

Assay Kit (Invitrogen, Carlsbad, CA) was used following the manufacturer's staining protocol with one modification. Keratinocytes were not brought into suspension; rather, all enzyme solutions were made in the same proportions suggested by the manufacturer, and were added directly to the coverslip. Coverslips were then imaged using a Nikon Eclipse E800 epifluorescent microscope using a 10x oil immersion objective. For analysis, four images of each condition were taken and the numbers of adherent cells staining positive for TUNEL (total cell number positive for apoptosis) or propidium iodide (total cell number) were counted and the percentage of cells staining positive for TUNEL was calculated.

Measurement of Intracellular Calcium

Fluo-4 AM (Invitrogen, Carlsbad, CA) was used to assay intracellular calcium levels in keratinocytes after exposure to BCM or PCM. Two mls of a 3 μM solution of Fluo-4 AM was prepared in fresh EPI and incubated at room temperature with 80-90% confluent keratinocytes grown in glass bottom microwell dishes (MatTek Corporation, Ashland, MA) for 30 minutes. Cells were washed twice with room temperature PBS for 5 minutes. Three mls of EPI, BCM, or PCM were then added to fluo-4 AM loaded cells. Images were captured every 45 seconds for four and one half hours on a Leica TCS-SP2 AOBS confocal microscope with a 63X water immersion objective.

Cytokine Detection by Enzyme-Linked Immunoassays (ELISA)

Confluent HaCaT keratinocytes in 6-well plates were cultured in the presence of 2 ml bacterial conditioned medium (BCM or PCM) or EPI for various exposure times. Cell

culture supernatants were collected and analyzed by colorimetric sandwich ELISA for IL-1β, IL-6, TNF-α, CXCL-8, CXCL-1, and GM-CSF (R&D Systems, Minneapolis, MN) following the manufacturer's instructions. ELISA data were normalized to adherent, non-apoptotic cell numbers using the delta method.

Detection of MAPK Phosphorylation Using Cell-Based ELISAs

HaCaT keratinocytes were grown to confluency in clear bottom black 96-well plates. HaCaT cells were treated with 100 µl BCM, PCM, or EPI for various times. Total and phosphorylated MAPKs (JNK, p38, and ERK) were detected simultaneously using a cell-based ELISA (R&D Systems, Minneapolis, MN) following the manufacturer's instructions.

Inhibition of MAPK

The p38 MAPK inhibitor, SB203580 (4-[4-fluorophenyl]-5-[4-pyridyl]-1*H*-imidazole); the ERK inhibitor, U0126 (1,4-diamino-2,3-dicyano-1,4-bis[2-aminophenyl-thio]butadiene); and the JNK inhibitor, SP600125 (anthrax(1–9-c-d)pyrazol-6(2*H*)-one; 1,9-pyrazoloanthrone) were prepared as 10 mM DMSO stocks (Cayman Chemicals, Ann Arbor, MI). HaCaT keratinocytes were pretreated with individual inhibitors or a combination of all three inhibitors (10 µM each, 0.1% DMSO) in EPI growth medium for one hour. Cells were then treated with PCM or BCM supplemented with 10 µM inhibitor(s) for four hours. Cell culture supernatants were collected and analyzed by ELISA for cytokine production. HaCaT keratinocytes treated with PCM or BCM supplemented with 0.1% DMSO were prepared as vehicle controls.

Results

Epithelialization

S. aureus Biofilms Induce Changes in Keratinocyte Morphology. Initial experiments with both the co-culture biofilm and BCM models revealed massive changes in cell morphology in keratinocytes. Similar changes in morphology were observed in primary human fibroblasts exposed to BCM as well (Appendix E). Keratinocytes exposed to BCM underwent rapid changes in morphology with the first signs occurring about an hour after exposure and major changes occurring after 90 minutes (Figure 19). BCM induced changes included the formation of spiny dendritic-like structures, rounding of the cell body, cell retraction, and condensation of the nucleus. Keratinocytes exposed to *S. aureus* biofilm in the co-culture model showed the same morphological changes, but on a longer timescale with changes occurring after 10-12 hours.

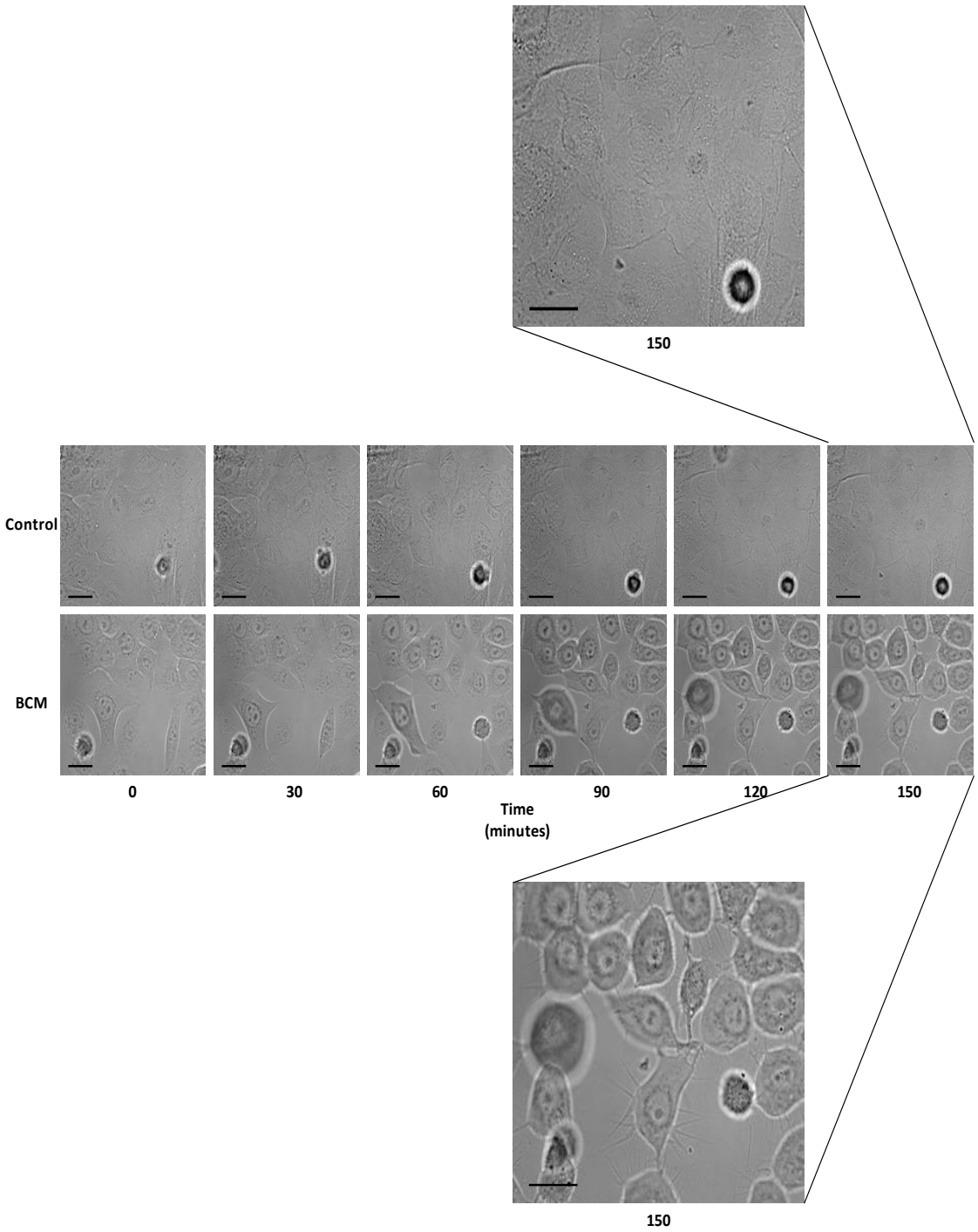

Figure 20. Time lapse microscopy of foreskin keratinocytes in contact with BCM. BCM induces a rapid change in cell morphology with cells losing adhesion to the bottom of the plate and each other as cells begin to retract. At 90 minutes the cell body rounds and comes out of the focal plane while spiny dendritic like extensions extend from the cell in the focal plane indicating that the dendritic like extensions are formed on the surface of the dish. Dendritic like extensions and rounded cell bodies can be viewed in the enlarged image of BCM treated keratinocytes at 150 minutes. Control and PCM treated cells do not show these characteristic changes in morphology. 60x water immersion objective, bar represents 20 µm.

The observed morphological changes induced by both BCM and *S. aureus* biofilm in the co-culture model likely involved re-arrangement of major cytoskeletal structure proteins such as filamentous actin (F-actin) and tubulin. F-actin and β-tubulin were imaged by LSCM to obtain more insight into the specific morphologies of these major cytoskeletal components in keratinocytes treated with BCM and PCM. HFKs and HaCaT keratinocytes were exposed to BCM, PCM, or EPI, stained, and imaged using LSCM (Figure 20).

Microtubules in BCM treated cells formed dense cables around the periphery of severely affected keratinocytes with projections protruding from the body of the cell. Stabilization of microtubules with the anti-cancer drug Taxol (Paclitaxel) inhibited the characteristic BCM induced morphology changes (Figure 21). The actin cytoskeleton formed several spiny dendritic like structures that did not positively stain for β-tubulin after exposure to both *S. aureus* biofilm and BCM (Figure 20).

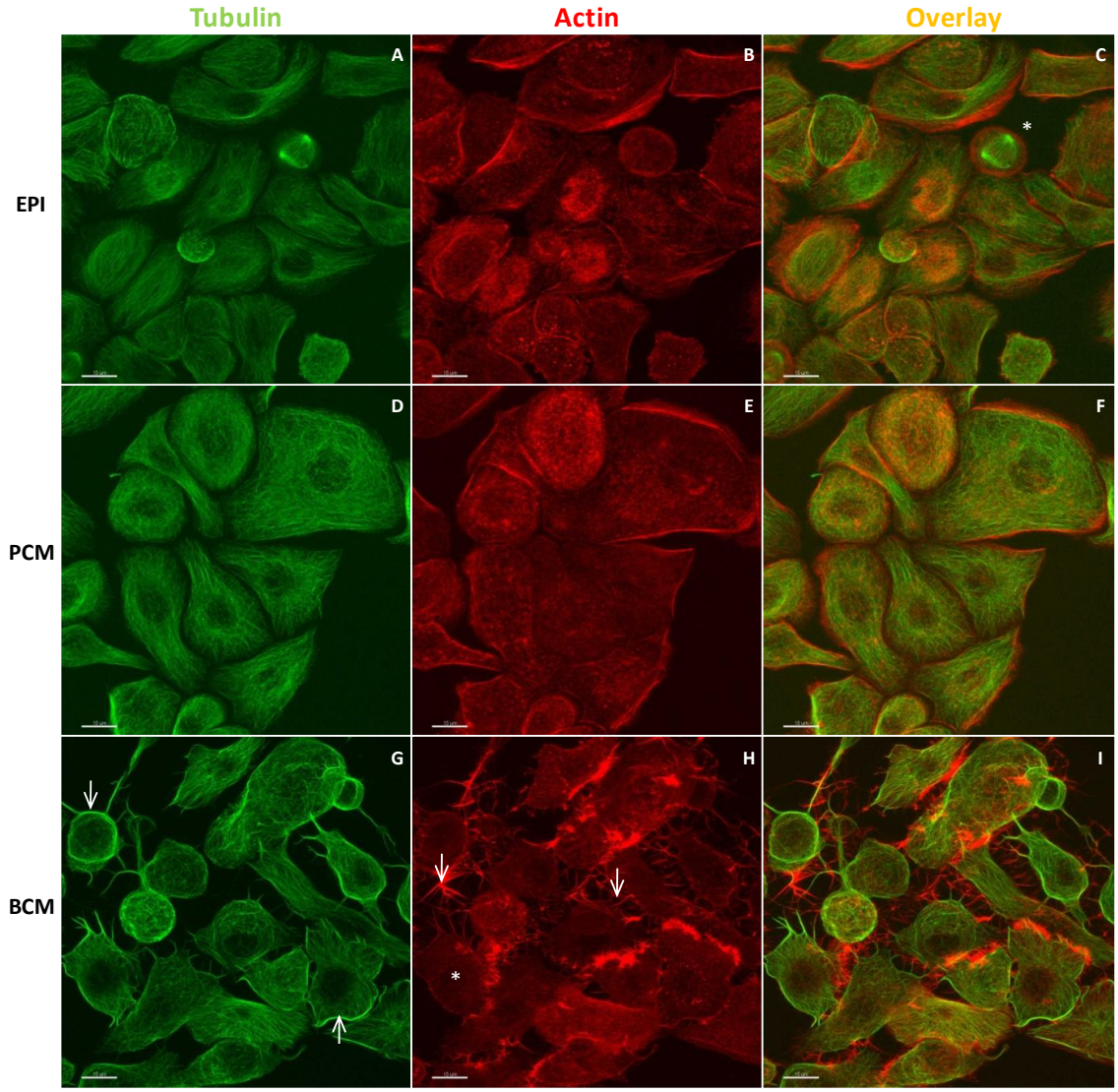

Figure 21. CSLM of HaCaT keratinocytes exposed to EPI, PCM, or BCM. BCM treated cells have an altered microtubule (Green) structure with microtubules polymerizing around the periphery of the cell body (arrows, G). The actin cytoskeleton (Red) formed several spikes extending from the cell body (arrows, H), which itself stains weakly for F-actin (*, H). Morphology of PCM treated cells was similar to that of control cells with the notable exception that no cells were observed to be undergoing mitosis, as observed in control cells (*, C). 100x oil objective, bars represent 15 µm.

PCM treated cells and control cells shared a similar morphology of branched networks of microtubules and microfilament structures. Identical morphological changes were observed in both the HaCaT cell line and HFKs (Compare Figure 20 and Figure 22) and with BCM derived from several different strains of *S. aureus* including methicillin resistant and susceptible strains. Disorganization of the microtubule and microfilament

networks in keratinocytes stimulated with BCM likely inhibits keratinocyte proliferation and migration which would lead to impaired wound healing. In addition to cytoskeletal rearrangements, microarray analysis revealed that BCM induced the expression of the small GTPase Gem, which is involved in regulating cytoskeletal architecture (Appendix F).

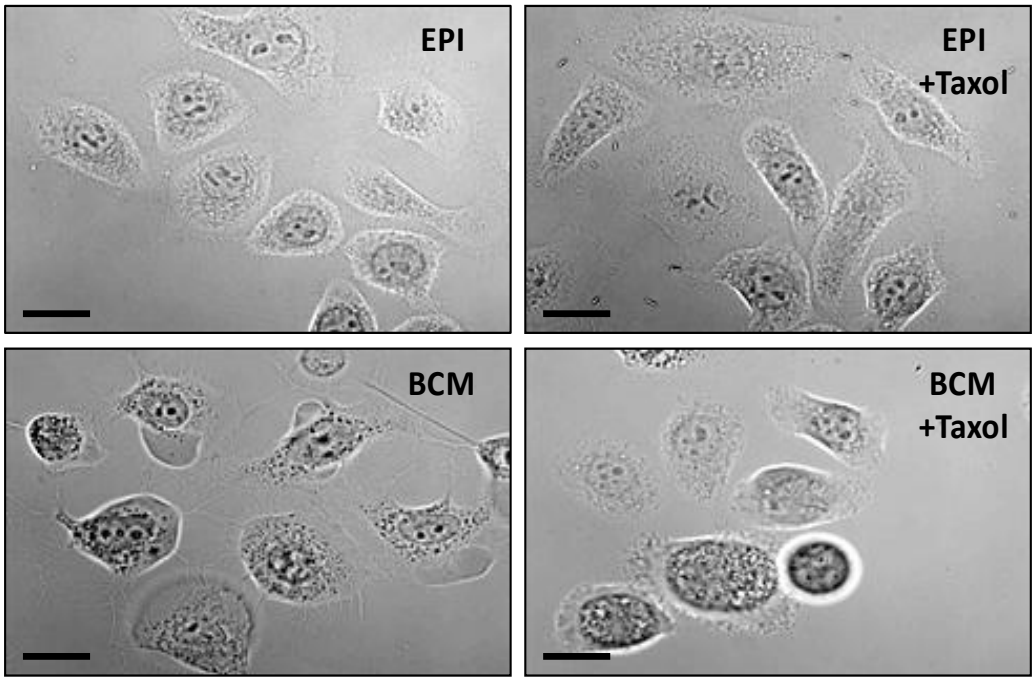

Figure 22. Pretreatment of keratinocytes with Taxol prior to exposure to BCM prevented the characteristic morphology changes induced by BCM. BCM +Taxol treated cells resemble the morphology of EPI +Taxol treated cells. 60x water immersion objective, bar represents 20 µm.

S. aureus Biofilms Induce Apoptosis in Human Keratinocytes

In addition to the formation of dendritic like extensions, changes in nuclear morphologies were apparent in BCM treated keratinocytes. Nuclei of BCM treated cells were highly fragmented indicating late stage apoptosis while control and PCM treated cells retained normal nuclear morphologies (Figure 22). BCM was also found to reduce peroxisome and lysosome levels in BCM treated HFKs (Appendix G).

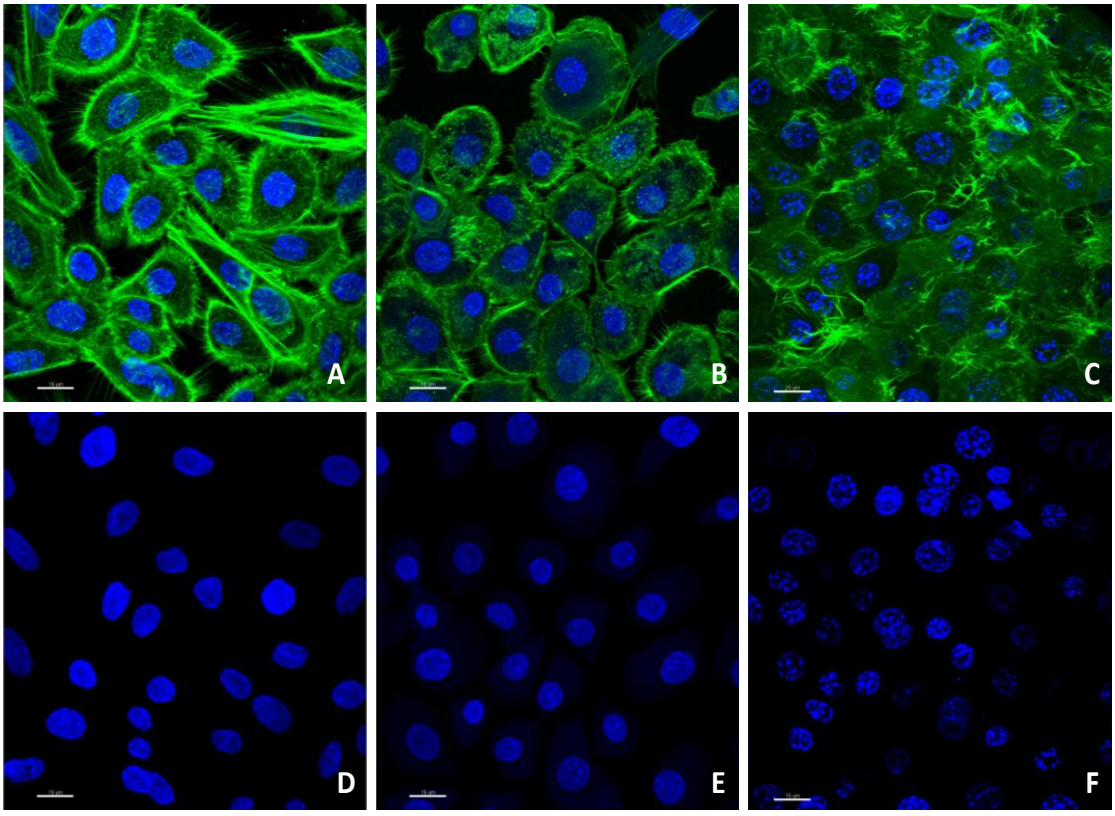

Figure 23. HFKs stained for F-actin (green) and nuclei (blue) after 24 hours of exposure to BCM, PCM, or EPI. Top row: Overlaid images of F-actin and nuclei. Bottom row: Images of nuclei associated with images in top row. Keratinocyte control cells (A, D). Keratinocytes treated with PCM (B, E). Keratinocytes treated with BCM (C, F). PCM treated cells and control cells have normal nuclear morphologies (D, E) while BCM treated cells show highly fragmented nuclei indicating late stage apoptosis (F). 100x oil objective, bars represent 15µm.

Nuclear fragmentation associated with late stage apoptosis in BCM treated keratinocytes was further examined using TUNEL. The percentage of HFKs and HaCaT keratinocytes staining positive for apoptosis is shown in Figure 23 and Figure 24, respectively. Additionally, it was found that BCM treated HFKs and HaCaT cells detached from the bottom of the culture dish after 24 hours (Figure 24). Human foreskin fibroblasts were also observed to undergo apoptosis after exposure to BCM (Appendix E).

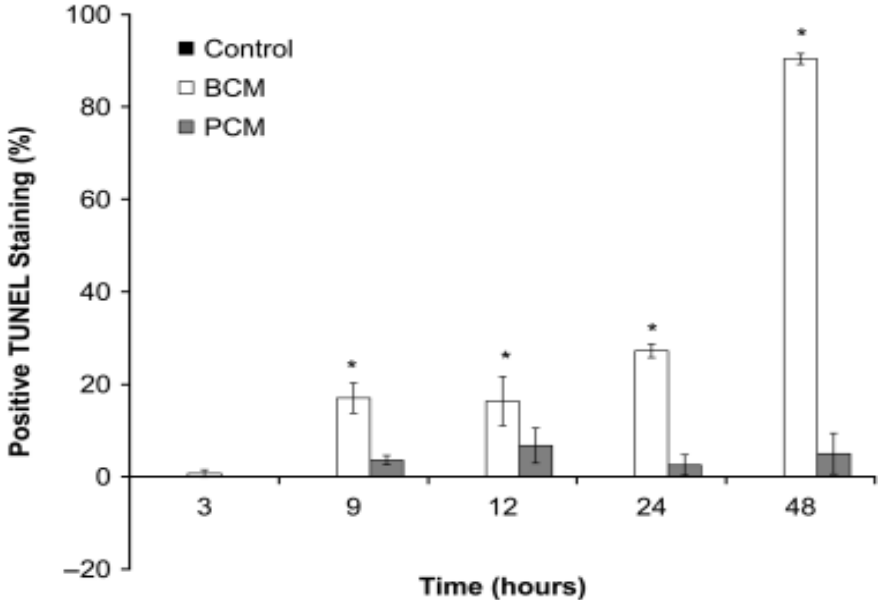

Figure 24. Percentage of HFK cultures staining positive for terminal deoxynucleotidyl transferase dUTP nick end labeling (TUNEL). Note: The control cultures had zero positive TUNEL staining in adherent cells at all time points. Results represented as mean ±standard deviation, n=3. *Significantly different from controls at $p < 0.005$.

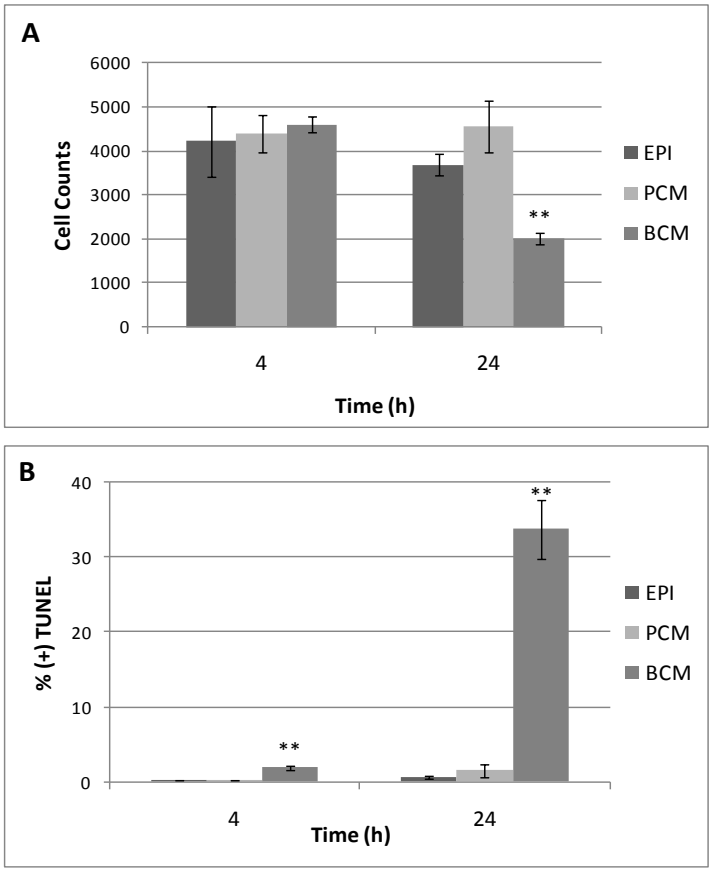

Figure 25. A. Total cell counts from propidium iodide stained HKs. B. Percentage of HKs staining positive for TUNEL, indicating late stage apoptosis. TUNEL data represents positive TUNEL cell counts over total cell counts from (A). Results represented as mean ± standard deviation, n=4 (**, $p<0.01$).

Apoptosis was induced at significantly greater levels in both HFK and HaCaT keratinocytes compared to controls after exposure to BCM. Apoptotic cell levels were similar in both control and PCM treated cells. Interestingly, unknown cell types present in the HFK culture and absent in the HaCaT cell line were found to be resistant to apoptosis after 48 hours of exposure to BCM (Appendix H). These novel results show that soluble products secreted by *S. aureus* biofilm are sufficient for the induction of apoptosis and direct contact is not required while soluble products from planktonic *S. aureus* do not induce apoptosis in HFKs or HaCaT keratinocytes.

Increase of Intracellular Calcium
Levels in BCM Stimulated Keratinocytes

Release of intracellular calcium stores often mediate changes in cell morphology and apoptosis. The calcium sensitive dye fluo-4 AM was used to measure relative levels of intracellular calcium release in human keratinocytes exposed to PCM or BCM.

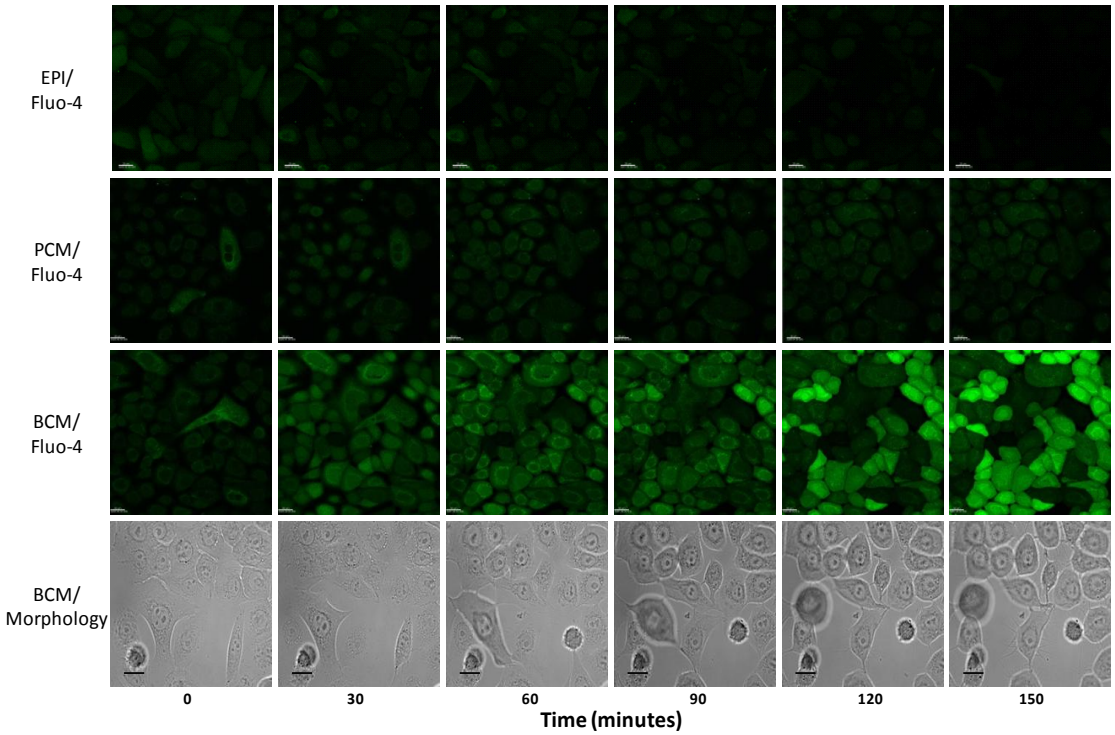

Figure 26. CSLM time lapse microscopy revealed intracellular calcium levels increase in BCM treated HFKs (green fluorescing cells) as indicated by the calcium sensitive dye Fluo-4 AM. Intracellular levels of calcium began to increase significantly at about the same time changes in morphology were observed in BCM treated cells. The lack of fluorescence in PCM treated cells indicates that intracellular calcium levels do not increase in response to PCM. 60x water immersion objective, bars represent 15 µm.

A significant increase in calcium levels in BCM treated cells over control levels correlated well with the time the observed morphology changes took place (Figure 25). Intracellular calcium levels were increased after 4 hours of exposure to BCM while PCM induced intracellular calcium levels remained near or below background. When keratinocytes were incubated with BCM or PCM for 21 hours and spiked with Fluo-4, a

rapid increase in intracellular calcium was again observed in BCM stimulated keratinocytes (Figure 26). These data indicate that BCM induces continual stimulation of intracellular calcium in keratinocytes.

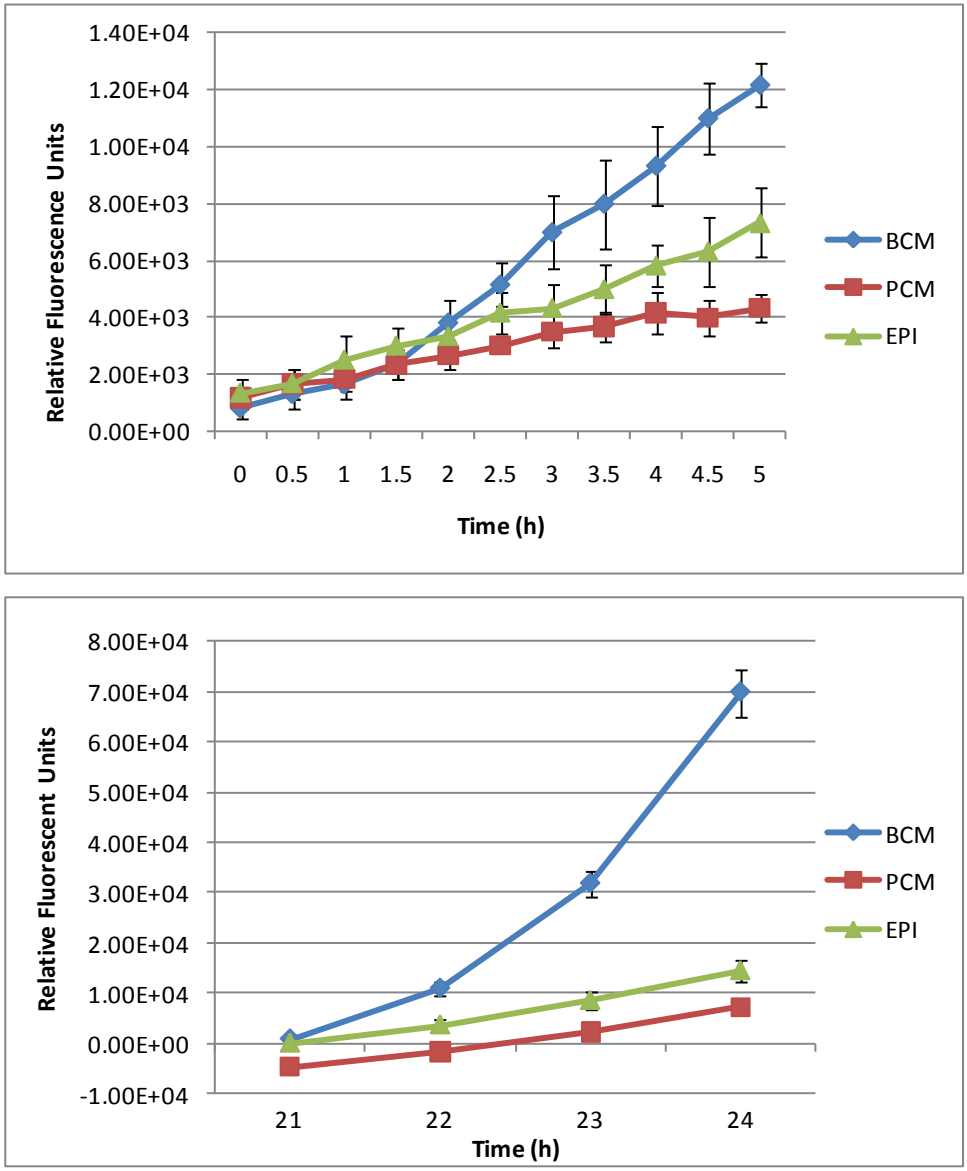

Figure 27. Relative levels of intracellular calcium in HaCaT cells exposed to BCM, PCM, or EPI were measured with a fluorescent plate reader using the calcium sensitive dye fluo-4 AM. BCM induces the release of relatively more intracellular calcium than control or PCM treated cells. Error bars represent standard deviation of the mean of 6 experiments.

Inflammation

S. aureus Biofilm Upregulates Genes Associated with Inflammation in Human Keratinocytes. The transcriptional response of HFKs exposed to BCM or *S. aureus* biofilm in the co-culture model were examined. Transcriptional responses in HFKs exposed to PCM or BCM were analyzed after 4 hours of stimulation. The effects of *S. aureus* biofilm on the transcriptome of HFKs in the co-culture model were examined after 24 hours of co-culture. This 24 hour time point is comparable to the conditioned medium experiments since BCM and PCM were harvested after 24 hours of bacterial conditioning. A shorter exposure time (4 hours) to bacterial conditioned medium was examined since bacterial products present in the growth medium were assumed to be at higher initial concentrations. Additionally, at 4 hours keratinocytes exposed to BCM had already undergone the observed morphology changes but had not yet started late stage apoptotic programs. These two approaches were taken to evaluate transcriptional response of keratinocytes exposed to planktonic or biofilm bacterial products in the conditioned medium or continual communication through secreted products between keratinocytes and *S. aureus* biofilm in the co-culture model.

Analysis of microarray data revealed changes in several genes related to a pro-inflammatory response. Several of the inflammatory genes upregulated by BCM included pro-inflammatory cytokines and chemokines (Table 7).

Table 7. Pro-inflammatory genes upregulated in BCM treated HFKs.

Gene Name	Gene Symbol	Fold Change (4 h) PCM v control	BCM v Control	BCM v PCM	p-value
Pro-Inflammatory					
interleukin 8	IL8	6.14	64.43	10.49	4.01E-07
chemokine (C-X-C motif) ligand 2	CXCL2	6.21	62.11	10.00	3.08E-07
tumor necrosis factor alpha	TNF α	3.05	27.73	9.10	4.00E-05
chemokine (C-X-C motif) ligand 3	CXCL3	1.82	12.23	6.72	6.65E-04
interleukin 6	IL6	1.06	3.40	3.20	1.79E-03
vascular endothelial growth factor A	VEGFA	3.93	8.08	2.05	1.12E-04
colony stimulating factor 3 (granulocyte)	CSF3/G-CSF	1.54	2.84	1.84	6.73E-05
colony stimulating factor 2 (granulocyte-macrophage)	CSF2/GM-CSF	2.43	4.24	1.75	5.36E-04
chemokine (C-X-C motif) ligand 1	CXCL1	13.86	20.81	1.50	5.34E-04
chemokine (C-C motif) ligand 20	CCL20	12.01	13.92	1.16	2.94E-03

These pro-inflammatory genes were upregulated in PCM treated cells relative to control cells as well, with the exception of IL-6, which was not significantly induced in HFKs exposed to PCM. BCM treated keratinocytes showed a much stronger induction of pro-inflammatory genes indicating that *S. aureus* BCM induced a stronger pro-inflammatory transcriptional response than PCM.

Table 8. Inflammatory genes significantly regulated in HFKs in the *S. aureus* biofilm co-culture model after 24 hours of co-culture. P<0.01.

Gene Name	Gene Symbol	Fold Change (24 h) Biofilm v control
Cytokines and Chemokines		
Interleukin 6	IL6	12.31
Interleukin 8	IL8	11.41
Chemokine (C-C Motif) Ligand 7	CCL7	11.25
Interleukin 24	IL24	9.83
Colony Stimulating Factor 2 (Grannulocyte/Macrophage)	CSF2/GM-CSF	7.75
Interleukin 1 β	IL1B	6.97
Chemokine (C-X-C motif) ligand 2	CXCL2	4.34
Chemokine (C-X-C motif) ligand 3	CXCL3	3.75
Chemokine (C-X-C motif) ligand 5	CXCL5	3.66
Chemokine (C-C Motif) Ligand 2	CCL2	3.44
Chemokine (C-X-C motif) ligand 1	CXCL1	3.24
Chemokine (C-X-C motif) ligand 6	CXCL6	3.10
Colony Stimulating Factor 3 (Grannulocyte)	CSF3/G-CSF	2.41
Interleukin 1 α	IL1α	2.32
Tumor Necrosis Factor Ligand Superfamily Member 15	TNFSF15	2.11
Prostaglandin Production		
Cylcooxygenase 2	PTGS2/COX-2	4.46
Prostaglandin E Synthase	PTGES	2.09
Phospholipase A2, Group Iva	PLA2G4A	1.50

A similar pro-inflammatory transcription profile was observed in the 24 hour co-culture microarray data (Table 8). Genes involved in prostaglandin synthesis were upregulated in keratinocytes in the co-culture model indicating further activation of pro-inflammatory networks. Several transcription factors that regulate inflammation were upregulated in keratinocytes treated with BCM (Table 9). Many of the upregulated transcription factor genes belong to the AP-1 family of transcription factors.

Table 9. Transcription factors induced in PCM and BCM treated HFKs after four hours of contact. Several members of the AP-1 family of transcription factors were induced in BCM treated cells. Other transcription factors such as EGR1 and NFkBIA indicate the regulation of other signaling pathways known to mediate inflammatory responses.

		Fold Change (4 h)			
Gene Name	Gene Symbol	PCM v control	BCM v Control	BCM v PCM	p-value
Transcription					
AP-1 family of transcription factors					
v-fos FBJ murine osteosarcoma viral oncogene homolog	c-FOS	1.01	43.58	42.97	2.59E-03
activating transcription factor 3	ATF3	1.42	13.63	9.61	1.06E-03
jun oncogene	c-JUN	1.78	3.64	2.05	3.54E-05
jun B proto-oncogene	JUNB	2.31	3.65	1.58	1.48E-05
Other transcription factors					
early growth response 1	EGR1	-1.10	17.79	19.58	4.80E-03
basic helix-loop-helix family, member e40	BHLHE40	1.44	13.58	9.46	1.40E-03
hairy and enhancer of split 1, (Drosophila)	HES1	1.80	13.71	7.62	8.00E-05
zinc finger protein 36, C3H type, homolog (mouse)	ZFP36	1.76	7.08	4.02	4.99E-05
RanBP-type and C3HC4-type zinc finger containing 1	RBCK1	1.05	1.84	1.76	4.46E-03
nuclear factor of kappa light polypeptide gene enhancer in B-cells	NFKBIA	2.35	3.65	1.55	1.17E-04

S. aureus BCM and PCM Induce Differential Temporal Cytokine and Chemokine Production in Human Keratinocytes

ELISA assays were used for further investigation of cytokine and chemokine production induced in HFKs by BCM or PCM. The cytokines IL-1β, IL-6, TNF-α, GM-CSF, and chemokines CXCL-8 and CXCL-1 were selected for further study. This battery of cytokines and chemokines were selected based on the microarray data and for comparison to other investigations of inflammatory responses induced by bacteria.

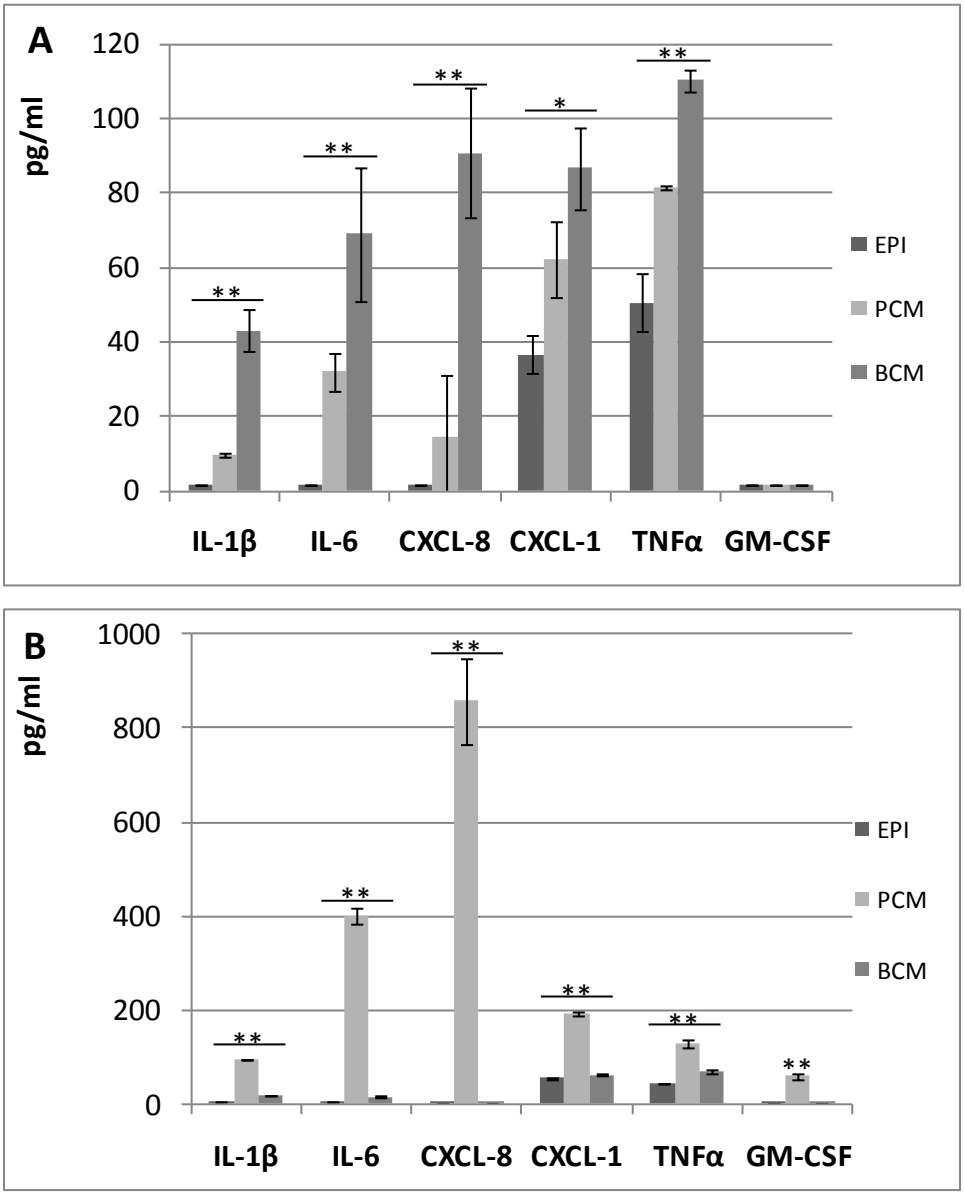

Figure 28. Cytokine and chemokine levels in keratinocytes after 4 (A) or 24 (B) hours of exposure to PCM, BCM, or EPI (pg/ml). Error bars represent standard deviation of the average of three experiments (*, $p<0.05$, **, $p<0.01$).

Cytokine production after 4 hours of stimulation was greater in BCM treated keratinocytes than in PCM treated keratinocytes (Figure 28). After 24 hours, PCM treated keratinocytes produced substantially more cytokines and chemokines than BCM treated keratinocytes. The observed decrease in cell numbers and apoptotic cell death induced by BCM were assumed to impact cytokine production. To adjust for this, cell numbers were counted for each time point and treatment condition. The percentage of apoptotic HaCaT keratinocytes at 4 and 24 hours (Figure 24) was used to calculate pg of cytokine produced per 100,000 adherent, non-apoptotic cells (Figure 29).

Normalized cytokine levels revealed that BCM treated HaCaT cells initially produced more cytokines and chemokines after four hours, in agreement with microarray data for HFKs. Surprisingly, normalized cytokine levels in PCM treated HaCaT cells still exhibited the highest production of all cytokines and chemokines tested after four hours, with the exception of normalized levels of TNF-α.

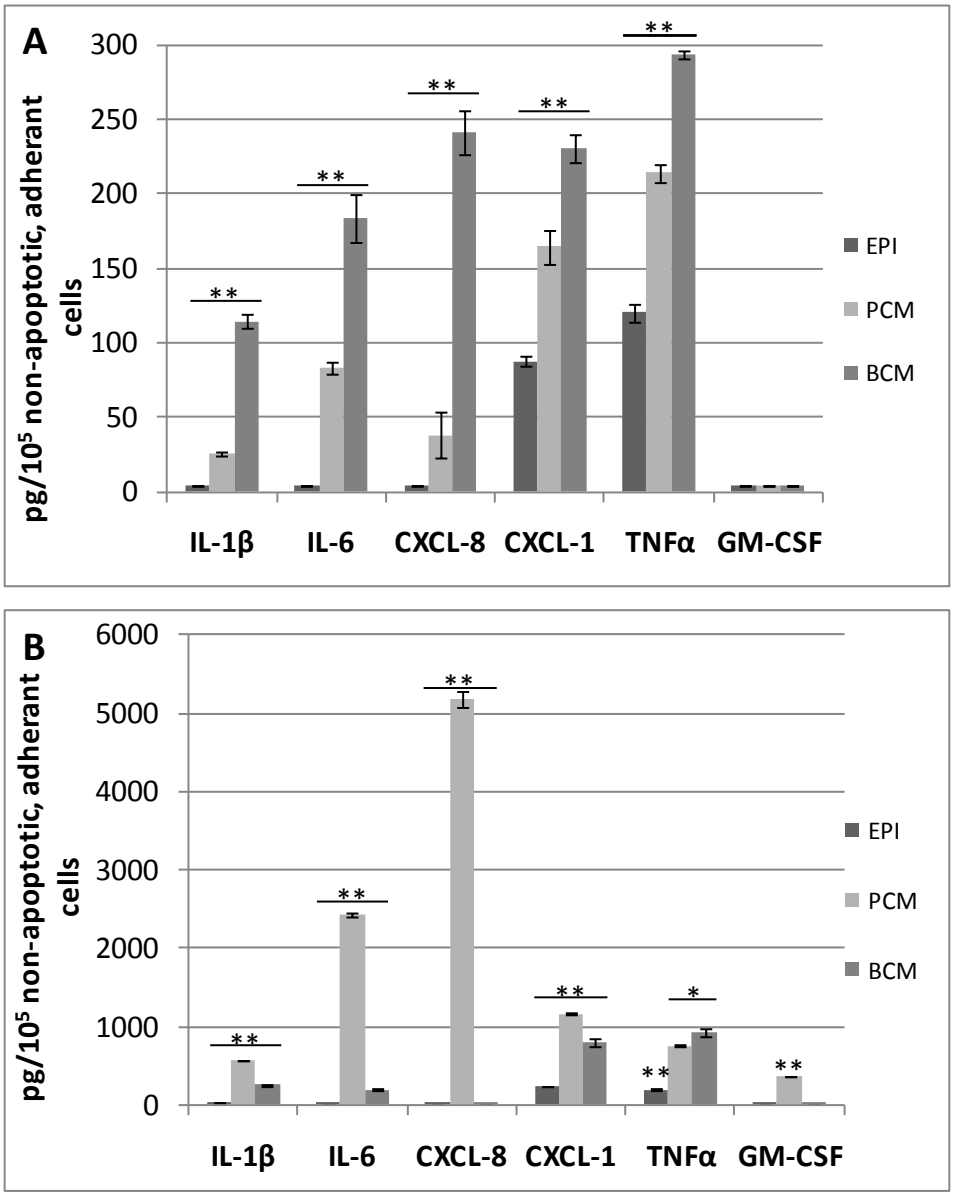

Figure 29. Cytokine and chemokine levels in keratinocytes after 4 (A) or 24 (B) hours of exposure to PCM, BCM, or EPI (pg protein / 100,000 non-apoptotic, adherent cells). Error bars represent standard deviation of the average of three experiments (*, $p<0.05$, **, $p<0.01$).

S. aureus BCM and PCM Differentially Modulate MAPK Phosphorylation in Human Keratinocytes

An enrichment analysis conducted using the DAVID functional annotation clustering tool revealed that genes associated with apoptosis, inflammation, serine/threonine kinase cascades, and NFkB signaling were significantly overrepresented ($p < 0.05$) in the set of genes upregulated in keratinocytes exposed to BCM. These data suggested that MAPK signaling may be differentially activated in HKs treated with BCM. Additionally, DUSP genes were more highly upregulated in BCM treated keratinocytes relative to PCM treated keratinocytes indicating differential regulation of MAPK cascades (Table 10). The role of MAPK signaling in PCM and BCM treated keratinocytes was investigated by measuring phosphorylation levels of JNK, p38, and ERK (Figure 29).

Table 10. DUSP genes are activated in keratinocytes exposed to both BCM (top) and *S. aureus* biofilm in the co-culture model (bottom), but not in PCM treated keratinocytes. Differential activation of DUSP genes in BCM and PCM treated cells indicates that MAPK pathways are differentially regulated under these conditions.

		Fold Change (4 h)			
Gene Name	Gene Symbol	PCM v control	BCM v Control	BCM v PCM	p-value
dual specificity phosphatase 1	DUSP-1	1.62	10.13	6.24	4.82E-04
dual specificity phosphatase 5	DUSP-5	2.88	2.96	1.03	5.72E-03

		Fold Change (24 h)
Gene Name	Gene Symbol	Biofilm v control
dual specificity phosphatase 1	DUSP-1	4.13
dual specificity phosphatase 10	DUSP-10	2.95

Levels of phosphorylated p38 and JNK in PCM treated keratinocytes increased after exposure to PCM while exposure to BCM reduced phosphorylation of both JNK and

p38. ERK phosphorylation was slightly increased in BCM treated keratinocytes and was not affected in PCM treated cells.

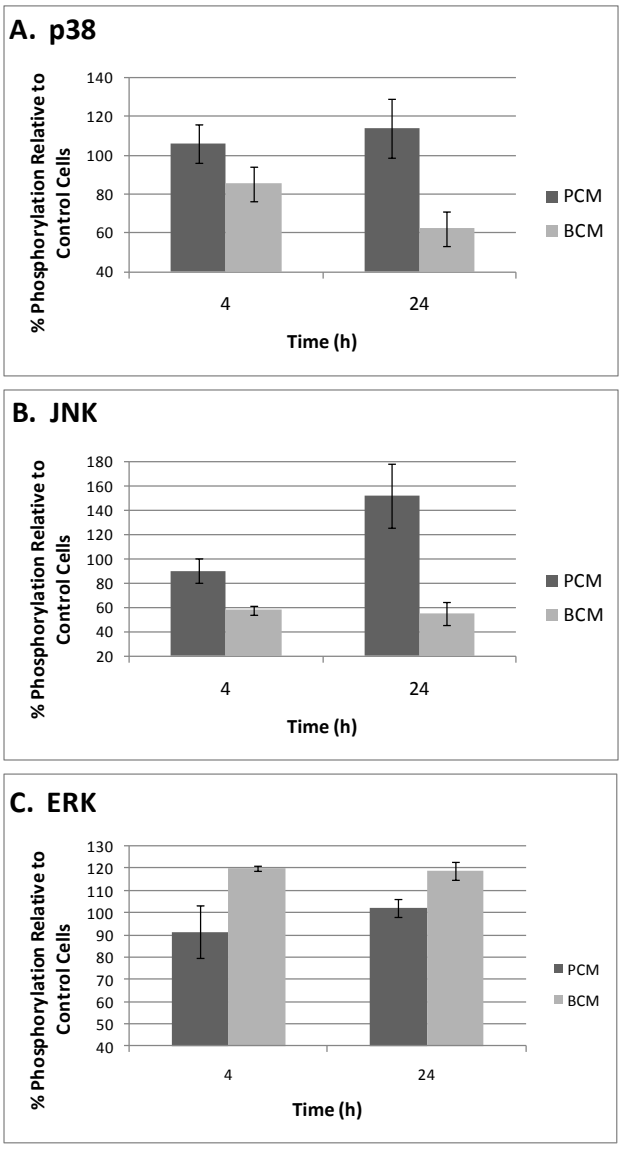

Figure 30. MAPK phosphorylation in HKs exposed to PCM or BCM. Data represented as percentage of phosphorylated p38, JNK, or ERK in control (EPI) cells. Error bars represent standard deviation, n=6, $p<0.005$.

If factors present in BCM were suppressing MAPK signaling cascades, then inhibition of MAPK signaling would not have as great of an impact on downstream targets such as cytokine and chemokine genes.

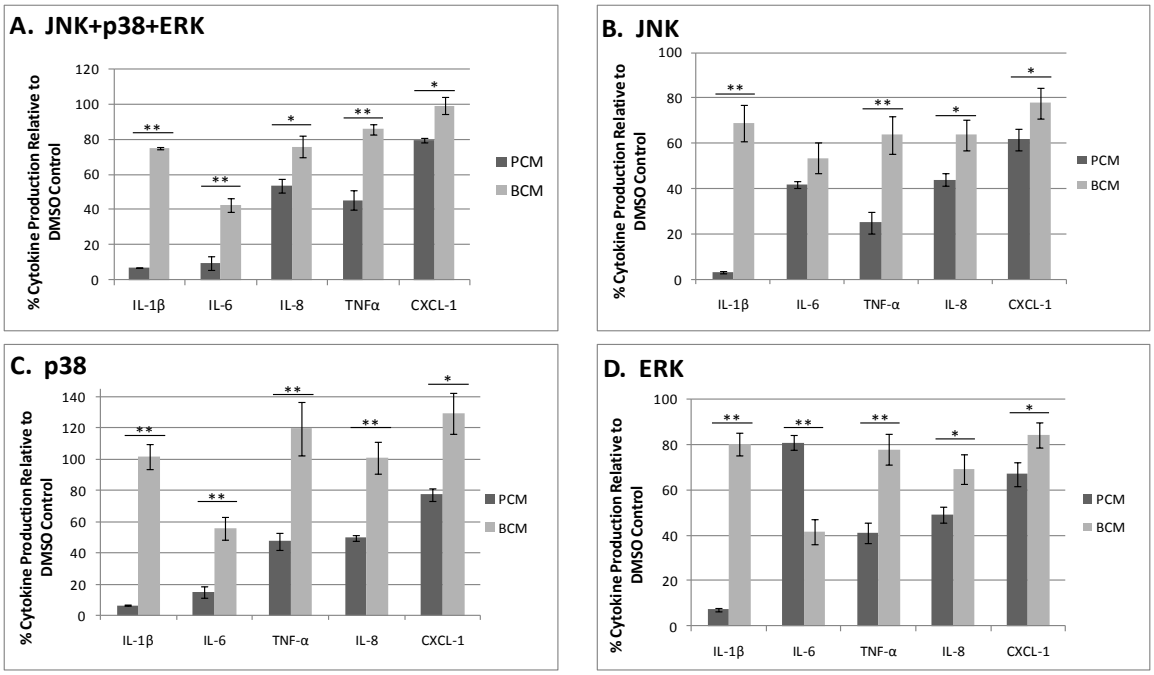

Figure 31. Percent cytokine production in MAPK inhibited HK after 4 hours of exposure to PCM or BCM. Data represented as percent DMSO control (BCM or PCM supplemented with DMSO). Error bars represent standard deviation of the average of triplicate experiments (*, $p<0.05$, **, $p<0.01$).

To investigate the role of MAPK signaling in BCM and PCM induced cytokine and chemokine production, the MAPK family members JNK, p38, and ERK, were inhibited using the inhibitors SP600125, SB203580, and U0126, respectively. Levels of GM-CSF were not analyzed in these experiments due to nearly undetectable levels at all time points except for 24 hours of exposure to PCM (Figure 28). Inhibition of JNK, p38, and ERK led to significant ($p<0.05$) decreases in cytokine and chemokine production in PCM-treated HKs relative to BCM-treated HKs with the exception of IL-6 production in ERK-inhibited HKs (Figure 30). The data demonstrate that in keratinocytes, MAPK signaling is responsible for a greater percentage of PCM mediated cytokine production than BCM mediated cytokine production. This may indicate that BCM induces cytokine production through alternative mechanisms in keratinocytes.

The effects of MAPK inhibitors on cell morphology were also investigated (Figure 31). It was found that inhibition of individual MAPKs (JNK, p38, or ERK) or the inhibition of all three combined did not prevent the characteristic biofilm induced morphology in HaCaT keratinocytes. These results indicate that morphological changes induced by BCM act through MAPK independent mechanisms. No apparent changes in morphology were observed by light microscopy in control cells with the exception of cells treated with all three MAPK inhibitors. Simultaneous inhibition of JNK, p38, and ERK in control cells lead to an abnormal morphology with formation of lamellipodia like structures along the entire perimeter of the cell and loss of cell/cell contact.

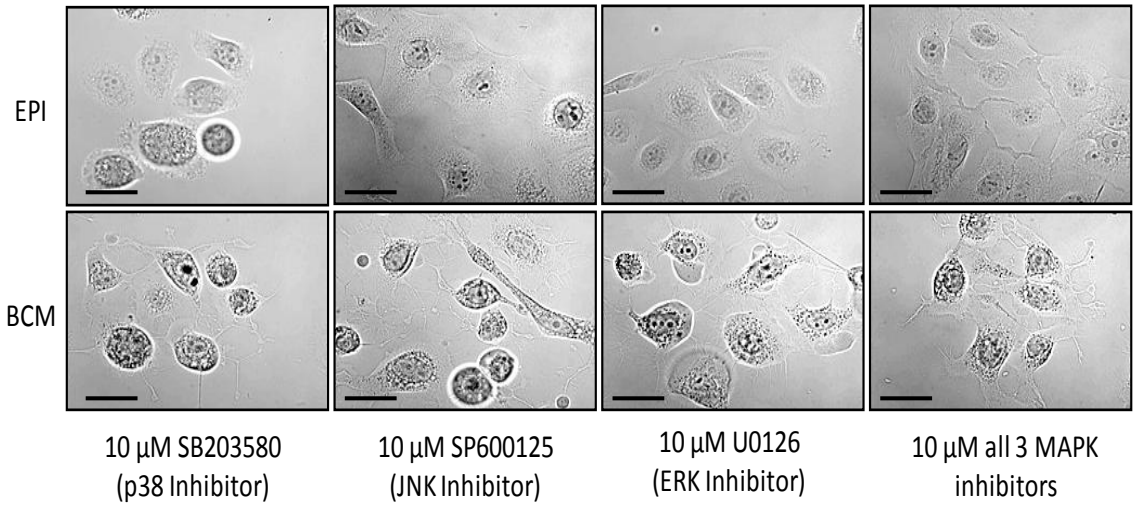

Figure 32. Inhibition of all or individual MAPKs did not have an impact on the morphology changes induced by BCM. This indicates a MAPK independent process for cytoskeletal rearrangements induced by *S. aureus* biofilm secreted factors. Control cells maintained apparently normal morphologies with the exception of treatment with all three inhibitors. Control cells treated with all inhibitors displayed an abnormal morphology and lost contact with one and other. 60x water immersion objective, bars represent 20 µm.

XME Genes Upregulated in Human
Keratinocytes Exposed to Bacterial Secreted Products

Transcriptional analysis of keratinocytes exposed to BCM revealed that, in the biofilm co-culture model, the monooxygenase cytochrome P450 1B1 (CYP1B1) was the most highly upregulated gene (Table 12). A closely related family member, CYP1A1, was the 24th most highly upregulated gene in BCM treated keratinocytes. No CYP450 family members were found to be significantly regulated in control or PCM treated keratinocytes. Additionally, genes of the aryl hydrocarbon receptor pathway (Figure 33) were induced by *S. aureus* biofilm in the co-culture model (Table 13).

Table 11. Genes with xenobiotic metabolic activity upregulated in BCM treated keratinocytes (left) and keratinocytes in the biofilm co-culture model (right). Genes in these groups include phase I (CYP1A1/CYP1B1) and phase II (ALDH3B2, GSTM2, GSTM1, MPST, SHMT2, UGT1A6, and UAP1L1) XME genes. Metabolites produced by CYP1A1 are further metabolized by aldehyde dehydrogenases, glutathione S-transferases, and UDP-glucuronosyltransferase (UGT) transferases. Several solute carrier (SLC) proteins are also induced in the co-culture model which function to shuttle electrphilic intermediates throughout the cell preventing them from reacting with random cellular components causing cellular damage.

	Gene Symbol	PCM v Control 4h	BCM v Control 4h		Gene Symbol	24h Co-culture
Phase I	CYP1A1	1.12	2.63	Phase I	CYP1B1	12.67
Phase II	ALDH3B2	1.50	1.93	Phase II	SLC16A6	6.86
	GSTM2	1.16	1.88		SLCO4A1	4.13
	GSTM1	1.08	1.87		SLC2A3	2.89
	MPST	1.47	1.75		UGT1A6	2.25
	SHMT2	1.07	1.58		UAP1L1	1.93

Table 12. Genes involved in the aryl hydrocarbon receptor pathway are regulated by *S. aureus* biofilm secreted factors in human keratinocytes.

Gene Symbol	Fold Change
ARNT	2.04
AHRR	1.59
p23	1.58
Hsp90	-1.68

CYP1A1/1B1 transcript levels were confirmed by RT-qPCR in BCM treated keratinocytes and keratinocytes exposed to *S. aureus* biofilm in the co-culture model (Figure 32). Keratinocytes in co-culture with *S. aureus* biofilm had higher CYP1A1/1B1 transcript levels indicating that continual contact with secreted products from the biofilm induced a stronger induction of CYP1A1/1B1.

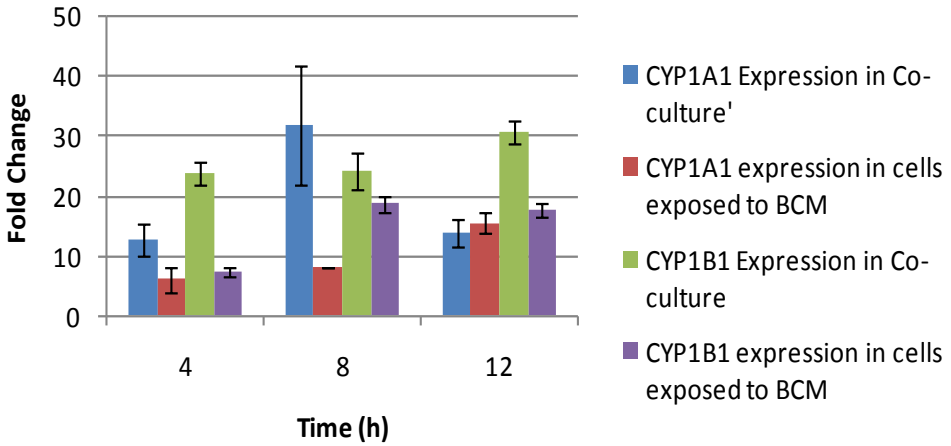

Figure 33. CYP1A1 and CYP1B1 expression in HFKs exposed to either BCM or *S. aureus* biofilm in the co-culture model. BCM induced lower levels of CYP1A1and CYP1B1 than did direct contact with the biofilm in the co-culture model indicating that the biofilm may have to continuously produce virulence factors to induce CYP1A1/1B1 expression. Fold change calculated by the ΔΔCt method with GAPD as the house keeping gene. Error bars represent standard deviation of the mean of three experiments.

Genes relating to oxidative stress and DNA damage were induced in keratinocytes in the biofilm co-culture and in keratinocytes exposed to BCM (Table 14). The phase II XME genes ALDH3B2 and GSTM1 and GSTM2 were induced by BCM in keratinocytes (Table 12).

Table 13. Functional enrichment using the DAVID functional analysis tool revealed several genes related to oxidative stress and DNA damage in response to BCM.

	Enrichment Score: 6.45	Count	P_Value	Benjamini
GOTERM_BP_FAT	DNA metabolic process	54	2.50E-10	3.60E-07
GOTERM_BP_FAT	DNA repair	34	6.00E-08	4.30E-05
GOTERM_BP_FAT	response to DNA damage stimulus	39	2.00E-07	9.40E-05
GOTERM_BP_FAT	cellular response to stress	48	3.00E-06	1.00E-03
SP_PIR_KEYWORDS	DNA damage	23	8.10E-06	4.80E-04
SP_PIR_KEYWORDS	dna repair	21	2.90E-05	1.60E-03

Discussion

Inflammation

Host-pathogen interactions were investigated between a clinical isolate of *S. aureus* and human keratinocytes. *S. aureus* BCM and PCM induced distinct inflammatory responses in human keratinocytes, *in vitro*. Transcriptional responses of keratinocytes to BCM revealed the upregulation of pro-inflammatory genes, including pro-inflammatory transcription factors and several cytokines and chemokines. ELISA analysis of cytokine and chemokine production in keratinocytes revealed that over time, BCM induced cytokine and chemokine levels were reduced relative to PCM treated keratinocytes. Phosphorylation of the MAPKs JNK and p38 were also found to be reduced by BCM while the ERK was not. Inhibition of MAPK pathways revealed that MAPK signaling was responsible for a larger percentage of cytokine and chemokine production in PCM treated keratinocytes compared to BCM treated keratinocytes. BCM also induced pro-inflammatory genes involved in the aryl hydrocarbon receptor pathway and xenobiotic metabolizing.

Transcriptional Analysis of Human Keratinocytes Exposed to BCM. Microarray analysis indicated an increase of cytokine and chemokine transcripts in keratinocytes exposed to BCM and PCM. Several studies have investigated the inflammatory effects of planktonic bacterial supernatants or bacterial conditioned medium on various mammalian cell types [52, 53, 184-190]; however much less is known about the effects of biofilm formation and the impacts on mammalian cell cultures.

Genes upregulated by PCM were in agreement with microarray data presented in Moreilhon et al on the upregulation of pro-inflammatory genes in epithelial cells exposed to *S. aureus* bacterial supernatant that was similar to PCM [52]. Peterson et al showed similar cytokine/chemokine gene expression patterns in human vaginal epithelial cells when exposed to late exponential phase *S. aureus* cultures [53]. Kumar et al reported that mid-logarithmic-phase cultures of *S. aureus* planktonic-conditioned medium induce IL-6, CXCL-8, and TNF-α in human-corneal-epithelial cells [185]. Different species of dental bacteria were found to induce different levels of cytokine production (IL-1β, IL-6 and CXCL-8 (IL-8)) after 4 or 24 hours of challenge in human gingival epithelial cells [48]. These differences were correlated to the virulence of the strains tested.

After four hours of contact with BCM, several genes encoding proteins belonging to the AP-1 complex were upregulated in BCM treated cells. In BCM treated cells AP-1 components c-Fos and ATF3 were strongly induced while their change in expression in PCM treated cells was not significant (Table 9). JUN and JUNB were upregulated by 2.05 fold and 1.58 fold in BCM treated cells, respectively, relative to PCM treated cells.

After 24 hours of co-culture with *S. aureus* biofilm, AP-1 family members c-Fos, ATF3, and ATF4 were induced +1.5, +4.99, and +1.90 fold, respectively.

The NFκB negative regulators TNFAIP3 (A20) and NFκBIA were upregulated 3.10 fold and 1.55 fold, respectively, in BCM treated cells relative to PCM treated cells. Although components of the activated NFκB complex were not directly upregulated in BCM treated cells, the expression of the negative regulators NFκBIA and TNFAIP3 indicates active regulation of the NFκB pathway.

The early growth response 1 gene (EGR1) was upregulated 19.6 fold in cells exposed to BCM while there was not a significant change in expression levels of EGR1 in PCM treated cells. EGR1 was not significantly regulated after 24 hours in the co-culture model. EGR1 is an early response transcription factor and regulates a variety of cellular functions including injury induced gene expression, regulation of pathophysiologically important genes, inflammation, apoptosis, differentiation, growth, and development [191-193]. This result suggests that EGR1 may be important for the biofilm induced production of an early inflammatory response in human keratinocytes.

Cytokine Production in BCM Treated Keratinocytes. The upregulation of cytokine and chemokine transcripts in BCM stimulated keratinocytes indicated that BCM induced a stronger inflammatory response in keratinocytes after four hours of exposure to BCM. ELISA analysis of cytokines produced after 4 hours of BCM stimulation confirmed microarray results. However, cytokine production in BCM treated keratinocytes was reduced after 24 hours of contact. It was hypothesized that reduced cell numbers and apoptotic cell death may have been responsible for the reduced level of

cytokine and chemokine secretion in BCM treated cells. Cytokine and chemokine levels normalized to non-apoptotic, adherent cells revealed that PCM treated cells still induced higher levels of cytokines and chemokines at 24 hours compared to keratinocytes exposed to BCM. The observed patterns of cytokine and chemokine production from keratinocytes exposed to either PCM or BCM is analogous to the levels of cytokines produced in sepsis and chronic inflammatory diseases.

Sepsis is characterized by uncontrollable release of massive amounts of cytokines and is comparable to the effects of PCM on keratinocyte cytokine production. Chronic inflammation, on the other hand, is more comparable to the effects of BCM on keratinocytes were inflammation is induced, but a runaway self inducing inflammatory response is not produced. The absence of GM-CSF in BCM treated cells at all time points analyzed and GM-CSF production in PCM treated keratinocytes at 24 hours was interesting given that GM-CSF is a mitogen for keratinocytes, and its absence in BCM treated keratinocytes may contribute to delayed re-epithelialization.

MAPK Signaling. The transcription factors NFkB, EGR1, and AP-1 are upregulated in several cell lines by diverse extracellular signals that activate MAPK signaling resulting in increased production of cytokines and chemokines [194-196]. Additionally, keratinocytes function in innate immunity through the activation of MAPK signaling cascades mainly through TLR activation resulting in cytokine and chemokine production in response to bacterial infection [164, 197, 198].

S. aureus BCM and PCM induced differential responses in MAPK signaling in keratinocytes. Phosphorylation of JNK and p38 MAPK family members was (i) low and

decreased overtime in keratinocytes exposed to BCM and (ii) unchanged or increased in keratinocytes exposed to PCM. Transcriptional analysis of BCM treated keratinocytes revealed the upregulation of DUSP MAPK regulators which may be responsible for the de-phosphorylation of JNK and p38. These data indicate that factors secreted by *S. aureus* biofilm may be suppressing JNK and p38 signaling leading to the observed reduction of cytokines and chemokines in BCM treated keratinocytes.

An increase in phosphorylation levels of p38 and JNK in PCM treated keratinocytes coincided with large increases in cytokine and chemokine production relative to BCM treated keratinocytes. This agrees with other reports of p38 and JNK activation in mammalian cell cultures in response to bacterial cultures similar to the planktonic cultures described in this dissertation [92, 120, 185, 199-201].

Chemical inhibition of MAPKs confirmed that BCM stimulation induced more MAPK independent cytokine production than PCM stimulated keratinocytes after 4 hours. The relative ineffectiveness of the MAPK inhibitors on BCM mediated cytokine production in addition to the reduced phosphorylation status of JNK and p38 would suggest that BCM and PCM induced production of cytokines is mediated through different signaling cascades in keratinocytes. The possibility of a secreted *S. aureus* biofilm factor(s) that suppress MAPK signal transduction in human keratinocytes may lead to reduced local cytokine and chemokine production establishing a chronic level of inflammation that disrupts the immune response and is detrimental to the healing process.

The suppression of MAPK signaling by BCM could potentially impact other wound related activities involving MAPK cascades in keratinocytes. These include

keratinocyte differentiation [100], the secretion of antimicrobial peptides [101], response to mechanical stress [102], and response to osmotic stress [103]. Suppression of MAPK signal transduction in keratinocytes could be detrimental to all phases of wound healing, possibly contributing to the formation and/or persistence of chronic wounds. The upregulation of AP-1 transcription factors may be an attempt by the cell to compensate for reduced MAPK signaling and subsequent cytokine production induced by BCM.

MAPK suppression in various mammalian cell types by bacterial products has been observed. *Bacillus anthracis* secretes lethal toxin, which cleaves most isoforms of MAPKs, reducing pro-inflammatory cytokine secretion from immune cells [202]. *Shigella Flexneri, Yersinia* spp., and *Salmonella* spp. deliver toxins which inhibit MAPK signal transduction through a type III secretion mechanism resulting in the repression of genes such as TNF-α, IL-6, and CXCL-8 [203, 204]. *S. aureus* has not been shown to produce a toxin that inhibits MAPK signaling. This indicates a novel mechanism responsible for the observed suppression of p38 and JNK MAPK signaling and reduced cytokine and chemokine secretion in BCM treated keratinocytes.

Xenobiotic Metabolism Enzymes are Induced by BCM in Human Keratinocytes

Any foreign chemical found in the body including drugs, pollution, certain foods, and chemicals liberated through combustion are known collectively as xenobiotic chemicals. Xenobiotics are typically hydrophobic in nature and readily penetrate cellular membranes. To combat the everyday exposure to these chemicals, the body utilizes xenobiotic metabolizing enzymes (XMEs) which are broken into two groups, Phase I and Phase II XMEs. Phase I XMEs generally prime Phase II XMEs through the formation of

electrophilic intermediates. Phase II XMEs are then able to conjugate the metabolite with a number of different moieties (glutathione, sulphate, glycine, etc) producing a hydrophilic product. The combined effects of Phase I and Phase II XMEs results in the detoxication of foreign chemicals through their excretion from the body.

The skin is the largest organ in the body and is a major barrier to the outside world. Xenobiotic metabolism has been shown to be active in human keratinocytes, albeit at a lower level when compared to other detoxifying organs such as the liver [205]. Major classes of phase I XMEs include members of the cytochrome P450 (CYP450) family of monooxygenases. CYP450s contain a heme cofactor and catalyze the insertion of one atom of oxygen into an organic substrate while the other oxygen atom is reduced to water. CYP1A1 and CYP1B1 are inducible members of the CYP1A family which are characterized by their ability to metabolize xenobiotic chemicals, mainly hydrophobic polycyclic aromatic hydrocarbons (PAHs) and polyhalogenated aromatic hydrocarbons [206]. CYP1A1 is classified as a phase I XME which is notorious for the metabolic activation of several carcinogens/toxins producing reactive oxygenated metabolites that are often more harmful than the parent compound. CYP1A1 is one of the most important detoxification enzymes because of its wide distribution in the body and its broad substrate specificity. PAHs show strong affinity towards the aryl hydrocarbon receptor (AHR), which dimerizes with its binding partner ARNT to regulate the expression of CYP1A family members and other genes involved in xenobiotic metabolism (Figure 33).

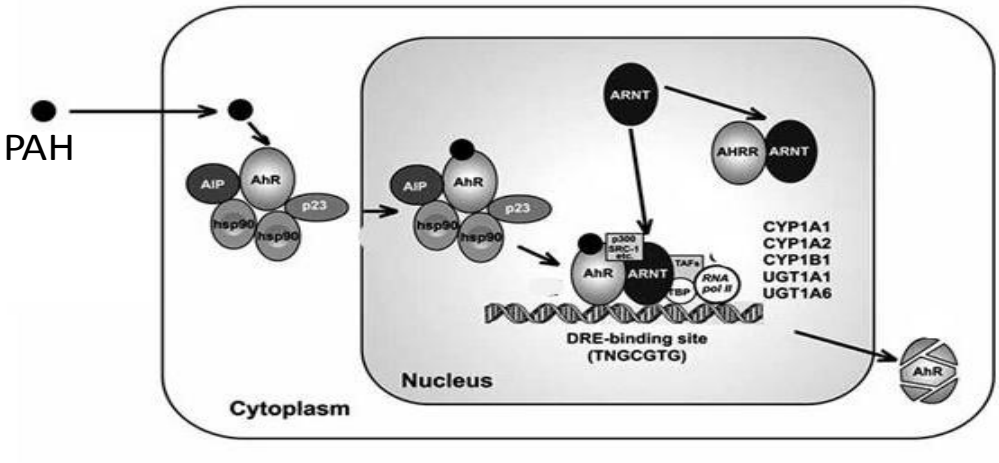

Figure 34. Illustration of the aryl hydrocarbon receptor (AhR) pathway. Xenobiotics (polycyclic aromatic hydrocarbons (PAHs) in this case) readily penetrate lipid membranes. Upon entry to the cell, xenobiotics activate the AhR complex which leads to its translocation into the nucleus were it dimerizes with its binding partner, ARNT. The AhR/ARNT complex acts as a transcription factor for several genes important to xenobiotic metabolism, including CYP1A1/1B1. Image adapted from reference [205].

CYP1A1 and CYP1B1 expression are considered to be diagnostic for AHR activation [207]. In addition to producing activated intermediate metabolites, the CYP1A family of XMEs induces oxidative stress through the generation of reactive oxygen species (ROS) which is coupled to its monooxygenase catalytic activities [208].

The expression of both phase I and phase II XME genes geared towards the metabolism of hydrophobic aryl hydrocarbons in BCM treated keratinocytes and in keratinocytes in the biofilm co-culture model, but not in PCM or control cells, is significant and points towards the existence of small hydrophobic virulence factors secreted by *S. aureus* biofilm. It is possible that the aureusimines could be metabolized by this metabolic pathway. Xenobiotic metabolism and inflammatory responses have an intimate relationship. CYP450 transcription is widely known to be inhibited by inflammation [209-211]. CYP450 genes are likely downregulated during inflammation due to the unavoidable generation of ROS and oxidative stress by CYP450. Oxidative

stress is known to induce inflammation through several processes including MAPK signaling [212]. Excessive ROS production during an inflammatory response, especially in the skin, which is exposed to high levels of ultraviolet radiation and oxygen tension, results in the damage of lipid membranes and nucleic acids, and induction of apoptosis [213-215]. Given the presence of CYP450 gene expression in addition to the upregulation of genes related to oxidative stress and DNA damage, ROS may be partially responsible for the observed apoptosis in keratinocytes exposed to *S. aureus* biofilm.

CYP1A1 and CYP1B1 have been demonstrated to have an inverse expression pattern when inflammation is induced where CYP1B1 is not affected by inflammatory responses to the degree that CYP1A1 is [206, 216]. The common *Staphylococcal* toxins *Staphylococcal* enterotoxin B and *S. aureus* protein A depresses CYP450 dependent drug biotransformation through inflammatory responses from the cell [210]. The expression patterns of CYP450 genes observed in keratinocytes in co-culture with *S. aureus* biofilm show different expression patterns over time, though a clear inverse expression pattern was not evident (Figure 32).

It is possible that BCM induces lower levels of CYP1A1/1B1 in keratinocytes relative to co-culture keratinocytes because the responsible *S. aureus* biofilm secreted products are metabolized and deactivated leading to the downregulation of CYP1A1/1B1 genes. Higher CYP1A1/1B1 levels in the co-culture model may be due to the continual replacement of biofilm secreted products which may lead to higher levels of CYP1A1/1B1 transcripts. The upregulation of more phase II XMEs in BCM treated cells may indicate that phase I XME metabolism is progressing resulting in decreased CYP1

levels and increased phase II XMEs responsible for the final metabolic steps prior to elimination from the cell. To my knowledge, an infectious disease has never been shown to directly induce xenobiotic metabolism while simultaneously generating an inflammatory response. These results are in conflict with reports on the relationship between xenobiotic metabolism and inflammation [206, 216].

The transcription of CYP450 genes under inflammatory conditions may be the consequence of deranged MAPK signaling. MAPKs are involved in the regulation of CYP450 genes [207, 217] and disruption of this regulation could potentially lead to inappropriate CYP1A1/1B1 transcription and the production of more oxygen radicals.

These data provide insights into the mechanisms of sustained inflammation and persistence in biofilm-based chronic-wound infections. Suppression of MAPK signaling and the corresponding reduction in cytokine production could help to explain the local, chronic inflammation observed in biofilm infected tissues. MAPK alternative inflammatory mechanisms potentially induced by BCM may include the production of lipid derived mediators of inflammation (i.e. arachadonic acid metabolites) and ROS generated by CYP450.

Epithelialization

Keratinocytes stimulated with BCM underwent morphological changes including the formation of actin rich dendritic like structures, rounding of the cell body, polymerization of tubulin around the periphery of the cell, and fragmentation of the nucleus. Additionally, BCM induced the release of intracellular calcium which correlated well with changes in morphology. PCM did not induce the release of

intracellular calcium stores. Apoptosis was also induced in BCM treated keratinocytes accompanied by cell detachment. ROS production induced by BCM may also contribute to apoptosis.

Morphologic Changes and Apoptosis Induced by BCM. *S. aureus* BCM induced morphological changes and apoptosis in HFKs. BCM also inhibits keratinocyte migration and increases the wounded area in a scratch based wound model [218]. The same morphological changes and activation of apoptosis that occur in BCM stimulated HFKs were also observed in HaCaT keratinocytes. Additionally, the same effects were observed in keratinocytes exposed to biofilm secreted products in the co-culture model, albeit on a longer timescale. The differences in the time during which the morphology changes occurred after exposure to BCM as opposed to co-culture is logical, since BCM treated cells received a large, concentrated dose of secreted bacterial factors while keratinocytes in the co-culture model are initially in fresh growth medium and are exposed to bacterial factors that build up to active concentrations over a longer period of time.

Temporal changes in cell morphology correlated with an increase in intracellular calcium levels, suggesting a calcium-dependent mechanism (Figure 25). The disruption of microtubules in keratinocytes exposed to BCM likely inhibits cell proliferation since microtubules are intimately involved in the cell division process. Microtubule and microfilament structures are also essential to locomotion in keratinocytes. The observed rearrangements in cytoskeletal structure likely explain the inhibition of scratch closure we previously described for BCM treated keratinocytes [218]. These data support the

hypothesis that cytoskeletal rearrangements induced by secreted factors from *S. aureus* biofilm in human keratinocytes impacts the epithelialization phase of wound healing.

Alterations of cytoskeletal architecture by direct contact with bacteria have been portrayed as a means for pathogenic bacteria to induce pathogenesis (i.e., apoptosis) through invasion of host cells [219-221]. The observed cytoskeletal rearrangements induced by BCM may play a role in the internalization of *S. aureus* and could potentially modulate immune responses.

Previous studies have shown co-culturing planktonic *S. aureus* and keratinocytes induces apoptosis, but direct contact and internalization of *S. aureus* was necessary [222-225]. Keratinocytes treated with BCM contained highly fragmented nuclei and stained positive in the TUNEL assay, consistent with late stage apoptosis (Figures 22-24). Apoptosis induced by BCM coincided with increases in intracellular calcium after 24 hours of exposure to BCM (Figures 22, 23, and 26). Intracellular calcium regulates differentiation and apoptotic programs in human keratinocytes [226]. Apoptosis in BCM treated keratinocytes was accompanied by a decrease in adherent cell numbers over time (Figure 24). Secreted biofilm factors capable of inducing apoptosis in keratinocytes would have major impacts on epithelialization. Apoptosis in cells not in direct contact with *S. aureus*, such as cells at the wound margin, could be induced to undergo programmed cell death leading to advancement of the wound front, further inhibiting the epithelialization phase of wound healing.

A Model of the Effects of Bacteria on Wound Healing

An overview of *S. aureus* infection as related to the work outlined in this dissertation is detailed in Figure 34. The initial colonization of a wound would theoretically be primarily by bacteria with a more planktonic phenotype. This infection would either result in a failed attempt to evade the host's immune response or successful infection of the wound. If the bacteria were successful in initiating an infection that was not cleared by the host, the infection would either become systemic and spread to the blood resulting in sepsis or the infection would remain localized and become chronic.

If the route of infection were to turn chronic, bacteria colonizing the wound would likely revert from a predominantly planktonic phenotype into a predominantly biofilm phenotype. The ability of *S. aureus* biofilms to induce apoptosis and induce abnormal cell morphology in human epidermal keratinocytes would likely impact wound healing through inhibition of the second phase of wound healing, re-epithelialization. Relatively low production of inflammatory cytokines by keratinocytes exposed to BCM and the suppression of MAPK signaling would lead to a deranged local inflammatory response contributing to the persistent nature of chronic wounds. Many factors could potentially influence the route of the infection. One of the most important factors to consider are underlying medical conditions of the host known to complicate the wound healing process including: immunosuppression, diabetes, pulmonary disease, and obesity.

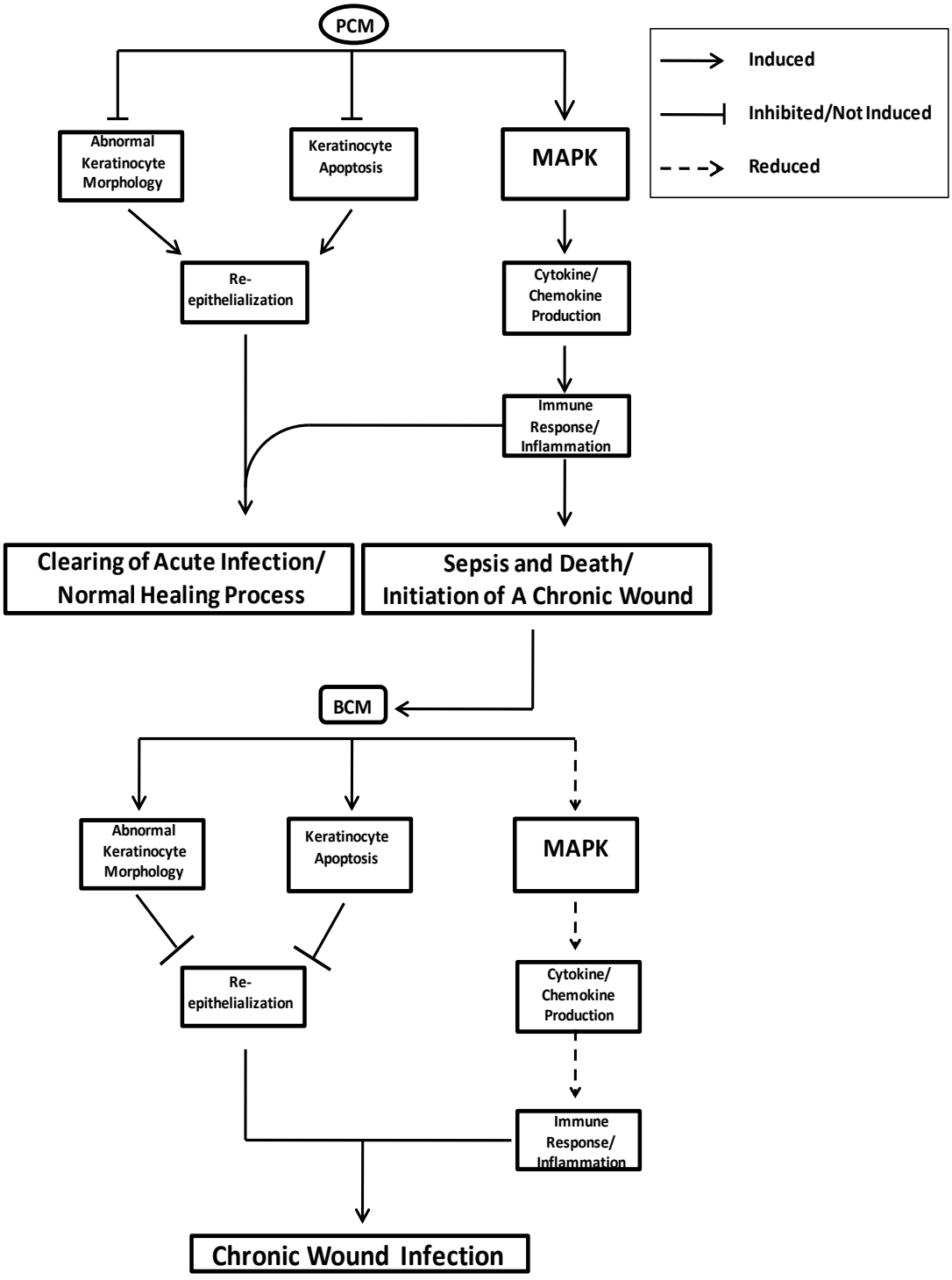

Figure 35. An overview of the potential mechanisms of pathogenesis induced by secreted factors from either *S. aureus* biofilm or planktonic cultures.

The many differential effects induced in human keratinocytes by secreted factors from *S. aureus* biofilm and planktonic cultures described in this dissertation underscore the importance in considering the formation of a biofilm when studying bacterial based diseases. A wide range of bacteria with varying degrees of phenotypes ranging from "100% planktonic" to "100% biofilm" are likely present in chronic infections. This phenotypic plasticity (in addition to population diversity) is what is assumed to lend bacterial biofilms resistance to several factors including antibiotics and attacks from the immune system. Data presented here revealed distinct characteristics in inflammatory and epithelialization processes in keratinocytes stimulated with BCM or PCM. These data further implicate biofilms as a causative agent of localized, persistent infections and underscore the need to investigate the impact of biofilm formation not only in studies investigating infectious disease, but in all studies were bacterial biofilm formation is a possibility.

CHAPTER 6

CONCLUSIONS AND SUMMARY OF RESULTS

S. aureus BCM and PCM differentially impacted inflammation and processes associated with epithelialization in human keratinocytes. Phylogenetic characterization of chronic wound biofilm communities revealed that chronic wounds contain a diverse community of microorganisms. Among the most prevalent organisms in chronic wound infections was *S. aureus.* Work described in this dissertation was one of the earlier documented cases of phylogenetic characterization of bacterial populations in diabetic foot ulcers, venous leg ulcers, and pressure ulcers using molecular methods. Molecular methods are utilized more frequently to characterize chronic-wound bacterial communities in clinical settings.

A novel *in vitro* biofilm-disease model was developed to study interactions between *S. aureus* BCM and human keratinocytes. The model allowed for a direct comparison between conditioned medium from *S. aureus* biofilm and planktonic cultures. Metabolite profiling of BCM indicated that amino acids were selectively consumed. Mixed-acid fermentation products were produced by *S. aureus* biofilm suggesting an anoxic niche. This indicates an important role for anoxic metabolism in bacterial biofilms and biofilm-based disease.

Aureusimine A and B were recently discovered to regulate virulence in *S. aureus* [167]. The production of the two virulence factors correlated with biofilm formation, anoxia, and were found to be present in a variety of Gram positive organisms. The inhibition of the production of these molecules could be a potential therapeutic/diagnostic

target for biofilm-based diseases. Additionally, activities induced in host cells by the aureusimines could also be targeted for therapeutic intervention.

S. aureus BCM impacted the inflammatory response by stalling cytokine production and suppressing MAPK phosphorylation in human keratinocytes. BCM also inhibited epithelialization-related processes through disruption of the cytoskeleton and induction of apoptosis. Cytoskeletal rearrangements and apoptosis were correlated with the mobilization of intracellular calcium, suggesting a calcium-dependent mechanism.

With the *in vitro* biofilm-disease model, important elements of host-pathogen relationships between mammalian cell lines and bacterial strains can be elucidated. Our current model could be expanded to include multi-species biofilms and more complex tissue cultures. Incorporation of specific strains of bacteria and mammalian cell types in our model expands the utility of this model to other biofilm-related diseases. This work highlights important host-pathogen interactions that may lead to discoveries associated with the healing and prevention of biofilm-based infections.

APPENDICES

APPENDIX A

MS2 DATA FOR AUREUSIMINE A

Highlighted peaks correspond to ions generated by MS2 fragmentation. MS2 spectra were averaged over low to high fragmentation energies (10-100 Volts) to obtain a representative spectrum. All major ions are accounted for when fragment masses from logical breaks in chemical bonds are calculated. The blue diamond represents the parent ion.

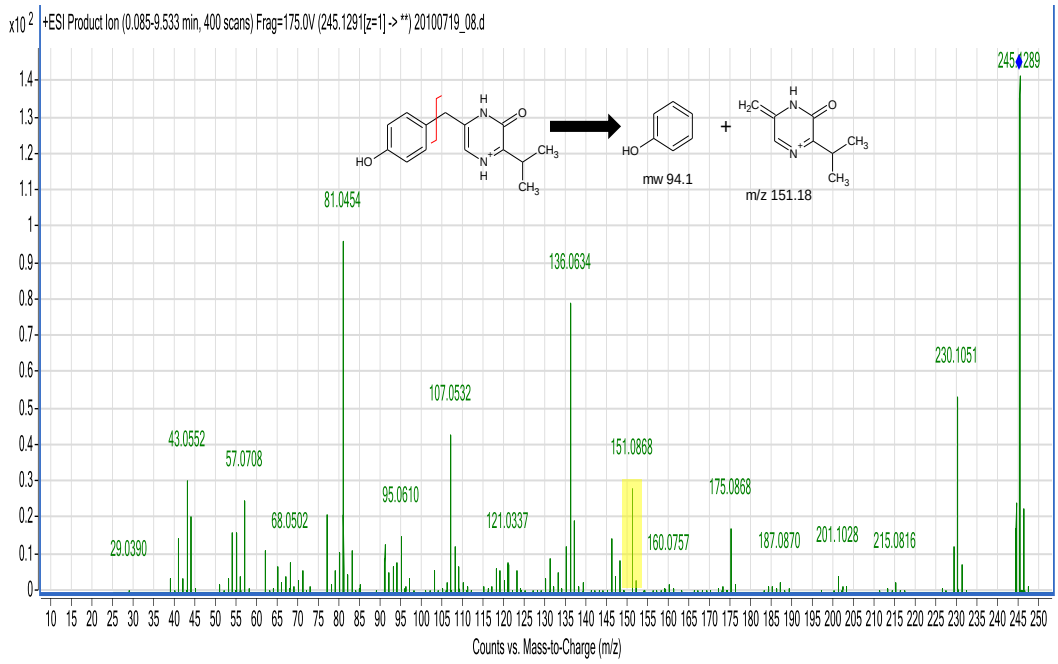

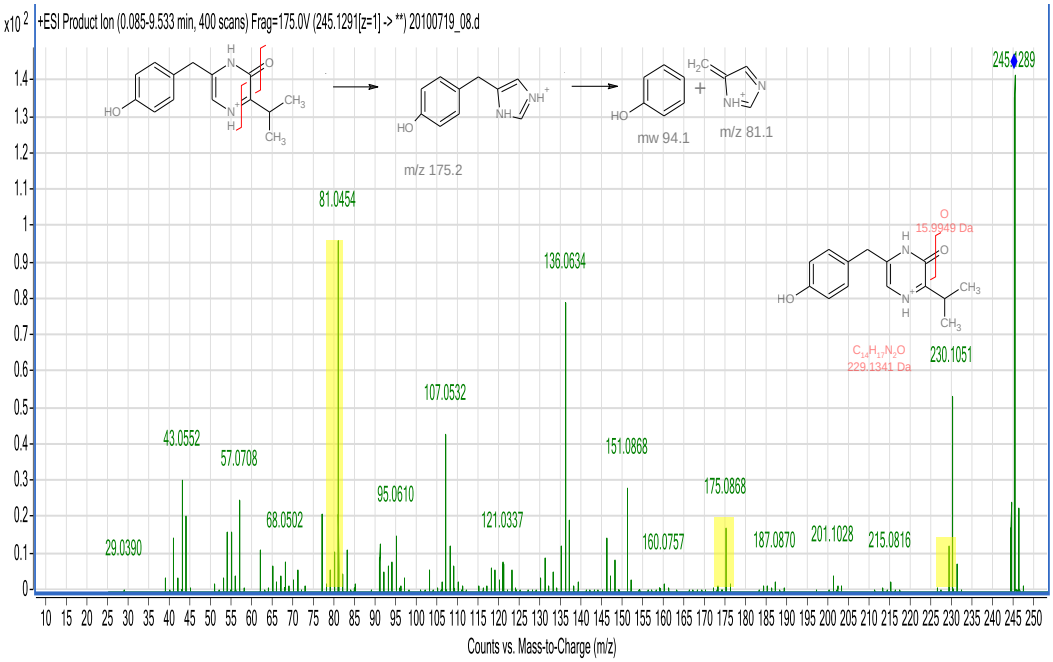
x10 2
+ESI Product Ion (0.085-9.533 min, 400 scans) Frag=175.0V (245.1291[z=1] -> **) 20100719_08.d
m/z 175.2
mw 94.1
m/z 81.1
245.1289
81.0454
136.0634
107.0532
43.0552
57.0708
151.0868
95.0610
175.0868
68.0502
121.0337
160.0757
187.0870
201.1028
215.0816
29.0390
230.1051
O
15.9949 Da
C14H17N2O
229.1341 Da
Counts vs. Mass-to-Charge (m/z)

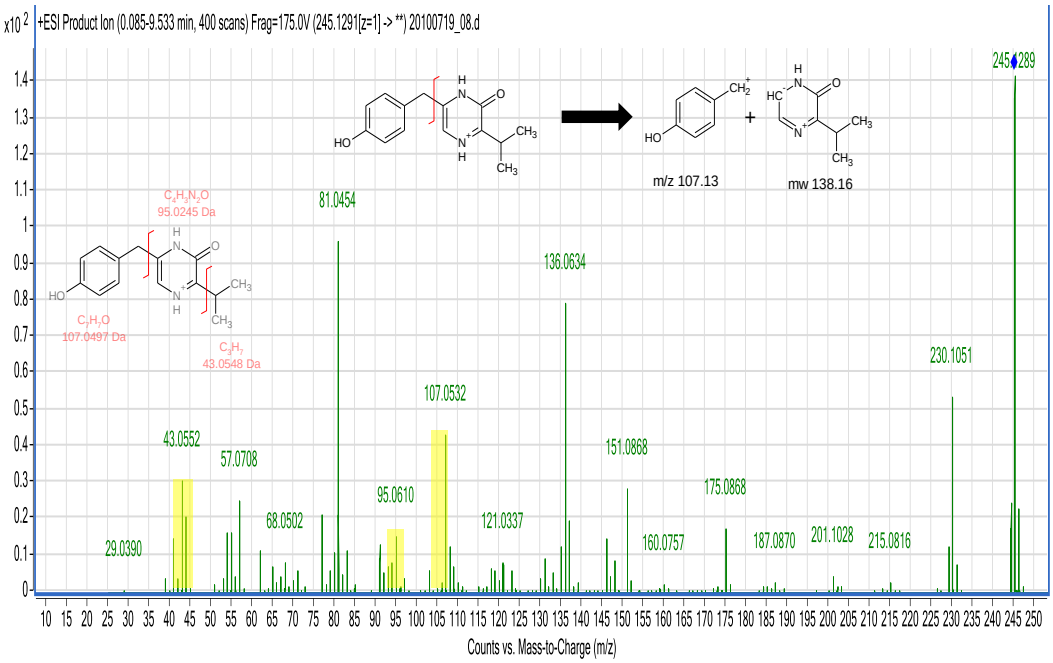
x10 2
+ESI Product Ion (0.085-9.533 min, 400 scans) Frag=175.0V (245.1291[z=1] -> **) 20100719_08.d
m/z 107.13
mw 138.16
245.1289
81.0454
136.0634
C7H9N2O
95.0245 Da
C7H7O
107.0497 Da
C3H7
43.0548 Da
107.0532
43.0552
57.0708
151.0868
95.0610
175.0868
68.0502
121.0337
160.0757
187.0870
201.1028
215.0816
29.0390
230.1051
Counts vs. Mass-to-Charge (m/z)

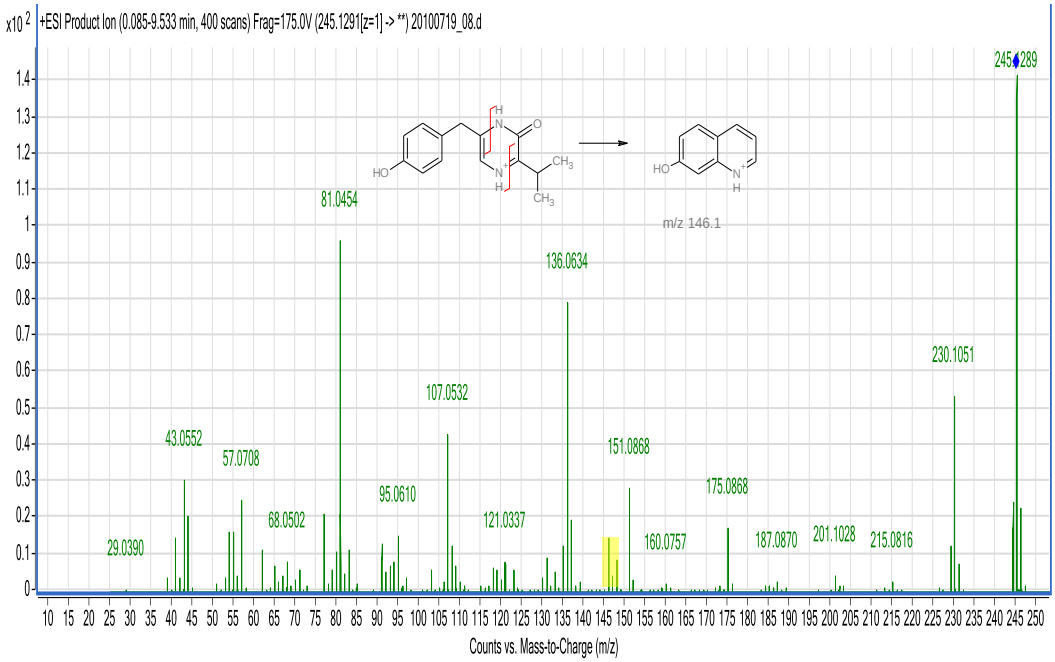
x10 2 +ESI Product Ion (0.085-9.533 min, 400 scans) Frag=175.0V (245.1291[z=1] -> **) 20100719_08.d
245.1289
81.0454
136.0634
230.1051
107.0532
43.0552
57.0708
151.0868
175.0868
95.0610
68.0502
121.0337
160.0757
187.0870
201.1028
215.0816
29.0390
m/z 146.1
Counts vs. Mass-to-Charge (m/z)

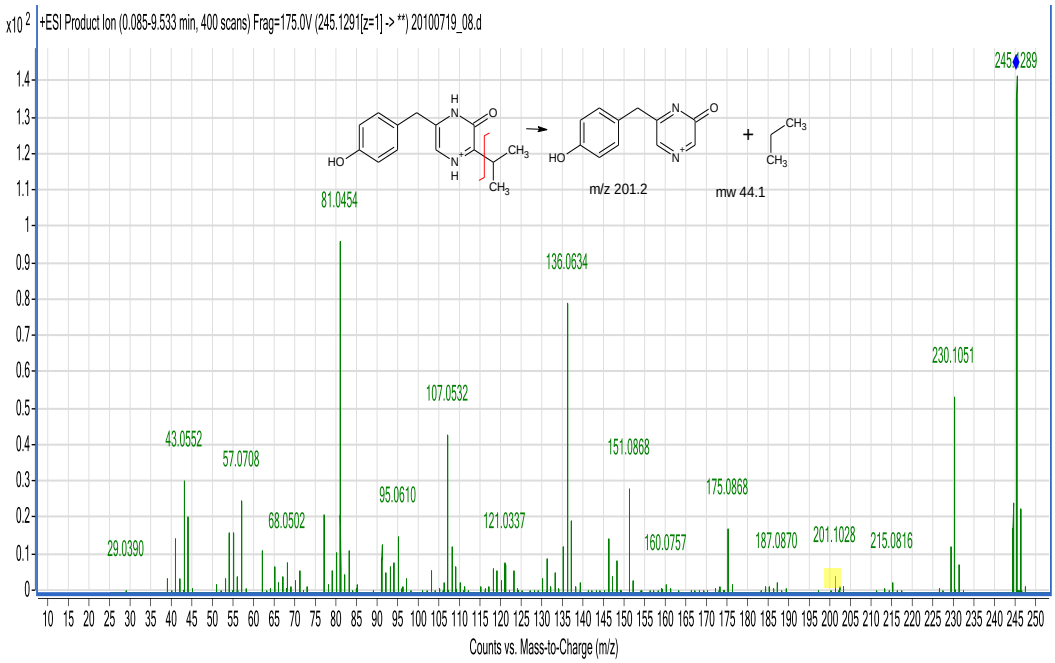
x10 2 +ESI Product Ion (0.085-9.533 min, 400 scans) Frag=175.0V (245.1291[z=1] -> **) 20100719_08.d
245.1289
81.0454
136.0634
230.1051
107.0532
43.0552
57.0708
151.0868
175.0868
95.0610
68.0502
121.0337
160.0757
187.0870
201.1028
215.0816
29.0390
m/z 201.2
mw 44.1
Counts vs. Mass-to-Charge (m/z)

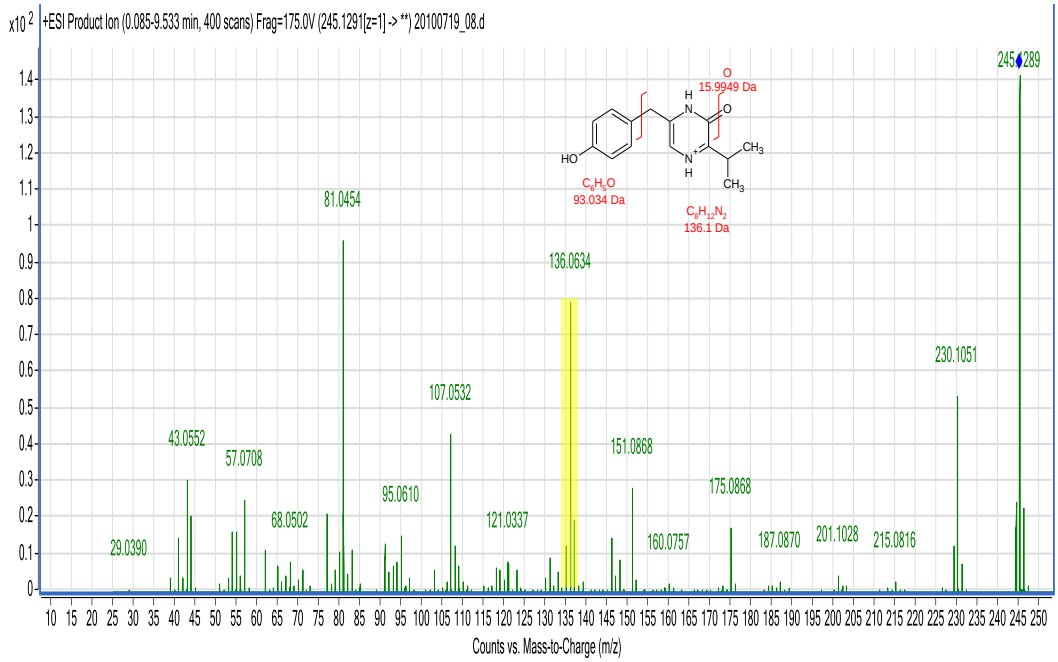
x10 2 +ESI Product Ion (0.085-9.533 min, 400 scans) Frag=175.0V (245.1291[z=1] -> **) 20100719_08.d
245.1289
81.0454
136.0634
230.1051
107.0532
43.0552
57.0708
151.0868
175.0868
95.0610
68.0502
121.0337
160.0757
187.0870
201.1028
215.0816
29.0390
O
15.9949 Da
HO
C6H6O
93.034 Da
C9H12N2
136.1 Da
CH3
Counts vs. Mass-to-Charge (m/z)

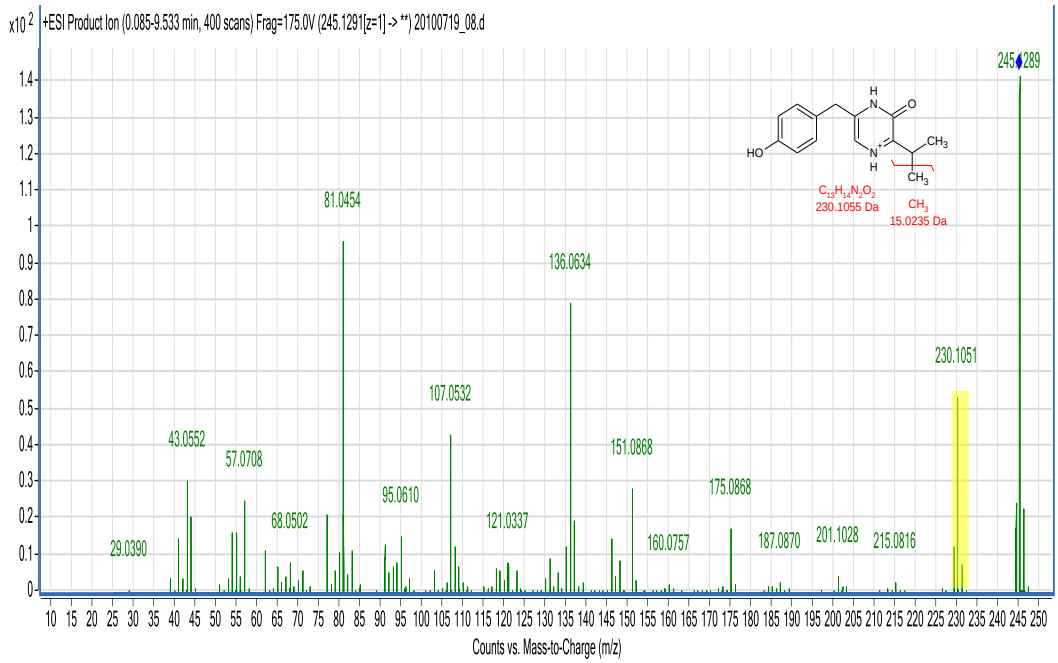
x10 2 +ESI Product Ion (0.085-9.533 min, 400 scans) Frag=175.0V (245.1291[z=1] -> **) 20100719_08.d
245.1289
81.0454
136.0634
230.1051
107.0532
43.0552
57.0708
151.0868
175.0868
95.0610
68.0502
121.0337
160.0757
187.0870
201.1028
215.0816
29.0390
HO
C13H14N2O2
230.1055 Da
CH3
15.0235 Da
Counts vs. Mass-to-Charge (m/z)

APPENDIX B

MS2 DATA FOR AUREUSIMINE B

Highlighted peaks correspond to ions generated by MS2 fragmentation. MS2 spectra were averaged over low to high fragmentation energies (10-100 Volts) to obtain a representative spectrum. All major ions are accounted for when fragment masses from logical breaks in chemical bonds are calculated. The blue diamond represents the parent ion.

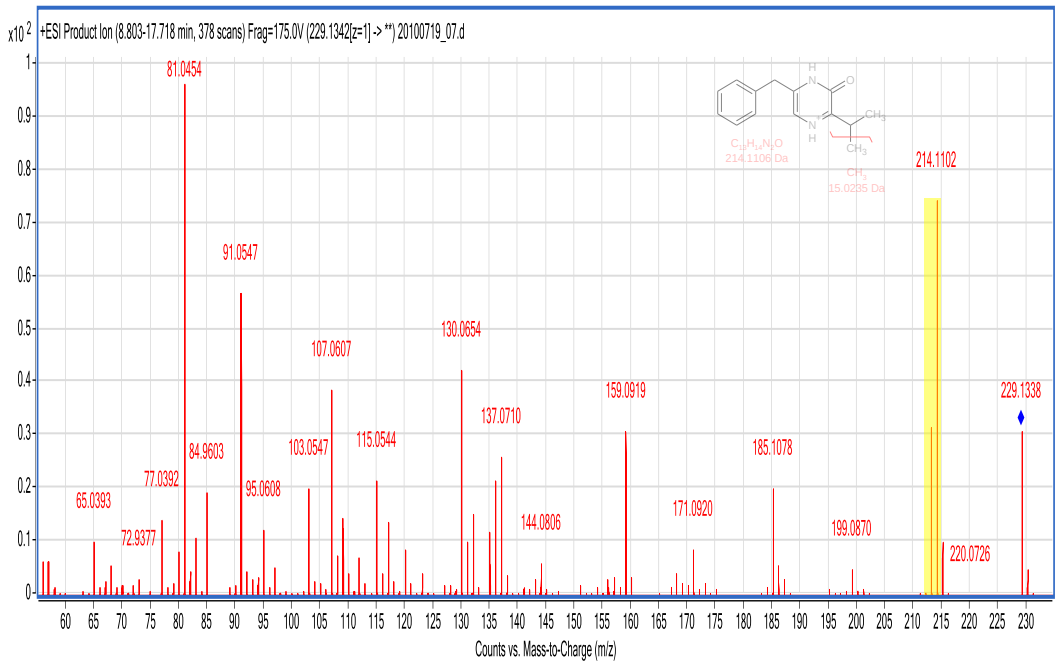

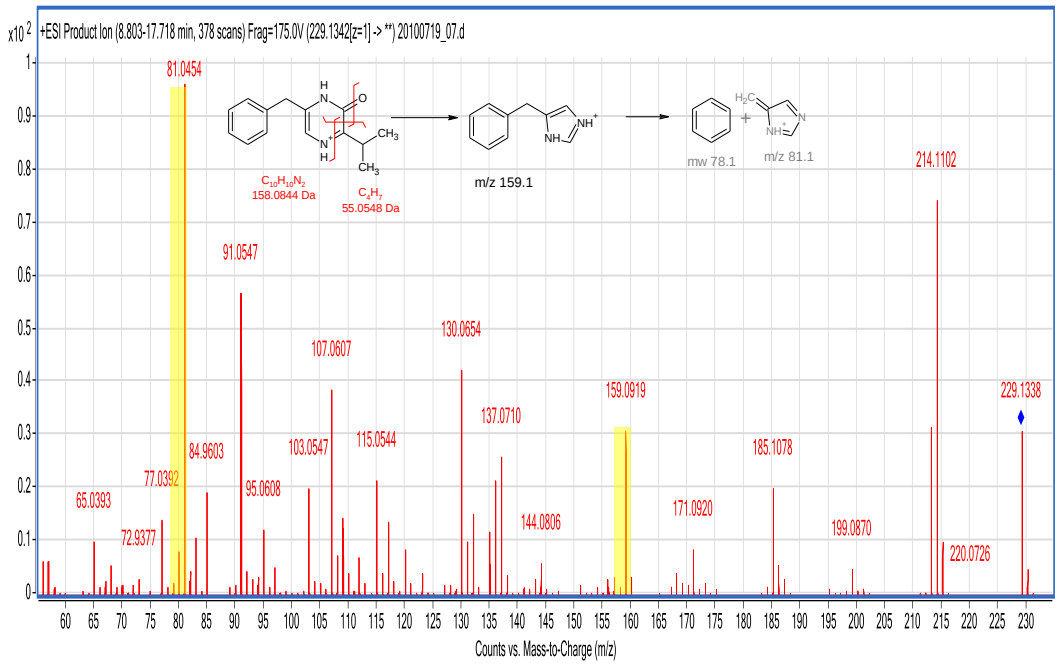
x10 2
+ESI Product Ion (8.803-17.718 min, 378 scans) Frag=175.0V (229.1342[z=1] -> **) 20100719_07.d
81.0454
91.0547
107.0607
130.0654
159.0919
137.0710
229.1338
214.1102
84.9603
103.0547
115.0544
185.1078
77.0392
95.0608
65.0393
144.0806
171.0920
72.9377
199.0870
220.0726
C10H10N2
158.0844 Da
C4H7
55.0548 Da
m/z 159.1
mw 78.1
m/z 81.1
Counts vs. Mass-to-Charge (m/z)

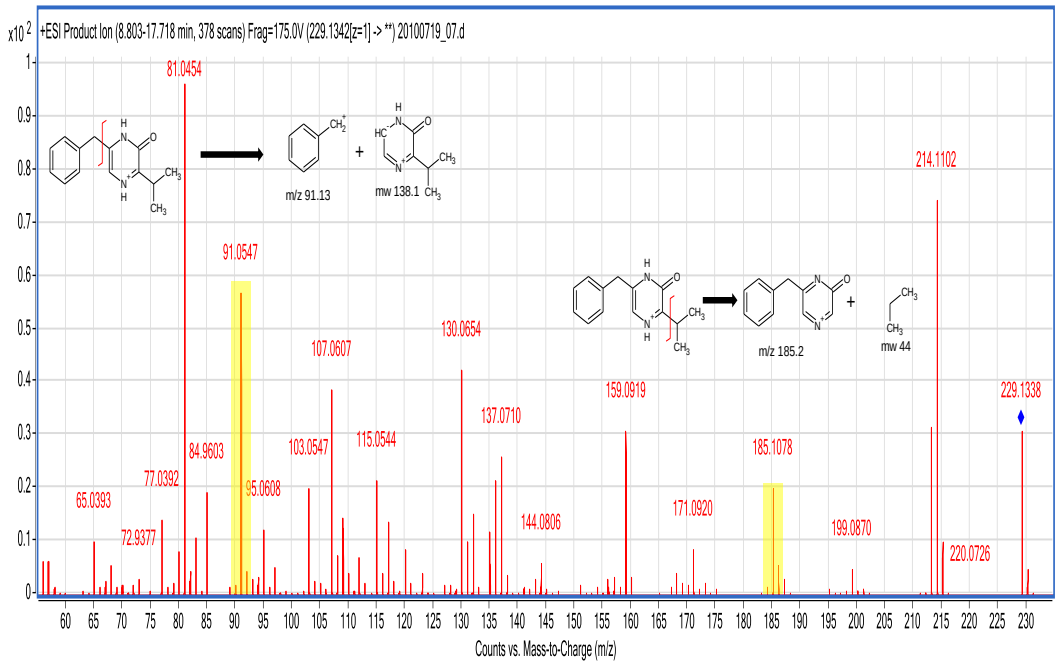
x10 2
+ESI Product Ion (8.803-17.718 min, 378 scans) Frag=175.0V (229.1342[z=1] -> **) 20100719_07.d
81.0454
91.0547
107.0607
130.0654
159.0919
137.0710
229.1338
214.1102
84.9603
103.0547
115.0544
185.1078
77.0392
95.0608
65.0393
144.0806
171.0920
72.9377
199.0870
220.0726
m/z 91.13
mw 138.1
m/z 185.2
mw 44
Counts vs. Mass-to-Charge (m/z)

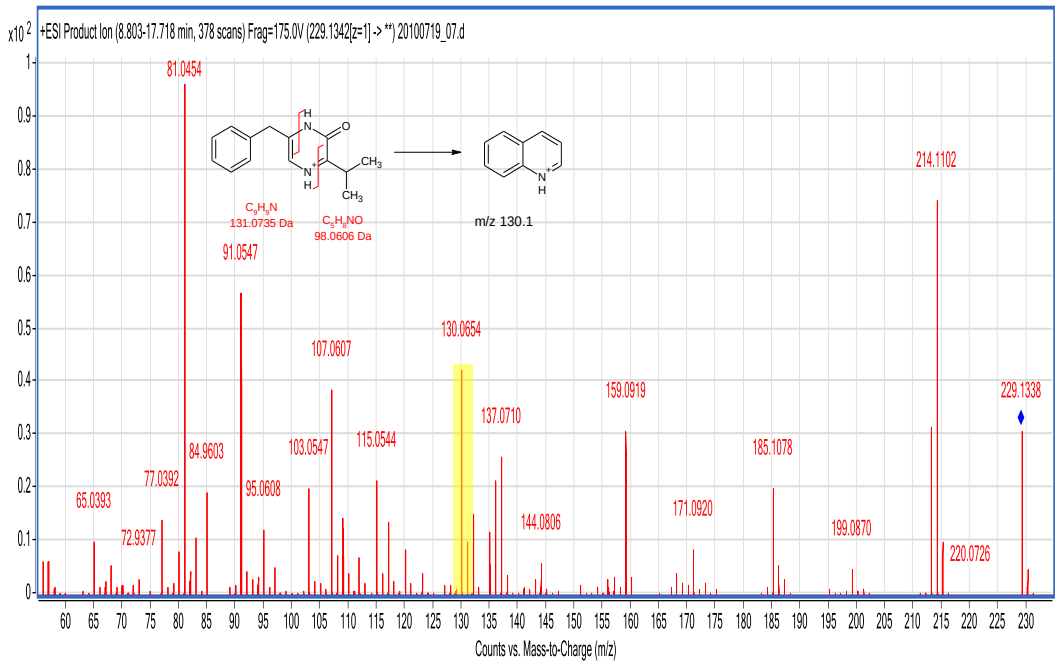
x10 2
+ESI Product Ion (8.803-17.718 min, 378 scans) Frag=175.0V (229.1342[z=1] -> **) 20100719_07.d
81.0454
214.1102
91.0547
130.0654
107.0607
159.0919
229.1338
137.0710
84.9603
103.0547
115.0544
185.1078
77.0392
95.0608
65.0393
144.0806
171.0920
72.9377
199.0870
220.0726
C7H9N
131.0735 Da
C5H9NO
98.0606 Da
m/z 130.1
Counts vs. Mass-to-Charge (m/z)

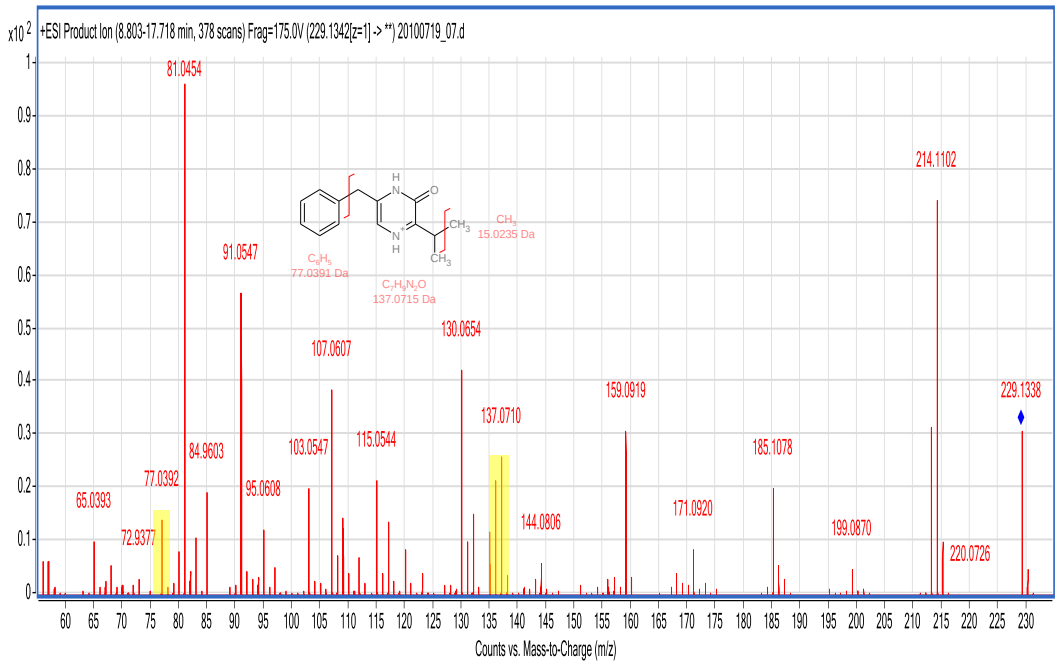
x10 2
+ESI Product Ion (8.803-17.718 min, 378 scans) Frag=175.0V (229.1342[z=1] -> **) 20100719_07.d
81.0454
214.1102
91.0547
130.0654
107.0607
159.0919
229.1338
137.0710
84.9603
103.0547
115.0544
185.1078
77.0392
95.0608
65.0393
144.0806
171.0920
72.9377
199.0870
220.0726
C6H5
77.0391 Da
CH2
15.0235 Da
C7H9N2O
137.0715 Da
Counts vs. Mass-to-Charge (m/z)

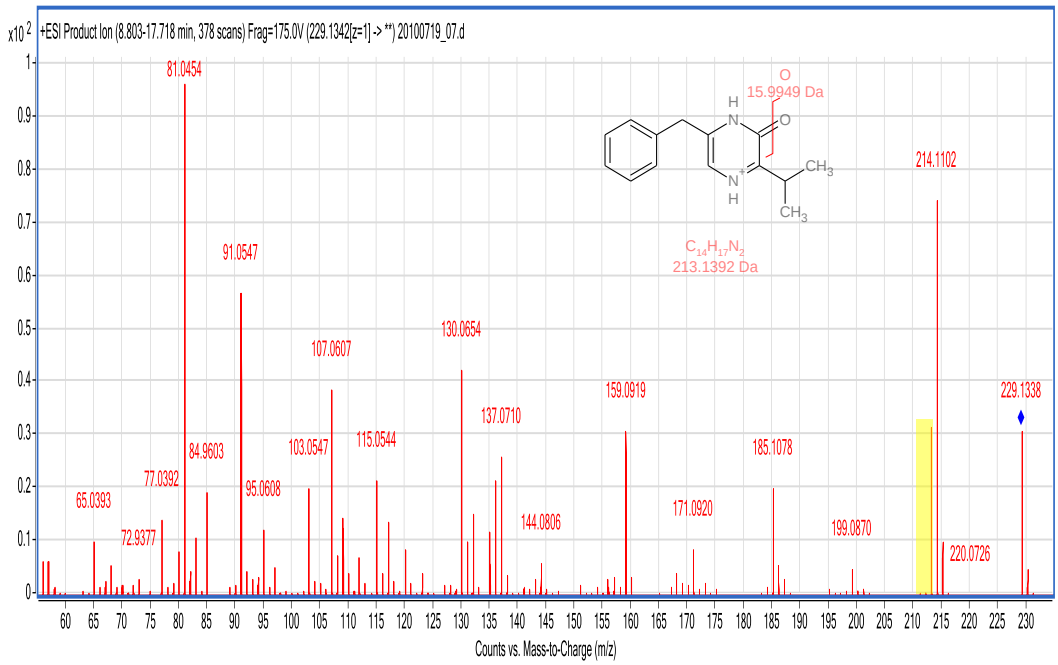
x10 2
+ESI Product Ion (8.803-17.718 min, 378 scans) Frag=175.0V (229.1342[z=1] -> **) 20100719_07.d
81.0454
91.0547
107.0607
130.0654
159.0919
229.1338
137.0710
84.9603
103.0547
115.0544
185.1078
77.0392
95.0608
65.0393
171.0920
144.0806
72.9377
199.0870
214.1102
220.0726
O
15.9949 Da
C14H17N2
213.1392 Da
Counts vs. Mass-to-Charge (m/z)

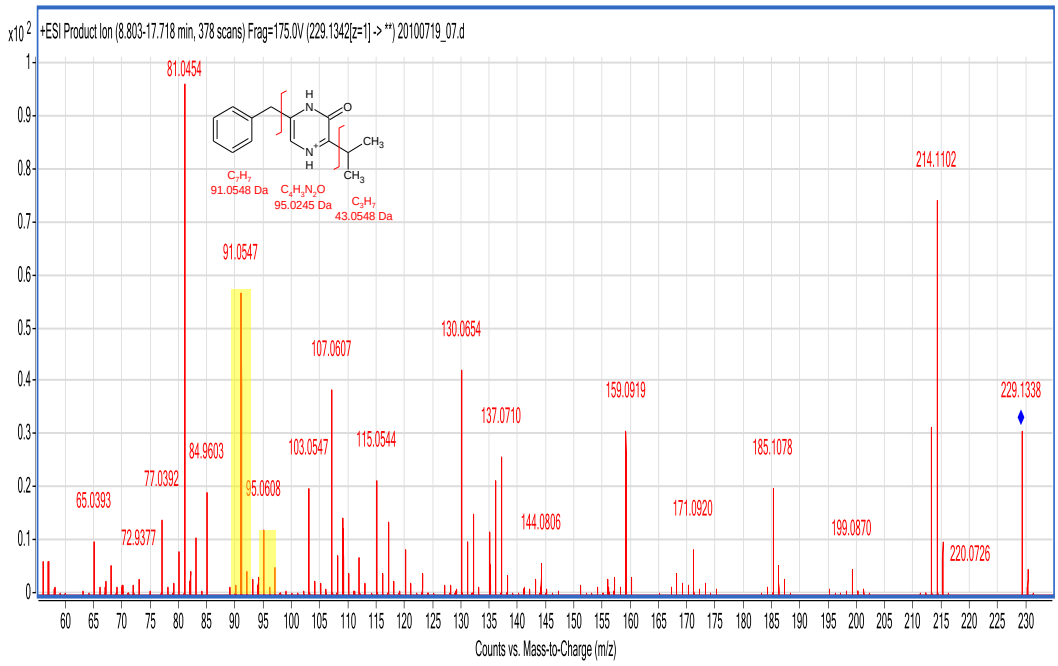
x10 2
+ESI Product Ion (8.803-17.718 min, 378 scans) Frag=175.0V (229.1342[z=1] -> **) 20100719_07.d
81.0454
91.0547
107.0607
130.0654
159.0919
229.1338
137.0710
84.9603
103.0547
115.0544
185.1078
77.0392
95.0608
65.0393
171.0920
144.0806
72.9377
199.0870
214.1102
220.0726
C7H7
91.0548 Da
C4H5N2O
95.0245 Da
C3H7
43.0548 Da
Counts vs. Mass-to-Charge (m/z)

APPENDIX C

BCM/PCM MICROARRAY DATA

RefSeq Transcript ID	Gene Symbol	OWA pval	FC PCMvEPI	FC BCMvEPI	FC BCMvPCM
NM_005252	c-FOS	2.59E-03	1.01	43.58	42.97
NM_001964	EGR1	4.80E-03	-1.10	17.79	19.58
NM_000584	IL8	4.01E-07	6.14	64.43	10.49
NM_002089	CXCL2	3.08E-07	6.21	62.11	10.00
NM_001030287	ATF3	1.06E-03	1.42	13.63	9.61
NM_003670	BHLHE40	1.40E-03	1.44	13.58	9.46
NM_000594	TNF alpha	4.00E-05	3.05	27.73	9.10
NM_005524	HES1	8.00E-05	1.80	13.71	7.62
NM_002090	CXCL3	6.65E-04	1.82	12.23	6.72
NM_004417	DUSP1	4.82E-04	1.62	10.13	6.24
NM_000584	IL8	6.39E-07	10.59	59.10	5.58
NM_004417	DUSP1	1.05E-06	2.88	15.96	5.54
NM_005524	HES1	7.06E-05	1.70	7.26	4.28
NM_003407	ZFP36	4.99E-05	1.76	7.08	4.02
NM_000600	IL6	1.79E-03	1.06	3.40	3.20
NM_006290	TNFAIP3	1.06E-07	4.39	13.59	3.10
NM_005261	GEM	1.28E-05	5.93	18.02	3.04
NM_001040874	HIST2H2AA3 /// HIST2H2AA4	6.43E-03	-1.01	2.95	2.99
NM_001040874	HIST2H2AA3 /// HIST2H2AA4	7.78E-03	1.08	3.08	2.85
NM_020307	CCNL1	7.92E-03	1.03	2.86	2.78
NM_020317	C1orf63	1.14E-03	1.34	3.61	2.70
NM_014330	PPP1R15A	7.47E-05	3.42	8.87	2.59
NM_015675	GADD45B	6.74E-03	-1.06	2.30	2.44
NM_000499	CYP1A1	9.05E-03	1.12	2.63	2.35
NM_005066	SFPQ	1.74E-04	1.51	3.52	2.34
NM_005980	S100P	1.98E-03	1.29	2.86	2.21
---	H2BFS	4.65E-03	1.06	2.32	2.19
NM_015675	GADD45B	7.18E-03	1.01	2.18	2.15
NM_014330	PPP1R15A	4.04E-05	4.47	9.57	2.14
NM_001025366	VEGFA	1.12E-04	3.93	8.08	2.05
NM_002228	c-JUN	3.54E-05	1.78	3.64	2.05
NM_003164	STX5	4.89E-03	1.04	1.93	1.86
NM_018217	EDEM2	6.00E-03	1.13	2.09	1.86
NM_000759	CSF3	6.73E-05	1.54	2.84	1.84
NM_022772	EPS8L2	3.40E-03	1.11	2.05	1.84
NM_005851	CDK2AP2	6.25E-03	1.03	1.89	1.83
NM_021063	HIST1H2BD	9.86E-03	1.30	2.37	1.82
NM_002228	JUN	1.20E-03	1.29	2.30	1.79
NM_006462	RBCK1	4.46E-03	1.05	1.84	1.76
NM_000758	CSF2	5.36E-04	2.43	4.24	1.75
NM_000561	GSTM1	1.16E-03	1.08	1.87	1.73
NM_001127603	C9orf95	5.25E-03	1.25	2.12	1.69
NM_016086	STYXL1	3.26E-03	1.18	1.98	1.68
NM_003945	ATP6V0E1	9.09E-03	1.07	1.81	1.68
NM_004428	EFNA1	1.59E-04	3.84	6.44	1.68
NM_006290	TNFAIP3	1.06E-05	2.93	4.90	1.67
NM_012088	PGLS	8.60E-03	-1.04	1.61	1.67
NM_007350	PHLDA1	4.33E-03	1.13	1.88	1.66
NM_000520	HEXA	9.81E-03	1.09	1.81	1.65
NM_018075	ANO10	9.14E-03	-1.05	1.56	1.64
NM_017670	OTUB1	6.04E-03	1.14	1.86	1.64
NM_000848	GSTM2	2.98E-03	1.16	1.88	1.62
NM_001142464	ECSIT	3.26E-04	1.19	1.92	1.62
NM_004596	SNRPA	9.27E-03	-1.00	1.61	1.61
NM_080593	HIST1H2BK	8.52E-03	1.03	1.64	1.59
NM_000917	P4HA1	5.60E-03	1.23	1.95	1.59
NM_002229	JUNB	1.48E-05	2.31	3.65	1.58
NM_000612	IGF2 /// INS-IGF2	2.11E-04	1.46	2.31	1.58
NM_024112	C9orf16	6.34E-04	1.18	1.86	1.58

NM_013349	NENF	6.15E-03	1.03	1.63	1.58
NM_007233	TP53TG1	8.16E-03	1.07	1.68	1.58
NM_000089	COL1A2	1.30E-03	1.08	1.70	1.57
NM_005529	HSPG2	4.02E-03	1.13	1.78	1.57
NM_001025234	TSPAN4	2.51E-03	1.02	1.60	1.56
NM_020529	NFKBIA	1.17E-04	2.35	3.65	1.55
NM_013402	FADS1	3.99E-03	1.02	1.58	1.55
NM_207340	ZDHHC24	8.63E-03	1.11	1.72	1.54
NM_006712	FASTK	5.53E-03	1.02	1.57	1.54
NM_016429	COPZ2	1.93E-03	1.08	1.63	1.52
NM_001155	ANXA6	8.45E-03	1.07	1.61	1.51
NM_001511	CXCL1	5.35E-04	13.86	20.81	1.50
NM_021178	CCNB1IP1	6.72E-03	1.04	1.56	1.50
NM_002016	FLG	6.67E-03	1.72	2.58	1.49
NM_001122	ADFP	4.71E-03	1.48	2.21	1.49
NM_001300	KLF6	9.10E-03	1.57	2.33	1.49
NM_005412	SHMT2	6.82E-03	1.07	1.58	1.48
NM_013402	FADS1	5.14E-03	1.12	1.65	1.48
NM_172341	PSENEN	5.63E-03	1.14	1.67	1.47
NM_001124	ADM	1.19E-04	2.53	3.67	1.45
NM_001101669	INPP4B	8.85E-03	1.11	1.61	1.45
NM_002831	PTPN6	1.49E-03	1.27	1.84	1.44
NM_003258	TK1	8.23E-03	1.15	1.64	1.43
NM_001122837	RAG1AP1	3.22E-03	1.08	1.53	1.42
NM_007350	PHLDA1	1.29E-04	1.15	1.63	1.42
NM_018999	KIAA1128	3.07E-03	1.09	1.54	1.42
NM_006623	PHGDH	4.57E-03	1.25	1.77	1.41
NM_016145	C19orf56	3.95E-03	1.08	1.52	1.41
NM_001040437	C6orf48	3.79E-04	1.18	1.66	1.41
NM_012323	MAFF	5.97E-04	2.56	3.61	1.41
NM_001136032	KLK11	5.16E-03	1.24	1.73	1.40
NM_001659	ARF3	6.61E-03	1.13	1.57	1.40
NM_002961	S100A4	3.41E-04	1.35	1.88	1.39
NM_000431	MVK	2.14E-03	1.29	1.80	1.39
NM_002228	JUN	2.46E-03	1.13	1.56	1.38
NM_000077	CDKN2A	2.61E-03	1.13	1.56	1.38
NM_001196	BID	5.27E-05	1.20	1.64	1.36
NM_022477	NDRG3	6.90E-03	1.17	1.58	1.35
NM_002032	FTH1	4.70E-03	1.31	1.78	1.35
NM_025079	ZC3H12A	2.73E-03	2.45	3.30	1.34
NM_001913	CUX1	1.56E-03	1.39	1.86	1.34
NM_003670	BHLHE40	2.39E-03	1.57	2.10	1.33
NM_003915	CPNE1	6.98E-03	1.22	1.61	1.32
NM_006462	RBCK1	4.82E-03	1.15	1.51	1.32
NM_000874	IFNAR2	1.68E-03	1.16	1.52	1.31
NM_012323	MAFF	9.37E-04	2.56	3.35	1.31
NM_002475	MYL6B	6.47E-03	1.32	1.72	1.30
NM_001018016	MUC1	1.67E-03	1.31	1.69	1.29
NM_006346	PIBF1	7.74E-03	1.46	1.89	1.29
NM_000695	ALDH3B2	1.78E-03	1.50	1.93	1.29
NM_014357	LCE2B	1.88E-03	2.32	2.98	1.29
NM_021922	FANCE	2.97E-03	1.25	1.60	1.28
NM_020412	CHMP1B	9.37E-04	1.71	2.18	1.28
NM_001130964	PLCD1	8.44E-03	1.27	1.59	1.25
NM_001551	IGBP1	4.07E-03	1.36	1.67	1.23
NM_004323	BAG1	1.63E-03	1.62	1.96	1.21
NM_000247	MICA	4.76E-03	1.29	1.53	1.19
NM_001013436	MPST	9.06E-03	1.47	1.75	1.19
NM_001880	ATF2	8.10E-03	1.51	1.79	1.18
NM_001130046	CCL20	2.94E-03	12.01	13.92	1.16
NM_002093	GSK3B	9.86E-03	1.51	1.72	1.14
NM_001098478	HLA-F	2.36E-03	1.37	1.56	1.14
NM_006121	KRT1	1.86E-03	1.81	2.02	1.12
NM_006931	SLC2A3	1.54E-03	2.28	2.54	1.11
NM_000045	ARG1	2.69E-03	1.92	2.14	1.11
NM_001172	ARG2	4.64E-03	1.52	1.68	1.11
NM_001042483	NUPR1	2.66E-03	2.58	2.86	1.11
NM_005730	CTDSP2	5.86E-03	1.48	1.63	1.10
NM_006026	H1FX	4.24E-03	1.59	1.72	1.08
NM_003897	IER3	1.94E-03	2.70	2.88	1.07

NM_015721	GEMIN4	6.82E-03	-5.02	-4.72	1.07
NM_001015881	TSC22D3	4.20E-03	2.68	2.85	1.06
NM_024598	C16orf57	3.59E-03	1.45	1.54	1.06
NM_000314	PTEN /// PTENP1	5.05E-03	2.17	2.28	1.05
NM_001039199	TTPAL	8.80E-03	-2.25	-2.14	1.05
NM_016470	C20orf111	4.98E-03	2.87	2.98	1.04
NM_001136007	FXYD3	2.15E-03	2.40	2.49	1.04
NM_019058	DDIT4	1.58E-03	1.55	1.60	1.03
NM_004419	DUSP5	5.72E-03	2.88	2.96	1.03
NM_001008211	OPTN	9.58E-03	1.54	1.55	1.01
NM_001539	DNAJA1	6.71E-03	-2.36	-2.34	1.01
NM_022717	SNRNP35	4.83E-03	-1.85	-1.83	1.01
NM_018321	BXDC2	5.78E-03	-2.65	-2.64	1.01
NM_015014	RBM34	6.44E-03	-2.46	-2.45	1.00
NM_014976	PDCD11	5.99E-03	-1.51	-1.51	-1.00
NM_003290	TPM4	8.14E-03	-1.58	-1.59	-1.01
NM_014597	DNTTIP2	4.40E-03	-1.82	-1.86	-1.02
NM_001033059	AMD1	4.73E-03	-1.52	-1.56	-1.03
NM_017446	MRPL39	8.13E-03	-1.83	-1.91	-1.05
NM_001099638	ZNF146	4.43E-03	-1.49	-1.56	-1.05
NM_000378	WT1	7.23E-03	-2.27	-2.40	-1.05
NM_015036	ENDOD1	8.65E-03	-1.65	-1.75	-1.06
NM_002703	PPAT	4.93E-03	-2.11	-2.24	-1.06
NM_025065	BXDC5	9.31E-03	-1.51	-1.61	-1.07
NM_014452	TNFRSF21	2.61E-03	-1.41	-1.51	-1.08
NM_017897	OXSM	9.69E-03	-2.75	-2.95	-1.08
NM_024808	C13orf34	7.03E-03	-2.87	-3.10	-1.08
NM_023940	RASL11B	3.45E-03	-1.67	-1.80	-1.08
NM_014864	FAM20B	2.10E-03	-1.50	-1.63	-1.09
NM_015475	FAM98A	1.66E-03	-1.66	-1.81	-1.09
NM_001539	DNAJA1	6.59E-04	-1.45	-1.59	-1.09
NM_014793	LCMT2	3.25E-03	-2.95	-3.24	-1.10
NM_016037	UTP11L	3.61E-04	-1.53	-1.68	-1.10
NM_001102397	HNRNPR	3.69E-04	-1.51	-1.67	-1.10
NM_031218	ZNF93	1.05E-03	-1.41	-1.55	-1.10
NM_014777	URB2	9.62E-03	-2.37	-2.62	-1.11
NM_006527	SLBP	2.38E-03	-1.40	-1.56	-1.11
NM_005415	SLC20A1	2.33E-03	-1.53	-1.70	-1.11
NM_001135650	EEF1E1	9.23E-03	-1.88	-2.10	-1.12
NM_006784	WDR3	2.28E-03	-4.01	-4.48	-1.12
NM_006805	HNRNPA0	1.25E-03	-1.82	-2.04	-1.12
NM_000418	IL4R	2.45E-03	-2.09	-2.37	-1.13
NM_012341	GTPBP4	3.84E-03	-2.34	-2.66	-1.14
NM_016077	PTRH2	7.77E-04	-2.12	-2.41	-1.14
NM_032195	SON	1.82E-03	-1.54	-1.76	-1.14
NM_001035521	GTF3C2	6.49E-03	-1.50	-1.72	-1.14
NM_017810	ZNF434	1.78E-03	-1.90	-2.18	-1.15
NM_025141	TM2D3	3.81E-03	-1.44	-1.66	-1.15
NM_198514	NHLRC2	3.23E-03	-2.61	-3.02	-1.16
NM_022366	TFB2M	7.47E-03	-1.94	-2.25	-1.16
NM_015062	PPRC1	4.43E-03	-2.35	-2.73	-1.16
NM_001113378	FANCI	7.29E-03	-1.52	-1.78	-1.17
NM_021732	AVPI1	8.17E-03	7.17	6.13	-1.17
NM_000693	ALDH1A3	4.25E-04	-2.30	-2.69	-1.17
NM_000430	PAFAH1B1	7.66E-03	-1.91	-2.25	-1.18
NM_018072	HEATR1	3.18E-03	-1.48	-1.74	-1.18
NM_001099415	POM121 /// POM121C	7.29E-04	-1.58	-1.87	-1.18
NM_002915	RFC3	6.10E-03	-2.46	-2.90	-1.18
NM_018225	SMU1	1.01E-05	-1.30	-1.54	-1.19
NM_024094	DSCC1	9.57E-03	-1.45	-1.73	-1.19
NM_003086	SNAPC4	1.14E-03	-1.48	-1.76	-1.19
NM_006622	PLK2	1.09E-03	-1.53	-1.82	-1.19
NM_001135191	ASAP2	1.16E-03	-1.33	-1.59	-1.19
NM_002915	RFC3	7.65E-03	-3.24	-3.88	-1.20
NM_016448	DTL	5.23E-03	-2.77	-3.33	-1.20
NM_006372	SYNCRIP	2.75E-03	-1.30	-1.57	-1.20
NM_024831	TGS1	5.39E-03	-1.61	-1.94	-1.20
NM_001009182	SIP1	2.84E-03	-1.83	-2.20	-1.21
NM_017676	GIN1	4.59E-03	-3.33	-4.02	-1.21
NM_004760	STK17A	1.26E-03	-1.64	-1.99	-1.21

NM_001554	CYR61	4.02E-03	-1.24	-1.50	-1.21
NM_003290	TPM4	7.11E-03	-1.36	-1.64	-1.21
NM_003246	THBS1	3.67E-05	-1.35	-1.64	-1.21
NM_012341	GTPBP4	7.62E-04	-2.35	-2.86	-1.21
NM_017955	CDCA4	8.20E-04	-1.33	-1.61	-1.21
NM_001085458	CTNND1	2.74E-03	-1.61	-1.96	-1.22
NM_003824	FADD	1.14E-03	-1.87	-2.28	-1.22
NM_004457	ACSL3	3.99E-03	-1.29	-1.58	-1.23
NM_006029	PNMA1	2.00E-03	-2.15	-2.63	-1.23
NM_005791	MPHOSPH10	4.45E-03	-1.91	-2.36	-1.23
NM_004508	IDI1	1.93E-04	-1.28	-1.58	-1.24
---	---	4.21E-04	-1.22	-1.51	-1.24
NM_004111	FEN1	8.39E-04	-1.38	-1.71	-1.24
NM_019008	SMCR7L	2.82E-03	-1.76	-2.18	-1.24
NM_022720	DGCR8	1.09E-04	-1.45	-1.80	-1.24
NM_014613	FAF2	1.12E-03	-1.61	-1.99	-1.24
NM_017730	QRICH1	4.16E-04	-1.27	-1.57	-1.24
NM_006810	PDIA5	4.69E-03	-1.28	-1.60	-1.24
NM_002890	RASA1	1.88E-03	-1.46	-1.81	-1.24
NM_012207	HNRNPH3	1.47E-03	-1.71	-2.13	-1.25
NM_006306	SMC1A	5.31E-03	-1.27	-1.58	-1.25
NM_001135650	EEF1E1	3.42E-03	-1.28	-1.60	-1.25
NM_003309	TSPYL1	1.49E-04	-1.43	-1.79	-1.25
NM_016333	SRRM2	4.10E-04	-1.21	-1.53	-1.26
NM_003246	THBS1	9.35E-05	-1.34	-1.69	-1.26
NM_006963	ZNF22	4.83E-03	-2.17	-2.75	-1.27
NM_022720	DGCR8	2.99E-03	-1.66	-2.11	-1.27
NR_015350	KIAA0040	6.27E-04	-1.23	-1.58	-1.28
NM_003885	CDK5R1	6.60E-03	-3.19	-4.09	-1.28
NM_014706	SART3	2.57E-03	-1.74	-2.24	-1.28
NM_012245	SNW1	1.52E-04	-1.22	-1.57	-1.29
NM_002267	KPNA3	5.75E-03	-1.23	-1.58	-1.29
NM_024775	GEMIN6	7.69E-04	-2.35	-3.03	-1.29
NM_000430	PAFAH1B1	6.14E-04	-2.58	-3.34	-1.29
NM_001007239	KIAA0859	1.74E-03	-1.57	-2.03	-1.30
NM_004124	GMFB	6.24E-03	-1.24	-1.61	-1.30
NM_002890	RASA1	1.68E-03	-1.48	-1.92	-1.30
NM_003405	YWHAH	1.50E-04	-1.41	-1.83	-1.30
NM_014458	KLHL20	5.96E-03	-2.53	-3.29	-1.30
NM_018639	WSB2	1.96E-03	-1.15	-1.50	-1.30
NM_014825	URB1	2.01E-03	-1.69	-2.21	-1.30
NM_018993	RIN2	3.11E-04	-1.35	-1.76	-1.31
NM_006322	TUBGCP3	6.87E-03	-2.26	-2.95	-1.31
NM_001008895	CUL4A	9.39E-03	-1.27	-1.66	-1.31
NM_015338	ASXL1	4.86E-03	-1.67	-2.19	-1.31
NM_003859	DPM1	2.66E-03	-1.15	-1.51	-1.31
NM_001096	ACLY	2.87E-03	-1.21	-1.59	-1.32
NM_000254	MTR	4.69E-03	-1.74	-2.29	-1.32
NM_001025247	TAF5L	1.62E-03	-1.62	-2.13	-1.32
NM_005754	G3BP1	5.78E-04	-1.27	-1.68	-1.32
NM_005334	HCFC1	4.36E-05	-1.25	-1.65	-1.32
NM_014740	EIF4A3	8.78E-04	-1.19	-1.58	-1.32
NM_004508	IDI1	1.17E-03	-1.18	-1.56	-1.32
NM_001130849	CAB39	4.08E-05	-1.20	-1.59	-1.33
NM_001957	EDNRA	1.83E-03	-2.07	-2.75	-1.33
NM_000888	ITGB6	6.90E-03	-1.80	-2.41	-1.34
NM_022081	HPS4	2.81E-03	-1.25	-1.68	-1.35
NM_018380	DDX28	1.42E-03	-1.85	-2.49	-1.35
NM_001127321	CBX5	1.40E-03	-1.13	-1.52	-1.35
NM_001128918	MARK3	3.33E-03	-1.32	-1.79	-1.36
NM_001007024	GOSR1	8.45E-03	-2.01	-2.73	-1.36
NM_015131	WDR43	4.33E-05	-1.60	-2.18	-1.36
NM_002834	PTPN11	5.67E-04	-1.43	-1.94	-1.36
NM_007192	SUPT16H	4.89E-04	-1.47	-2.01	-1.37
NM_001018090	GCOM1 /// GRINL1A	9.74E-03	-1.37	-1.88	-1.37
NM_018117	BRWD2	5.23E-03	-1.32	-1.81	-1.37
NM_014504	RABGEF1	1.33E-03	-1.27	-1.75	-1.38
NM_001241	CCNT2	1.64E-03	-2.15	-2.96	-1.38
NM_018657	MYNN	5.55E-03	-1.45	-2.00	-1.38
NM_015957	APIP	2.59E-04	-1.33	-1.84	-1.38

NM_005643	TAF11	3.25E-05	-1.32	-1.82	-1.38
NM_017736	THUMPD1	1.53E-03	-1.65	-2.29	-1.38
NM_007375	TARDBP	5.88E-03	-1.11	-1.54	-1.39
NM_001130678	EIF4E	2.32E-03	-1.21	-1.67	-1.39
NM_001100626	ERLIN1	4.06E-03	-1.12	-1.56	-1.39
NM_002911	UPF1	3.55E-04	-1.18	-1.64	-1.39
NM_014388	C1orf107	3.03E-03	-1.17	-1.63	-1.39
NM_004856	KIF23	1.41E-04	-2.14	-2.97	-1.39
NM_005429	VEGFC	7.88E-05	-1.22	-1.70	-1.39
NM_001031701	NT5DC3	2.61E-03	-1.26	-1.76	-1.40
NM_000373	UMPS	5.38E-04	-2.73	-3.81	-1.40
NM_198256	E2F6	4.20E-03	-1.44	-2.03	-1.41
NM_004697	PRPF4	2.67E-03	-2.45	-3.45	-1.41
NM_017953	ZNHIT6	8.23E-03	-2.18	-3.07	-1.41
NM_024644	C14orf169	3.38E-04	-3.28	-4.62	-1.41
NM_030755	TXNDC1	6.72E-03	-1.15	-1.63	-1.41
NM_000662	NAT1	2.36E-03	-2.90	-4.09	-1.41
NM_014166	MED4	6.22E-03	-1.36	-1.93	-1.42
NM_003800	RNGTT	9.58E-03	-1.10	-1.56	-1.42
NM_014941	MORC2	8.82E-03	-1.41	-2.00	-1.42
NM_004580	RAB27A	7.17E-03	-2.07	-2.94	-1.42
NM_003170	SUPT6H	5.67E-03	-1.08	-1.54	-1.42
NM_014388	C1orf107	9.08E-03	-1.57	-2.24	-1.43
NM_025222	WDR82	4.25E-03	-1.12	-1.60	-1.43
NM_018361	AGPAT5	1.61E-03	-1.82	-2.60	-1.43
NM_025076	UXS1	1.35E-05	-1.24	-1.78	-1.43
NM_001007239	KIAA0859	3.56E-04	-1.75	-2.52	-1.44
NM_003486	SLC7A5	4.37E-04	-1.12	-1.61	-1.44
NM_018469	TEX2	3.62E-04	-1.11	-1.59	-1.44
NM_001358	DHX15	3.65E-04	-1.14	-1.64	-1.44
NM_015462	NOL11	4.69E-04	-2.06	-2.96	-1.44
NM_001083914	CTBP2	6.53E-03	-1.21	-1.74	-1.44
NM_003925	MBD4	2.70E-03	-1.54	-2.21	-1.44
NM_003350	UBE2V2	8.92E-04	-1.26	-1.82	-1.44
NM_030628	INTS5	2.17E-03	-1.46	-2.11	-1.44
NM_001003690	MAD2L1BP	1.98E-03	-1.24	-1.79	-1.44
NM_017665	ZCCHC10	8.17E-03	-2.39	-3.48	-1.45
NM_199072	MDFIC	6.79E-03	-1.40	-2.03	-1.45
NM_014657	KIAA0406	1.85E-03	-2.12	-3.09	-1.46
NM_004549	NDUFC2	2.75E-04	-1.16	-1.68	-1.46
NM_002417	MKI67	2.46E-03	-1.10	-1.60	-1.46
NM_001085458	CTNND1	4.49E-05	-1.27	-1.85	-1.46
NM_000361	THBD	1.01E-04	-2.51	-3.66	-1.46
NM_014616	ATP11B	7.75E-03	-1.14	-1.66	-1.46
NM_000788	DCK	4.94E-03	-1.57	-2.29	-1.46
NM_001135943	MADD	9.27E-03	-1.05	-1.53	-1.46
NM_0043188	ASPH	1.48E-03	-1.23	-1.79	-1.46
NM_001085458	CTNND1	1.49E-03	-1.15	-1.68	-1.46
NM_003934	FUBP3	1.52E-03	-1.47	-2.14	-1.46
NM_014078	MRPL13	2.30E-04	-1.18	-1.73	-1.47
NM_018082	POLR3B	1.12E-03	-2.37	-3.51	-1.48
NM_024747	HPS6	3.07E-05	-2.80	-4.13	-1.48
NM_001033521	CSTF1	3.22E-03	-2.04	-3.01	-1.48
NM_001024808	BCL7A	1.66E-03	-1.31	-1.94	-1.48
NM_014751	MTSS1	3.01E-04	-1.24	-1.83	-1.48
NM_003600	AURKA	1.89E-03	-1.33	-1.98	-1.48
NM_001128844	SMARCA4	3.40E-03	-1.03	-1.54	-1.49
NM_001098424	DLG1	4.05E-03	-1.10	-1.64	-1.50
NM_001042510	ZNF706	6.43E-04	-1.15	-1.73	-1.50
NM_004953	EIF4G1	5.12E-04	-1.11	-1.67	-1.51
NM_022470	ZMAT3	3.01E-03	-1.04	-1.57	-1.51
NM_001005739	VPS54	3.64E-03	-2.09	-3.15	-1.51
NM_001042388	PPP4R1	2.85E-03	-1.14	-1.73	-1.51
NM_005926	MFAP1	6.93E-03	-1.27	-1.92	-1.51
NM_080686	BAT2	8.22E-04	-1.18	-1.78	-1.51
NM_005466	MED6	7.22E-05	-1.33	-2.01	-1.51
NM_000373	UMPS	2.15E-04	-2.41	-3.65	-1.51
NM_003615	SLC4A7	7.34E-05	-1.48	-2.24	-1.51
NM_024745	SHCBP1	8.11E-03	-1.95	-2.95	-1.51
NM_006624	ZMYND11	6.07E-03	-1.32	-1.99	-1.52

NM_004161	RAB1A	1.58E-03	-1.16	-1.76	-1.52
NM_014820	TOMM70A	1.44E-03	-1.20	-1.83	-1.52
NM_002182	IL1RAP	6.90E-04	-1.40	-2.13	-1.52
NM_004729	ZBED1	1.03E-04	-1.31	-2.00	-1.52
NM_018380	DDX28	8.17E-05	-2.01	-3.07	-1.52
NM_000445	PLEC1	3.74E-03	-1.21	-1.84	-1.52
NM_020368	UTP3	1.19E-05	-1.68	-2.57	-1.53
NM_001128615	ARHGEF3	2.40E-03	-1.26	-1.92	-1.53
NM_007114	TMF1	2.17E-03	-1.35	-2.06	-1.53
NM_015073	SIPA1L3	1.88E-03	-1.11	-1.70	-1.53
NM_006267	RANBP2	7.93E-04	-1.44	-2.21	-1.54
NM_001009993	FAM168B	5.93E-03	1.00	-1.53	-1.54
NM_002956	CLIP1	1.04E-03	-1.27	-1.96	-1.54
NM_005607	PTK2	2.54E-03	-1.08	-1.66	-1.54
NM_012408	ZMYND8	2.37E-03	-2.26	-3.48	-1.54
NM_013286	RBM15B	3.56E-03	-1.30	-2.00	-1.54
NM_018994	FBXO42	3.22E-03	-1.27	-1.96	-1.54
NM_003198	TCEB3	2.21E-04	-2.50	-3.87	-1.55
---	---	2.25E-03	-1.49	-2.31	-1.55
NM_024620	ZNF329	6.54E-03	-1.62	-2.52	-1.55
NM_006387	CHERP	3.80E-04	-1.79	-2.77	-1.55
NM_001457	FLNB	7.53E-03	-1.02	-1.59	-1.56
NM_003201	TFAM	3.55E-03	-1.74	-2.72	-1.56
NM_001100398	GARNL4	1.09E-03	-1.23	-1.93	-1.57
NM_030628	INTS5	2.57E-03	-1.89	-2.97	-1.57
NM_003640	IKBKAP	6.82E-04	-1.25	-1.97	-1.57
NM_003796	C19orf2	1.45E-03	-1.27	-1.99	-1.57
NM_016284	CNOT1	5.72E-04	-1.37	-2.15	-1.57
NM_017669	ERCC6L	7.17E-05	-2.00	-3.15	-1.57
NM_012207	HNRNPH3	7.80E-03	-1.09	-1.71	-1.58
NM_002748	MAPK6 (erk 3)	3.46E-03	-1.23	-1.95	-1.58
NM_020336	KIAA1219	4.05E-03	-1.59	-2.51	-1.58
NM_001007024	GOSR1	1.29E-05	-1.68	-2.65	-1.58
NM_012164	FBXW2	9.92E-03	-1.19	-1.88	-1.58
NM_012406	PRDM4	3.34E-03	-1.14	-1.80	-1.58
NM_012207	HNRNPH3	2.15E-03	-1.14	-1.80	-1.58
NM_006363	SEC23B	5.39E-03	-1.48	-2.34	-1.58
NM_003170	SUPT6H	5.02E-03	-1.05	-1.68	-1.59
NM_015283	DPY19L1	3.01E-03	-1.11	-1.78	-1.60
NM_003439	ZKSCAN1	3.61E-03	-2.09	-3.35	-1.60
NM_006565	CTCF	1.66E-03	-2.57	-4.13	-1.60
NM_002834	PTPN11	7.64E-03	-1.06	-1.70	-1.61
NM_001136115	FBXO28	7.44E-03	-1.39	-2.24	-1.61
NM_003463	PTP4A1	4.17E-03	-1.02	-1.65	-1.61
NM_001033085	HAT1	1.13E-03	-1.11	-1.79	-1.61
NM_004318	ASPH	2.29E-05	-1.25	-2.02	-1.61
NM_003584	DUSP11	1.49E-05	-1.56	-2.53	-1.62
NM_016248	AKAP11	4.89E-03	-1.60	-2.59	-1.62
NM_015110	SMC5	9.34E-03	-1.37	-2.21	-1.62
NM_005760	CEBPZ	7.48E-04	-1.49	-2.43	-1.63
NM_001241	CCNT2	5.17E-04	-1.84	-2.99	-1.63
NM_004973	JARID2	3.42E-04	-1.21	-1.97	-1.64
NM_003107	SOX4	4.07E-04	-1.40	-2.29	-1.64
NM_001130107	KLC1	4.03E-03	-1.22	-2.00	-1.65
NM_001624	AIM1	1.49E-03	-1.08	-1.79	-1.65
NM_022754	SFXN1	4.04E-03	-1.13	-1.88	-1.66
NM_002408	MGAT2	1.16E-03	-1.71	-2.84	-1.66
---	---	7.20E-03	-1.05	-1.75	-1.66
NM_012346	NUP62	1.61E-03	-1.25	-2.08	-1.67
NM_018492	PBK	1.70E-03	-1.32	-2.20	-1.67
NM_015500	C2CD2	7.20E-04	-1.64	-2.74	-1.67
NM_015634	KIAA1279	1.45E-03	-1.71	-2.87	-1.67
NM_003590	CUL3	9.25E-04	-2.59	-4.34	-1.68
NM_001042426	CENPA	6.16E-04	-1.30	-2.20	-1.69
NM_001114978	TP63	5.51E-04	-1.15	-1.95	-1.70
NM_005680	TAF1B	6.29E-03	-1.16	-1.98	-1.71
NM_012406	PRDM4	8.36E-03	1.01	-1.70	-1.71
NM_025126	RNF34	3.66E-03	-1.66	-2.84	-1.71
NM_001137550	LRRFIP1	4.08E-03	-1.04	-1.78	-1.72
NM_016195	KIF20B	6.21E-04	-1.28	-2.20	-1.72

NM_005724	TSPAN3	6.59E-03	1.01	-1.70	-1.72
NM_000376	VDR	3.46E-06	-1.52	-2.62	-1.73
NM_001128930	ENTPD4	7.39E-03	-2.05	-3.55	-1.74
NM_017542	POGK	4.67E-06	-2.28	-3.96	-1.74
NM_003129	SQLE	3.02E-03	-1.01	-1.76	-1.74
NM_015056	RRP1B	2.14E-03	-1.18	-2.07	-1.75
NM_015409	EP400	5.11E-05	-1.28	-2.23	-1.75
NM_003401	XRCC4	9.61E-05	-1.39	-2.43	-1.75
NM_016441	CRIM1	8.46E-03	-1.05	-1.84	-1.75
NM_019589	YLPM1	5.06E-03	-1.22	-2.14	-1.75
NM_000361	THBD	3.56E-05	-2.17	-3.82	-1.75
NM_003750	EIF3A	4.26E-03	-2.43	-4.28	-1.76
NM_002589	PCDH7	2.60E-04	-2.10	-3.70	-1.76
NM_001358	DHX15	6.63E-03	1.01	-1.75	-1.77
NM_016258	YTHDF2	1.14E-03	-1.31	-2.31	-1.77
NM_001717	BNC1	6.41E-03	-1.04	-1.84	-1.77
NM_001618	PARP1	6.49E-03	1.02	-1.75	-1.77
NM_001042635	NGDN	4.20E-03	-1.49	-2.65	-1.78
NM_001040020	FAM3C	8.51E-03	-1.13	-2.03	-1.79
NM_002589	PCDH7	8.54E-04	-1.69	-3.03	-1.79
NM_021960	MCL1	2.53E-03	-1.12	-2.00	-1.79
NM_004747	DLG5	2.01E-03	-1.05	-1.89	-1.80
NM_001100819	MOBKL3	5.01E-03	-1.50	-2.70	-1.80
NM_001025107	ADAR	6.62E-03	-1.03	-1.87	-1.81
NM_030621	DICER1	2.59E-04	-2.93	-5.31	-1.81
NM_024513	FYCO1	1.17E-03	-1.31	-2.38	-1.81
NM_000376	VDR	7.98E-04	-1.38	-2.52	-1.82
NM_015339	ADNP	1.28E-04	-1.97	-3.62	-1.84
NM_001130674	CALU	4.17E-03	-1.13	-2.08	-1.85
NM_017582	UBE2Q1	9.56E-03	-1.16	-2.15	-1.85
NM_002902	RCN2	1.64E-03	-1.07	-1.99	-1.85
NM_005737	ARL4C	8.49E-03	1.01	-1.84	-1.86
NM_001005476	PKP4	6.64E-03	-1.01	-1.88	-1.87
NM_016604	JMJD1B	1.03E-03	-1.34	-2.50	-1.87
NM_006822	RAB40B	5.79E-03	-1.36	-2.53	-1.87
NM_012167	FBXO11	2.03E-03	-1.29	-2.41	-1.87
NM_004705	PRKRIR	6.44E-04	-1.67	-3.12	-1.87
NM_002816	PSMD12	2.06E-03	-1.09	-2.04	-1.88
NM_018092	NETO2	1.35E-03	-1.68	-3.16	-1.88
NM_003794	SNX4	6.28E-03	-1.37	-2.58	-1.88
NM_024654	NOL9	3.01E-03	-1.10	-2.08	-1.89
NM_003045	SLC7A1	4.54E-03	-1.04	-1.96	-1.89
NM_015354	NUP188	6.39E-03	-1.25	-2.37	-1.89
NM_015134	MPRIP	7.14E-03	1.01	-1.89	-1.91
NM_000176	NR3C1	1.39E-04	-1.42	-2.71	-1.91
NM_152758	YTHDF3	1.70E-03	-1.48	-2.84	-1.91
NM_018200	HMG20A	7.30E-03	-1.19	-2.28	-1.92
NM_002938	RNF4	7.78E-03	1.01	-1.90	-1.92
NM_004346	CASP3	6.63E-03	-1.02	-1.96	-1.92
NM_198834	ACACA	7.24E-03	1.03	-1.89	-1.93
NM_017782	C10orf18	3.29E-03	-1.42	-2.76	-1.94
NM_001105515	ABCC4	7.23E-03	-1.07	-2.08	-1.94
NM_015134	MPRIP	9.28E-03	1.01	-1.92	-1.94
NM_013231	FLRT2	7.98E-04	-1.10	-2.14	-1.95
NM_006391	IPO7	4.00E-03	-1.08	-2.11	-1.96
NM_002408	MGAT2	7.07E-04	-1.70	-3.34	-1.97
NM_003470	USP7	2.60E-03	-1.42	-2.80	-1.97
NM_003681	PDXK	9.33E-03	-1.04	-2.06	-1.98
NM_000346	SOX9	4.23E-04	-1.68	-3.34	-1.99
NM_015315	LARP1	9.94E-03	1.06	-1.87	-1.99
NM_003898	SYNJ2	2.62E-03	-1.68	-3.37	-2.00
NM_003796	C19orf2	1.61E-04	-1.41	-2.83	-2.01
NM_005116	SLC23A2	6.34E-03	-1.18	-2.38	-2.02
NM_015342	PPWD1	5.29E-03	-1.32	-2.67	-2.02
NM_000179	MSH6	1.12E-03	-1.31	-2.66	-2.03
NM_000214	JAG1	7.81E-03	-1.08	-2.20	-2.03
NM_004776	B4GALT5	6.67E-04	-1.21	-2.46	-2.03
NM_002816	PSMD12	5.71E-04	-1.24	-2.52	-2.03
NM_001143667	ZBED5	5.69E-03	-1.49	-3.03	-2.04
NM_001142522	FBXO5	1.60E-03	-1.61	-3.27	-2.04

NM_001083924	C1orf116	1.31E-03	-1.81	-3.70	-2.04
NM_001018009	SH3BP5	8.23E-03	-1.35	-2.78	-2.05
NM_032195	SON	2.15E-03	-1.21	-2.49	-2.06
NM_014866	SEC16A	1.99E-03	-1.25	-2.58	-2.07
NM_152260	RPUSD2	2.54E-03	-1.36	-2.81	-2.07
NM_003414	ZNF267	4.18E-03	-1.27	-2.63	-2.07
NM_006311	NCOR1	4.66E-03	-1.15	-2.40	-2.08
NM_178812	MTDH	5.19E-03	-1.05	-2.21	-2.10
NM_015048	SETD1B	1.64E-03	-1.16	-2.44	-2.11
NM_001100819	MOBKL3	1.67E-03	-1.20	-2.57	-2.13
NM_002834	PTPN11	3.40E-03	-1.24	-2.65	-2.14
NM_003325	HIRA	4.51E-03	-1.23	-2.62	-2.14
NM_001048166	STIL	4.93E-03	-1.40	-3.00	-2.14
NM_017798	YTHDF1	9.76E-03	1.04	-2.07	-2.15
NM_015158	KANK1	2.22E-04	-1.51	-3.28	-2.16
NM_003794	SNX4	3.58E-03	-1.23	-2.67	-2.17
NM_007034	DNAJB4	3.49E-03	-1.34	-2.91	-2.18
NM_006267	RANBP2	6.46E-03	-1.03	-2.27	-2.19
---	---	3.76E-03	-1.39	-3.05	-2.20
NM_012164	FBXW2	5.04E-03	-1.20	-2.64	-2.20
NM_004645	COIL	7.63E-04	-2.20	-4.91	-2.24
NM_012334	MYO10	2.30E-06	-1.61	-3.62	-2.25
NM_002430	MN1	8.56E-04	-1.46	-3.31	-2.26
NM_003489	NRIP1	3.39E-04	-1.62	-3.68	-2.27
NM_004093	EFNB2	5.72E-04	-1.19	-2.74	-2.30
NM_032195	SON	7.93E-04	-1.13	-2.60	-2.30
NM_014264	PLK4	8.52E-03	-1.07	-2.47	-2.30
NM_014016	SACM1L	9.94E-03	-1.05	-2.42	-2.32
NM_018343	RIOK2	9.31E-04	-2.23	-5.19	-2.32
NM_005513	GTF2E1	1.75E-04	-1.56	-3.62	-2.32
NM_016604	JMJD1B	3.38E-03	-1.60	-3.72	-2.32
NM_001755	CBFB	6.18E-04	-1.63	-3.81	-2.35
NM_002296	LBR	9.91E-03	1.05	-2.23	-2.35
NM_199072	MDFIC	6.57E-03	-1.19	-2.79	-2.35
NM_001079673	FNDC3A	9.25E-03	1.01	-2.33	-2.36
NM_015070	ZC3H13	5.00E-03	-1.93	-4.58	-2.37
NM_004627	WRB	9.69E-04	-1.76	-4.26	-2.42
NM_014671	UBE3C	1.60E-03	-1.14	-2.79	-2.44
NM_005895	GOLGA3	2.21E-03	-1.14	-2.78	-2.44
NM_014633	CTR9	1.40E-03	-1.14	-2.82	-2.48
NM_006420	ARFGEF2	1.59E-03	-1.16	-2.88	-2.48
NM_014838	ZBED4	5.08E-03	-1.13	-2.83	-2.51
NR_024275	LOC151162	8.58E-03	1.02	-2.46	-2.51
NM_003590	CUL3	1.85E-03	-1.12	-2.84	-2.53
NM_007034	DNAJB4	6.85E-03	-1.20	-3.04	-2.53
NM_015113	ZZEF1	4.67E-03	-1.02	-2.58	-2.54
NM_015123	FRMD4B	7.37E-03	-1.17	-3.02	-2.58
NM_001008925	RCHY1	3.50E-03	-1.47	-3.82	-2.59
NM_018149	C17orf71	7.84E-05	-1.94	-5.09	-2.62
NM_012096	APPL1	6.16E-03	-1.13	-2.97	-2.63
NM_002417	MKI67	8.93E-03	1.05	-2.52	-2.64
NM_001135820	TMEM2	7.08E-03	1.07	-2.48	-2.65
NM_001127231	AUTS2	9.36E-03	-1.06	-2.81	-2.67
NM_004815	ARHGAP29	3.06E-03	-1.04	-2.78	-2.67
NM_017742	ZCCHC2	7.06E-03	-1.23	-3.30	-2.68
NM_003129	SQLE	3.53E-04	-1.44	-3.89	-2.70
NM_032139	ANKRD27	8.14E-03	-1.13	-3.06	-2.70
NM_006267	RANBP2	1.60E-03	-1.10	-3.04	-2.77
---	---	6.84E-03	1.09	-2.56	-2.79
NM_024546	RNF219	5.28E-04	-1.69	-4.75	-2.81
NM_015168	ZC3H4	8.07E-05	-2.07	-5.85	-2.83
NM_014048	MKL2	4.30E-03	-1.33	-3.79	-2.84
NM_001004065	AKAP2 /// PALM2 /// PALM2-AKAP2	9.73E-03	1.10	-2.59	-2.86
NM_001412	EIF1AX	3.39E-03	-1.30	-3.76	-2.89
NM_001142546	LUZP1	8.48E-03	-1.02	-3.00	-2.93
NM_003797	EED	1.03E-03	-1.93	-5.75	-2.99
NM_005859	PURA	3.68E-03	-1.14	-3.41	-2.99
NM_001548	IFIT1	3.86E-04	-1.30	-3.92	-3.01
NM_005206	CRK	5.54E-03	1.07	-2.83	-3.03
NM_001102653	OTUD4	4.02E-03	-1.04	-3.17	-3.06

NM_012161	FBXL5	3.85E-03	-1.14	-3.52	-3.09
NM_014319	LEMD3	8.32E-03	1.04	-2.99	-3.12
NM_001042369	TROVE2	8.56E-03	-1.00	-3.23	-3.21
NM_015156	RCOR1	7.38E-03	1.04	-3.11	-3.22
NM_025164	KIAA0999	2.95E-03	-1.19	-3.87	-3.25
NM_012416	RANBP6	2.66E-04	-1.86	-6.13	-3.30
NM_014918	CHSY1	2.32E-03	-1.22	-4.11	-3.36
NM_152301	MRFAP1L1	5.04E-03	-1.04	-3.53	-3.41
NM_014023	WDR37	4.94E-03	-1.26	-4.44	-3.51
NM_003478	CUL5	6.91E-03	-1.17	-4.14	-3.54
NM_015325	KIAA0947	9.34E-03	-1.01	-3.75	-3.70
NM_016436	PHF20	8.79E-03	-1.19	-4.44	-3.72
NM_021194	SLC30A1	8.59E-03	1.00	-3.78	-3.78
NM_001100594	SNRK	9.61E-03	1.06	-3.65	-3.88
NM_014705	DOCK4	9.72E-03	-1.20	-4.73	-3.93
NM_004973	JARID2	7.58E-03	-1.18	-4.68	-3.95
NM_001100590	KIAA0232	4.47E-03	-1.15	-4.62	-4.01
NM_145290	GPR125	9.66E-03	1.08	-3.77	-4.08
NM_007172	NUP50	5.36E-04	-1.26	-5.36	-4.27
NM_001079846	CREBBP	6.66E-03	1.07	-4.12	-4.40
NM_015045	WAPAL	2.42E-03	-1.42	-6.24	-4.40
NM_014602	PIK3R4	2.79E-03	-1.03	-4.59	-4.47
NM_001142597	CLP1	4.15E-03	1.02	-5.07	-5.19
NM_001003698	RREB1	4.17E-03	-1.06	-6.17	-5.84
NM_015322	FEM1B	8.06E-03	1.10	-5.91	-6.50
NM_018136	ASPM	6.90E-03	1.12	-7.67	-8.55

APPENDIX D

CO-CULTURE MICROARRAY DATA

P value	Fold Change	GENBANK_ACCESSION	Gene Name
2.54E-04	12.67	NM_000104	CYTOCHROME P450, FAMILY 1, SUBFAMILY B, POLYPEPTIDE 1
5.26E-06	12.31	NM_000600	INTERLEUKIN 6 (INTERFERON, BETA 2)
4.95E-05	11.54	NM_005261	GTP BINDING PROTEIN OVEREXPRESSED IN SKELETAL MUSCLE
1.20E-05	11.41	NM_000584	INTERLEUKIN 8
3.48E-06	11.39	NM_000600	INTERLEUKIN 6 (INTERFERON, BETA 2)
4.79E-05	11.25	NM_006273	CHEMOKINE (C-C MOTIF) LIGAND 7
4.79E-09	9.83	NM_006850	INTERLEUKIN 24
3.71E-05	9.38	NM_001122	ADIPOSE DIFFERENTIATION-RELATED PROTEIN
1.20E-03	9.37	BC016934	SUPEROXIDE DISMUTASE 2, MITOCHONDRIAL
1.14E-03	9.06	NM_153607	ADULT RETINA PROTEIN
3.18E-06	8.12	NM_002422	MATRIX METALLOPEPTIDASE 3 (STROMELYSIN 1, PROGELATINASE)
7.98E-04	7.98	NM_007115	TUMOR NECROSIS FACTOR, ALPHA-INDUCED PROTEIN 6
4.99E-04	7.75	NM_000758	COLONY STIMULATING FACTOR 2 (GRANULOCYTE-MACROPHAGE)
3.74E-05	7.41	NM_006850	INTERLEUKIN 24
1.11E-03	6.97	NM_000576	INTERLEUKIN 1, BETA
1.08E-04	6.86	NM_004694	SOLUTE CARRIER FAMILY 16 (MONOCARBOXYLIC ACID TRANSPORTERS), MEMBER 6
1.01E-03	6.58	NM_005524	HAIRY AND ENHANCER OF SPLIT 1, (DROSOPHILA)
1.09E-03	6.40	NM_134260	RAR-RELATED ORPHAN RECEPTOR A
5.90E-04	6.36	NM_000640	INTERLEUKIN 13 RECEPTOR, ALPHA 2
5.24E-05	6.25	NM_005524	HAIRY AND ENHANCER OF SPLIT 1, (DROSOPHILA)
1.30E-03	6.18	NM_003064	SECRETORY LEUKOCYTE PEPTIDASE INHIBITOR
1.41E-04	5.92	NM_001040708	
1.39E-05	5.82	NM_017644	KELCH-LIKE 24 (DROSOPHILA)
1.23E-04	5.77	NM_170744	UNC-5 HOMOLOG B (C. ELEGANS)
1.12E-04	5.69	BM129308	STANNIOCALCIN 1
2.29E-04	5.69	NM_000576	INTERLEUKIN 1, BETA
1.49E-05	5.51	NM_005524	HAIRY AND ENHANCER OF SPLIT 1, (DROSOPHILA)
6.19E-04	5.43	NM_152431	PIWI-LIKE 4 (DROSOPHILA)
6.68E-05	5.24	AW138903	NOTCH HOMOLOG 3 (DROSOPHILA)
1.00E-03	5.14	NM_138461	TRANSMEMBRANE 4 L SIX FAMILY MEMBER 19
1.78E-05	5.13	NM_005980	S100 CALCIUM BINDING PROTEIN P
3.73E-04	4.99	NM_001040619	
6.49E-04	4.99	NM_014079	KRUPPEL-LIKE FACTOR 15
2.53E-07	4.91	NM_003900	SEQUESTOSOME 1
2.56E-05	4.66	NM_000574	CD55 ANTIGEN, DECAY ACCELERATING FACTOR FOR COMPLEMENT (CROMER BLOOD GROUP)
4.49E-05	4.65	THC2698311	
2.62E-04	4.62	NM_006290	TUMOR NECROSIS FACTOR, ALPHA-INDUCED PROTEIN 3
1.36E-04	4.55	NM_005114	HEPARAN SULFATE (GLUCOSAMINE) 3-O-SULFOTRANSFERASE 1
1.87E-07	4.53	NM_001920	DECORIN
7.09E-04	4.52	NM_001200	BONE MORPHOGENETIC PROTEIN 2
5.62E-04	4.51	NM_002575	SERPIN PEPTIDASE INHIBITOR, CLADE B (OVALBUMIN), MEMBER 2
4.73E-04	4.50	NM_000574	CD55 ANTIGEN, DECAY ACCELERATING FACTOR FOR COMPLEMENT (CROMER BLOOD GROUP)
1.26E-03	4.46	NM_000963	PROSTAGLANDIN-ENDOPEROXIDE SYNTHASE 2 (PROSTAGLANDIN G/H SYNTHASE AND CYCLOOXYGENASE)
9.87E-04	4.44	AA969200	CD55 ANTIGEN, DECAY ACCELERATING FACTOR FOR COMPLEMENT (CROMER BLOOD GROUP)
5.78E-04	4.42	NM_000963	PROSTAGLANDIN-ENDOPEROXIDE SYNTHASE 2 (PROSTAGLANDIN G/H SYNTHASE AND CYCLOOXYGENASE)
1.53E-05	4.38	NM_002345	LUMICAN
1.05E-05	4.37	NM_000963	PROSTAGLANDIN-ENDOPEROXIDE SYNTHASE 2 (PROSTAGLANDIN G/H SYNTHASE AND CYCLOOXYGENASE)
2.08E-05	4.34	NM_000963	PROSTAGLANDIN-ENDOPEROXIDE SYNTHASE 2 (PROSTAGLANDIN G/H SYNTHASE AND CYCLOOXYGENASE)
4.26E-04	4.34	NM_002089	CHEMOKINE (C-X-C MOTIF) LIGAND 2
1.58E-05	4.29	CD743044	SUPEROXIDE DISMUTASE 2, MITOCHONDRIAL
5.78E-06	4.26	NM_000963	PROSTAGLANDIN-ENDOPEROXIDE SYNTHASE 2 (PROSTAGLANDIN G/H SYNTHASE AND CYCLOOXYGENASE)
3.97E-04	4.25	BQ004014	DECORIN
4.09E-04	4.22	NM_002421	MATRIX METALLOPEPTIDASE 1 (INTERSTITIAL COLLAGENASE)
2.87E-05	4.17	NM_001945	HEPARIN-BINDING EGF-LIKE GROWTH FACTOR
2.57E-04	4.17	NM_000963	PROSTAGLANDIN-ENDOPEROXIDE SYNTHASE 2 (PROSTAGLANDIN G/H SYNTHASE AND CYCLOOXYGENASE)
5.56E-04	4.13	NM_016354	SOLUTE CARRIER ORGANIC ANION TRANSPORTER FAMILY, MEMBER 4A1
3.06E-04	4.13	NM_004417	DUAL SPECIFICITY PHOSPHATASE 1
8.98E-04	4.10	NM_002421	MATRIX METALLOPEPTIDASE 1 (INTERSTITIAL COLLAGENASE)
4.28E-04	4.09	NM_002421	MATRIX METALLOPEPTIDASE 1 (INTERSTITIAL COLLAGENASE)
1.21E-04	4.08	NM_000963	PROSTAGLANDIN-ENDOPEROXIDE SYNTHASE 2 (PROSTAGLANDIN G/H SYNTHASE AND CYCLOOXYGENASE)
2.54E-04	4.05	NM_000963	PROSTAGLANDIN-ENDOPEROXIDE SYNTHASE 2 (PROSTAGLANDIN G/H SYNTHASE AND CYCLOOXYGENASE)
3.17E-04	4.05	NM_000963	PROSTAGLANDIN-ENDOPEROXIDE SYNTHASE 2 (PROSTAGLANDIN G/H SYNTHASE AND CYCLOOXYGENASE)
5.75E-04	4.02	ENST00000299502	
2.28E-04	4.00	NM_002421	MATRIX METALLOPEPTIDASE 1 (INTERSTITIAL COLLAGENASE)
8.34E-04	4.00	NM_021724	NUCLEAR RECEPTOR SUBFAMILY 1, GROUP D, MEMBER 1
1.87E-04	3.99	NM_005168	RHO FAMILY GTPASE 3

3.85E-04	3.95	NM_002421	MATRIX METALLOPEPTIDASE 1 (INTERSTITIAL COLLAGENASE)
4.52E-04	3.94	NM_002421	MATRIX METALLOPEPTIDASE 1 (INTERSTITIAL COLLAGENASE)
2.39E-05	3.94	NM_005168	RHO FAMILY GTPASE 3
5.88E-05	3.93	NM_005168	RHO FAMILY GTPASE 3
9.28E-04	3.93	NM_001024465	SUPEROXIDE DISMUTASE 2, MITOCHONDRIAL
2.40E-04	3.92	NM_002421	MATRIX METALLOPEPTIDASE 1 (INTERSTITIAL COLLAGENASE)
3.51E-05	3.91	BF760214	COLLAGEN, TYPE III, ALPHA 1 (EHLERS-DANLOS SYNDROME TYPE IV, AUTOSOMAL DOMINANT)
6.63E-04	3.90	NM_002421	MATRIX METALLOPEPTIDASE 1 (INTERSTITIAL COLLAGENASE)
3.55E-05	3.87	NM_018440	PHOSPHOPROTEIN ASSOCIATED WITH GLYCOSPHINGOLIPID MICRODOMAINS 1
2.58E-04	3.85	AI620901	WINGLESS-TYPE MMTV INTEGRATION SITE FAMILY, MEMBER 5A
8.96E-06	3.82	NM_000076	CYCLIN-DEPENDENT KINASE INHIBITOR 1C (P57, KIP2)
2.07E-04	3.82	NM_001025370	VASCULAR ENDOTHELIAL GROWTH FACTOR
6.64E-05	3.80	NM_005168	RHO FAMILY GTPASE 3
1.74E-04	3.80	AW276332	LUMICAN
2.52E-04	3.76	NM_002421	MATRIX METALLOPEPTIDASE 1 (INTERSTITIAL COLLAGENASE)
9.69E-05	3.76	NM_005168	RHO FAMILY GTPASE 3
8.25E-05	3.75	NM_005168	RHO FAMILY GTPASE 3
1.75E-04	3.75	NM_002090	CHEMOKINE (C-X-C MOTIF) LIGAND 3
3.23E-04	3.73	NM_001005404	YIPPEE-LIKE 2 (DROSOPHILA)
8.26E-04	3.72	NM_015009	PDZ DOMAIN CONTAINING RING FINGER 3
6.51E-04	3.71	NM_000146	FERRITIN, LIGHT POLYPEPTIDE
4.62E-05	3.71	NM_005168	RHO FAMILY GTPASE 3
3.15E-04	3.70	NM_014330	PROTEIN PHOSPHATASE 1, REGULATORY (INHIBITOR) SUBUNIT 15A
6.86E-06	3.66	NM_002994	CHEMOKINE (C-X-C MOTIF) LIGAND 5
1.06E-05	3.63	NM_003392	WINGLESS-TYPE MMTV INTEGRATION SITE FAMILY, MEMBER 5A
2.19E-04	3.63	NM_002421	MATRIX METALLOPEPTIDASE 1 (INTERSTITIAL COLLAGENASE)
2.78E-04	3.61	NM_173842	INTERLEUKIN 1 RECEPTOR ANTAGONIST
3.78E-05	3.61	NM_005168	RHO FAMILY GTPASE 3
4.94E-04	3.58	NM_005168	RHO FAMILY GTPASE 3
1.75E-05	3.56	NM_005168	RHO FAMILY GTPASE 3
2.92E-04	3.51	NM_182663	RAS ASSOCIATION (RALGDS/AF-6) DOMAIN FAMILY 5
5.95E-08	3.49	ENST00000339446	
2.06E-05	3.44	NM_002982	CHEMOKINE (C-C MOTIF) LIGAND 2
3.44E-04	3.44	NM_002971	SPECIAL AT-RICH SEQUENCE BINDING PROTEIN 1 (BINDS TO NUCLEAR MATRIX/SCAFFOLD-ASSOCIATING DNA'S)
1.41E-05	3.38	NM_004177	SYNTAXIN 3A
3.54E-05	3.36	NM_003013	SECRETED FRIZZLED-RELATED PROTEIN 2
1.03E-04	3.32	NM_033035	THYMIC STROMAL LYMPHOPOIETIN
8.21E-04	3.32	NM_002982	CHEMOKINE (C-C MOTIF) LIGAND 2
2.55E-04	3.31	NM_002089	CHEMOKINE (C-X-C MOTIF) LIGAND 2
6.54E-04	3.28	NM_001706	B-CELL CLL/LYMPHOMA 6 (ZINC FINGER PROTEIN 51)
2.39E-05	3.28	NM_002982	CHEMOKINE (C-C MOTIF) LIGAND 2
4.54E-04	3.24	NM_001511	CHEMOKINE (C-X-C MOTIF) LIGAND 1 (MELANOMA GROWTH STIMULATING ACTIVITY, ALPHA)
1.75E-05	3.24	NM_002982	CHEMOKINE (C-C MOTIF) LIGAND 2
7.21E-06	3.23	NM_002006	FIBROBLAST GROWTH FACTOR 2 (BASIC)
1.47E-03	3.21	NM_002006	FIBROBLAST GROWTH FACTOR 2 (BASIC)
2.56E-05	3.19	NM_002982	CHEMOKINE (C-C MOTIF) LIGAND 2
4.27E-04	3.17	NM_002982	CHEMOKINE (C-C MOTIF) LIGAND 2
1.97E-05	3.17	NM_002982	CHEMOKINE (C-C MOTIF) LIGAND 2
7.32E-04	3.16	NM_002982	CHEMOKINE (C-C MOTIF) LIGAND 2
5.52E-04	3.16	NM_006813	PROLINE-RICH NUCLEAR RECEPTOR COACTIVATOR 1
2.49E-04	3.15	AI367654	CCAAT/ENHANCER BINDING PROTEIN (C/EBP), BETA
5.54E-05	3.14	NM_002006	FIBROBLAST GROWTH FACTOR 2 (BASIC)
1.52E-06	3.13	NM_016315	GULP, ENGULFMENT ADAPTOR PTB DOMAIN CONTAINING 1
3.59E-04	3.11	ENST00000381826	
1.35E-03	3.11	NM_001025366	VASCULAR ENDOTHELIAL GROWTH FACTOR
2.42E-04	3.11	NM_001005404	YIPPEE-LIKE 2 (DROSOPHILA)
9.53E-05	3.10	NM_001025366	VASCULAR ENDOTHELIAL GROWTH FACTOR
5.65E-04	3.10	NM_002993	CHEMOKINE (C-X-C MOTIF) LIGAND 6 (GRANULOCYTE CHEMOTACTIC PROTEIN 2)
1.57E-04	3.10	NM_002982	CHEMOKINE (C-C MOTIF) LIGAND 2
2.56E-07	3.09	NM_018661	DEFENSIN, BETA 103A
1.02E-04	3.08	NM_002648	PIM-1 ONCOGENE
6.95E-05	3.06	NM_001025366	VASCULAR ENDOTHELIAL GROWTH FACTOR
9.32E-04	3.05	NM_021732	ARGININE VASOPRESSIN-INDUCED 1
2.29E-05	3.02	NM_001338	COXSACKIE VIRUS AND ADENOVIRUS RECEPTOR
7.67E-04	2.99	NM_000090	COLLAGEN, TYPE III, ALPHA 1 (EHLERS-DANLOS SYNDROME TYPE IV, AUTOSOMAL DOMINANT)
1.41E-04	2.97	AK054921	CEREBELLAR DEGENERATION-RELATED PROTEIN 1, 34KDA
1.15E-06	2.95	BC089388	
1.03E-06	2.95	AK022913	UBIQUITIN SPECIFIC PEPTIDASE 36
9.60E-04	2.95	NM_007207	DUAL SPECIFICITY PHOSPHATASE 10
6.95E-05	2.94	NM_021229	NETRIN 4

1.09E-03	2.93	ENST00000390271	
6.29E-05	2.90	NM_017705	PROGESTIN AND ADIPOQ RECEPTOR FAMILY MEMBER V
1.00E-04	2.89	NM_003013	SECRETED FRIZZLED-RELATED PROTEIN 2
3.80E-04	2.89	NM_032784	R-SPONDIN 3 HOMOLOG (XENOPUS LAEVIS)
5.45E-04	2.89	NM_006931	SOLUTE CARRIER FAMILY 2 (FACILITATED GLUCOSE TRANSPORTER), MEMBER 3
1.30E-03	2.88	NM_181755	HYDROXYSTEROID (11-BETA) DEHYDROGENASE 1
6.32E-04	2.87	NM_001031746	CHROMOSOME 10 OPEN READING FRAME 72
3.88E-04	2.86	NM_001935	DIPEPTIDYL-PEPTIDASE 4 (CD26, ADENOSINE DEAMINASE COMPLEXING PROTEIN 2)
8.48E-04	2.86	THC2562557	
1.01E-03	2.85	NM_004925	AQUAPORIN 3 (GILL BLOOD GROUP)
6.81E-04	2.83	NM_203391	GLYCEROL KINASE
1.21E-03	2.79	NM_016315	GULP, ENGULFMENT ADAPTOR PTB DOMAIN CONTAINING 1
4.04E-04	2.79	BC090920	SIMILAR TO F-BOX ONLY PROTEIN 25
1.02E-03	2.79	THC2575688	
4.67E-05	2.79	NM_002006	FIBROBLAST GROWTH FACTOR 2 (BASIC)
1.46E-04	2.76	NM_005384	NUCLEAR FACTOR, INTERLEUKIN 3 REGULATED
8.52E-04	2.76	NM_001048226	
1.30E-04	2.76	NM_033647	HELICASE (DNA) B
2.44E-05	2.75	NM_005194	CCAAT/ENHANCER BINDING PROTEIN (C/EBP), BETA
1.40E-05	2.74	NM_005194	CCAAT/ENHANCER BINDING PROTEIN (C/EBP), BETA
1.80E-04	2.74	NM_002581	PREGNANCY-ASSOCIATED PLASMA PROTEIN A, PAPPALYSIN 1
2.31E-04	2.73	NM_003064	SECRETORY LEUKOCYTE PEPTIDASE INHIBITOR
2.40E-04	2.73	NM_004925	AQUAPORIN 3 (GILL BLOOD GROUP)
8.54E-05	2.72	NM_001042483	
1.19E-03	2.72	NM_007036	ENDOTHELIAL CELL-SPECIFIC MOLECULE 1
6.80E-06	2.72	NM_005194	CCAAT/ENHANCER BINDING PROTEIN (C/EBP), BETA
6.36E-04	2.70	NM_183422	TSC22 DOMAIN FAMILY, MEMBER 1
7.76E-05	2.70	NM_002006	FIBROBLAST GROWTH FACTOR 2 (BASIC)
7.32E-04	2.69	THC2642537	
3.26E-04	2.67	NM_033397	KIAA1754
7.94E-05	2.65	NM_001338	COXSACKIE VIRUS AND ADENOVIRUS RECEPTOR
7.72E-06	2.64	NM_001338	COXSACKIE VIRUS AND ADENOVIRUS RECEPTOR
2.28E-04	2.62	NR_000041	RNA, U12 SMALL NUCLEAR
4.59E-04	2.62	NM_003897	IMMEDIATE EARLY RESPONSE 3
7.61E-05	2.61	NM_005194	CCAAT/ENHANCER BINDING PROTEIN (C/EBP), BETA
1.40E-03	2.61	NM_032573	COILED-COIL DOMAIN CONTAINING 62
9.81E-05	2.59	NM_005194	CCAAT/ENHANCER BINDING PROTEIN (C/EBP), BETA
2.93E-04	2.59	NM_001570	INTERLEUKIN-1 RECEPTOR-ASSOCIATED KINASE 2
1.25E-03	2.58	NM_000167	GLYCEROL KINASE
1.42E-03	2.57	BG950086	DUAL SPECIFICITY PHOSPHATASE 1
2.57E-04	2.57	NM_005194	CCAAT/ENHANCER BINDING PROTEIN (C/EBP), BETA
5.72E-06	2.57	NM_001957	ENDOTHELIN RECEPTOR TYPE A
3.91E-04	2.57	NM_002357	MAX DIMERIZATION PROTEIN 1
1.42E-04	2.56	NM_005194	CCAAT/ENHANCER BINDING PROTEIN (C/EBP), BETA
2.81E-04	2.55	BQ010172	MATRIX METALLOPEPTIDASE 2 (GELATINASE A, 72KDA GELATINASE, 72KDA TYPE IV COLLAGENASE)
1.65E-04	2.55	NM_012413	GLUTAMINYL-PEPTIDE CYCLOTRANSFERASE (GLUTAMINYL CYCLASE)
2.35E-04	2.55	NM_006504	PROTEIN TYROSINE PHOSPHATASE, RECEPTOR TYPE, E
1.30E-04	2.55	NM_006147	INTERFERON REGULATORY FACTOR 6
8.48E-05	2.55	NM_005194	CCAAT/ENHANCER BINDING PROTEIN (C/EBP), BETA
1.25E-03	2.55	AI915259	PLATELET-DERIVED GROWTH FACTOR RECEPTOR, BETA POLYPEPTIDE
4.46E-04	2.53	NM_000710	BRADYKININ RECEPTOR B1
9.93E-04	2.52	NM_003196	TRANSCRIPTION ELONGATION FACTOR A (SII), 3
5.83E-04	2.52	AL547890	GROWTH ARREST-SPECIFIC 5
6.36E-04	2.51	NM_000877	INTERLEUKIN 1 RECEPTOR, TYPE I
2.23E-04	2.50	NM_020422	PROMETHIN
5.65E-04	2.49	NM_181671	PHOSPHATIDYLINOSITOL TRANSFER PROTEIN, CYTOPLASMIC 1
7.07E-04	2.49	NM_001025370	VASCULAR ENDOTHELIAL GROWTH FACTOR
3.26E-04	2.49	AI669361	SOLUTE CARRIER FAMILY 38, MEMBER 2
6.44E-05	2.48	NM_020651	PELLINO HOMOLOG 1 (DROSOPHILA)
1.81E-04	2.48	NM_001042507	
5.73E-05	2.48	NM_000618	INSULIN-LIKE GROWTH FACTOR 1 (SOMATOMEDIN C)
1.81E-04	2.47	AF349445	MAXI-K CHANNEL HSLO
1.81E-04	2.47	AF349445	POTASSIUM LARGE CONDUCTANCE CALCIUM-ACTIVATED CHANNEL, SUBFAMILY M, ALPHA MEMBER 1
6.58E-04	2.47	NM_000710	BRADYKININ RECEPTOR B1
5.14E-04	2.45	NM_152586	UBIQUITIN SPECIFIC PEPTIDASE 54
6.02E-04	2.44	NM_138411	HYPOTHETICAL PROTEIN LOC284361
6.02E-04	2.44	NM_138411	HYPOTHETICAL PROTEIN BC004941
2.32E-04	2.44	NM_000081	LYSOSOMAL TRAFFICKING REGULATOR
1.92E-04	2.44	NM_005194	CCAAT/ENHANCER BINDING PROTEIN (C/EBP), BETA
4.34E-04	2.44	NM_005194	CCAAT/ENHANCER BINDING PROTEIN (C/EBP), BETA

2.65E-04	2.43	NM_019060	CHROMOSOME 1 OPEN READING FRAME 42
1.33E-03	2.42	NM_002970	SPERMIDINE/SPERMINE N1-ACETYLTRANSFERASE
1.16E-04	2.41	BC047030	URIDINE PHOSPHORYLASE 1
1.14E-03	2.41	NM_002166	INHIBITOR OF DNA BINDING 2, DOMINANT NEGATIVE HELIX-LOOP-HELIX PROTEIN
9.01E-05	2.41	NM_000759	COLONY STIMULATING FACTOR 3 (GRANULOCYTE)
1.15E-03	2.41	NR_002578	GROWTH ARREST-SPECIFIC 5
4.60E-04	2.41	NM_003004	SECRETED AND TRANSMEMBRANE 1
3.20E-05	2.40	AL834140	
1.77E-04	2.39	S73202	ARGININOSUCCINATE SYNTHETASE PROTEIN
1.18E-04	2.36	NM_133372	KIAA1961 GENE
1.36E-03	2.36	NM_020529	NUCLEAR FACTOR OF KAPPA LIGHT POLYPEPTIDE GENE ENHANCER IN B-CELLS INHIBITOR, ALPHA
2.65E-06	2.35	NM_024867	KPL2 PROTEIN
1.02E-03	2.35	NM_001628	ALDO-KETO REDUCTASE FAMILY 1, MEMBER B1 (ALDOSE REDUCTASE)
6.64E-05	2.35	NM_006504	PROTEIN TYROSINE PHOSPHATASE, RECEPTOR TYPE, E
5.25E-04	2.34	NM_003991	ENDOTHELIN RECEPTOR TYPE B
8.74E-04	2.34	THC2565422	
8.21E-04	2.34	NR_003605	
3.25E-04	2.34	AL833749	HYPOTHETICAL LOC146439
4.15E-04	2.33	NM_004323	BCL2-ASSOCIATED ATHANOGENE
3.55E-04	2.33	NM_018566	YOD1 OTU DEUBIQUINATING ENZYME 1 HOMOLOG (YEAST)
4.98E-04	2.32	AL109695	SOLUTE CARRIER ORGANIC ANION TRANSPORTER FAMILY, MEMBER 3A1
2.47E-04	2.32	NM_000575	INTERLEUKIN 1, ALPHA
6.51E-04	2.32	NM_018976	SOLUTE CARRIER FAMILY 38, MEMBER 2
3.27E-04	2.31	NM_133639	RAS HOMOLOG GENE FAMILY, MEMBER V
4.24E-04	2.31	NR_000039	RAB9, MEMBER RAS ONCOGENE FAMILY, PSEUDOGENE 1
8.69E-05	2.31	NM_018357	LA RIBONUCLEOPROTEIN DOMAIN FAMILY, MEMBER 6
7.20E-04	2.30	NM_005779	LIPOMA HMGIC FUSION PARTNER-LIKE 2
4.60E-04	2.30	BC094756	MYOTUBULARIN RELATED PROTEIN 11
1.64E-04	2.28	NM_003013	SECRETED FRIZZLED-RELATED PROTEIN 2
2.89E-05	2.28	NM_000050	ARGININOSUCCINATE SYNTHETASE
5.05E-04	2.27	NM_182767	SOLUTE CARRIER FAMILY 6, MEMBER 15
1.22E-03	2.27	AF011794	CELL CYCLE PROGRESSION 1
2.28E-04	2.26	NM_001042610	
1.52E-04	2.26	AA573434	KRUPPEL-LIKE FACTOR 4 (GUT)
1.03E-03	2.25	NM_152405	JUNCTION-MEDIATING AND REGULATORY PROTEIN
1.35E-03	2.25	NM_001072	UDP GLUCURONOSYLTRANSFERASE 1 FAMILY, POLYPEPTIDE A6
2.61E-04	2.24	NM_012153	ETS HOMOLOGOUS FACTOR
1.17E-03	2.24	NM_000362	TIMP METALLOPEPTIDASE INHIBITOR 3 (SORSBY FUNDUS DYSTROPHY, PSEUDOINFLAMMATORY)
9.49E-04	2.23	NM_003662	PIRIN (IRON-BINDING NUCLEAR PROTEIN)
1.12E-03	2.22	NM_018433	JUMONJI DOMAIN CONTAINING 1A
7.36E-04	2.22	NM_002237	POTASSIUM VOLTAGE-GATED CHANNEL, SUBFAMILY G, MEMBER 1
1.10E-03	2.22	NM_017771	PX DOMAIN CONTAINING SERINE/THREONINE KINASE
5.22E-05	2.21	NM_080629	COLLAGEN, TYPE XI, ALPHA 1
4.58E-04	2.21	NM_000575	INTERLEUKIN 1, ALPHA
9.07E-05	2.21	NM_003670	BASIC HELIX-LOOP-HELIX DOMAIN CONTAINING, CLASS B, 2
1.46E-03	2.19	NM_005746	PRE-B-CELL COLONY ENHANCING FACTOR 1
8.11E-04	2.19	NM_001042413	
1.06E-03	2.19	NM_018371	CHONDROITIN BETA1,4 N-ACETYLGALACTOSAMINYLTRANSFERASE
1.44E-04	2.19	NM_012257	HMG-BOX TRANSCRIPTION FACTOR 1
1.94E-04	2.18	NM_000575	INTERLEUKIN 1, ALPHA
6.41E-04	2.18	NM_015021	
1.51E-04	2.18	NM_000575	INTERLEUKIN 1, ALPHA
9.16E-05	2.18	AW952039	ZINC FINGER PROTEIN 496
1.95E-04	2.17	NM_001408	CADHERIN, EGF LAG SEVEN-PASS G-TYPE RECEPTOR 2 (FLAMINGO HOMOLOG, DROSOPHILA)
4.25E-04	2.17	NM_003713	PHOSPHATIDIC ACID PHOSPHATASE TYPE 2B
9.71E-04	2.17	NM_004530	MATRIX METALLOPEPTIDASE 2 (GELATINASE A, 72KDA GELATINASE, 72KDA TYPE IV COLLAGENASE)
4.50E-04	2.17	NM_004071	CDC-LIKE KINASE 1
9.32E-04	2.16	NM_020422	PROMETHIN
1.30E-04	2.16	NM_002994	CHEMOKINE (C-X-C MOTIF) LIGAND 5
1.18E-04	2.15	NM_018976	SOLUTE CARRIER FAMILY 38, MEMBER 2
1.66E-04	2.15	NM_020962	LIKELY ORTHOLOG OF MOUSE NEIGHBOR OF PUNC E11
1.02E-03	2.14	NM_144697	CHROMOSOME 1 OPEN READING FRAME 51
4.90E-04	2.14	NM_000575	INTERLEUKIN 1, ALPHA
1.10E-03	2.14	NM_004530	MATRIX METALLOPEPTIDASE 2 (GELATINASE A, 72KDA GELATINASE, 72KDA TYPE IV COLLAGENASE)
1.34E-03	2.13	BC041893	TETRATRICOPEPTIDE REPEAT DOMAIN 17
2.93E-04	2.13	NM_001001661	ZINC FINGER PROTEIN 425
5.27E-04	2.12	NM_002032	FERRITIN, HEAVY POLYPEPTIDE 1
9.93E-04	2.12	NM_001800	CYCLIN-DEPENDENT KINASE INHIBITOR 2D (P19, INHIBITS CDK4)
8.87E-05	2.11	NM_018566	YOD1 OTU DEUBIQUINATING ENZYME 1 HOMOLOG (YEAST)
5.86E-04	2.11	NM_005118	TUMOR NECROSIS FACTOR (LIGAND) SUPERFAMILY, MEMBER 15

1.39E-03	2.11	NM_052885	SOLUTE CARRIER FAMILY 2 (FACILITATED GLUCOSE TRANSPORTER), MEMBER 13
5.84E-04	2.10	AK124426	
1.43E-03	2.09	AB188491	OTU DOMAIN CONTAINING 1
1.29E-03	2.09	NM_021818	SALVADOR HOMOLOG 1 (DROSOPHILA)
6.48E-05	2.09	NM_004878	PROSTAGLANDIN E SYNTHASE
1.15E-03	2.09	NM_032412	PUTATIVE NUCLEAR PROTEIN ORF1-FL49
7.48E-04	2.08	NM_000575	INTERLEUKIN 1, ALPHA
3.58E-04	2.08	NM_001037132	NEURONAL CELL ADHESION MOLECULE
1.24E-03	2.08	THC2587036	
6.46E-06	2.08	AI803364	HYPOTHETICAL PROTEIN MGC16037
3.77E-04	2.08	NM_019034	RAS HOMOLOG GENE FAMILY, MEMBER F (IN FILOPODIA)
3.67E-04	2.07	H45075	PROTEIN PHOSPHATASE 1, REGULATORY (INHIBITOR) SUBUNIT 3F
3.87E-04	2.07	NM_032521	PAR-6 PARTITIONING DEFECTIVE 6 HOMOLOG BETA (C. ELEGANS)
2.50E-04	2.07	NM_018252	CHROMOSOME 1 OPEN READING FRAME 75
3.89E-04	2.06	NM_004331	BCL2/ADENOVIRUS E1B 19KDA INTERACTING PROTEIN 3-LIKE
3.89E-04	2.06	CB123670	
2.05E-04	2.06	NM_015526	CLIP-170-RELATED PROTEIN
1.81E-04	2.05	NM_032573	COILED-COIL DOMAIN CONTAINING 62
8.99E-05	2.05	NM_001007245	INTERFERON-RELATED DEVELOPMENTAL REGULATOR 1
2.20E-04	2.05	NM_032251	HYPOTHETICAL PROTEIN DKFZP434G0920
4.63E-04	2.05	BX537786	NUCLEAR RECEPTOR SUBFAMILY 1, GROUP D, MEMBER 2
6.03E-04	2.05	THC2742812	
6.47E-04	2.04	NM_152756	KIAA1999 PROTEIN
7.49E-04	2.04	NM_001030273	ARYL HYDROCARBON RECEPTOR NUCLEAR TRANSLOCATOR-LIKE
1.33E-04	2.03	NM_004071	CDC-LIKE KINASE 1
5.27E-05	2.03	NM_001008219	AMYLASE, ALPHA 2A; PANCREATIC
5.27E-05	2.03	NM_001008219	AMYLASE, ALPHA 1A; SALIVARY
2.04E-04	2.03	NM_005126	NUCLEAR RECEPTOR SUBFAMILY 1, GROUP D, MEMBER 2
5.50E-04	2.03	NM_012090	MICROTUBULE-ACTIN CROSSLINKING FACTOR 1
9.19E-05	2.02	XM_928637	SIMILAR TO ACTIVATING TRANSCRIPTION FACTOR 4
5.21E-04	2.02	NM_003831	RIO KINASE 3 (YEAST)
1.05E-03	2.02	NM_001001417	TBC1 DOMAIN FAMILY, MEMBER 3
1.04E-04	2.02	NM_006948	STRESS 70 PROTEIN CHAPERONE, MICROSOME-ASSOCIATED, 60KDA
6.12E-04	2.01	NM_199330	HOMER HOMOLOG 2 (DROSOPHILA)
3.47E-04	2.01	NM_020387	RAB25, MEMBER RAS ONCOGENE FAMILY
3.01E-04	2.01	NM_005685	GTF2I REPEAT DOMAIN CONTAINING 1
7.73E-04	2.00	NM_007102	GUANYLATE CYCLASE ACTIVATOR 2B (UROGUANYLIN)
3.05E-04	2.00	THC2511310	
7.66E-04	2.00	NM_002245	POTASSIUM CHANNEL, SUBFAMILY K, MEMBER 1
7.79E-04	2.00	NM_001206	KRUPPEL-LIKE FACTOR 9
3.61E-04	1.99	NM_012421	REARRANGED L-MYC FUSION
2.54E-04	1.98	NM_017933	HYPOTHETICAL PROTEIN FLJ20701
5.41E-04	1.98	BI521983	
1.25E-03	1.98	NM_017712	PYROGLUTAMYL-PEPTIDASE I
8.57E-04	1.97	NM_001080467	
9.46E-04	1.96	AK023572	
5.23E-04	1.95	NM_203391	GLYCEROL KINASE
1.45E-03	1.95	NM_024422	DESMOCOLLIN 2
4.75E-07	1.95	NM_016621	PHD FINGER PROTEIN 21A
8.90E-04	1.94	NM_001896	CASEIN KINASE 2, ALPHA PRIME POLYPEPTIDE
4.17E-05	1.94	BF366211	
8.22E-04	1.94	NM_004126	GUANINE NUCLEOTIDE BINDING PROTEIN (G PROTEIN), GAMMA 11
4.02E-04	1.94	NM_006912	RAS-LIKE WITHOUT CAAX 1
2.95E-04	1.93	NM_207309	UDP-N-ACTEYLGLUCOSAMINE PYROPHOSPHORYLASE 1-LIKE 1
6.40E-04	1.93	NM_014781	RB1-INDUCIBLE COILED-COIL 1
2.83E-04	1.93	NM_001042471	
5.35E-04	1.93	AF258583	RAB24, MEMBER RAS ONCOGENE FAMILY
8.88E-04	1.92	NM_002771	PROTEASE, SERINE, 3 (MESOTRYPSIN)
6.32E-05	1.92	NM_006769	LIM DOMAIN ONLY 4
9.63E-04	1.92	NM_016531	KRUPPEL-LIKE FACTOR 3 (BASIC)
1.10E-03	1.92	AF117233	MAKORIN, RING FINGER PROTEIN, 1
1.29E-03	1.92	NM_016848	SHC (SRC HOMOLOGY 2 DOMAIN CONTAINING) TRANSFORMING PROTEIN 3
4.55E-04	1.91	NM_052937	PROTEIN-L-ISOASPARTATE (D-ASPARTATE) O-METHYLTRANSFERASE DOMAIN CONTAINING 1
1.08E-03	1.91	NM_006465	AT RICH INTERACTIVE DOMAIN 3B (BRIGHT- LIKE)
3.95E-04	1.90	ENST00000400104	
1.16E-03	1.90	NM_001675	ACTIVATING TRANSCRIPTION FACTOR 4 (TAX-RESPONSIVE ENHANCER ELEMENT B67)
1.21E-03	1.90	NM_152352	CHROMOSOME 18 OPEN READING FRAME 19
9.35E-04	1.89	BQ009471	RING FINGER PROTEIN 130
1.46E-03	1.89	NM_001007245	INTERFERON-RELATED DEVELOPMENTAL REGULATOR 1
1.38E-03	1.88	NR_015377	

2.25E-04	1.88	NM_003442	ZINC FINGER PROTEIN 143 (CLONE PHZ-1)
9.35E-04	1.88	NM_138714	NUCLEAR FACTOR OF ACTIVATED T-CELLS 5, TONICITY-RESPONSIVE
9.34E-04	1.87	NM_014028	OSTEOPETROSIS ASSOCIATED TRANSMEMBRANE PROTEIN 1
2.81E-04	1.86	NM_025160	WD REPEAT DOMAIN 26
9.74E-04	1.85	NM_032095	PROTOCADHERIN GAMMA SUBFAMILY C, 3
9.74E-04	1.85	NM_032095	PROTOCADHERIN GAMMA SUBFAMILY B, 1
1.02E-03	1.85	NM_001675	ACTIVATING TRANSCRIPTION FACTOR 4 (TAX-RESPONSIVE ENHANCER ELEMENT B67)
6.62E-04	1.85	NM_182565	FAMILY WITH SEQUENCE SIMILARITY 100, MEMBER B
7.66E-04	1.85	NM_003254	TIMP METALLOPEPTIDASE INHIBITOR 1
9.72E-04	1.85	NM_004425	EXTRACELLULAR MATRIX PROTEIN 1
1.26E-03	1.85	NM_018420	SOLUTE CARRIER FAMILY 22 (ORGANIC CATION TRANSPORTER), MEMBER 15
1.47E-03	1.85	BX460543	CDC-LIKE KINASE 1
8.09E-04	1.85	NM_152230	INOSITOL POLYPHOSPHATE MULTIKINASE
4.25E-04	1.84	ENST00000357303	
1.22E-03	1.84	NM_031477	YIPPEE-LIKE 3 (DROSOPHILA)
7.19E-04	1.84	NM_052858	MARVEL DOMAIN CONTAINING 3
8.35E-04	1.83	NM_001042413	
3.43E-04	1.83	ENST00000337682	
5.71E-04	1.82	NM_000855	GUANYLATE CYCLASE 1, SOLUBLE, ALPHA 2
1.02E-03	1.82	THC2740750	
7.56E-04	1.82	NM_018963	BROMODOMAIN AND WD REPEAT DOMAIN CONTAINING 1
1.34E-03	1.82	NM_006371	CARTILAGE ASSOCIATED PROTEIN
4.73E-04	1.82	NM_001109	ADAM METALLOPEPTIDASE DOMAIN 8
1.39E-03	1.81	NM_015626	WD REPEAT AND SOCS BOX-CONTAINING 1
5.50E-04	1.81	NM_032258	TBC1 DOMAIN FAMILY, MEMBER 3
9.29E-05	1.81	NM_182851	CYCLIN B1 INTERACTING PROTEIN 1
1.23E-03	1.81	NM_004582	RAB GERANYLGERANYLTRANSFERASE, BETA SUBUNIT
4.55E-04	1.80	NM_153218	HYPOTHETICAL PROTEIN FLJ38725
1.11E-03	1.80	AK021668	FERM DOMAIN CONTAINING 4A
3.51E-05	1.80	NM_181795	PROTEIN KINASE (CAMP-DEPENDENT, CATALYTIC) INHIBITOR BETA
4.47E-04	1.79	NM_006526	ZINC FINGER PROTEIN 217
7.82E-04	1.79	NM_015972	HYPOTHETICAL PROTEIN MGC9850
7.82E-04	1.79	NM_015972	POLYMERASE (RNA) I POLYPEPTIDE D, 16KDA
4.98E-04	1.79	NM_016474	CHROMOSOME 3 OPEN READING FRAME 19
1.05E-03	1.78	NM_017664	ANKYRIN REPEAT DOMAIN 10
9.90E-04	1.78	NM_000396	CATHEPSIN K (PYCNODYSOSTOSIS)
5.53E-04	1.78	AB007870	NUCLEOPORIN LIKE 1
1.11E-03	1.78	AI470277	CYSTEINE-RICH SECRETORY PROTEIN LCCL DOMAIN CONTAINING 2
1.20E-03	1.77	NM_007314	V-ABL ABELSON MURINE LEUKEMIA VIRAL ONCOGENE HOMOLOG 2 (ARG, ABELSON-RELATED GENE)
9.87E-04	1.77	NM_000633	B-CELL CLL/LYMPHOMA 2
7.80E-05	1.77	NM_133484	TRAF FAMILY MEMBER-ASSOCIATED NFKB ACTIVATOR
6.14E-04	1.76	NM_032333	CHROMOSOME 10 OPEN READING FRAME 58
2.98E-05	1.75	NR_003500	
3.66E-04	1.75	NM_178815	ADP-RIBOSYLATION FACTOR-LIKE 5B
4.30E-04	1.74	NM_002214	INTEGRIN, BETA 8
4.11E-06	1.74	NM_198459	DENN/MADD DOMAIN CONTAINING 2C
2.20E-04	1.74	NM_198581	ZINC FINGER CCCH-TYPE CONTAINING 6
4.53E-04	1.73	NM_016217	HEADCASE HOMOLOG (DROSOPHILA)
2.68E-04	1.72	NM_007289	MEMBRANE METALLO-ENDOPEPTIDASE (NEUTRAL ENDOPEPTIDASE, ENKEPHALINASE, CALLA, CD10)
1.14E-03	1.72	CR613361	
3.78E-04	1.72	NM_015209	KAZRIN
1.46E-04	1.72	NM_147780	CATHEPSIN B
5.75E-04	1.71	NM_017747	ANKYRIN REPEAT AND KH DOMAIN CONTAINING 1
6.90E-04	1.70	BC063703	SLC7A5 PSEUDOGENE
6.90E-04	1.70	BC063703	KIAA0220-LIKE PROTEIN
2.27E-04	1.70	NM_001114938	
8.43E-04	1.70	XR_018444	
2.63E-04	1.70	NM_002214	INTEGRIN, BETA 8
4.40E-04	1.69	BI828537	
3.03E-04	1.68	NM_058181	CHROMOSOME 21 OPEN READING FRAME 57
1.09E-03	1.68	XM_001718704	
1.07E-03	1.68	NM_145807	HYPOTHETICAL PROTEIN BC018697
1.15E-03	1.68	ENST00000326470	
4.86E-04	1.68	BC032312	TRANSFORMING GROWTH FACTOR BETA REGULATOR 1
7.03E-04	1.68	NP1252191	
8.08E-04	1.68	NM_052885	SOLUTE CARRIER FAMILY 2 (FACILITATED GLUCOSE TRANSPORTER), MEMBER 13
1.19E-03	1.68	NM_021127	PHORBOL-12-MYRISTATE-13-ACETATE-INDUCED PROTEIN 1
5.09E-04	1.68	NM_002292	LAMININ, BETA 2 (LAMININ S)
7.93E-04	1.68	NM_014007	ZINC FINGER PROTEIN 297B
8.91E-04	1.67	NM_024552	LAG1 LONGEVITY ASSURANCE HOMOLOG 4 (S. CEREVISIAE)

1.42E-03	1.67	XM_292021	HYPOTHETICAL LOC341346
2.20E-04	1.67	NM_007075	WD REPEAT DOMAIN 45
7.49E-04	1.67	NM_000201	INTERCELLULAR ADHESION MOLECULE 1 (CD54), HUMAN RHINOVIRUS RECEPTOR
2.35E-04	1.67	AJ420378	CARNITINE PALMITOYLTRANSFERASE 1A (LIVER)
5.50E-04	1.66	NM_031412	GABA(A) RECEPTOR-ASSOCIATED PROTEIN LIKE 1
7.19E-04	1.66	NM_181782	NUCLEAR RECEPTOR COACTIVATOR 7
1.03E-03	1.66	NM_018368	LMBR1 DOMAIN CONTAINING 1
8.21E-04	1.66	AF000984	DEAD (ASP-GLU-ALA-ASP) BOX POLYPEPTIDE 3, Y-LINKED
7.31E-04	1.66	NM_015322	FEM-1 HOMOLOG B (C. ELEGANS)
8.85E-04	1.66	BG108194	HYPOXIA-INDUCIBLE FACTOR 1, ALPHA SUBUNIT (BASIC HELIX-LOOP-HELIX TRANSCRIPTION FACTOR)
1.04E-03	1.65	BC010943	ONCOSTATIN M RECEPTOR
1.94E-04	1.65	NM_015308	FORMIN BINDING PROTEIN 4
1.29E-03	1.65	NM_004506	HEAT SHOCK TRANSCRIPTION FACTOR 2
1.61E-04	1.64	ENST00000373457	
5.82E-04	1.64	NM_006079	CBP/P300-INTERACTING TRANSACTIVATOR, WITH GLU/ASP-RICH CARBOXY-TERMINAL DOMAIN, 2
1.17E-03	1.64	M32220	
1.30E-03	1.64	NM_030627	CYTOPLASMIC POLYADENYLATION ELEMENT BINDING PROTEIN 4
5.52E-05	1.64	NM_000201	INTERCELLULAR ADHESION MOLECULE 1 (CD54), HUMAN RHINOVIRUS RECEPTOR
1.39E-03	1.64	XR_018025	
9.29E-04	1.63	NM_007289	MEMBRANE METALLO-ENDOPEPTIDASE (NEUTRAL ENDOPEPTIDASE, ENKEPHALINASE, CALLA, CD10)
7.49E-04	1.63	NM_003850	SUCCINATE-COA LIGASE, ADP-FORMING, BETA SUBUNIT
7.00E-05	1.63	NM_000201	INTERCELLULAR ADHESION MOLECULE 1 (CD54), HUMAN RHINOVIRUS RECEPTOR
7.99E-04	1.62	ENST00000333156	
7.47E-04	1.62	NM_032867	MICAL C-TERMINAL LIKE
8.64E-04	1.62	NM_181721	FORKHEAD BOX R1
8.81E-04	1.62	THC2583971	
4.50E-06	1.62	NM_005667	RING FINGER PROTEIN 103
3.68E-05	1.62	NM_017881	CHROMOSOME 9 OPEN READING FRAME 95
1.04E-04	1.62	NM_181782	NUCLEAR RECEPTOR COACTIVATOR 7
4.17E-04	1.61	AA743218	PROTEIN PHOSPHATASE 1A (FORMERLY 2C), MAGNESIUM-DEPENDENT, ALPHA ISOFORM
6.43E-04	1.61	NM_000201	INTERCELLULAR ADHESION MOLECULE 1 (CD54), HUMAN RHINOVIRUS RECEPTOR
1.29E-03	1.61	NM_003999	ONCOSTATIN M RECEPTOR
7.64E-04	1.61	NM_018434	RING FINGER PROTEIN 130
8.39E-04	1.61	NM_020412	CHROMATIN MODIFYING PROTEIN 1B
1.36E-04	1.61	NM_181715	CREB REGULATED TRANSCRIPTION COACTIVATOR 2
1.38E-03	1.61	NM_015312	
1.14E-03	1.60	NM_024101	MELANOPHILIN
4.13E-04	1.60	NM_181354	OXIDATION RESISTANCE 1
3.82E-04	1.60	AK127420	SIMILAR TO FLJ43276 PROTEIN
4.27E-04	1.60	NM_016525	UBIQUITIN ASSOCIATED PROTEIN 1
1.05E-03	1.60	NM_152350	CHROMOSOME 17 OPEN READING FRAME 45
1.06E-03	1.60	NM_033305	VACUOLAR PROTEIN SORTING 13A (YEAST)
1.17E-03	1.60	NM_138363	COILED-COIL DOMAIN CONTAINING 45
4.61E-04	1.60	NM_000201	INTERCELLULAR ADHESION MOLECULE 1 (CD54), HUMAN RHINOVIRUS RECEPTOR
1.08E-03	1.60	NM_000036	ADENOSINE MONOPHOSPHATE DEAMINASE 1 (ISOFORM M)
2.02E-04	1.59	NM_020731	ARYL-HYDROCARBON RECEPTOR REPRESSOR
2.02E-04	1.59	NM_020731	PROGRAMMED CELL DEATH 6
1.33E-04	1.59	AK128047	SEC31-LIKE 1 (S. CEREVISIAE)
1.14E-04	1.59	NM_001002233	RAB11 FAMILY INTERACTING PROTEIN 1 (CLASS I)
3.35E-04	1.59	NM_031412	GABA(A) RECEPTOR-ASSOCIATED PROTEIN LIKE 1
9.56E-04	1.59	NM_014765	TRANSLOCASE OF OUTER MITOCHONDRIAL MEMBRANE 20 HOMOLOG (YEAST)
2.58E-04	1.59	NM_005407	SAL-LIKE 2 (DROSOPHILA)
1.46E-03	1.58	NM_003295	TUMOR PROTEIN, TRANSLATIONALLY-CONTROLLED 1
1.30E-03	1.58	NM_004064	CYCLIN-DEPENDENT KINASE INHIBITOR 1B (P27, KIP1)
3.00E-04	1.57	NM_016304	CHROMOSOME 15 OPEN READING FRAME 15
9.33E-04	1.57	THC2537829	
1.49E-03	1.57	NM_004064	CYCLIN-DEPENDENT KINASE INHIBITOR 1B (P27, KIP1)
3.48E-04	1.57	NM_181597	URIDINE PHOSPHORYLASE 1
5.28E-04	1.57	NM_001001555	GROWTH FACTOR RECEPTOR-BOUND PROTEIN 10
9.33E-04	1.57	NM_021127	PHORBOL-12-MYRISTATE-13-ACETATE-INDUCED PROTEIN 1
2.71E-04	1.56	NM_003162	STRIATIN, CALMODULIN BINDING PROTEIN
1.29E-03	1.56	BC040195	
1.46E-03	1.55	NM_020370	G PROTEIN-COUPLED RECEPTOR 84
7.18E-04	1.55	NM_021003	PROTEIN PHOSPHATASE 1A (FORMERLY 2C), MAGNESIUM-DEPENDENT, ALPHA ISOFORM
2.65E-05	1.55	NM_181805	PROTEIN KINASE (CAMP-DEPENDENT, CATALYTIC) INHIBITOR GAMMA
7.98E-05	1.55	NM_174899	F-BOX PROTEIN 36
8.09E-04	1.55	NM_177550	SODIUM-COUPLED CITRATE TRANSPORTER
9.45E-05	1.55	AK093811	HYPOTHETICAL PROTEIN FLJ36492
5.30E-05	1.53	NM_000393	COLLAGEN, TYPE V, ALPHA 2
3.11E-04	1.53	NM_000201	INTERCELLULAR ADHESION MOLECULE 1 (CD54), HUMAN RHINOVIRUS RECEPTOR

1.10E-03	1.52	NM_006623	PHOSPHOGLYCERATE DEHYDROGENASE
7.43E-04	1.52	NM_005587	MADS BOX TRANSCRIPTION ENHANCER FACTOR 2, POLYPEPTIDE A (MYOCYTE ENHANCER FACTOR 2A)
3.57E-07	1.51	NM_000861	HISTAMINE RECEPTOR H1
8.03E-04	1.51	NM_003565	UNC-51-LIKE KINASE 1 (C. ELEGANS)
8.19E-04	1.51	AF158383	ATPASE, (NA+)/K+ TRANSPORTING, BETA 4 POLYPEPTIDE
6.57E-04	1.50	NM_024420	PHOSPHOLIPASE A2, GROUP IVA (CYTOSOLIC, CALCIUM-DEPENDENT)
1.28E-03	1.50	NM_004428	EPHRIN-A1
5.67E-04	1.50	NM_001684	ATPASE, CA++ TRANSPORTING, PLASMA MEMBRANE 4
9.34E-04	-1.50	NM_054114	T-CELL ACTIVATION GTPASE ACTIVATING PROTEIN
4.74E-04	-1.50	NM_014063	DREBRIN-LIKE
1.28E-03	-1.51	AF130050	HYPOTHETICAL LOC654434
6.39E-04	-1.51	NM_000059	BREAST CANCER 2, EARLY ONSET
3.14E-04	-1.51	BC010526	HYPOTHETICAL LOC401127
6.86E-04	-1.51	NM_052893	
8.49E-05	-1.51	THC2748419	
1.37E-03	-1.51	NM_016819	8-OXOGUANINE DNA GLYCOSYLASE
3.31E-04	-1.51	NM_138408	CHROMOSOME 6 OPEN READING FRAME 51
1.20E-03	-1.52	BE388027	CHROMOSOME 9 OPEN READING FRAME 74
1.22E-03	-1.52	NM_002028	FARNESYLTRANSFERASE, CAAX BOX, BETA
1.21E-04	-1.52	NM_005891	ACETYL-COENZYME A ACETYLTRANSFERASE 2 (ACETOACETYL COENZYME A THIOLASE)
4.86E-04	-1.52	NM_025040	ZINC FINGER PROTEIN 614
7.15E-04	-1.52	NM_004091	E2F TRANSCRIPTION FACTOR 2
5.45E-04	-1.52	NM_017491	WD REPEAT DOMAIN 1
1.09E-03	-1.53	NM_025189	ZINC FINGER PROTEIN 430
7.78E-04	-1.53	AK124175	SIMILAR TO RPE-SPONDIN
6.61E-04	-1.53	AK097637	CDNA FLJ40318 FIS, CLONE TESTI2030556
1.06E-04	-1.53	NM_017443	POLYMERASE (DNA DIRECTED), EPSILON 3 (P17 SUBUNIT)
7.33E-04	-1.53	BC008667	PANTOTHENATE KINASE 2 (HALLERVORDEN-SPATZ SYNDROME)
7.33E-04	-1.53	BC008667	HYPOTHETICAL PROTEIN
5.74E-04	-1.53	NM_004687	MYOTUBULARIN RELATED PROTEIN 4
5.84E-05	-1.54	NM_002716	PROTEIN PHOSPHATASE 2 (FORMERLY 2A), REGULATORY SUBUNIT A (PR 65), BETA ISOFORM
8.33E-04	-1.54	ENST00000390253	
3.69E-04	-1.54	AK025669	RING FINGER PROTEIN 169
2.04E-04	-1.54	NM_138463	TLC DOMAIN CONTAINING 1
4.19E-05	-1.54	NM_007126	VALOSIN-CONTAINING PROTEIN
1.27E-03	-1.54	THC2616573	
7.92E-04	-1.54	NM_001040458	
1.07E-03	-1.55	NR_015350	
1.07E-03	-1.55	NM_004814	WD REPEAT DOMAIN 57 (U5 SNRNP SPECIFIC)
4.88E-04	-1.55	NM_024662	N-ACETYLTRANSFERASE 10
2.33E-04	-1.55	NM_015697	COENZYME Q2 HOMOLOG, PRENYLTRANSFERASE (YEAST)
1.01E-03	-1.55	NM_178517	PHOSPHATIDYLINOSITOL GLYCAN, CLASS W
1.26E-03	-1.55	NM_145865	ANKYRIN REPEAT AND STERILE ALPHA MOTIF DOMAIN CONTAINING 4B
1.12E-03	-1.56	NM_002947	REPLICATION PROTEIN A3, 14KDA
7.61E-04	-1.56	NM_138999	NEUROPILIN (NRP) AND TOLLOID (TLL)-LIKE 1
6.71E-04	-1.56	NM_152577	ZINC FINGER PROTEIN 645
5.84E-04	-1.57	NM_004393	DYSTROGLYCAN 1 (DYSTROPHIN-ASSOCIATED GLYCOPROTEIN 1)
1.15E-03	-1.57	NM_005968	HETEROGENEOUS NUCLEAR RIBONUCLEOPROTEIN M
9.46E-04	-1.57	NM_017794	KIAA1797
3.60E-04	-1.57	NM_012247	SELENOPHOSPHATE SYNTHETASE 1
1.23E-03	-1.58	NM_018098	EPITHELIAL CELL TRANSFORMING SEQUENCE 2 ONCOGENE
1.40E-03	-1.58	NM_033418	CHROMOSOME 1 OPEN READING FRAME 156
1.09E-03	-1.58	NM_031844	HETEROGENEOUS NUCLEAR RIBONUCLEOPROTEIN U (SCAFFOLD ATTACHMENT FACTOR A)
1.35E-03	-1.58	NM_144682	LIKLEY ORTHOLOG OF MOUSE SCHLAFEN 10
1.16E-03	-1.58	AF220264	CHROMOSOME 8 OPEN READING FRAME 17
1.40E-03	-1.58	X15667	GLUTATHIONE PEROXIDASE 1
3.23E-05	-1.58	NM_198461	LON PEPTIDASE N-TERMINAL DOMAIN AND RING FINGER 2
7.26E-05	-1.59	NM_144573	NEXILIN (F ACTIN BINDING PROTEIN)
6.88E-04	-1.59	NM_031944	MIX1 HOMEOBOX-LIKE 1 (XENOPUS LAEVIS)
1.13E-03	-1.59	NM_003029	SHC (SRC HOMOLOGY 2 DOMAIN CONTAINING) TRANSFORMING PROTEIN 1
8.26E-04	-1.59	BC037919	
6.57E-05	-1.59	AK055372	
4.42E-04	-1.59	NM_001079	ZETA-CHAIN (TCR) ASSOCIATED PROTEIN KINASE 70KDA
3.73E-05	-1.59	NM_177987	TUBULIN, BETA 8
1.08E-03	-1.59	NM_033238	PROMYELOCYTIC LEUKEMIA
5.19E-04	-1.60	NM_152754	SEMA DOMAIN, IMMUNOGLOBULIN DOMAIN (IG), SHORT BASIC DOMAIN, SECRETED, (SEMAPHORIN) 3D
1.17E-03	-1.60	NM_001077482	
7.26E-04	-1.60	ENST00000382378	
1.27E-03	-1.60	AK023683	CENTROSOMAL PROTEIN 135KDA
7.52E-04	-1.61	NM_004326	B-CELL CLL/LYMPHOMA 9

6.14E-04	-1.61	NM_007126	VALOSIN-CONTAINING PROTEIN
1.39E-03	-1.61	NM_001039690	DECREASED EXPRESSION IN RENAL AND PROSTATE
3.63E-05	-1.61	NM_013293	TRANSFORMER-2 ALPHA
1.29E-03	-1.61	NM_006306	SMC1 STRUCTURAL MAINTENANCE OF CHROMOSOMES 1-LIKE 1 (YEAST)
1.48E-03	-1.61	NM_003029	SHC (SRC HOMOLOGY 2 DOMAIN CONTAINING) TRANSFORMING PROTEIN 1
1.17E-03	-1.62	NM_002945	REPLICATION PROTEIN A1, 70KDA
7.40E-04	-1.62	NM_021095	SOLUTE CARRIER FAMILY 5 (SODIUM-DEPENDENT VITAMIN TRANSPORTER), MEMBER 6
6.96E-05	-1.62	NM_000059	BREAST CANCER 2, EARLY ONSET
1.08E-04	-1.62	NM_015050	KIAA0082
3.08E-04	-1.62	NM_007137	ZINC FINGER PROTEIN 81 (HFZ20)
2.36E-04	-1.63	NM_181699	PROTEIN PHOSPHATASE 2 (FORMERLY 2A), REGULATORY SUBUNIT A (PR 65), BETA ISOFORM
1.29E-04	-1.63	NM_001111	ADENOSINE DEAMINASE, RNA-SPECIFIC
5.98E-05	-1.63	NM_014730	KIAA0152
1.20E-03	-1.64	AB040937	KIAA1504 PROTEIN
1.40E-04	-1.64	NM_013322	SORTING NEXIN 10
4.40E-04	-1.64	DarkCorner	
9.31E-04	-1.65	THC2684874	
2.16E-04	-1.65	NM_006716	DBF4 HOMOLOG (S. CEREVISIAE)
7.96E-04	-1.65	NM_000692	ALDEHYDE DEHYDROGENASE 1 FAMILY, MEMBER B1
5.93E-04	-1.65	NM_183001	SHC (SRC HOMOLOGY 2 DOMAIN CONTAINING) TRANSFORMING PROTEIN 1
3.70E-04	-1.66	NM_006809	TRANSLOCASE OF OUTER MITOCHONDRIAL MEMBRANE 34
8.63E-04	-1.66	CR592968	ROUND SPERMATID BASIC PROTEIN 1-LIKE
1.82E-04	-1.66	AK095359	HYPOTHETICAL PROTEIN LOC221362
6.86E-04	-1.66	NM_138287	DELTEX 3-LIKE (DROSOPHILA)
1.18E-03	-1.66	AL050122	
8.47E-04	-1.66	THC2677118	
1.62E-04	-1.67	ENST00000249776	
1.19E-04	-1.67	NM_004499	HETEROGENEOUS NUCLEAR RIBONUCLEOPROTEIN A/B
9.12E-04	-1.67	NM_030577	HYPOTHETICAL PROTEIN MGC10993
1.26E-05	-1.67	NM_006099	PROTEIN INHIBITOR OF ACTIVATED STAT, 3
2.84E-04	-1.67	NM_153705	KDEL (LYS-ASP-GLU-LEU) CONTAINING 2
3.80E-04	-1.67	NM_015531	HYPOTHETICAL PROTEIN
2.05E-04	-1.68	NM_018319	TYROSYL-DNA PHOSPHODIESTERASE 1
1.88E-04	-1.68	NM_003029	SHC (SRC HOMOLOGY 2 DOMAIN CONTAINING) TRANSFORMING PROTEIN 1
1.07E-03	-1.68	NM_005348	HEAT SHOCK PROTEIN 90KDA ALPHA (CYTOSOLIC), CLASS A MEMBER 1
1.14E-04	-1.68	NM_003824	FAS (TNFRSF6)-ASSOCIATED VIA DEATH DOMAIN
1.19E-04	-1.69	BC011660	
1.14E-03	-1.69	NM_032389	ZINC FINGER PROTEIN 289, ID1 REGULATED
3.61E-04	-1.69	AK095300	FERM, RHOGEF AND PLECKSTRIN DOMAIN PROTEIN 2
3.61E-04	-1.69	AK095300	CDNA FLJ37981 FIS, CLONE CTONG2010566
5.89E-04	-1.69	ENST00000379156	
1.77E-04	-1.70	THC2638232	
2.67E-06	-1.70	NM_001559	INTERLEUKIN 12 RECEPTOR, BETA 2
5.18E-04	-1.70	AK095108	CHROMOBOX HOMOLOG 5 (HP1 ALPHA HOMOLOG, DROSOPHILA)
5.65E-04	-1.70	NM_003115	UDP-N-ACTEYLGLUCOSAMINE PYROPHOSPHORYLASE 1
1.65E-04	-1.71	NM_018320	RING FINGER PROTEIN 121
4.48E-04	-1.71	NM_003029	SHC (SRC HOMOLOGY 2 DOMAIN CONTAINING) TRANSFORMING PROTEIN 1
6.73E-04	-1.71	AK057261	MITOCHONDRIAL RIBOSOMAL PROTEIN L38
5.30E-04	-1.71	NM_025077	HYPOTHETICAL PROTEIN FLJ13949
8.87E-04	-1.71	NM_005184	CALMODULIN 1 (PHOSPHORYLASE KINASE, DELTA)
1.17E-03	-1.72	NM_000446	PARAOXONASE 1
2.49E-04	-1.72	NM_080873	ANKYRIN REPEAT AND SOCS BOX-CONTAINING 11
1.10E-04	-1.72	AB007937	SYNDECAN 3 (N-SYNDECAN)
8.87E-04	-1.72	NM_022731	NUCLEAR CASEIN KINASE AND CYCLIN-DEPENDENT KINASE SUBSTRATE 1
4.89E-05	-1.72	NM_017882	CEROID-LIPOFUSCINOSIS, NEURONAL 6, LATE INFANTILE, VARIANT
3.42E-05	-1.74	NM_017785	HYPOTHETICAL PROTEIN FLJ20364
1.42E-03	-1.74	NM_001078166	
5.33E-04	-1.74	NM_003016	SPLICING FACTOR, ARGININE/SERINE-RICH 2
7.67E-04	-1.74	NM_015426	WD REPEAT DOMAIN 51A
1.33E-04	-1.75	NM_018294	CWF19-LIKE 1, CELL CYCLE CONTROL (S. POMBE)
1.19E-05	-1.75	NM_001316	CSE1 CHROMOSOME SEGREGATION 1-LIKE (YEAST)
1.21E-03	-1.75	NM_001111	ADENOSINE DEAMINASE, RNA-SPECIFIC
3.07E-04	-1.75	AF426262	CHROMOSOME 21 OPEN READING FRAME 85
3.07E-04	-1.75	AF426262	MCM3 MINICHROMOSOME MAINTENANCE DEFICIENT 3 (S. CEREVISIAE) ASSOCIATED PROTEIN ANTISENSE
3.95E-04	-1.75	NM_002875	RAD51 HOMOLOG (RECA HOMOLOG, E. COLI) (S. CEREVISIAE)
5.71E-04	-1.75	NM_006001	TUBULIN, ALPHA 2
3.27E-04	-1.75	ENST00000390369	
1.45E-03	-1.76	NM_014657	KIAA0406 GENE PRODUCT
4.36E-04	-1.76	NM_017785	HYPOTHETICAL PROTEIN FLJ20364
1.02E-04	-1.76	NM_025077	HYPOTHETICAL PROTEIN FLJ13949

6.29E-04	-1.76	NM_017613	DOWNSTREAM NEIGHBOR OF SON
1.40E-03	-1.76	NM_024625	ZINC FINGER CCCH-TYPE, ANTIVIRAL 1
1.34E-03	-1.76	NM_005517	HIGH-MOBILITY GROUP NUCLEOSOMAL BINDING DOMAIN 2
8.12E-04	-1.77	NM_004265	FATTY ACID DESATURASE 2
4.70E-04	-1.77	NM_015340	LEUCYL-TRNA SYNTHETASE 2, MITOCHONDRIAL
7.16E-04	-1.77	ENST00000375806	
8.99E-04	-1.78	NM_203467	PEPTIDYLPROLYL ISOMERASE (CYCLOPHILIN)-LIKE 5
5.89E-04	-1.78	NM_002828	PROTEIN TYROSINE PHOSPHATASE, NON-RECEPTOR TYPE 2
1.33E-03	-1.78	XR_019306	
1.02E-03	-1.79	NM_017785	HYPOTHETICAL PROTEIN FLJ20364
7.30E-04	-1.79	NM_004688	N-MYC (AND STAT) INTERACTOR
2.52E-05	-1.79	NM_198468	CHROMOSOME 6 OPEN READING FRAME 167
1.14E-04	-1.80	NM_032166	THREE PRIME REPAIR EXONUCLEASE 1
9.65E-04	-1.80	NM_017785	HYPOTHETICAL PROTEIN FLJ20364
1.44E-03	-1.80	NM_021067	DNA REPLICATION COMPLEX GINS PROTEIN PSF1
1.46E-04	-1.81	NM_001017963	HEAT SHOCK PROTEIN 90KDA ALPHA (CYTOSOLIC), CLASS A MEMBER 1
1.33E-03	-1.81	NM_032456	BH-PROTOCADHERIN (BRAIN-HEART)
9.34E-04	-1.81	NM_005914	MCM4 MINICHROMOSOME MAINTENANCE DEFICIENT 4 (S. CEREVISIAE)
1.28E-04	-1.81	NM_024808	FLJ22624 PROTEIN
3.58E-04	-1.82	NM_000251	MUTS HOMOLOG 2, COLON CANCER, NONPOLYPOSIS TYPE 1 (E. COLI)
1.29E-03	-1.82	NM_014859	KIAA0672 GENE PRODUCT
1.15E-04	-1.82	AT_T_3	
2.12E-05	-1.83	NM_003368	UBIQUITIN SPECIFIC PEPTIDASE 1
1.33E-03	-1.83	NM_001211	BUB1 BUDDING UNINHIBITED BY BENZIMIDAZOLES 1 HOMOLOG BETA (YEAST)
5.85E-04	-1.85	NM_032525	TUBULIN, BETA 6
1.32E-03	-1.86	AT_ssH_AB_3	
5.09E-05	-1.86	NM_032704	TUBULIN, ALPHA, UBIQUITOUS
5.17E-05	-1.86	NM_145175	FAMILY WITH SEQUENCE SIMILARITY 84, MEMBER A
1.49E-03	-1.87	NM_001040152	
1.01E-03	-1.87	NM_014109	ATPASE FAMILY, AAA DOMAIN CONTAINING 2
9.72E-06	-1.87	NM_002266	KARYOPHERIN ALPHA 2 (RAG COHORT 1, IMPORTIN ALPHA 1)
1.06E-03	-1.87	NR_022014	
2.59E-04	-1.88	D31765	PROCESSING OF PRECURSOR 1, RIBONUCLEASE P/MRP SUBUNIT (S. CEREVISIAE)
1.04E-03	-1.88	NM_006084	INTERFERON-STIMULATED TRANSCRIPTION FACTOR 3, GAMMA 48KDA
1.10E-03	-1.88	NM_005441	CHROMATIN ASSEMBLY FACTOR 1, SUBUNIT B (P60)
1.50E-03	-1.89	NM_006176	NEUROGRANIN (PROTEIN KINASE C SUBSTRATE, RC3)
1.32E-03	-1.90	NM_000251	MUTS HOMOLOG 2, COLON CANCER, NONPOLYPOSIS TYPE 1 (E. COLI)
1.21E-04	-1.91	NM_018944	CHROMOSOME 21 OPEN READING FRAME 45
1.98E-05	-1.91	NM_017955	CELL DIVISION CYCLE ASSOCIATED 4
7.98E-04	-1.92	AK091439	TRANSMEMBRANE PROTEIN 48
1.41E-03	-1.92	NM_001999	FIBRILLIN 2 (CONGENITAL CONTRACTURAL ARACHNODACTYLY)
6.45E-05	-1.92	NM_198188	ASTROTACTIN 2
1.66E-04	-1.92	DB363547	LOC440111
1.09E-03	-1.93	AW168145	
2.03E-04	-1.93	NM_002692	POLYMERASE (DNA DIRECTED), EPSILON 2 (P59 SUBUNIT)
2.21E-04	-1.93	NM_017785	HYPOTHETICAL PROTEIN FLJ20364
1.32E-03	-1.93	NM_032015	RING FINGER PROTEIN 26
4.14E-05	-1.93	NM_018697	LANC LANTIBIOTIC SYNTHETASE COMPONENT C-LIKE 2 (BACTERIAL)
9.19E-04	-1.94	THC2572108	
3.53E-04	-1.94	NM_139266	SIGNAL TRANSDUCER AND ACTIVATOR OF TRANSCRIPTION 1, 91KDA
8.20E-04	-1.94	NM_000251	MUTS HOMOLOG 2, COLON CANCER, NONPOLYPOSIS TYPE 1 (E. COLI)
4.06E-05	-1.94	NM_006187	2'-5'-OLIGOADENYLATE SYNTHETASE 3, 100KDA
1.45E-03	-1.94	NM_032525	TUBULIN, BETA 6
1.43E-03	-1.95	NM_020810	TRM5 TRNA METHYLTRANSFERASE 5 HOMOLOG (S. CEREVISIAE)
8.18E-04	-1.95	NM_001101	ACTIN, BETA
8.78E-04	-1.95	NM_006086	MELANOCORTIN 1 RECEPTOR (ALPHA MELANOCYTE STIMULATING HORMONE RECEPTOR)
4.46E-04	-1.96	BF761348	
8.87E-04	-1.97	XR_019461	
1.41E-03	-1.97	NM_024094	DEFECTIVE IN SISTER CHROMATID COHESION HOMOLOG 1 (S. CEREVISIAE)
2.41E-04	-1.98	NM_017955	CELL DIVISION CYCLE ASSOCIATED 4
1.55E-04	-1.98	NM_015907	LEUCINE AMINOPEPTIDASE 3
5.42E-04	-1.99	NM_017554	POLY (ADP-RIBOSE) POLYMERASE FAMILY, MEMBER 14
2.98E-04	-1.99	AK074711	HEDGEHOG INTERACTING PROTEIN
1.53E-04	-1.99	XR_017251	
5.02E-04	-1.99	NM_003141	TRIPARTITE MOTIF-CONTAINING 21
6.89E-04	-1.99	NM_005441	CHROMATIN ASSEMBLY FACTOR 1, SUBUNIT B (P60)
5.22E-04	-1.99	NM_000251	MUTS HOMOLOG 2, COLON CANCER, NONPOLYPOSIS TYPE 1 (E. COLI)
1.13E-03	-2.00	NM_007086	WD REPEAT AND HMG-BOX DNA BINDING PROTEIN 1
2.88E-04	-2.00	NM_022836	DNA CROSS-LINK REPAIR 1B (PSO2 HOMOLOG, S. CEREVISIAE)
1.35E-03	-2.00	NM_006597	HEAT SHOCK 70KDA PROTEIN 8

5.08E-04	-2.00	NM_001490	GLUCOSAMINYL (N-ACETYL) TRANSFERASE 1, CORE 2 (BETA-1,6-N-ACETYLGLUCOSAMINYLTRANSFERASE)
9.04E-05	-2.00	NM_139266	SIGNAL TRANSDUCER AND ACTIVATOR OF TRANSCRIPTION 1, 91KDA
1.13E-04	-2.00	NM_005441	CHROMATIN ASSEMBLY FACTOR 1, SUBUNIT B (P60)
6.32E-04	-2.00	NM_139266	SIGNAL TRANSDUCER AND ACTIVATOR OF TRANSCRIPTION 1, 91KDA
4.81E-05	-2.02	NM_003642	HISTONE ACETYLTRANSFERASE 1
4.96E-04	-2.02	NM_006087	TUBULIN, BETA 4
3.11E-04	-2.04	NM_139266	SIGNAL TRANSDUCER AND ACTIVATOR OF TRANSCRIPTION 1, 91KDA
7.03E-04	-2.04	NM_007295	BREAST CANCER 1, EARLY ONSET
8.12E-05	-2.05	NM_001031684	SPLICING FACTOR, ARGININE/SERINE-RICH 7, 35KDA
1.93E-04	-2.05	AF193046	FIBRILLIN 2 (CONGENITAL CONTRACTURAL ARACHNODACTYLY)
5.66E-05	-2.05	AK027667	HYPOTHETICAL PROTEIN FLJ14761
1.10E-03	-2.05	NM_000251	MUTS HOMOLOG 2, COLON CANCER, NONPOLYPOSIS TYPE 1 (E. COLI)
1.03E-03	-2.05	NM_007295	BREAST CANCER 1, EARLY ONSET
1.15E-03	-2.06	NM_032704	TUBULIN, ALPHA, UBIQUITOUS
1.38E-03	-2.06	NM_005517	HIGH-MOBILITY GROUP NUCLEOSOMAL BINDING DOMAIN 2
1.27E-03	-2.06	NM_001024847	TRANSFORMING GROWTH FACTOR, BETA RECEPTOR II (70/80KDA)
5.20E-04	-2.07	NM_007295	BREAST CANCER 1, EARLY ONSET
1.09E-03	-2.07	NM_139266	SIGNAL TRANSDUCER AND ACTIVATOR OF TRANSCRIPTION 1, 91KDA
1.85E-04	-2.07	NM_138287	DELTEX 3-LIKE (DROSOPHILA)
2.00E-04	-2.07	AA065042	CHROMOSOME 21 OPEN READING FRAME 45
1.57E-04	-2.08	NM_139266	SIGNAL TRANSDUCER AND ACTIVATOR OF TRANSCRIPTION 1, 91KDA
2.57E-04	-2.08	NM_018186	CHROMOSOME 1 OPEN READING FRAME 112
4.88E-04	-2.09	NM_006074	TRIPARTITE MOTIF-CONTAINING 22
6.95E-04	-2.09	NM_005441	CHROMATIN ASSEMBLY FACTOR 1, SUBUNIT B (P60)
9.63E-04	-2.10	NM_139266	SIGNAL TRANSDUCER AND ACTIVATOR OF TRANSCRIPTION 1, 91KDA
1.36E-03	-2.10	BU731317	HEAT SHOCK 70KDA PROTEIN 8
5.56E-04	-2.10	NM_015474	SAM DOMAIN AND HD DOMAIN 1
2.67E-04	-2.11	NM_173084	TRIPARTITE MOTIF-CONTAINING 59
4.86E-04	-2.12	NM_024094	DEFECTIVE IN SISTER CHROMATID COHESION HOMOLOG 1 (S. CEREVISIAE)
7.68E-04	-2.12	THC2611110	
1.03E-03	-2.13	NM_198468	CHROMOSOME 6 OPEN READING FRAME 167
4.52E-05	-2.13	NM_032043	BRCA1 INTERACTING PROTEIN C-TERMINAL HELICASE 1
8.82E-04	-2.14	NM_000251	MUTS HOMOLOG 2, COLON CANCER, NONPOLYPOSIS TYPE 1 (E. COLI)
2.44E-05	-2.14	NM_001618	POLY (ADP-RIBOSE) POLYMERASE FAMILY, MEMBER 1
1.25E-04	-2.15	NM_001042762	
1.43E-03	-2.15	BC019599	
2.14E-04	-2.15	NM_014502	PRP19/PSO4 PRE-MRNA PROCESSING FACTOR 19 HOMOLOG (S. CEREVISIAE)
7.16E-05	-2.15	NM_001618	POLY (ADP-RIBOSE) POLYMERASE FAMILY, MEMBER 1
6.99E-04	-2.16	THC2762149	
1.49E-03	-2.17	NM_007295	BREAST CANCER 1, EARLY ONSET
8.16E-04	-2.18	NM_001618	POLY (ADP-RIBOSE) POLYMERASE FAMILY, MEMBER 1
1.02E-03	-2.18	NM_002388	MCM3 MINICHROMOSOME MAINTENANCE DEFICIENT 3 (S. CEREVISIAE)
2.10E-04	-2.18	NM_139266	SIGNAL TRANSDUCER AND ACTIVATOR OF TRANSCRIPTION 1, 91KDA
9.05E-05	-2.18	AK055960	SIMILAR TO HIGH MOBILITY GROUP PROTEIN 4 (HMG-4) (HIGH MOBILITY GROUP PROTEIN 2A) (HMG-2A)
1.07E-04	-2.18	NM_022770	HYPOTHETICAL PROTEIN FLJ13912
4.71E-04	-2.18	NM_182751	MCM10 MINICHROMOSOME MAINTENANCE DEFICIENT 10 (S. CEREVISIAE)
6.36E-04	-2.18	NM_002130	3-HYDROXY-3-METHYLGLUTARYL-COENZYME A SYNTHASE 1 (SOLUBLE)
9.43E-04	-2.18	NM_001042762	
4.63E-04	-2.19	NM_001618	POLY (ADP-RIBOSE) POLYMERASE FAMILY, MEMBER 1
3.07E-05	-2.19	XM_497547	SIMILAR TO HIGH-MOBILITY GROUP BOX 3
4.64E-04	-2.20	NM_018042	LIKELY ORTHOLOG OF MOUSE SCHLAFEN 3
2.56E-04	-2.21	NM_139266	SIGNAL TRANSDUCER AND ACTIVATOR OF TRANSCRIPTION 1, 91KDA
6.73E-05	-2.21	CR749256	X-RAY REPAIR COMPLEMENTING DEFECTIVE REPAIR IN CHINESE HAMSTER CELLS 2
3.28E-04	-2.22	NM_001618	POLY (ADP-RIBOSE) POLYMERASE FAMILY, MEMBER 1
5.46E-04	-2.22	NM_001155	ANNEXIN A6
6.40E-04	-2.24	NM_033219	TRIPARTITE MOTIF-CONTAINING 14
1.34E-04	-2.26	NM_182625	HYPOTHETICAL PROTEIN FLJ40869
1.40E-03	-2.26	NM_153026	PRICKLE-LIKE 1 (DROSOPHILA)
1.07E-04	-2.26	NM_001618	POLY (ADP-RIBOSE) POLYMERASE FAMILY, MEMBER 1
1.98E-04	-2.26	NM_006088	TUBULIN, BETA 2C
9.88E-04	-2.27	NM_000059	BREAST CANCER 2, EARLY ONSET
5.80E-05	-2.28	NM_001618	POLY (ADP-RIBOSE) POLYMERASE FAMILY, MEMBER 1
2.49E-04	-2.29	NM_002592	PROLIFERATING CELL NUCLEAR ANTIGEN
2.76E-04	-2.32	NM_139266	SIGNAL TRANSDUCER AND ACTIVATOR OF TRANSCRIPTION 1, 91KDA
8.56E-04	-2.32	NM_016195	M-PHASE PHOSPHOPROTEIN 1
8.25E-05	-2.33	THC2738878	
7.79E-04	-2.34	NM_006000	TUBULIN, ALPHA 1 (TESTIS SPECIFIC)
7.68E-04	-2.36	AK027859	HYPOTHETICAL PROTEIN MGC11266
3.41E-04	-2.36	NM_152562	CELL DIVISION CYCLE ASSOCIATED 2
5.17E-04	-2.38	NM_198965	PARATHYROID HORMONE-LIKE HORMONE

3.27E-05	-2.39	NM_001618	POLY (ADP-RIBOSE) POLYMERASE FAMILY, MEMBER 1
5.82E-04	-2.39	NM_003173	SUPPRESSOR OF VARIEGATION 3-9 HOMOLOG 1 (DROSOPHILA)
2.88E-04	-2.39	NM_002592	PROLIFERATING CELL NUCLEAR ANTIGEN
6.52E-05	-2.40	NM_001618	POLY (ADP-RIBOSE) POLYMERASE FAMILY, MEMBER 1
2.08E-04	-2.41	NM_004111	FLAP STRUCTURE-SPECIFIC ENDONUCLEASE 1
5.79E-04	-2.41	NM_002592	PROLIFERATING CELL NUCLEAR ANTIGEN
7.74E-04	-2.42	NM_001618	POLY (ADP-RIBOSE) POLYMERASE FAMILY, MEMBER 1
1.42E-04	-2.42	AK091289	ZINC FINGER PROTEIN 367
2.00E-04	-2.43	NM_001071	THYMIDYLATE SYNTHETASE
5.68E-04	-2.43	XR_018533	
1.16E-03	-2.45	AB040957	KIAA1524
1.98E-04	-2.45	NM_002592	PROLIFERATING CELL NUCLEAR ANTIGEN
7.93E-05	-2.46	NM_057749	CYCLIN E2
2.39E-04	-2.46	NM_002592	PROLIFERATING CELL NUCLEAR ANTIGEN
5.64E-05	-2.46	NM_020890	KIAA1524
1.28E-03	-2.47	NM_018154	ASF1 ANTI-SILENCING FUNCTION 1 HOMOLOG B (S. CEREVISIAE)
6.54E-04	-2.50	THC2677432	
9.16E-04	-2.51	NM_017414	UBIQUITIN SPECIFIC PEPTIDASE 18
2.69E-04	-2.51	NM_002017	FRIEND LEUKEMIA VIRUS INTEGRATION 1
1.23E-04	-2.51	NM_004111	FLAP STRUCTURE-SPECIFIC ENDONUCLEASE 1
5.87E-04	-2.52	NM_002915	REPLICATION FACTOR C (ACTIVATOR 1) 3, 38KDA
8.88E-04	-2.53	NM_017912	HECT DOMAIN AND RLD 6
2.20E-04	-2.54	NM_002592	PROLIFERATING CELL NUCLEAR ANTIGEN
5.68E-05	-2.54	NM_002592	PROLIFERATING CELL NUCLEAR ANTIGEN
3.84E-05	-2.55	NM_002592	PROLIFERATING CELL NUCLEAR ANTIGEN
2.51E-04	-2.56	NM_002592	PROLIFERATING CELL NUCLEAR ANTIGEN
1.34E-03	-2.56	NM_032704	TUBULIN, ALPHA, UBIQUITOUS
6.93E-05	-2.58	NM_002534	2',5'-OLIGOADENYLATE SYNTHETASE 1, 40/46KDA
1.17E-03	-2.59	XR_018797	
5.81E-04	-2.59	NM_002592	PROLIFERATING CELL NUCLEAR ANTIGEN
2.68E-04	-2.61	NM_000958	PROSTAGLANDIN E RECEPTOR 4 (SUBTYPE EP4)
2.02E-04	-2.62	NM_001549	INTERFERON-INDUCED PROTEIN WITH TETRATRICOPEPTIDE REPEATS 3
3.35E-06	-2.62	AA865794	BREAST CANCER 1, EARLY ONSET
6.64E-04	-2.63	NM_001813	CENTROMERE PROTEIN E, 312KDA
1.45E-03	-2.64	NM_018492	PDZ BINDING KINASE
2.46E-04	-2.64	NM_005915	MCM6 MINICHROMOSOME MAINTENANCE DEFICIENT 6 (MIS5 HOMOLOG, S. POMBE) (S. CEREVISIAE)
5.66E-04	-2.68	X98261	ZW10 INTERACTOR ANTISENSE
5.66E-04	-2.68	X98261	ZW10 INTERACTOR
7.15E-04	-2.68	NM_001753	CAVEOLIN 1, CAVEOLAE PROTEIN, 22KDA
1.16E-03	-2.71	NM_194298	SOLUTE CARRIER FAMILY 16 (MONOCARBOXYLIC ACID TRANSPORTERS), MEMBER 9
2.71E-04	-2.73	NM_198433	AURORA KINASE A
1.01E-03	-2.76	NM_002417	ANTIGEN IDENTIFIED BY MONOCLONAL ANTIBODY KI-67
7.24E-04	-2.77	DB356469	TUBULIN, ALPHA, UBIQUITOUS
4.02E-04	-2.78	NM_001753	CAVEOLIN 1, CAVEOLAE PROTEIN, 22KDA
1.06E-03	-2.81	NM_005573	LAMIN B1
8.73E-04	-2.82	NM_024094	DEFECTIVE IN SISTER CHROMATID COHESION HOMOLOG 1 (S. CEREVISIAE)
5.44E-04	-2.83	NM_001753	CAVEOLIN 1, CAVEOLAE PROTEIN, 22KDA
2.37E-05	-2.91	NM_031458	POLY (ADP-RIBOSE) POLYMERASE FAMILY, MEMBER 9
1.31E-03	-2.95	NM_001753	CAVEOLIN 1, CAVEOLAE PROTEIN, 22KDA
5.77E-06	-2.96	AW291149	THYMOPOIETIN
7.78E-04	-2.98	NM_004336	BUB1 BUDDING UNINHIBITED BY BENZIMIDAZOLES 1 HOMOLOG (YEAST)
2.76E-04	-2.98	NM_173529	CHROMOSOME 18 OPEN READING FRAME 54
1.16E-03	-3.00	NM_001753	CAVEOLIN 1, CAVEOLAE PROTEIN, 22KDA
5.34E-04	-3.04	BF195408	CARBOXYPEPTIDASE, VITELLOGENIC-LIKE
1.13E-04	-3.11	NM_017669	FLJ20105 PROTEIN
1.56E-04	-3.23	AL359052	INTEGRIN, BETA-LIKE 1 (WITH EGF-LIKE REPEAT DOMAINS)
5.99E-04	-3.25	NM_016192	TRANSMEMBRANE PROTEIN WITH EGF-LIKE AND TWO FOLLISTATIN-LIKE DOMAINS 2
2.31E-06	-3.28	NM_003276	THYMOPOIETIN
6.43E-04	-3.29	NM_016448	DENTICLELESS HOMOLOG (DROSOPHILA)
8.87E-04	-3.31	NM_006417	INTERFERON-INDUCED PROTEIN 44
1.45E-05	-3.32	NM_017957	EPSIN 3
5.07E-04	-3.39	XR_019065	
1.48E-04	-3.45	NM_016448	DENTICLELESS HOMOLOG (DROSOPHILA)
5.22E-04	-3.48	BC007360	HYPOTHETICAL PROTEIN MGC16121
1.47E-04	-3.51	NM_016448	DENTICLELESS HOMOLOG (DROSOPHILA)
9.46E-04	-3.54	NM_016448	DENTICLELESS HOMOLOG (DROSOPHILA)
1.55E-04	-3.60	NM_016448	DENTICLELESS HOMOLOG (DROSOPHILA)
9.33E-04	-3.66	NM_016448	DENTICLELESS HOMOLOG (DROSOPHILA)
1.13E-05	-3.72	NM_016448	DENTICLELESS HOMOLOG (DROSOPHILA)
9.44E-04	-3.81	NM_016448	DENTICLELESS HOMOLOG (DROSOPHILA)

9.85E-04	-3.90	NM_016817	2'-5'-OLIGOADENYLATE SYNTHETASE 2, 69/71KDA
5.25E-05	-3.94	NM_005733	KINESIN FAMILY MEMBER 20A
1.33E-03	-3.97	NM_017631	HYPOTHETICAL PROTEIN FLJ10787
8.83E-05	-3.99	NM_005733	KINESIN FAMILY MEMBER 20A
3.91E-05	-4.01	NM_005733	KINESIN FAMILY MEMBER 20A
7.46E-05	-4.14	NM_005733	KINESIN FAMILY MEMBER 20A
4.01E-04	-4.15	NM_016817	2'-5'-OLIGOADENYLATE SYNTHETASE 2, 69/71KDA
1.26E-03	-4.17	NM_005733	KINESIN FAMILY MEMBER 20A
1.10E-03	-4.36	NM_005733	KINESIN FAMILY MEMBER 20A
1.34E-03	-4.37	NM_030919	CHROMOSOME 20 OPEN READING FRAME 129
2.23E-05	-4.43	NM_017631	HYPOTHETICAL PROTEIN FLJ10787
1.37E-04	-4.99	NM_006408	ANTERIOR GRADIENT 2 HOMOLOG (XENOPUS LAEVIS)
2.96E-05	-5.11	NM_001548	INTERFERON-INDUCED PROTEIN WITH TETRATRICOPEPTIDE REPEATS 1
4.55E-05	-5.24	NM_005733	KINESIN FAMILY MEMBER 20A
4.70E-04	-5.37	THC2731029	
6.53E-06	-5.57	NM_016448	DENTICLELESS HOMOLOG (DROSOPHILA)
1.71E-04	-5.76	NM_005733	KINESIN FAMILY MEMBER 20A
1.32E-03	-5.94	NM_018177	NEDD4 BINDING PROTEIN 2

APPENDIX E

FIBROBLAST MORPHOLOGY AND APOPTOSIS

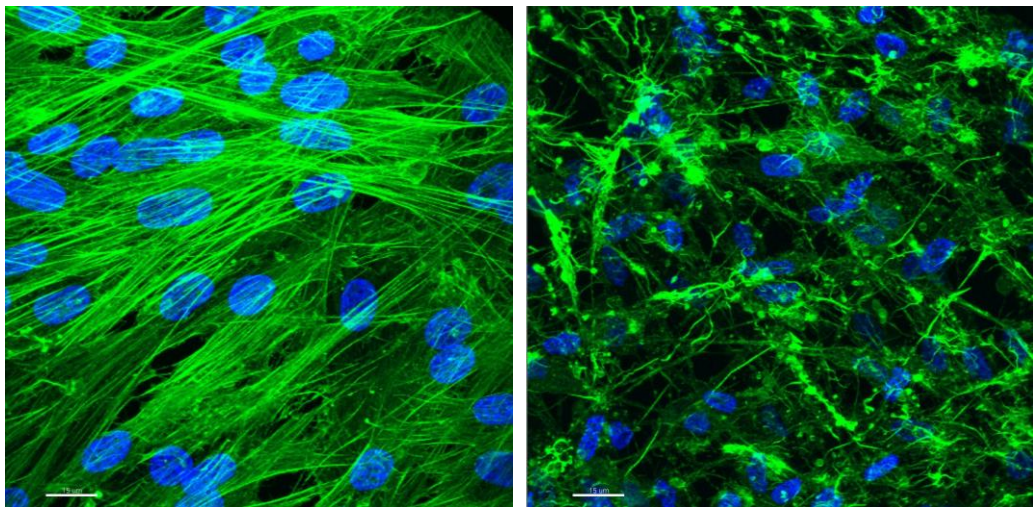

Figure Appdx. 1. CSLM of primary human fibroblasts reveal that fibroblasts undergo a similar disruption of the cytoskeleton as human keratinocytes when exposed to BCM. Green, F-actin, blue, nuclei. 100x oil objective, bars represent 15 µm.

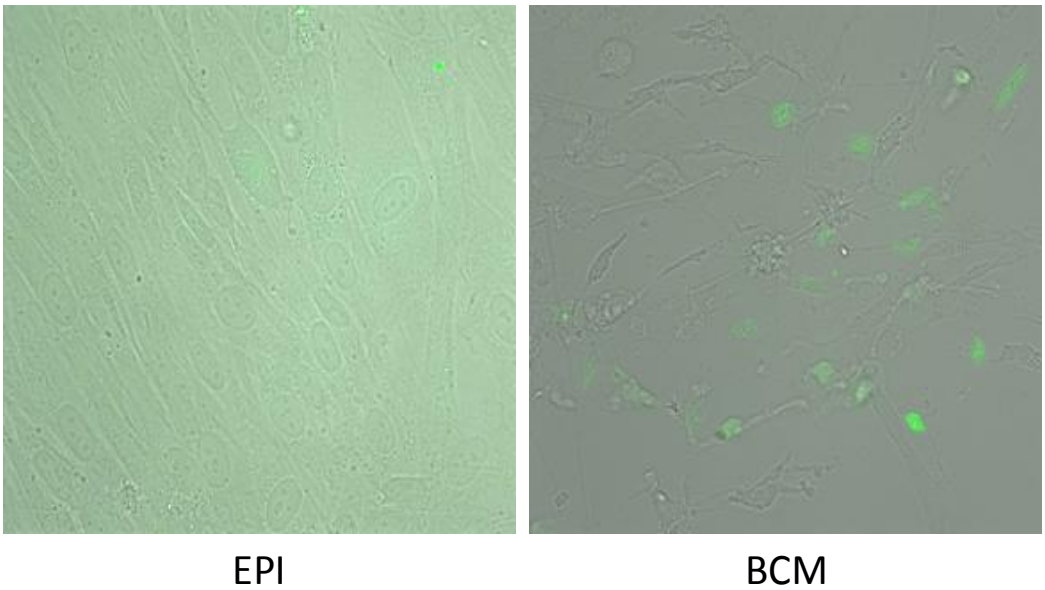

Figure Appdx. 2. TUNEL staining reveals that apoptosis is induced in human foreskin fibroblasts after 24 hours of exposure to BCM (green fluorescing nuclei).

APPENDIX F

THE SMALL GTPASE GEM AND CELL MORPHOLOGY

Introduction

The RGK (Rem, Rem2, Rad, Gem/Kir) subfamily of Ras related GTPases are regulated by both transcriptional and post transcriptional mechanisms in response to environmental stimuli. RGK family members are associated with cytoskeletal re-arrangements including cell sprouting and formation of **l**amellipodia and filopodia. Intracellular levels of Gem have been found to have dramatic effects on the architecture of the cytoskeleton [227]. RGK family members differ from other Ras like GTPases in several ways. Firstly, RGK family members display an extended C-terminal residue containing a calmodulin binding region linking these proteins to intracellular calcium levels [228]. Secondly, RGK family members contain significant modifications in the catalytic domain responsible for GTP hydrolysis lending RGK members extremely low intrinsic GTPase activity [229]. Two functions have been described for Gem, including inhibition of voltage-gated calcium channel activity and inhibition of Rho kinase mediated cytoskeletal reorganization [230, 231]. These activities are attributed to the direct association of Gem with the calcium channel β-unit or Rho kinase- β through distinct mechanisms. PKC dependant phosphorylation of Gem mediates the inhibition of Rho kinase and thus cytoskeletal architecture [232]. Gem is also regulated through sub-cellular localization. Gem is thought to act upon cytoskeletal organization through interactions in the cytosol and thus can be regulated through either binding by regulatory partners in the cytosol, or through sequestration in the nucleus [233]. The calcium dependent nature of Gem in addition to its role in cytoskeletal re-arrangements makes Gem an interesting target for responses observed in BCM treated keratinocytes.

Materials and Methods

Microarray

See Chapter 5.

RT-qPCR

See Chapter 4. Validated qPCR primer sets for Gem were purchased from SA Biosciences (Frederick, MD).

Gem Immunostaining

The GEM (H-85) polyclonal antibody was purchased from Santa Cruz Biotechnology (Santa Cruz, CA). Cell preparations and staining protocols were based on manufacturer's recommendations. The secondary goat anti-rabbit IgG-FITC antibody was used at a 1:100 dilution for detection of GEM (H-85) following the manufacturer's instructions. Cells were mounted using Vectashield® H-1000 (Vector Laboratories, Burlingame, CA) and imaged using a Leica TCS-SP2 AOBS confocal microscope.

Protein Kinase C Detection

Fim-1 diacetate was purchased from Invitrogen Corporation (Carlsbad, CA) and the manufacturer's instructions were followed. Cells were imaged by epifluorescent microscopy using a 100x oil objective.

shRNA Interference

A SureSilencing shRNA kit with a GFP marker for human GEM was purchased from SA Biosciences (Frederick, MD) and the manufacturer's instructions were followed.

Results and Discussion

Microarray analysis of HFKs in co-culture with *S. aureus* biofilm revealed several genes related to cytoskeletal organization to be upregulated (Figure Appdx. 3). Among these genes was Gem, which was the third most highly upregulated gene in the co-culture model (+11.54 fold) and the 17th most highly upregulated gene in keratinocytes exposed to conditioned medium (+18.01 fold, relative to control cells).

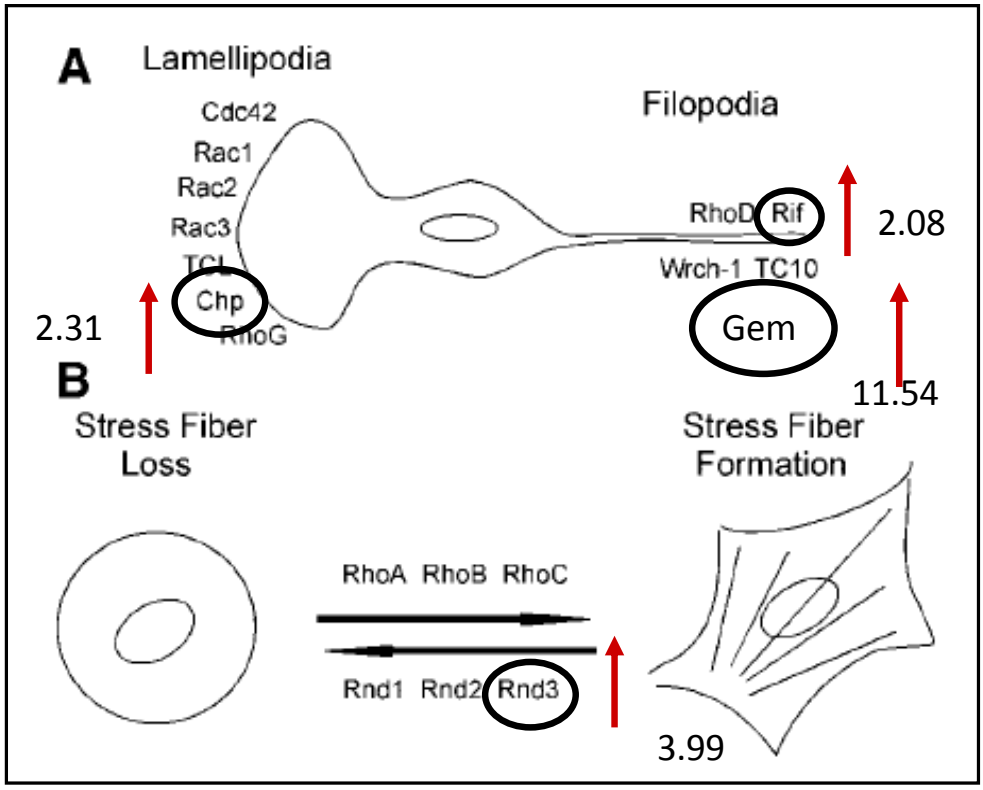

Figure Appdx. 3. A. Genes associated with lamellipodia formation are listed on the left while genes associated with filopodia are listed on the right. B. Genes associated with stress fiber formation are listed on top and genes associated with stress fiber loss are listed on the bottom. Microarray analysis reveled genes associated with cytoskeletal organization are expressed in HFKs exposed to *S. aureus* biofilm for 24 hours in the co-culture model. Many genes involved in filopodia formation and a key gene involved in stress fiber loss were induced relative to control cells. Image adapted from [234].

Expression of Gem was confirmed by RT-qPCR over the course of 24 hours (Figure Appdx. 4). Gem expression was increased relative to control cells at all time points peaking after 12 hours of exposure to BCM.

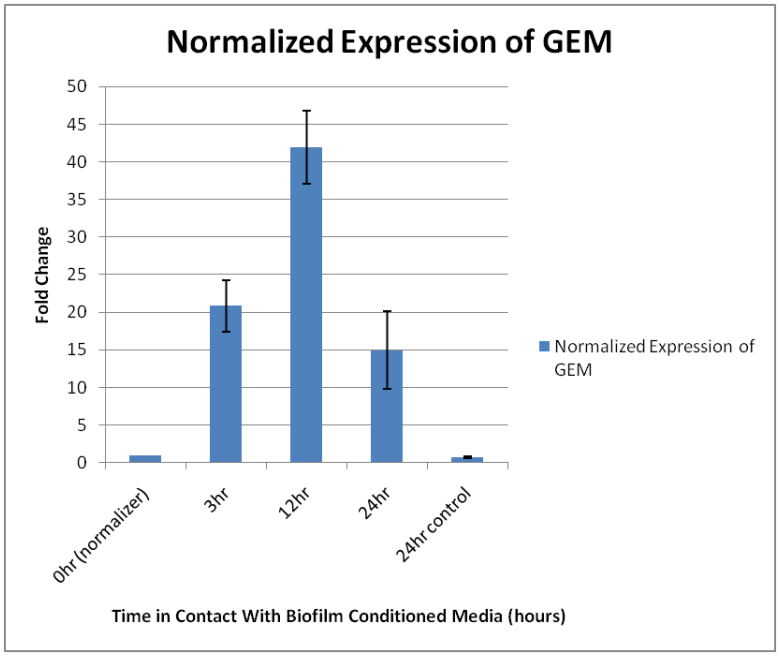

Figure Appdx. 4. RT-qPCR analysis of GEM expression revealed that GEM expression increases in keratinocytes exposed to BCM, peaking at 12 hours. GEM expression levels normalized to the housekeeping gene GAPDH. Error bars represent standard deviation of the mean of three experiments.

Immunostaining experiments revealed that Gem accumulated in BCM treated keratinocytes initially sequestered in the nucleus and later in the cytoplasm (Figure Appdx. 5). The effects of Gem on the cytoskeleton have been determined to be mediated through interactions in the cytosol. However, the temporal localization of Gem does not match with the rapid disruption of the cytoskeleton observed in BCM treated keratinocytes. Morphology changes were observed in keratinocytes exposed to BCM within hours while Gem was not observed in the cytosol until 24 hours of exposure to BCM. More evidence is needed to determine the exact role of Gem in this system.

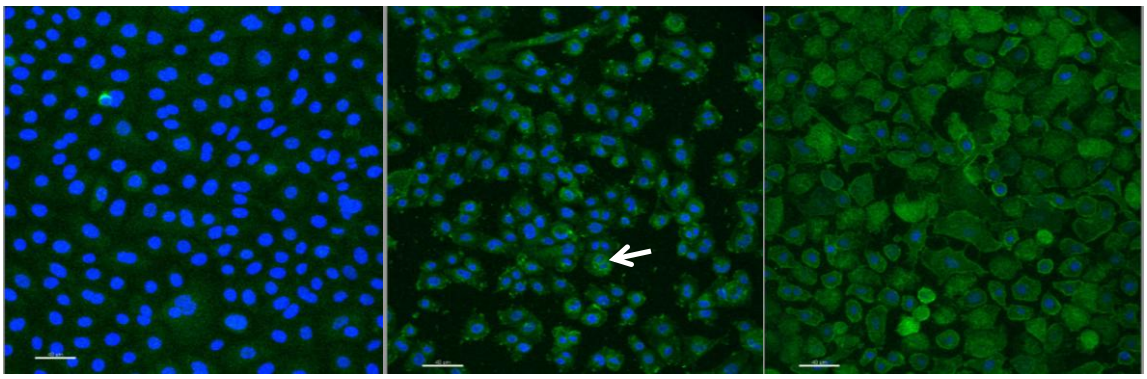

Figure Appdx. 5. Immonostaining using an antibody specific to GEM (green) reveals that the GEM protein is not highly expressed in un-stimulated cells (0hrs). After 12 hours of contact with BCM, GEM appears to be predominately associated with the nuclear compartment (arrow, 12hr). After 24 hours of exposure to BCM, the GEM protein seems to be predominant in the cytoplasm. Nuclei counterstained for clarity (blue). 60x oil objective, bar represents 40 µm.

Over expression of Gem has been shown to induce abnormal morphologies which are similar to the morphologies observed in BCM treated keratinocytes [235] (Figure Appdx. 6).

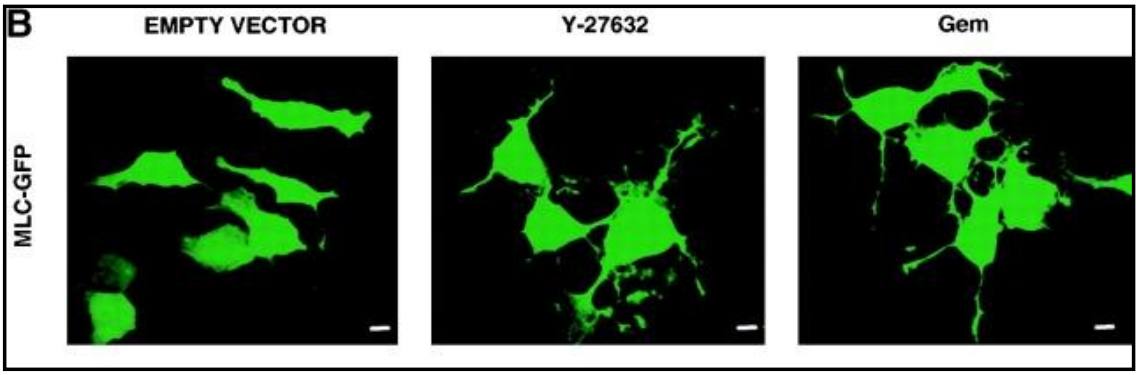

Figure Appdx. 6. Abnormal cell morphologies were observed by Ward, *et al*, in cells were Gem was over expressed (right image) [235]. These abnormal morphologies were similar to the morphologies observed in BCM treated keratinocytes. The Rho Kinase inhibitor Y-27632 produced similar effects on the cytoskeleton to those of Gem.

PKC mediated phosphorylation of Gem has been linked to its ability to inhibit Rho kinase and subsequent re-organization of the cytoskeleton. The PKC specific stain Fim-1 diacetate was used to probe live cells for PKC activity (Figure Appdx. 7). BCM treated keratinocytes showed much more intense Fim-1 staining than control cells, indicating that PKC was activated. The activation of PKC may or may not correlate with

Gem activity in BCM treated keratinocytes and further experiments will be needed to determine the relationship between PKC signaling, Gem, and cytoskeletal organization.

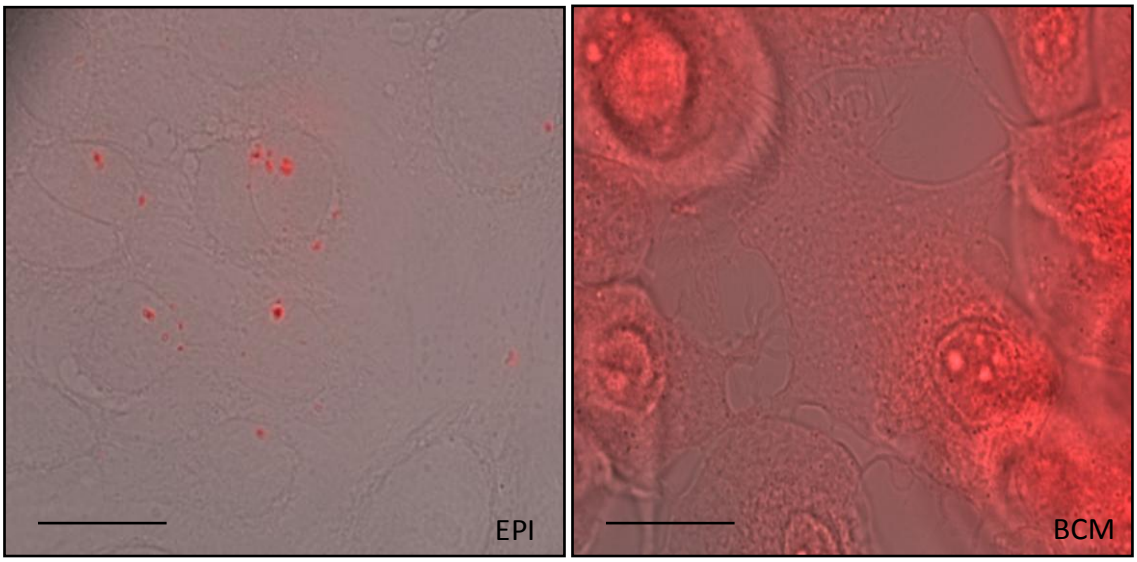

Figure Appdx. 7. Staining using a PKC specific dye revealed that PKC is activated in BCM treated keratinocytes after 24 hours but not in control cells. Bar represents 20 µm.

Short hairpin RNAs (shRNAs) were used to knock down Gem expression in HFKs (Figure Appdx. 8). Keratinocytes were transiently transfected with plasmids containing both shRNA sequences against Gem and a GFP marker. Cell morphologies were observed after 240 minutes of exposure to BCM. Non-transfected cells displayed the expected morphology while transfected cells appeared to have less of a cytoskeletal re-organization. However, without a quantitative measurement of morphological changes, these results are subjective to interpretation.

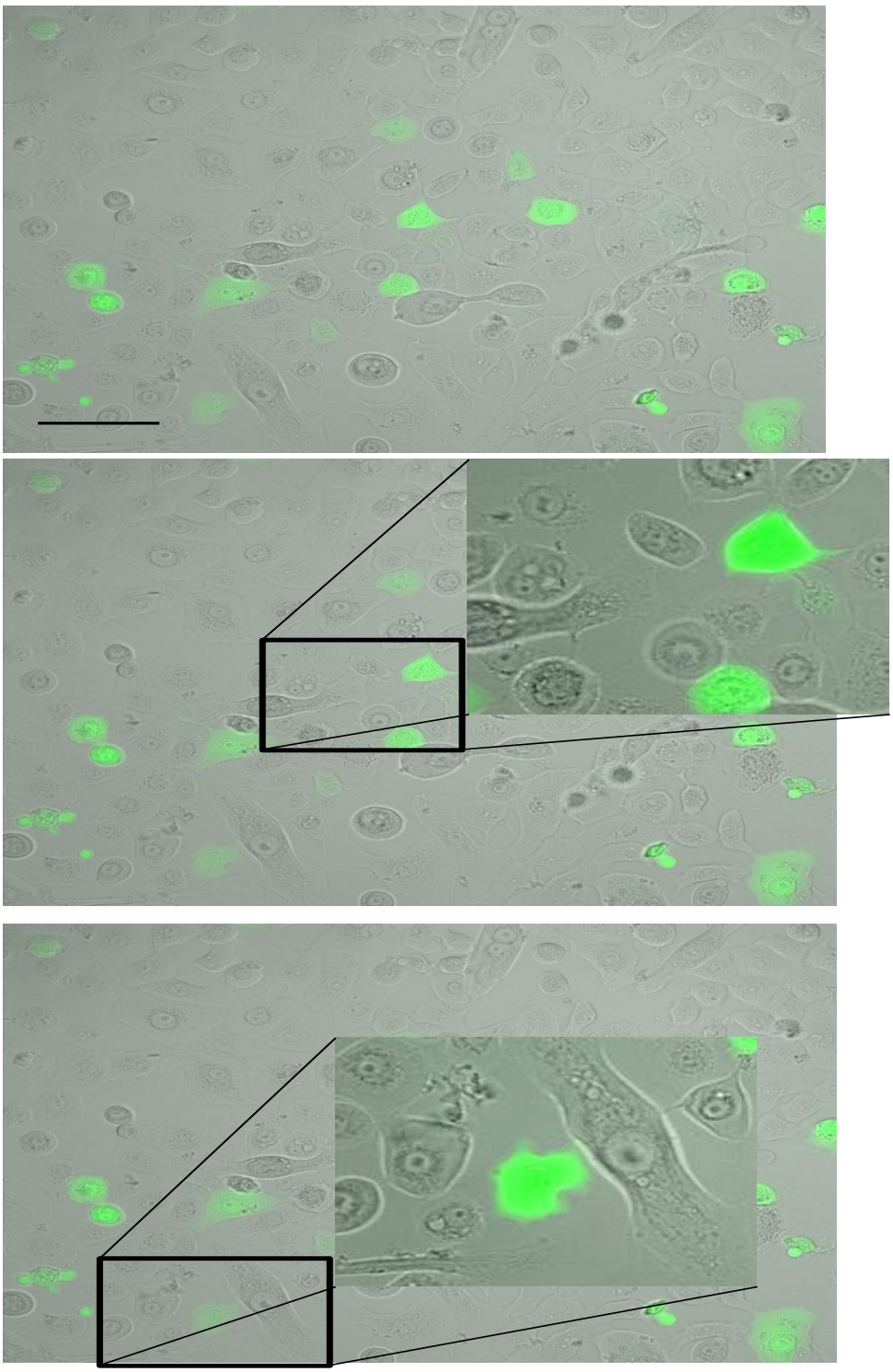

Figure Appdx. 8. shRNA knockdown of GEM by transient transfection (green fluorescing cells). Keratinocytes treated with BCM for 240 minutes post transfection. Enlarged images show that fluorescing cells do not contain as many dendritic like extensions as neighboring cells that were not transfected. Bar represents 40 µm.

APPENDIX G

PEROXISOME AND LYSOSOME DEPLETION IN KERATINOCYTES TREATED WITH BCM

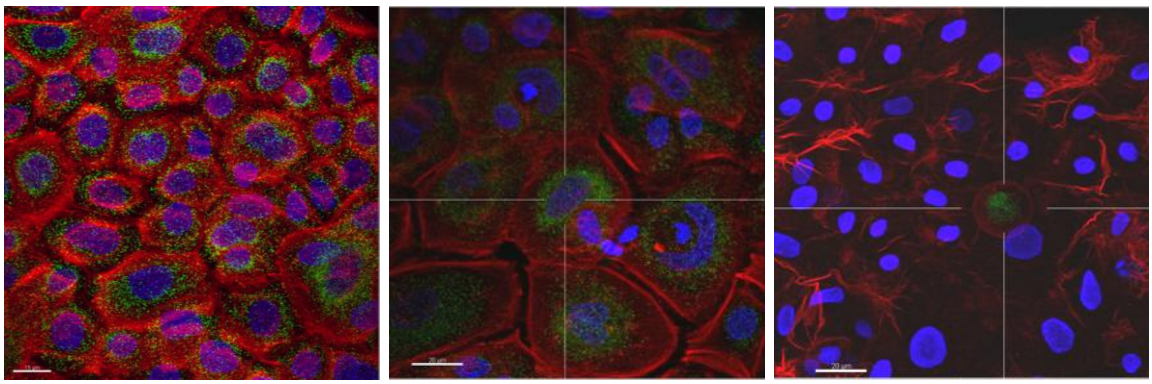

Figure Appdx. 9. Peroxisomes (green) were detected by immunostaining and imaging by CSLM. EPI and PCM treated keratinocytes show uniformly distributed peroxisomes while BCM treated keratinocytes showed no peroxisomes in any cell with the rare exception of rounded, detaching cells with no nuclei (see crosshairs in BCM image) after a 24 hour exposure. The actin cytoskeleton (Red) and nuclei (Blue) were counterstained for clarity. 100x oil objective, bar represents 20 µm.

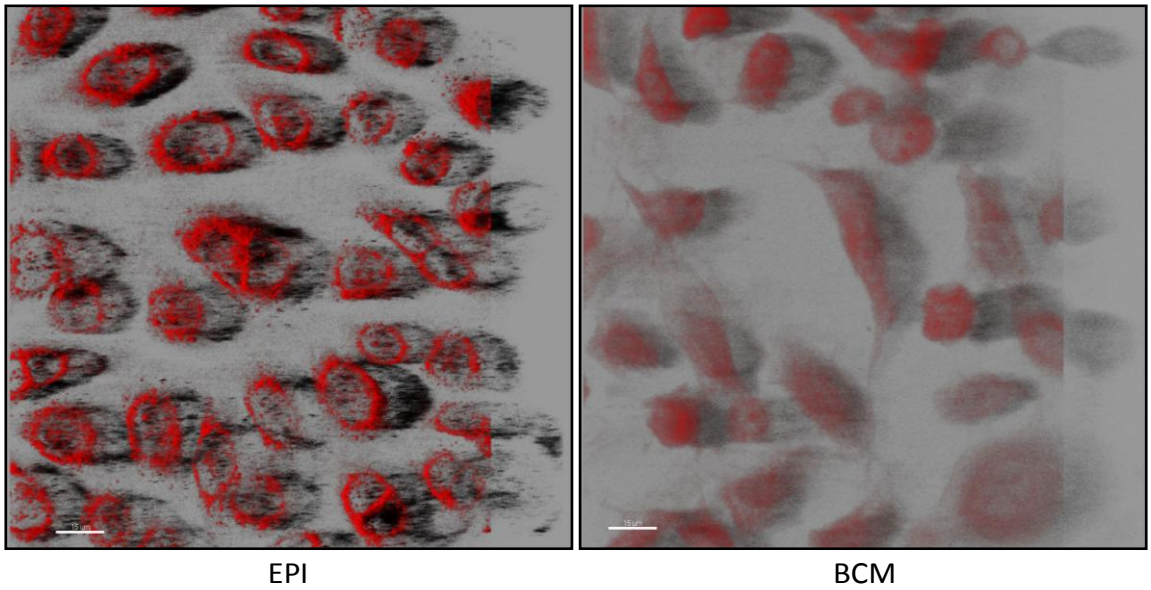

Figure Appdx. 10. Lysosomes were stained with LysoTracker Red. Cells were stained after 24 hours of exposure to BCM. Bar represents 15 µm.

APPENDIX H

UNKNOWN CELL TYPES PRESENT IN HFK CULTURE RESISTANT TO ILL EFFECTS OF BCM

Primary cell lines are never 100% pure cultures and often contain assorted cell types (i.e. fibroblasts, melanocytes) with the cell type of interest being dominant. While performing TUNEL assays on HFKs cultures after extended exposure to BCM, cell types with a specific morphology were found to be resistant to BCM induced apoptosis and cytoskeletal disruption (Figure Appdx. 11). These cells had a long and slender appearance and were full of dense granules. The same cell types were not observed in BCM treated HaCaT keratinocytes.

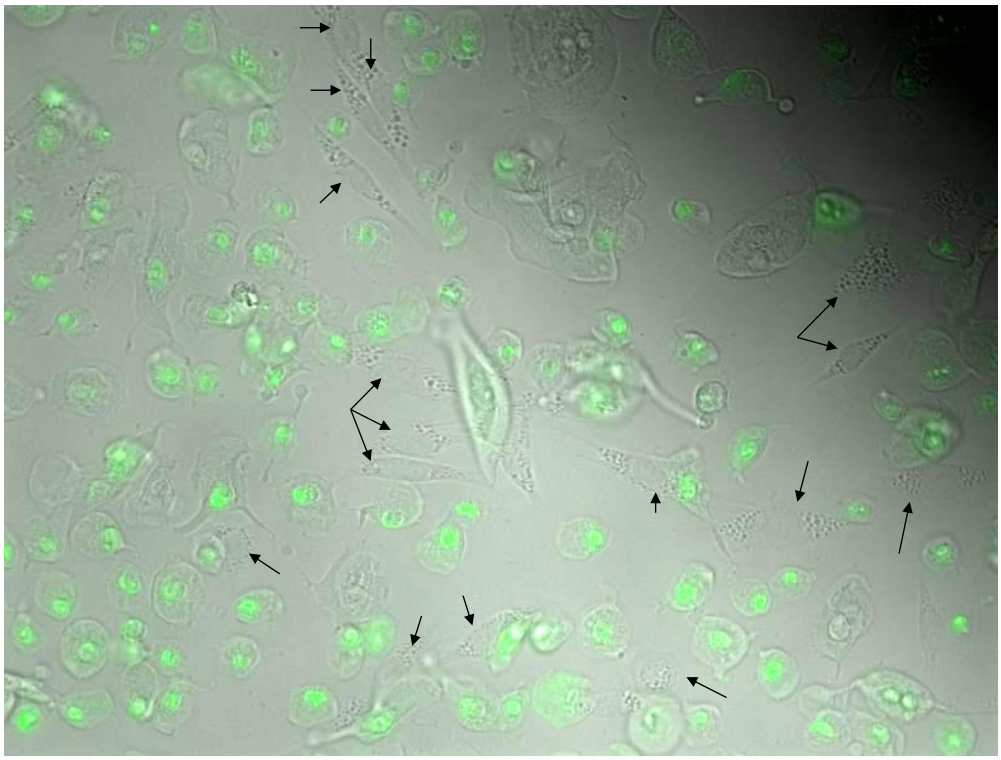

Figure Appdx. 11. TUNEL staining after 48 hours of exposure to BCM revealed several cells with a distinct morphology that were not undergoing apoptosis (arrows). 60x oil objective.

Upon closer examination of the cytoskeletal architecture of these cells, it was discovered that there were in fact two types of cells, long and slender cells, and round and flat cells (Figure Appdx. 12). Each cell type contained dense granules and their cytoskeletons remained intact, relative to neighboring keratinocytes.

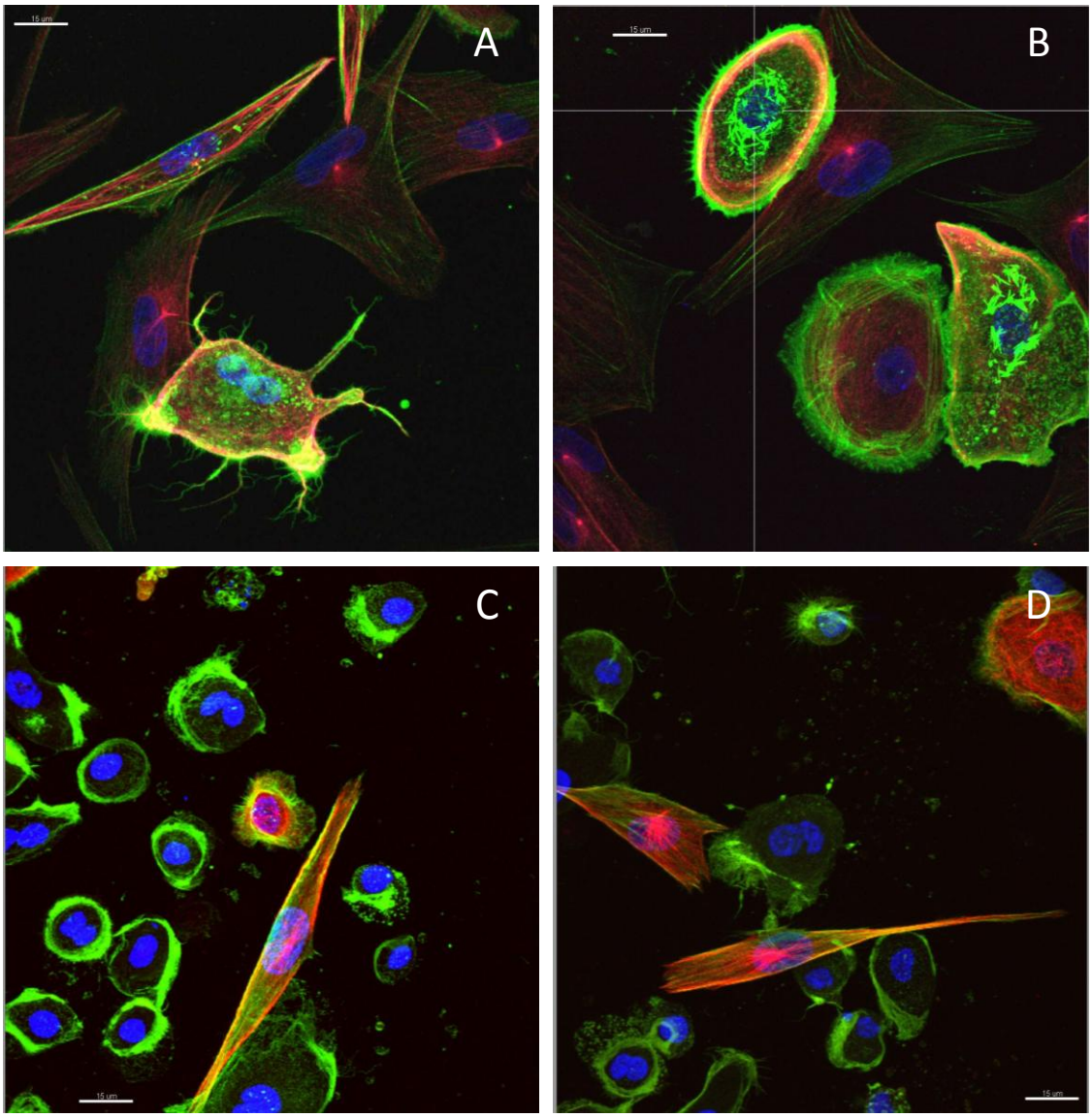

Figure Appdx. 12. Staining of cytoskeletal components (F-actin, green, β-tubulin, red, nuclei, blue) revealed two distinct morphologies of "biofilm resistant" cells. The "biofilm resistant" cells were found to be either long and skinny or round and flat. Keratinocytes visible in "A" and "C" can be seen with the expected morphology after exposure to BCM. 100x oil objective, bars represent 15 µm.

The PKC specific stain Fim-1 diacetate revealed that PKC was not activated in these "biofilm resistant" cells (Figure Appdx. 13). The lack of PKC activation together with the absence of dendritic like extensions in these cells may indicate a role for PKC in the cytoskeletal re-arrangements observed in keratinocytes exposed to BCM.

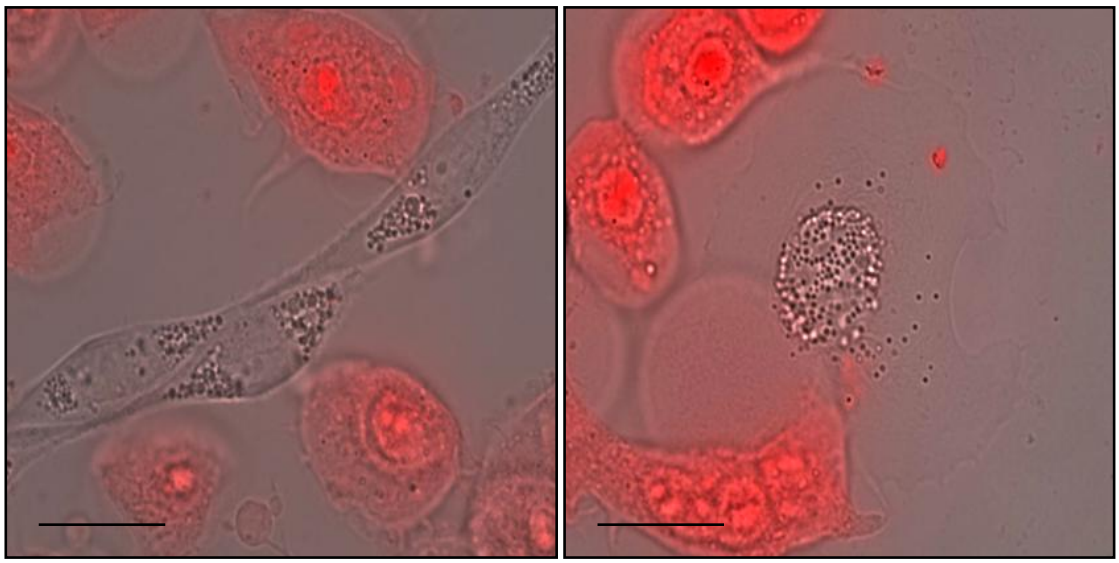

Figure Appdx. 13. PKC staining reveals that PKC is not activated in either the long and skinny (left) or the round and flat (right) biofilm resistant cells. 100x oil objective, bar represents 20 µm.

Treatment of HFKs with BCM for 24 hours followed by the removal of BCM and addition of fresh EPI growth medium for an additional 96 hours revealed that the cell culture was re-populated with different cell types with a morphology that resembled fibroblasts (Figure Appdx. 14). After 24 hours in fresh EPI, there were still many cells that detached from the culture well. This was likely due to apoptotic keratinocytes which were still attached to the culture well eventually detaching. By 72 hours, cells with long extended morphologies were beginning to re-populate the culture well. After 96 hours in fresh EPI growth medium, colonies of both fibroblast like cells and keratinocytes could be observed.

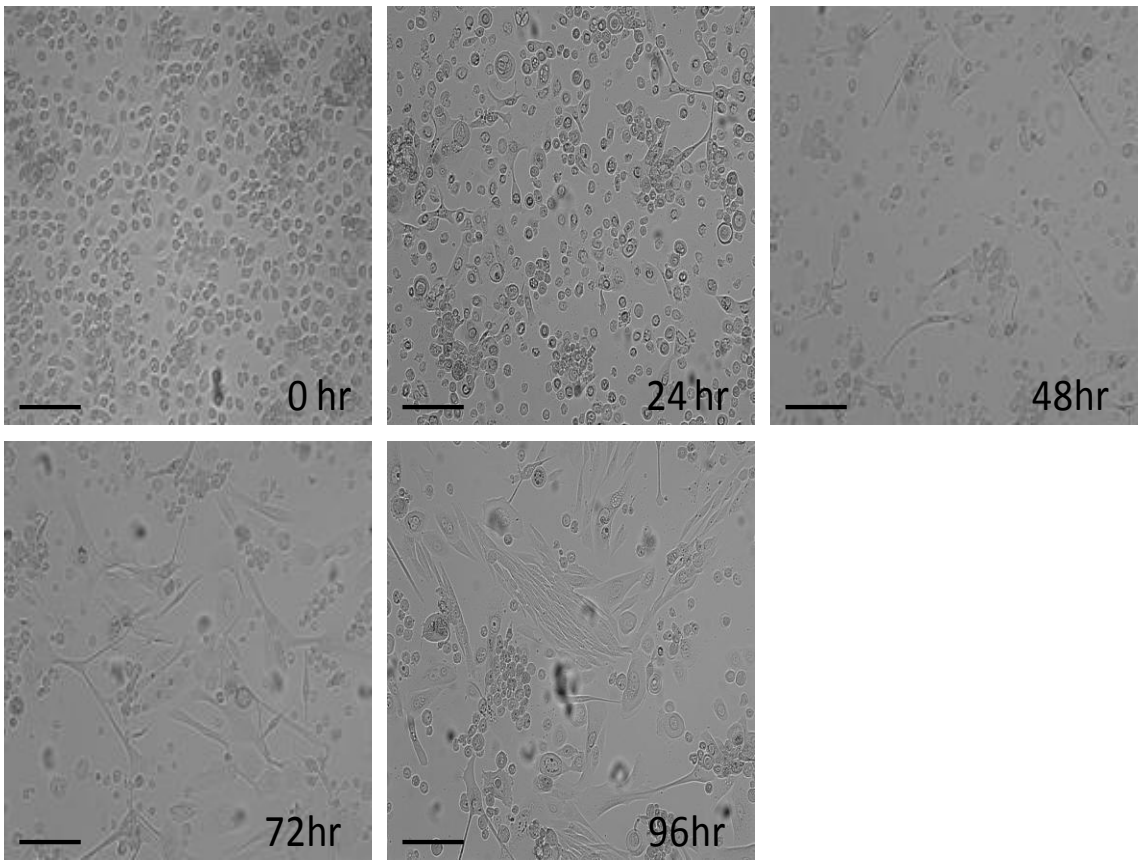

Figure Appdx. 14. HFKs were treated with BCM for 24 hours. Cells were then placed in fresh EPI growth medium and incubated for an additional 96 hours with the medium being replaced every 24 hours. Images above are from the same area in a single culture dish. After 24 hours in fresh EPI, many cells detach. These are likely cells undergoing apoptosis. An unknown cell type repopulates the dish after 96 hours with microcolonies of keratinocytes present as well. Bar=40 um.

Interestingly, no cells were found to contain the dense granules observed in "biofilm resistant" cells. This may be due to the removal of specific biofilm secreted factors responsible for the formation and maintenance of these structures. The dense granules could theoretically be microsomes. Microsomes are vesicles derived from the endoplasmic reticulum whose dense appearance is derived from the proteins contained within; most notably from heme groups contained within cytochrome P450 family members. Microsomes present in keratinocytes contain CYP1A1 and CYP1B1 in addition to other XMEs [236]. The possibility of xenobiotic metabolism in these

"biofilm resistant" cells is interesting given the expression of several XMEs in BCM treated keratinocytes, including CYP1A1 and CYP1B1.

REFERENCES CITED

1. Martin, P., *Wound healing--aiming for perfect skin regeneration.* Science, 1997. **276**(5309): p. 75-81.

2. Singer, A.J. and R.A. Clark, *Cutaneous wound healing.* N Engl J Med, 1999. **341**(10): p. 738-46.

3. Deuel, T.F., et al., *Chemotaxis of monocytes and neutrophils to platelet-derived growth factor.* J Clin Invest, 1982. **69**(4): p. 1046-9.

4. Newman, S.L., J.E. Henson, and P.M. Henson, *Phagocytosis of senescent neutrophils by human monocyte-derived macrophages and rabbit inflammatory macrophages.* J Exp Med, 1982. **156**(2): p. 430-42.

5. Duffield, J.S., *The inflammatory macrophage: a story of Jekyll and Hyde.* Clin Sci (Lond), 2003. **104**(1): p. 27-38.

6. Serhan, C.N. and J. Savill, *Resolution of inflammation: the beginning programs the end.* Nat Immunol, 2005. **6**(12): p. 1191-7.

7. Clark, R.A., et al., *Collagen matrices attenuate the collagen-synthetic response of cultured fibroblasts to TGF-beta.* J Cell Sci, 1995. **108 (Pt 3)**: p. 1251-61.

8. Gurtner, G.C., et al., *Wound repair and regeneration.* Nature, 2008. **453**(7193): p. 314-21.

9. Salo, T., et al., *Expression of matrix metalloproteinase-2 and -9 during early human wound healing.* Lab Invest, 1994. **70**(2): p. 176-82.

10. Gipson, I.K., S.J. Spurr-Michaud, and A.S. Tisdale, *Hemidesmosomes and anchoring fibril collagen appear synchronously during development and wound healing.* Dev Biol, 1988. **126**(2): p. 253-62.

11. Kurkinen, M., et al., *Sequential appearance of fibronectin and collagen in experimental granulation tissue.* Lab Invest, 1980. **43**(1): p. 47-51.

12. Welch, M.P., G.F. Odland, and R.A. Clark, *Temporal relationships of F-actin bundle formation, collagen and fibronectin matrix assembly, and fibronectin receptor expression to wound contraction.* J Cell Biol, 1990. **110**(1): p. 133-45.

13. Lovvorn, H.N., 3rd, et al., *Relative distribution and crosslinking of collagen distinguish fetal from adult sheep wound repair.* J Pediatr Surg, 1999. **34**(1): p. 218-23.

14. Li, J., J. Chen, and R. Kirsner, *Pathophysiology of acute wound healing.* Clin Dermatol, 2007. **25**(1): p. 9-18.

15. Falanga, V., *Wound healing and its impairment in the diabetic foot.* Lancet, 2005. **366**(9498): p. 1736-43.

16. Meluleni, G.J., et al., *Mucoid Pseudomonas aeruginosa growing in a biofilm in vitro are killed by opsonic antibodies to the mucoid exopolysaccharide capsule but not by antibodies produced during chronic lung infection in cystic fibrosis patients.* J Immunol, 1995. **155**(4): p. 2029-38.

17. Kristian, S.A., et al., *Biofilm formation induces C3a release and protects Staphylococcus epidermidis from IgG and complement deposition and from neutrophil-dependent killing.* J Infect Dis, 2008. **197**(7): p. 1028-35.

18. Jesaitis, A.J., et al., *Compromised host defense on Pseudomonas aeruginosa biofilms: characterization of neutrophil and biofilm interactions.* J Immunol, 2003. **171**(8): p. 4329-39.

19. Foster, T.J., *Immune evasion by staphylococci.* Nat Rev Microbiol, 2005. **3**(12): p. 948-58.

20. Donlan, R.M. and J.W. Costerton, *Biofilms: survival mechanisms of clinically relevant microorganisms.* Clin Microbiol Rev, 2002. **15**(2): p. 167-93.

21. Leid, J.G., et al., *Human leukocytes adhere to, penetrate, and respond to Staphylococcus aureus biofilms.* Infect Immun, 2002. **70**(11): p. 6339-45.

22. Edwards, J.V., et al., *Protease inhibition by oleic acid transfer from chronic wound dressings to albumin.* Int J Pharm, 2007. **340**(1-2): p. 42-51.

23. Diegelmann, R.F., *Excessive neutrophils characterize chronic pressure ulcers.* Wound Repair Regen, 2003. **11**(6): p. 490-5.

24. Akgul, C., D.A. Moulding, and S.W. Edwards, *Molecular control of neutrophil apoptosis.* FEBS Lett, 2001. **487**(3): p. 318-22.

25. Glynn, P.C., E. Henney, and I.P. Hall, *The selective CXCR2 antagonist SB272844 blocks interleukin-8 and growth-related oncogene-alpha-mediated inhibition of spontaneous neutrophil apoptosis.* Pulm Pharmacol Ther, 2002. **15**(2): p. 103-10.

26. Higley, H.R., et al., *Extravasation of macromolecules and possible trapping of transforming growth factor-beta in venous ulceration.* Br J Dermatol, 1995. **132**(1): p. 79-85.

27. Grinnell, F., C.H. Ho, and A. Wysocki, *Degradation of fibronectin and vitronectin in chronic wound fluid: analysis by cell blotting, immunoblotting, and cell adhesion assays.* J Invest Dermatol, 1992. **98**(4): p. 410-6.

28. Tarnuzzer, R.W. and G.S. Schultz, *Biochemical analysis of acute and chronic wound environments.* Wound Repair Regen, 1996. **4**(3): p. 321-5.

29. McCawley, L.J. and L.M. Matrisian, *Matrix metalloproteinases: they're not just for matrix anymore!* Curr Opin Cell Biol, 2001. **13**(5): p. 534-40.

30. Loot, M.A., et al., *Fibroblasts derived from chronic diabetic ulcers differ in their response to stimulation with EGF, IGF-I, bFGF and PDGF-AB compared to controls.* Eur J Cell Biol, 2002. **81**(3): p. 153-60.

31. Stojadinovic, O., et al., *Molecular pathogenesis of chronic wounds: the role of beta-catenin and c-myc in the inhibition of epithelialization and wound healing.* Am J Pathol, 2005. **167**(1): p. 59-69.

32. Waikel, R.L., et al., *Deregulated expression of c-Myc depletes epidermal stem cells.* Nat Genet, 2001. **28**(2): p. 165-8.

33. Krampert, M., et al., *Activities of the matrix metalloproteinase stromelysin-2 (MMP-10) in matrix degradation and keratinocyte organization in wounded skin.* Mol Biol Cell, 2004. **15**(12): p. 5242-54.

34. Sauer, K., et al., *Pseudomonas aeruginosa displays multiple phenotypes during development as a biofilm.* J Bacteriol, 2002. **184**(4): p. 1140-54.

35. Resch, A., et al., *Differential gene expression profiling of Staphylococcus aureus cultivated under biofilm and planktonic conditions.* Appl Environ Microbiol, 2005. **71**(5): p. 2663-76.

36. Stewart, P.S. and J.W. Costerton, *Antibiotic resistance of bacteria in biofilms.* Lancet, 2001. **358**(9276): p. 135-8.

37. Zhu, J., et al., *Quorum-sensing regulators control virulence gene expression in Vibrio cholerae.* Proc Natl Acad Sci U S A, 2002. **99**(5): p. 3129-34.

38. Cotter, P.A. and S. Stibitz, *c-di-GMP-mediated regulation of virulence and biofilm formation.* Curr Opin Microbiol, 2007. **10**(1): p. 17-23.

39. Fux, C.A., et al., *Survival strategies of infectious biofilms.* Trends Microbiol, 2005. **13**(1): p. 34-40.

40. Wolcott, R.D., J.P. Kennedy, and S.E. Dowd, *Regular debridement is the main tool for maintaining a healthy wound bed in most chronic wounds.* J Wound Care, 2009. **18**(2): p. 54-6.

41. James, G.A., et al., *Biofilms in chronic wounds.* Wound Repair Regen, 2008. **16**(1): p. 37-44.

42. Lin, Y.T., C.T. Wang, and B.L. Chiang, *Role of bacterial pathogens in atopic dermatitis.* Clin Rev Allergy Immunol, 2007. **33**(3): p. 167-77.

43. Kuehnert, M.J., et al., *Prevalence of Staphylococcus aureus nasal colonization in the United States, 2001-2002.* J Infect Dis, 2006. **193**(2): p. 172-9.

44. Kristian, S.A., et al., *The ability of biofilm formation does not influence virulence of Staphylococcus aureus and host response in a mouse tissue cage infection model.* Microb Pathog, 2004. **36**(5): p. 237-45.

45. Yarwood, J.M., et al., *Quorum sensing in Staphylococcus aureus biofilms.* J Bacteriol, 2004. **186**(6): p. 1838-50.

46. Caiazza, N.C. and G.A. O'Toole, *Alpha-toxin is required for biofilm formation by Staphylococcus aureus.* J Bacteriol, 2003. **185**(10): p. 3214-7.

47. Guggenheim, B., et al., *In vitro modeling of host-parasite interactions: the 'subgingival' biofilm challenge of primary human epithelial cells.* BMC Microbiol, 2009. **9**: p. 280.

48. Stathopoulou, P.G., et al., *Epithelial cell pro-inflammatory cytokine response differs across dental plaque bacterial species.* J Clin Periodontol. **37**(1): p. 24-9.

49. Haugwitz, U., et al., *Pore-forming Staphylococcus aureus alpha-toxin triggers epidermal growth factor receptor-dependent proliferation.* Cell Microbiol, 2006. **8**(10): p. 1591-600.

50. Kenzel, S., et al., *Role of p38 and early growth response factor 1 in the macrophage response to group B streptococcus.* Infect Immun, 2009. **77**(6): p. 2474-81.

51. Li, X., et al., *Epithelial Cell Gene Expression Induced by Intracellular Staphylococcus aureus.* Int J Microbiol, 2009. **2009**: p. 753278.

52. Moreilhon, C., et al., *Live Staphylococcus aureus and bacterial soluble factors induce different transcriptional responses in human airway cells.* Physiol Genomics, 2005. **20**(3): p. 244-55.

53. Peterson, M.L., et al., *The innate immune system is activated by stimulation of vaginal epithelial cells with Staphylococcus aureus and toxic shock syndrome toxin 1.* Infect Immun, 2005. **73**(4): p. 2164-74.

54. Sun, Y., et al., *Staphylococcus aureus-induced corneal inflammation is dependent on Toll-like receptor 2 and myeloid differentiation factor 88.* Infect Immun, 2006. **74**(9): p. 5325-32.

55. Veldkamp, K.E., et al., *Modulation of neutrophil chemokine receptors by Staphylococcus aureus supernate.* Infect Immun, 2000. **68**(10): p. 5908-13.

56. Dowd, S.E., et al., *Survey of bacterial diversity in chronic wounds using pyrosequencing, DGGE, and full ribosome shotgun sequencing.* BMC Microbiol, 2008. **8**: p. 43.

57. Sibbald, R.G., et al., *Preparing the wound bed 2003: focus on infection and inflammation.* Ostomy Wound Manage, 2003. **49**(11): p. 23-51.

58. Dowd, S.E., et al., *Polymicrobial nature of chronic diabetic foot ulcer biofilm infections determined using bacterial tag encoded FLX amplicon pyrosequencing (bTEFAP).* PLoS One, 2008. **3**(10): p. e3326.

59. Miller, L.S., *Toll-like receptors in skin.* Adv Dermatol, 2008. **24**: p. 71-87.

60. Lebre, M.C., et al., *Human keratinocytes express functional Toll-like receptor 3, 4, 5, and 9.* J Invest Dermatol, 2007. **127**(2): p. 331-41.

61. Albanesi, C., et al., *Keratinocytes in inflammatory skin diseases.* Curr Drug Targets Inflamm Allergy, 2005. **4**(3): p. 329-34.

62. Takeda, K. and S. Akira, *Toll-like receptors in innate immunity.* Int Immunol, 2005. **17**(1): p. 1-14.

63. Basham, T.Y. and T.C. Merigan, *Recombinant interferon-gamma increases HLA-DR synthesis and expression.* J Immunol, 1983. **130**(4): p. 1492-4.

64. Tokura, Y., et al., *Superantigenic staphylococcal exotoxins induce T-cell proliferation in the presence of Langerhans cells or class II-bearing keratinocytes and stimulate keratinocytes to produce T-cell-activating cytokines.* J Invest Dermatol, 1994. **102**(1): p. 31-8.

65. Meng, X., et al., *Transgenic TNF-alpha causes apoptosis in epidermal keratinocytes after subcutaneous injection of TNF-alpha DNA plasmid.* J Invest Dermatol, 1999. **113**(5): p. 856-7.

66. Van Antwerp, D.J., et al., *Suppression of TNF-alpha-induced apoptosis by NF-kappaB.* Science, 1996. **274**(5288): p. 787-9.

67. Victor, F.C. and A.B. Gottlieb, *TNF-alpha and apoptosis: implications for the pathogenesis and treatment of psoriasis.* J Drugs Dermatol, 2002. **1**(3): p. 264-75.

68. Bashir, M.M., M.R. Sharma, and V.P. Werth, *TNF-alpha production in the skin.* Arch Dermatol Res, 2009. **301**(1): p. 87-91.

69. Amiot, F., et al., *Lipopolysaccharide-induced cytokine cascade and lethality in LT alpha/TNF alpha-deficient mice.* Mol Med, 1997. **3**(12): p. 864-75.

70. Dinarello, C.A., *Immunological and inflammatory functions of the interleukin-1 family.* Annu Rev Immunol, 2009. **27**: p. 519-50.

71. Sims, J.E. and D.E. Smith, *The IL-1 family: regulators of immunity.* Nat Rev Immunol. **10**(2): p. 89-102.

72. Dinarello, C.A., *Biologic basis for interleukin-1 in disease.* Blood, 1996. **87**(6): p. 2095-147.

73. Kupper, T.S., *Immune and inflammatory processes in cutaneous tissues. Mechanisms and speculations.* J Clin Invest, 1990. **86**(6): p. 1783-9.

74. Delaleu, N. and M. Bickel, *Interleukin-1 beta and interleukin-18: regulation and activity in local inflammation.* Periodontol 2000, 2004. **35**: p. 42-52.

75. Cacabelos, R., et al., *Brain interleukin-1 beta in Alzheimer's disease and vascular dementia.* Methods Find Exp Clin Pharmacol, 1994. **16**(2): p. 141-51.

76. Chomarat, P., et al., *Balance of IL-1 receptor antagonist/IL-1 beta in rheumatoid synovium and its regulation by IL-4 and IL-10.* J Immunol, 1995. **154**(3): p. 1432-9.

77. Kornman, K.S., et al., *The interleukin-1 genotype as a severity factor in adult periodontal disease.* J Clin Periodontol, 1997. **24**(1): p. 72-7.

78. Rabinovitch, A., *An update on cytokines in the pathogenesis of insulin-dependent diabetes mellitus.* Diabetes Metab Rev, 1998. **14**(2): p. 129-51.

79. Shabo, Y., et al., *The myeloid blood cell differentiation-inducing protein MGI-2A is interleukin-6.* Blood, 1988. **72**(6): p. 2070-3.

80. Gauldie, J., et al., *Interferon beta 2/B-cell stimulatory factor type 2 shares identity with monocyte-derived hepatocyte-stimulating factor and regulates the major acute phase protein response in liver cells.* Proc Natl Acad Sci U S A, 1987. **84**(20): p. 7251-5.

81. Kishimoto, T., *Interleukin-6: from basic science to medicine--40 years in immunology.* Annu Rev Immunol, 2005. **23**: p. 1-21.

82. Ishihara, K. and T. Hirano, *IL-6 in autoimmune disease and chronic inflammatory proliferative disease.* Cytokine Growth Factor Rev, 2002. **13**(4-5): p. 357-68.

83. Harada, A., et al., *Essential involvement of interleukin-8 (IL-8) in acute inflammation.* J Leukoc Biol, 1994. **56**(5): p. 559-64.

84. Rosenkilde, M.M. and T.W. Schwartz, *The chemokine system -- a major regulator of angiogenesis in health and disease.* APMIS, 2004. **112**(7-8): p. 481-95.

85. Sheridan, J.W. and D. Metcalf, *Studies on the bone marrow colony stimulating factor (CSF): relation of tissue CSF to serum CSF.* J Cell Physiol, 1972. **80**(1): p. 129-40.

86. Hamilton, J.A., *GM-CSF in inflammation and autoimmunity.* Trends Immunol, 2002. **23**(8): p. 403-8.

87. Armitage, J.O., *Emerging applications of recombinant human granulocyte-macrophage colony-stimulating factor.* Blood, 1998. **92**(12): p. 4491-508.

88. Braunstein, S., et al., *GM-CSF activates regenerative epidermal growth and stimulates keratinocyte proliferation in human skin in vivo.* J Invest Dermatol, 1994. **103**(4): p. 601-4.

89. Kupper, T.S., et al., *Keratinocyte derived T-cell growth factor (KTGF) is identical to granulocyte macrophage colony stimulating factor (GM-CSF).* J Invest Dermatol, 1988. **91**(2): p. 185-8.

90. Medzhitov, R., *Toll-like receptors and innate immunity.* Nat Rev Immunol, 2001. **1**(2): p. 135-45.

91. Cobb, M.H. and E.J. Goldsmith, *How MAP kinases are regulated.* J Biol Chem, 1995. **270**(25): p. 14843-6.

92. Lang, R., M. Hammer, and J. Mages, *DUSP meet immunology: dual specificity MAPK phosphatases in control of the inflammatory response.* J Immunol, 2006. **177**(11): p. 7497-504.

93. Kyriakis, J.M. and J. Avruch, *Mammalian mitogen-activated protein kinase signal transduction pathways activated by stress and inflammation.* Physiol Rev, 2001. **81**(2): p. 807-69.

94. Pearson, G., et al., *Mitogen-activated protein (MAP) kinase pathways: regulation and physiological functions.* Endocr Rev, 2001. **22**(2): p. 153-83.

95. Liu, J. and A. Lin, *Role of JNK activation in apoptosis: a double-edged sword.* Cell Res, 2005. **15**(1): p. 36-42.

96. Park, J.M., et al., *Macrophage apoptosis by anthrax lethal factor through p38 MAP kinase inhibition.* Science, 2002. **297**(5589): p. 2048-51.

97. Xia, Z., et al., *Opposing effects of ERK and JNK-p38 MAP kinases on apoptosis.* Science, 1995. **270**(5240): p. 1326-31.

98. Matsubayashi, Y., et al., *ERK activation propagates in epithelial cell sheets and regulates their migration during wound healing.* Curr Biol, 2004. **14**(8): p. 731-5.

99. Sharma, G.D., J. He, and H.E. Bazan, *p38 and ERK1/2 coordinate cellular migration and proliferation in epithelial wound healing: evidence of cross-talk activation between MAP kinase cascades.* J Biol Chem, 2003. **278**(24): p. 21989-97.

100. Efimova, T., A.M. Broome, and R.L. Eckert, *A regulatory role for p38 delta MAPK in keratinocyte differentiation. Evidence for p38 delta-ERK1/2 complex formation.* J Biol Chem, 2003. **278**(36): p. 34277-85.

101. Niyonsaba, F., et al., *The human beta-defensins (-1, -2, -3, -4) and cathelicidin LL-37 induce IL-18 secretion through p38 and ERK MAPK activation in primary human keratinocytes.* J Immunol, 2005. **175**(3): p. 1776-84.

102. Kippenberger, S., et al., *Signaling of mechanical stretch in human keratinocytes via MAP kinases.* J Invest Dermatol, 2000. **114**(3): p. 408-12.

103. Garmyn, M., et al., *Human keratinocytes respond to osmotic stress by p38 map kinase regulated induction of HSP70 and HSP27.* J Invest Dermatol, 2001. **117**(5): p. 1290-5.

104. Johnson, G.L. and R. Lapadat, *Mitogen-activated protein kinase pathways mediated by ERK, JNK, and p38 protein kinases.* Science, 2002. **298**(5600): p. 1911-2.

105. Derijard, B., et al., *JNK1: a protein kinase stimulated by UV light and Ha-Ras that binds and phosphorylates the c-Jun activation domain.* Cell, 1994. **76**(6): p. 1025-37.

106. Kyriakis, J.M. and J. Avruch, *Sounding the alarm: protein kinase cascades activated by stress and inflammation.* J Biol Chem, 1996. **271**(40): p. 24313-6.

107. Pombo, C.M., et al., *The stress-activated protein kinases are major c-Jun amino-terminal kinases activated by ischemia and reperfusion.* J Biol Chem, 1994. **269**(42): p. 26546-51.

108. Angel, P., A. Szabowski, and M. Schorpp-Kistner, *Function and regulation of AP-1 subunits in skin physiology and pathology.* Oncogene, 2001. **20**(19): p. 2413-23.

109. Karin, M., Z. Liu, and E. Zandi, *AP-1 function and regulation.* Curr Opin Cell Biol, 1997. **9**(2): p. 240-6.

110. Javelaud, D., et al., *Disruption of basal JNK activity differentially affects key fibroblast functions important for wound healing.* J Biol Chem, 2003. **278**(27): p. 24624-8.

111. Ramet, M., et al., *JNK signaling pathway is required for efficient wound healing in Drosophila.* Dev Biol, 2002. **241**(1): p. 145-56.

112. Han, J., et al., *A MAP kinase targeted by endotoxin and hyperosmolarity in mammalian cells.* Science, 1994. **265**(5173): p. 808-11.

113. Lee, J.C., et al., *A protein kinase involved in the regulation of inflammatory cytokine biosynthesis.* Nature, 1994. **372**(6508): p. 739-46.

114. Klemke, R.L., et al., *Regulation of cell motility by mitogen-activated protein kinase.* J Cell Biol, 1997. **137**(2): p. 481-92.

115. Kyriakis, J.M. and J. Avruch, *Protein kinase cascades activated by stress and inflammatory cytokines.* Bioessays, 1996. **18**(7): p. 567-77.

116. Ip, Y.T. and R.J. Davis, *Signal transduction by the c-Jun N-terminal kinase (JNK)--from inflammation to development.* Curr Opin Cell Biol, 1998. **10**(2): p. 205-19.

117. Marshall, C.J., *Specificity of receptor tyrosine kinase signaling: transient versus sustained extracellular signal-regulated kinase activation.* Cell, 1995. **80**(2): p. 179-85.

118. Yang, C.S., et al., *Differential regulation of interleukin-12 and tumour necrosis factor-alpha by phosphatidylinositol 3-kinase and ERK 1/2 pathways during Mycobacterium tuberculosis infection.* Clin Exp Immunol, 2006. **143**(1): p. 150-60.

119. Farley, S.M., et al., *Fas ligand-induced proinflammatory transcriptional responses in reconstructed human epidermis. Recruitment of the epidermal growth factor receptor and activation of MAP kinases.* J Biol Chem, 2008. **283**(2): p. 919-28.

120. Kloft, N., et al., *Pore-forming toxins activate MAPK p38 by causing loss of cellular potassium.* Biochem Biophys Res Commun, 2009. **385**(4): p. 503-6.

121. Yates, S. and T.E. Rayner, *Transcription factor activation in response to cutaneous injury: role of AP-1 in reepithelialization.* Wound Repair Regen, 2002. **10**(1): p. 5-15.

122. Muller, R., et al., *Induction of c-fos gene and protein by growth factors precedes activation of c-myc.* Nature, 1984. **312**(5996): p. 716-20.

123. Abate, C., et al., *Dimerization and DNA binding alter phosphorylation of Fos and Jun.* Proc Natl Acad Sci U S A, 1993. **90**(14): p. 6766-70.

124. Akiba, H., et al., *CD27, a member of the tumor necrosis factor receptor superfamily, activates NF-kappaB and stress-activated protein kinase/c-Jun N-terminal kinase via TRAF2, TRAF5, and NF-kappaB-inducing kinase.* J Biol Chem, 1998. **273**(21): p. 13353-8.

125. Dziarski, R., Y.P. Jin, and D. Gupta, *Differential activation of extracellular signal-regulated kinase (ERK) 1, ERK2, p38, and c-Jun NH2-terminal kinase mitogen-activated protein kinases by bacterial peptidoglycan.* J Infect Dis, 1996. **174**(4): p. 777-85.

126. Barton, G.M. and R. Medzhitov, *Toll-like receptor signaling pathways.* Science, 2003. **300**(5625): p. 1524-5.

127. Kopp, E.B. and S. Ghosh, *NF-kappa B and rel proteins in innate immunity.* Adv Immunol, 1995. **58**: p. 1-27.

128. Stein, B., et al., *Cross-coupling of the NF-kappa B p65 and Fos/Jun transcription factors produces potentiated biological function.* EMBO J, 1993. **12**(10): p. 3879-91.

129. Sun, S.C., et al., *Human T-cell leukemia virus type I Tax activation of NF-kappa B/Rel involves phosphorylation and degradation of I kappa B alpha and RelA (p65)-mediated induction of the c-rel gene.* Mol Cell Biol, 1994. **14**(11): p. 7377-84.

130. Baldwin, A.S., Jr., *The NF-kappa B and I kappa B proteins: new discoveries and insights.* Annu Rev Immunol, 1996. **14**: p. 649-83.

131. Barnes, P.J. and M. Karin, *Nuclear factor-kappaB: a pivotal transcription factor in chronic inflammatory diseases.* N Engl J Med, 1997. **336**(15): p. 1066-71.

132. Arthur, J.S., *MSK activation and physiological roles.* Front Biosci, 2008. **13**: p. 5866-79.

133. Dent, P., et al., *Stress and radiation-induced activation of multiple intracellular signaling pathways.* Radiat Res, 2003. **159**(3): p. 283-300.

134. Hoffmann, A. and D. Baltimore, *Circuitry of nuclear factor kappaB signaling.* Immunol Rev, 2006. **210**: p. 171-86.

135. Schmitz, R., et al., *TNFAIP3 (A20) is a tumor suppressor gene in Hodgkin lymphoma and primary mediastinal B cell lymphoma.* J Exp Med, 2009. **206**(5): p. 981-9.

136. Gon, Y., et al., *A20 inhibits toll-like receptor 2- and 4-mediated interleukin-8 synthesis in airway epithelial cells.* Am J Respir Cell Mol Biol, 2004. **31**(3): p. 330-6.

137. Bond, M., et al., *Synergistic upregulation of metalloproteinase-9 by growth factors and inflammatory cytokines: an absolute requirement for transcription factor NF-kappa B.* FEBS Lett, 1998. **435**(1): p. 29-34.

138. Bond, M., A.H. Baker, and A.C. Newby, *Nuclear factor kappaB activity is essential for matrix metalloproteinase-1 and -3 upregulation in rabbit dermal fibroblasts.* Biochem Biophys Res Commun, 1999. **264**(2): p. 561-7.

139. Li, Z.W., et al., *The IKKbeta subunit of IkappaB kinase (IKK) is essential for nuclear factor kappaB activation and prevention of apoptosis.* J Exp Med, 1999. **189**(11): p. 1839-45.

140. Camerer, E., et al., *Binding of factor VIIa to tissue factor on keratinocytes induces gene expression.* J Biol Chem, 2000. **275**(9): p. 6580-5.

141. Pettit, E.J. and F.S. Fay, *Cytosolic free calcium and the cytoskeleton in the control of leukocyte chemotaxis.* Physiol Rev, 1998. **78**(4): p. 949-67.

142. Sharpe, G.R., J.I. Gillespie, and J.R. Greenwell, *An increase in intracellular free calcium is an early event during differentiation of cultured human keratinocytes.* FEBS Lett, 1989. **254**(1-2): p. 25-8.

143. Wakita, H., et al., *Staphylococcal enterotoxin B upregulates expression of ICAM-1 molecules on IFN-gamma-treated keratinocytes and keratinocyte cell lines.* J Invest Dermatol, 1995. **105**(4): p. 536-42.

144. Etienne, S., et al., *MHC class II engagement in brain endothelial cells induces protein kinase A-dependent IL-6 secretion and phosphorylation of cAMP response element-binding protein.* J Immunol, 1999. **163**(7): p. 3636-41.

145. Travers, J.B., D.A. Norris, and D.Y. Leung, *The keratinocyte as a target for staphylococcal bacterial toxins.* J Investig Dermatol Symp Proc, 2001. **6**(3): p. 225-30.

146. Al-Daccak, R., N. Mooney, and D. Charron, *MHC class II signaling in antigen-presenting cells.* Curr Opin Immunol, 2004. **16**(1): p. 108-13.

147. Hornig-Do, H.T., et al., *Human epidermal keratinocytes accumulate superoxide due to low activity of Mn-SOD, leading to mitochondrial functional impairment.* J Invest Dermatol, 2007. **127**(5): p. 1084-93.

148. Gethin, G.T., S. Cowman, and R.M. Conroy, *The impact of Manuka honey dressings on the surface pH of chronic wounds.* Int Wound J, 2008. **5**(2): p. 185-94.

149. Greener, B., et al., *Proteases and pH in chronic wounds.* J Wound Care, 2005. **14**(2): p. 59-61.

150. Sen, C.K., *Wound healing essentials: Let there be oxygen.* Wound Repair and Regeneration, 2009. **17**(1): p. 1-18.

151. Park, M.K., R.A.M. Myers, and L. Marzella, *Oxygen-tensions and infections - Modulation of microbial growth, activity of antimicrobial agents, and immunological resonses.* Clinical Infectious Diseases, 1992. **14**(3): p. 720-740.

152. Kranke, P., et al., *Hyperbaric oxygen therapy for chronic wounds.* Cochrane Database Syst Rev, 2004(2): p. CD004123.

153. Thackham, J.A., D.L. McElwain, and R.J. Long, *The use of hyperbaric oxygen therapy to treat chronic wounds: A review.* Wound Repair Regen, 2008. **16**(3): p. 321-30.

154. Sander, A.L., et al., *In vivo effect of hyperbaric oxygen on wound angiogenesis and epithelialization.* Wound Repair and Regeneration, 2009. **17**(2): p. 179-184.

155. Yoon, S.S., et al., *Pseudomonas aeruginosa anaerobic respiration in biofilms: relationships to cystic fibrosis pathogenesis.* Dev Cell, 2002. **3**(4): p. 593-603.

156. Rani, S.A., et al., *Spatial patterns of DNA replication, protein synthesis, and oxygen concentration within bacterial biofilms reveal diverse physiological states.* J Bacteriol, 2007. **189**(11): p. 4223-33.

157. Davey, M.E. and A. O'Toole G, *Microbial biofilms: from ecology to molecular genetics.* Microbiol Mol Biol Rev, 2000. **64**(4): p. 847-67.

158. Cotter, J.J., et al., *Oxygen-mediated regulation of biofilm development is controlled by the alternative sigma factor {sigma}B in Staphylococcus epidermidis.* Applied and Environmental Microbiology, 2009. **75**(1): p. 261-264.

159. Cramton, S.E., et al., *Anaerobic conditions induce expression of polysaccharide intercellular adhesin in Staphylococcus aureus and Staphylococcus epidermidis.* Infection and Immunity, 2001. **69**(6): p. 4079-4085.

160. Fuchs, S., et al., *Anaerobic gene expression in Staphylococcus aureus.* Journal of Bacteriology, 2007. **189**(11): p. 4275-4289.

161. Bowler, P.G., B.I. Duerden, and D.G. Armstrong, *Wound microbiology and associated approaches to wound management.* Clin Microbiol Rev, 2001. **14**(2): p. 244-69.

162. Price, L.B., et al., *Community analysis of chronic wound bacteria using 16S rRNA gene-based pyrosequencing: impact of diabetes and antibiotics on chronic wound microbiota.* PLoS One, 2009. **4**(7): p. e6462.

163. Davies, C.E., et al., *Use of 16S ribosomal DNA PCR and denaturing gradient gel electrophoresis for analysis of the microfloras of healing and nonhealing chronic venous leg ulcers.* J Clin Microbiol, 2004. **42**(8): p. 3549-57.

164. Olaru, F. and L.E. Jensen, *Chemokine expression by human keratinocyte cell lines after activation of Toll-like receptors.* Exp Dermatol.

165. Charvat, S., et al., *Ras-transfection up-regulated HaCaT cell migration: inhibition by Marimastat.* Clin Exp Metastasis, 1999. **17**(8): p. 677-85.

166. Fukano, Y., et al., *Characterization of an in vitro model for evaluating the interface between skin and percutaneous biomaterials.* Wound Repair Regen, 2006. **14**(4): p. 484-91.

167. Wyatt, M.A., et al., *Staphylococcus aureus Nonribosomal Peptide Secondary Metabolites Regulate Virulence.* Science.

168. Hemmi, H., et al., *A Toll-like receptor recognizes bacterial DNA.* Nature, 2000. **408**(6813): p. 740-5.

169. Molne, L., L.V. Collins, and A. Tarkowski, *Inflammatogenic properties of bacterial DNA following cutaneous exposure.* J Invest Dermatol, 2003. **121**(2): p. 294-9.

170. Dalton, S.J., et al., *Mechanisms of chronic skin ulceration linking lactate, transforming growth factor-beta, vascular endothelial growth factor, collagen remodeling, collagen stability, and defective angiogenesis.* J Invest Dermatol, 2007. **127**(4): p. 958-68.

171. Niinikoski, J., *Effect of oxygen supply on wound healing and formation of experimental granulation tissue.* Acta Physiol Scand Suppl, 1969. **334**: p. 1-72.

172. Hunt, T.K. and M.P. Pai, *The effect of varying ambient oxygen tensions on wound metabolism and collagen synthesis.* Surg Gynecol Obstet, 1972. **135**(4): p. 561-7.

173. Knighton, D.R., I.A. Silver, and T.K. Hunt, *Regulation of wound-healing angiogenesis-effect of oxygen gradients and inspired oxygen concentration.* Surgery, 1981. **90**(2): p. 262-70.

174. Hohn, D.C., et al., *Effect of O2 tension on microbicidal function of leukocytes in wounds and in vitro.* Surg Forum, 1976. **27**(62): p. 18-20.

175. Mader, J.T., et al., *A mechanism for the amelioration by hyperbaric oxygen of experimental staphylococcal osteomyelitis in rabbits.* J Infect Dis, 1980. **142**(6): p. 915-22.

176. Gordillo, G.M. and C.K. Sen, *Revisiting the essential role of oxygen in wound healing.* Am J Surg, 2003. **186**(3): p. 259-63.

177. Blackman, E., et al., *Topical wound oxygen therapy in the treatment of severe diabetic foot ulcers: a prospective controlled study.* Ostomy Wound Manage. **56**(6): p. 24-31.

178. Zhang, J. and S. Kashket, *Cytotoxic effects of short-chain carboxylic acids on human gingival epithelial cells.* Oral Microbiol Immunol, 1997. **12**(6): p. 345-9.

179. Sorkin, B.C. and R. Niederman, *Short chain carboxylic acids decrease human gingival keratinocyte proliferation and increase apoptosis and necrosis.* J Clin Periodontol, 1998. **25**(4): p. 311-5.

180. Rippke, F., et al., *Stratum corneum pH in atopic dermatitis: impact on skin barrier function and colonization with Staphylococcus Aureus.* Am J Clin Dermatol, 2004. **5**(4): p. 217-23.

181. Lenz, A.P., et al., *Localized gene expression in Pseudomonas aeruginosa biofilms.* Appl Environ Microbiol, 2008. **74**(14): p. 4463-71.

182. Sturn, A., J. Quackenbush, and Z. Trajanoski, *Genesis: cluster analysis of microarray data.* Bioinformatics, 2002. **18**(1): p. 207-8.

183. Dennis, G., Jr., et al., *DAVID: Database for Annotation, Visualization, and Integrated Discovery.* Genome Biol, 2003. **4**(5): p. P3.

184. Moreland, J.G., et al., *Organism-specific neutrophil-endothelial cell interactions in response to Escherichia coli, Streptococcus pneumoniae, and Staphylococcus aureus.* J Immunol, 2004. **172**(1): p. 426-32.

185. Kumar, A., J. Zhang, and F.S. Yu, *Innate immune response of corneal epithelial cells to Staphylococcus aureus infection: role of peptidoglycan in stimulating proinflammatory cytokine secretion.* Invest Ophthalmol Vis Sci, 2004. **45**(10): p. 3513-22.

186. van Langevelde, P., et al., *Antibiotic-induced release of lipoteichoic acid and peptidoglycan from Staphylococcus aureus: quantitative measurements and biological reactivities.* Antimicrob Agents Chemother, 1998. **42**(12): p. 3073-8.

187. Callegan, M.C., et al., *Corneal virulence of Staphylococcus aureus: roles of alpha-toxin and protein A in pathogenesis.* Infect Immun, 1994. **62**(6): p. 2478-82.

188. Dommisch, H., et al., *Protease-activated receptor 2 mediates human beta-defensin 2 and CC chemokine ligand 20 mRNA expression in response to proteases secreted by Porphyromonas gingivalis.* Infect Immun, 2007. **75**(9): p. 4326-33.

189. Yao, L., et al., *Prevention of endothelial cell cytokine induction by a Staphylococcus aureus lipoprotein.* FEMS Immunol Med Microbiol, 2000. **28**(4): p. 301-5.

190. Bantel, H., et al., *alpha-Toxin is a mediator of Staphylococcus aureus-induced cell death and activates caspases via the intrinsic death pathway independently of death receptor signaling.* J Cell Biol, 2001. **155**(4): p. 637-48.

191. Dieckgraefe, B.K. and D.M. Weems, *Epithelial injury induces egr-1 and fos expression by a pathway involving protein kinase C and ERK.* Am J Physiol, 1999. **276**(2 Pt 1): p. G322-30.

192. De Sousa, L.P., et al., *Plasminogen/plasmin regulates c-fos and egr-1 expression via the MEK/ERK pathway.* Biochem Biophys Res Commun, 2005. **329**(1): p. 237-45.

193. Lee, K.H. and J.R. Kim, *Hepatocyte growth factor induced up-regulations of VEGF through Egr-1 in hepatocellular carcinoma cells.* Clin Exp Metastasis, 2009. **26**(7): p. 685-92.

194. Granet, C., et al., *MAPK and SRC-kinases control EGR-1 and NF-kappa B inductions by changes in mechanical environment in osteoblasts.* Biochem Biophys Res Commun, 2001. **284**(3): p. 622-31.

195. Mishra, J.P., et al., *Differential involvement of calmodulin-dependent protein kinase II-activated AP-1 and c-Jun N-terminal kinase-activated EGR-1 signaling pathways in tumor necrosis factor-alpha and lipopolysaccharide-induced CD44 expression in human monocytic cells.* J Biol Chem, 2005. **280**(29): p. 26825-37.

196. Eder, J., *Tumour necrosis factor alpha and interleukin 1 signalling: do MAPKK kinases connect it all?* Trends Pharmacol Sci, 1997. **18**(9): p. 319-22.

197. Niyonsaba, F., et al., *The human antimicrobial peptide dermcidin activates normal human keratinocytes.* Br J Dermatol, 2009. **160**(2): p. 243-9.

198. Menzies, B.E. and A. Kenoyer, *Signal transduction and nuclear responses in Staphylococcus aureus-induced expression of human beta-defensin 3 in skin keratinocytes.* Infect Immun, 2006. **74**(12): p. 6847-54.

199. Li, Q., et al., *Staphylococcus aureus lipoproteins trigger human corneal epithelial innate response through toll-like receptor-2.* Microb Pathog, 2008. **44**(5): p. 426-34.

200. Chung, W.O. and B.A. Dale, *Innate immune response of oral and foreskin keratinocytes: utilization of different signaling pathways by various bacterial species.* Infect Immun, 2004. **72**(1): p. 352-8.

201. Esen, M., et al., *Mechanisms of Staphylococcus aureus induced apoptosis of human endothelial cells.* Apoptosis, 2001. **6**(6): p. 431-9.

202. Baldari, C.T., et al., *Anthrax toxins: A paradigm of bacterial immune suppression.* Trends Immunol, 2006. **27**(9): p. 434-40.

203. Shan, L., P. He, and J. Sheen, *Intercepting host MAPK signaling cascades by bacterial type III effectors.* Cell Host Microbe, 2007. **1**(3): p. 167-74.

204. Brodsky, I.E. and R. Medzhitov, *Targeting of immune signalling networks by bacterial pathogens.* Nat Cell Biol, 2009. **11**(5): p. 521-6.

205. Swanson, H.I., *Cytochrome P450 expression in human keratinocytes: an aryl hydrocarbon receptor perspective.* Chem Biol Interact, 2004. **149**(2-3): p. 69-79.

206. Umannova, L., et al., *Tumor necrosis factor-alpha potentiates genotoxic effects of benzo[a]pyrene in rat liver epithelial cells through upregulation of cytochrome P450 1B1 expression.* Mutat Res, 2008. **640**(1-2): p. 162-9.

207. Fujii-Kuriyama, Y. and J. Mimura, *Molecular mechanisms of AhR functions in the regulation of cytochrome P450 genes.* Biochem Biophys Res Commun, 2005. **338**(1): p. 311-7.

208. Barouki, R. and Y. Morel, *Repression of cytochrome P450 1A1 gene expression by oxidative stress: mechanisms and biological implications.* Biochem Pharmacol, 2001. **61**(5): p. 511-6.

209. Morgan, E.T., *Regulation of cytochrome p450 by inflammatory mediators: why and how?* Drug Metab Dispos, 2001. **29**(3): p. 207-12.

210. Renton, K.W., *Alteration of drug biotransformation and elimination during infection and inflammation.* Pharmacol Ther, 2001. **92**(2-3): p. 147-63.

211. McMillan, B.J. and C.A. Bradfield, *The aryl hydrocarbon receptor sans xenobiotics: endogenous function in genetic model systems.* Mol Pharmacol, 2007. **72**(3): p. 487-98.

212. Katiyar, S.K., et al., *Inhibition of UVB-induced oxidative stress-mediated phosphorylation of mitogen-activated protein kinase signaling pathways in cultured human epidermal keratinocytes by green tea polyphenol (-)-epigallocatechin-3-gallate.* Toxicol Appl Pharmacol, 2001. **176**(2): p. 110-7.

213. Simon, H.U., A. Haj-Yehia, and F. Levi-Schaffer, *Role of reactive oxygen species (ROS) in apoptosis induction.* Apoptosis, 2000. **5**(5): p. 415-8.

214. Darr, D. and I. Fridovich, *Free radicals in cutaneous biology.* J Invest Dermatol, 1994. **102**(5): p. 671-5.

215. Trenam, C.W., D.R. Blake, and C.J. Morris, *Skin inflammation: reactive oxygen species and the role of iron.* J Invest Dermatol, 1992. **99**(6): p. 675-82.

216. Malaplate-Armand, C., et al., *Astroglial CYP1B1 up-regulation in inflammatory/oxidative toxic conditions: IL-1beta effect and protection by N-acetylcysteine.* Toxicol Lett, 2003. **138**(3): p. 243-51.

217. Fradette, C. and P. Du Souich, *Effect of hypoxia on cytochrome P450 activity and expression.* Curr Drug Metab, 2004. **5**(3): p. 257-71.

218. Kirker, K.R., et al., *Loss of viability and induction of apoptosis in human keratinocytes exposed to Staphylococcus aureus biofilms in vitro.* Wound Repair Regen, 2009. **17**(5): p. 690-9.

219. Rosenshine, I., et al., *Signal transduction between enteropathogenic Escherichia coli (EPEC) and epithelial cells: EPEC induces tyrosine phosphorylation of host cell proteins to initiate cytoskeletal rearrangement and bacterial uptake.* EMBO J, 1992. **11**(10): p. 3551-60.

220. Zhou, D., et al., *A Salmonella inositol polyphosphatase acts in conjunction with other bacterial effectors to promote host cell actin cytoskeleton rearrangements and bacterial internalization.* Mol Microbiol, 2001. **39**(2): p. 248-59.

221. Jung, K.Y., et al., *Involvement of staphylococcal protein A and cytoskeletal actin in Staphylococcus aureus invasion of cultured human oral epithelial cells.* J Med Microbiol, 2001. **50**(1): p. 35-41.

222. Mempel, M., et al., *Invasion of human keratinocytes by Staphylococcus aureus and intracellular bacterial persistence represent haemolysin-independent virulence mechanisms that are followed by features of necrotic and apoptotic keratinocyte cell death.* Br J Dermatol, 2002. **146**(6): p. 943-51.

223. Nuzzo, I., et al., *Apoptosis of human keratinocytes after bacterial invasion.* FEMS Immunol Med Microbiol, 2000. **27**(3): p. 235-40.

224. Alexander, E.H., et al., *Staphylococcus aureus - induced tumor necrosis factor - related apoptosis - inducing ligand expression mediates apoptosis and caspase-8 activation in infected osteoblasts.* BMC Microbiol, 2003. **3**: p. 5.

225. Kahl, B.C., et al., *Staphylococcus aureus RN6390 replicates and induces apoptosis in a pulmonary epithelial cell line.* Infect Immun, 2000. **68**(9): p. 5385-92.

226. Gniadecki, R. and B. Gajkowska, *Intracellular calcium pool emptying induces DNA synthesis in HaCaT keratinocytes.* Exp Dermatol, 2003. **12**(4): p. 453-9.

227. Piddini, E., et al., *The Ras-like GTPase Gem is involved in cell shape remodelling and interacts with the novel kinesin-like protein KIF9.* EMBO J, 2001. **20**(15): p. 4076-87.

228. Fischer, R., et al., *Calmodulin binds to and inhibits GTP binding of the ras-like GTPase Kir/Gem.* J Biol Chem, 1996. **271**(41): p. 25067-70.

229. Cohen, L., et al., *Transcriptional activation of a ras-like gene (kir) by oncogenic tyrosine kinases.* Proc Natl Acad Sci U S A, 1994. **91**(26): p. 12448-52.

230. Aresta, S., et al., *A novel Rho GTPase-activating-protein interacts with Gem, a member of the Ras superfamily of GTPases.* Biochem J, 2002. **367**(Pt 1): p. 57-65.

231. Beguin, P., et al., *Regulation of Ca2+ channel expression at the cell surface by the small G-protein kir/Gem.* Nature, 2001. **411**(6838): p. 701-6.

232. Ward, Y., et al., *Phosphorylation of critical serine residues in Gem separates cytoskeletal reorganization from down-regulation of calcium channel activity.* Mol Cell Biol, 2004. **24**(2): p. 651-61.

233. Beguin, P., et al., *14-3-3 and calmodulin control subcellular distribution of Kir/Gem and its regulation of cell shape and calcium channel activity.* J Cell Sci, 2005. **118**(Pt 9): p. 1923-34.

234. Sorokina, E.M. and J. Chernoff, *Rho-GTPases: new members, new pathways.* J Cell Biochem, 2005. **94**(2): p. 225-31.

235. Ward, Y., et al., *The GTP binding proteins Gem and Rad are negative regulators of the Rho-Rho kinase pathway.* J Cell Biol, 2002. **157**(2): p. 291-302.

236. Baron, J.M., et al., *Expression of multiple cytochrome p450 enzymes and multidrug resistance-associated transport proteins in human skin keratinocytes.* J Invest Dermatol, 2001. **116**(4): p. 541-8.